

Declaration of Originality

I, Paul Justin Reichl declare that this thesis is my own work and has not been submitted in any form for another degree or diploma at any university or other institute of tertiary education. Information derived from the published and unpublished work of others has been acknowledged in the text and a list of references is given in the bibliography.

Paul Justin Reichl 20 July 2001

Flow Past A Cylinder Close To A Free Surface

This thesis is submitted in fulfillment of
the requirements for the degree of Doctor of Philosophy,
Department of Mechanical Engineering
Monash University
July 2001

By
Paul Reichl
B.Sc. (Honours)

Abstract

Two-dimensional flow past a cylinder close to a free surface at a Reynolds number of 180 is numerically investigated. The flow characteristics for Froude numbers between 0.00 and 0.70 and for gap ratios between 0.10 and 5.00 are examined, and a mechanism that explains the flows behaviour is proposed. The results reveal that this problem shares many features with flow past a cylinder close to a no-slip wall at low Froude numbers where the surface experiences little or no deformation. This suggests that the flow is largely governed by geometrical constraints at least in the low Froude number limit.

At the larger Froude numbers good agreement is obtained with the experimental findings of Sheridan *et al.* (1995), Sheridan *et al.* (1997) and Hoyt and Sellin (2000). The proposed mechanism suggests that the cessation of shedding at smaller gap ratios is due to a combination of lack of fluid for discrete vortex formation, and increasing levels of skew in the wake. The metastable wake states seen by both Sheridan *et al.* (1995) and Sheridan *et al.* (1997) are observed, and it is speculated here that these states result from the time dependent switching between an absolute and a convective instability.

An analogy with flow past two side-by-side cylinders and symmetrical flow past a cylinder is made, as common aspects with both of these flows are observed.

A larger portion of the parameter space is mapped out and the forces and shedding frequencies associated with the flow are provided, which to the author's knowledge was largely previously uncharted.

Acknowledgment

I would like to express my gratitude to my supervisor Professor Kerry Hourigan for his continuous guidance and enthusiasm and for managing to find the right balance between providing direction and encouraging independence. I would also like to express my thanks to Associate Professor Mark Thompson for his input and suggestions during the course of my candidature.

I am also grateful to the numerous people who have through shared experiences become both my colleagues and my friends. In particular I would like to thank my former office mates, Dr Tan Boon Thong, Dr Paul Morris, Michael Jones, Keith Liow and Mervyn Tan, who have all in their own way made sure that life was never dull.

The financial assistance in the form of an Australian Postgraduate Award (scholarship) is also gratefully acknowledged.

I would also like to express my appreciation to Melanie Franklyn for proof-reading parts of this document, as her effort has helped to reduce the number of grammatical and typographical mistakes in this thesis.

This document would never have been completed without the support of my family, and I would like to thank my late Aunty Margaret for always managing to help me see things from the best possible light. I would also like to thank my brother Craig and especially my parents, whose faith in me never wavered even when my own did, and whose honesty and kindness continue to inspire me.

Publications

Reichl, P. J., Morris, P., Hourigan, K., Thompson, M.C. & Stoneman, S.A.T. (1997), Coating flow simulations using smooth particle hydrodynamics, *in* ‘Computational Fluid Dynamics in Mineral & Metal Processing and Power Generation, Melbourne Australia’, pp. 345-352.

Reichl, P. J., Morris, P., Hourigan, K., Thompson, M.C. & Stoneman, S.A.T. (1997), Free surface flows using smooth particle hydrodynamics, *in* ‘ASME Fluids Engineering Division Summer Meeting, FEDSM97-3403, Vancouver, British Columbia, Canada’.

Reichl, P. J., Morris, P., Hourigan, K., Thompson, M. C. & Stoneman, S. A. T. (1998), ‘Smooth particle hydrodynamics simulation of surface coating’, *Applied Mathematical Modelling* **22**, 1037-1046.

Reichl, P. J., Morris, P., Stoneman, S.A.T., Thompson, M.C.& Hourigan, K. (1998), Smooth particle hydrodynamics modelling of vertical jet impingement’, *in* ‘Proceeding of the 13th Australasian Fluid Mechanics Conference, Melbourne, Australia’, pp. 103-106.

Reichl, P. J., Hourigan, K. & Thompson, M.C. (1998), Flow past a cylinder submerged under a free surface’, *in* ‘Proceeding of the 13th Australasian Fluid Mechanics Conference, Melbourne, Australia’, pp. 943-946.

Reichl, P. J., Hourigan, K. & Thompson, M.C. (1999), Flow past a cylinder near a free surface’, *in* ‘Proceeding of the 30th AIAA Fluid Dynamics Conference, AIAA paper 99-3808, Richmond, Virginia, U.S.A.’.

Abstracts for the following papers have already been accepted.

Reichl, P. J., Hourigan, K. & Thompson, M.C. (2001), Low Froude number frequency response for flow past a cylinder close to a free surface, *in* ‘Proceeding of the 14th Australasian Fluid Mechanics Conference, Adelaide, Australia’.

Reichl, P. J., Hourigan, K. & Thompson, M.C. (2001), Metastable wake states for flow past a cylinder close to a free surface, *in* ‘Proceeding of the 14th Australasian Fluid Mechanics Conference, Adelaide, Australia’.

Hourigan, K., Reichl, P.J. & Thompson, M.C. (2002), Unsteady separated flow near a free surface, *in* ‘Invited presentation for the IUTAM Symposium on Unsteady Separated Flows’, Toulouse, France.

Nomenclature

α	volume fraction
A	area
β	factor by which the resolution was altered
C_d	drag coefficient
C'_d	root mean square of the drag coefficient
C_l	lift coefficient
C'_l	root mean square of the lift coefficient
C_{pb}	base pressure coefficient
d	cylinder diameter
dA	integral area element
δ_{ij}	Kronecker delta
δ^*	displacement thickness
$d\mathbf{l}$	integral vector length element
ds	integral surface length element
dV	integral volume element
$D_{particle}$	particle diameter
\mathbf{e}_r	unit vector in the radial direction
\mathbf{e}_θ	unit vector in the azimuthal direction
\mathbf{e}_z	unit vector in the axial direction
f	shedding frequency
Fr	Froude Number
g	gravitational acceleration
\mathbf{g}	body force vector
$\nabla\phi$	body force vector (\mathbf{g})
Γ	Circulation
Γ_d	diffusion coefficient
h	submergence depth
h^*	gap ratio, or non-dimensionalized submergence depth
h_r	resolution parameter
κ	curvature ($\frac{1}{R}$)
L	lift force

$L1$	distance from the inlet to the cylinder center
$L2$	distance from the outlet to the cylinder center
$L3$	width of the computational domain
μ	dynamic viscosity of the fluid
\mathbf{n}	normal vector
n_j	j^{th} component of the normal vector
ν	kinematic viscosity
P	pressure
ϕ	general scalar quantity that is defined when used
r	radial coordinate
R	radius of curvature / radial distance
Re	Reynolds Number
ρ	fluid density
$\rho_{particle}$	particle density
s	distance
St	Strouhal Number
S_ϕ	momentum source term
σ	surface tension
\mathbf{u}	velocity vector
u	x component of the velocity
v	y component of the velocity
w	z component of the velocity
u_r	component of the velocity in the radial direction
u_θ	component of the velocity in the azimuthal direction
u_{part}	particle velocity
ω	vorticity
ω_x	x component of the vorticity
ω_y	y component of the vorticity
ω_z	z component of the vorticity
\mathbf{t}	stress vector
t_i	i^{th} component of the stress
T_{ij}	stress tensor
θ	azimuthal coordinate

θ_1	stagnation angle
θ_2	top separation angle
θ_3	bottom separation angle
θ_4	rear attachment angle
∇	gradient operator
\times	curl operator

Contents

1	Introduction and Literature Review	1
1.1	Flow Past a Cylinder in an Infinite Medium	2
1.2	Flow Instabilities	4
1.3	Wake Control	8
1.4	Flow Past a Cylinder Close to a No-slip Wall	10
1.5	Vorticity and the Free Surface	14
1.5.1	What is Vorticity?	14
1.5.2	Why Discuss Phenomena in Terms of Vorticity?	14
1.5.3	What is a Free Surface?	15
1.5.4	Conservation / Non-Conservation of Vorticity	17
1.5.5	Free Surface Vorticity	21
1.5.6	Interaction of Vorticity with a Free Surface	23
1.6	Flow Past a Body Close to a Free Surface	25
1.7	Scope of the Present Investigation	28
2	Numerical Method, Validation, Problem Setup and Post Processing	29
2.1	Foreword	29
2.2	Free-Surface Flows	30
2.3	Numerical Method	30
2.3.1	Spatial Discretization	33

2.3.2	Temporal Discretization	34
2.3.3	Spatial and Temporal Accuracy Tests	34
2.3.4	Modelling the Free Surface	35
2.3.5	Interpolation Near the Interface	37
2.4	Validation	38
2.4.1	Spinning Bowl	38
2.4.2	Breaking Dam	41
2.4.3	Fully Submerged Cylinder	42
2.4.4	Testing Domain Sizes	45
2.4.5	Resolution	46
2.4.6	Convergence	49
2.4.7	Time Step	50
2.5	Problem Setup and Post Processing	51
2.5.1	Lift and Drag Forces	52
2.5.2	Moment	53
2.5.3	Force and Moment Coefficients	53
2.5.4	Separation and Stagnation Points	53
2.5.5	Vortex Paths and Convective Speeds	53
2.5.6	Time Averaged Flow and Standard Deviation	54
2.5.7	Strouhal Number	54
2.5.8	Particle Transport Plots/Videos	55
2.5.9	Vorticity Plots/Videos	56
2.5.10	Free-Surface Position	56
2.5.11	Pressure Plots	57
2.6	Videos	58
2.7	Summary	59

3	Free Slip and Froude Number 0.20	60
3.1	Scope and Layout of the Chapter	61
3.2	Strouhal Number	62
3.3	Lift, Drag and Moment Coefficients	64
3.3.1	Lift Coefficient	65
3.3.2	Root Mean Square (RMS) Lift Coefficient	65
3.3.3	Drag Coefficient	67
3.3.4	RMS Drag Coefficient	68
3.3.5	Mean Moment Coefficient	68
3.4	Pressure Distribution, and the Stagnation and Separation Points	72
3.5	Surface Deformation	76
3.6	Formation Length	80
3.7	Flow Fields	81
3.7.1	Gap Ratios 5.00, 2.50, 1.50	82
3.7.2	Gap Ratios 1.00 to 0.10	83
3.8	Comparison with Experiment	96
3.9	Suppression of Vortex Shedding	101
3.10	Vorticity Distributions	102
3.11	Vortex Paths	105
3.12	Mechanism for the Cessation of Vortex Shedding	107
3.13	Summary	118
4	Froude Numbers 0.25, 0.30, 0.35 and 0.40	120
4.1	Flow Behaviour and Surface Deformation	122
4.2	Strouhal Number	129
4.3	Mass Flux	136
4.4	Lift, Drag and Moment Coefficients	139

4.4.1	Lift	139
4.4.2	RMS Lift	140
4.4.3	Drag	141
4.4.4	RMS Drag	141
4.4.5	Moment	143
4.5	Pressure Distribution, and the Stagnation and Separation Points	144
4.6	Formation Length	150
4.7	Vortex Paths and Convective Velocities	151
4.8	Comparison with Experiments	152
4.9	Wave Breaking	154
4.10	Mechanism	164
4.11	Summary	175
5	Froude Numbers 0.50, 0.60 and above	178
5.1	Flow Behaviour	180
5.1.1	Large Gap Ratios, 5.00, 2.50, 1.50, 1.00 and 0.85	181
5.1.2	Intermediate Gap Ratios 0.70, 0.55, 0.40, 0.25 and Metastable Wake States	184
5.1.3	Small Gap Ratios 0.22, 0.19, 0.16, 0.13 and 0.10	212
5.2	Strouhal Number and Lift	217
5.3	Drag	233
5.4	Moment	234
5.5	Mechanism and the Stability of the Wake States	235
5.6	Summary	239
6	Conclusion	240
6.1	Future Work	243

Chapter 1

Introduction and Literature Review

The problem being considered here is that of flow past a cylinder close to a free surface. Practically, situations containing the same underlying physics will include flows relating to: offshore structures, pipelines, water vehicles such as boats and submarines, and power generation equipment to harness energy from both rivers and tides. A basic schematic that illustrates the problem is shown in figure (1.1).

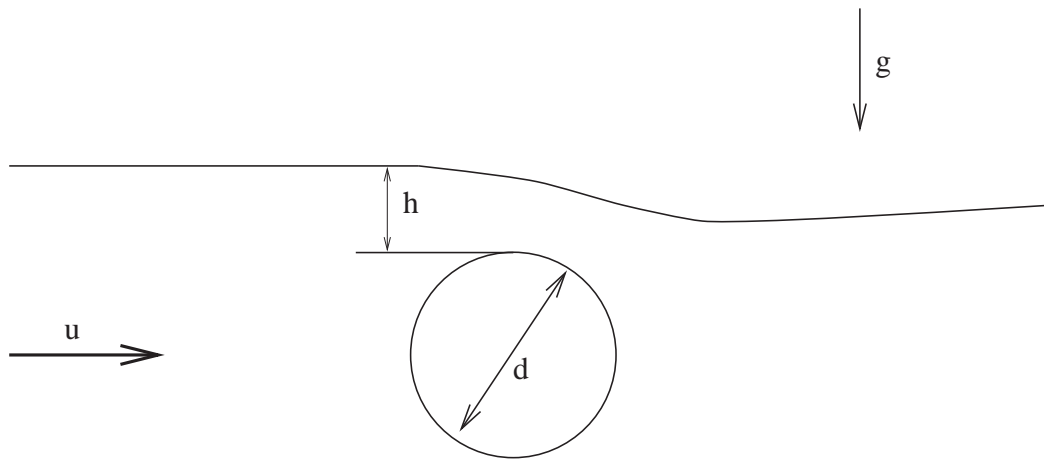


Figure 1.1: Schematic showing the problem setup, and some of the important parameters.

A broad discussion of some of the aspects that are potentially relevant to flow past a cylinder close to a free surface are examined. More attention has been given to some of the areas that are unique to this problem, such as the characteristics of the free surface, that are not as widely covered in the literature. The first section briefly examines some of the previous work on flow past a cylinder in an infinite medium, which is obviously of interest to the problem under consideration. The nature of the instabilities that govern the behaviour of the wake are

then discussed in section (1.2), as their impact on the observed flow is likely to be considerable. Previous work relevant to the control of the wake is then discussed in section (1.3) as aspects of this work have a direct bearing on what is observed here. Section (1.4) details previous work relating to flow past a cylinder close to a no-slip wall, which is found to share many common features with the current investigation, particularly at low Froude numbers. Following on from this, section (1.5) then provides a brief introduction to free surfaces and to vorticity, with section (1.6) highlighting some of the finding of others with regard to flow past a body close to a free surface. Finally section (1.7) then details the scope and aims of the present investigation.

1.1 Flow Past a Cylinder in an Infinite Medium

Flow past a cylinder in an infinite medium may be considered as one of the classical problems of fluid dynamics, with extensive investigation having been undertaken over a period of more than 120 years. One of the earliest studies was by Strouhal (1878), who examined the frequency response of wind blowing over a wire or a string in an Aeolian harp. As a testament to the extensive research which has been undertaken with regard to this geometry, many textbooks devote considerable attention to the problem, with Tritton (1988) providing just one example. A major attraction of the cylinder is its simple geometry, along with its immediate application to engineering problems. Indeed, the time-varying forces acting upon the cylinder are of immense importance in the design of buildings, offshore structures, bridges, vehicles, and power generation systems.

As considerable research has been previously undertaken in this area, the discussion here will largely restrict itself to some of the more recent work, with the reader recommended to consult review articles by Morkovin (1964), Berger & Wille (1972), and Williamson (1996) for more details.

While there are many aspects of flow past a cylinder which could be discussed, it is the establishment of Kármán vortex shedding which is of interest here. Such shedding arises when the Reynolds number of the flow ($Re = \rho dv/\mu$, where ρ is the fluid density, d is the cylinder diameter, v is the flow velocity, and μ is the dynamic viscosity of the fluid) exceeds the critical Reynolds number for vortex shedding, which is somewhere between 40 and 50 (the exact value seems to vary somewhat in the literature, with Williamson (1996) giving 49, while others such as Triantafyllou & Dimas (1989) indicate a value of about 40). At Reynolds numbers below this critical value, the flow is found to be steady with a symmetric pair of recirculation bubbles

observed at the rear of the cylinder.

When this critical value is exceeded, vortices form and are shed from each side of the cylinder in an alternating fashion, with the subsequent vortex pattern produced referred to as a von Kármán vortex street. The vortex street, which is made up of vortices (commonly referred to as Kármán vortices), is two dimensional for Reynolds numbers less than 180, although some three dimensional effects may be introduced experimentally by altering the end conditions on the cylinder, as demonstrated by Williamson (1991).

Williamson (1996) discusses the influence that increasing the Reynolds number has on the wake. For Reynolds numbers greater than 180 the flow field is found to become three dimensional, with mode A instabilities first developing at Reynolds numbers between 180 and 230, and mode B instabilities noted at Reynolds numbers above 230. These modes result in waviness in the third dimension, with the wavelength varying in size (3 to 4 diameters for mode A and about 1 diameter for mode B). As the Reynolds number is increased further, Morkovin (1964) indicates that there is a forward migration of turbulence within the shear layer and increasing three dimensionality. Williamson (1996) notes that three-dimensional structures of the scale of both the shear layer and of the Kármán vortices develop at the Reynolds number between 1000 and 200,000. The distance at which the vortices form behind the cylinder (often referred to as the formation length) also changes, with Unal & Rockwell (1988*a*), Lin et al. (1995) and Norberg (1998) all finding that the formation length initially increases (from roughly 1.5 diameters to 2.5 diameters for Reynolds numbers between 200 and 2000) before decreasing again as the Reynolds number is increased further (to roughly 1.25 diameters at a Reynolds number of 10,000).

Gerrard (1966) and Green & Gerrard (1993) give a descriptive process of vortex shedding. For Reynolds numbers above about 500, they describe the vortex shedding mechanism as one in which a forming vortex remains stationary relative to the cylinder as it grows, while at the same time drawing the shear layer from the other side of the cylinder toward itself. When the shear layer from the other side of the cylinder crosses the centerline, it cuts off the upstream supply of vorticity to the growing vortex, and a discrete ‘vortex’ is shed. The timing of this entire process then effectively determines the shedding frequency. Green & Gerrard (1993) note that this mechanism is not directly applicable at lower Reynolds numbers, as there is only very minor cross flow observed in the near wake. At lower Reynolds numbers, vortex shedding is characterized by a process in which the vorticity is split apart, a feature described by Freymuth et al. (1986) as vortex nipping. Green & Gerrard (1993) indicate that the shed vortex appears to develop from the area of vorticity bearing fluid that is subjected to the least viscous shear

stress. Furthermore they suggest that the Strouhal number ($St = fd/u$, where u is the flow velocity, d is the cylinder diameter, and f is the shedding frequency) versus Reynolds number relationship proposed by Williamson (1989) results from the changes in vorticity transport which occur as the Reynolds number is increased. They also propose that at lower Reynolds numbers the shedding mechanism involves the accumulation of vorticity from the separated boundary layer in the wake. This vorticity is then redistributed by the velocity field and split at locations downstream in regions of high shear. The growth of localized vorticity in the area outside of the high shear-stress region then develops, and a vortex is formed. Green & Gerrard (1993) describe vortex shedding as essentially a two-stage process: the first stage involves the formation of the vortices while the second involves them being shed. For low Reynolds numbers they indicate that it is the formation process which is the most critical, with the period of vortex shedding being determined by the time required for a coherent vortex structure to develop outside the high shear stress zone. At larger Reynolds numbers, the zone in which the viscous shear stress is high is considerably smaller, and as a consequence less time is required for vortex formation (hence the shortening of the period with increasing Reynolds number). At large enough Reynolds numbers where the shear stress contribution becomes very small, the self-induced velocity field (cross-flow) dominates the shedding process and the shedding frequency tends towards a constant.

Shariff et al. (1991) discuss the transport of fluid for flow past a cylinder in an infinite medium at low Reynolds numbers. They suggest that it is the wake fluid located just behind and slightly above the cylinder, which is shed from ‘the wake cavity’ during the course of one shedding cycle. The fluid which is to be ejected appears to broadly coincide with region of low viscous shear stress observed by Green & Gerrard (1993). Shariff et al. (1991) also indicate the region from which new fluid will be supplied to replace that lost during the last shedding cycle. For the case considered here (i.e. flow past a cylinder close to a free surface) the replacement fluid is likely to come from locations close to the free surface.

1.2 Flow Instabilities

Some of the underlying principles associated with linear stability theory and its application to related problems will now be discussed. Many assumptions are often made when studying fluid mechanics so as to simplify the mathematical models used to describe the physical behaviour. Common assumptions that are made about the nature of the fluid include: the treatment of the fluid as if it were Newtonian, the assumption that the fluid is incompressible and the neglect

of physical properties associated with the chemical structure of the material from which the fluid is composed. These assumptions must always be questioned before any model derived as a result may be applied. However, for the cases in which these assumptions are valid, the resulting mathematical model provides a point of reference from which much physical insight can be gained. Indeed, all numerical simulations are based upon the assumption that physical behaviour can be accurately modelled via a set of mathematical equations, with appropriate boundary conditions. In incompressible fluid mechanics, the flow behaviour is modelled via the time-dependent solution of both the momentum (often referred to as the Navier-Stokes equations for a Newtonian fluid) and continuity equations, which respectively ensure that both momentum and mass are conserved.

Stability analysis involves the further simplification of these governing equations and as such, caution must be taken when interpreting the results of such analysis. However, it is an invaluable tool when used appropriately.

Stability analysis involves solving for the impulse response of an unstable system to a given perturbation. Practically this involves first obtaining a steady-state flow field which is a solution of the steady Navier-Stokes equations, and then adding a small perturbation to each quantity being solved for. The subsequent time-dependent equations are then linearized with respect to the perturbation quantities. If the flow field is assumed to be parallel, then the resultant equations are commonly referred to as the Orr-Sommerfeld equations, which can then be solved for the perturbation quantities. In most instances, for a given velocity profile and Reynolds number, the spatial and temporal growth rates are solved for an impulse disturbance. The variation of these growth rates with Reynolds number and velocity profile can then be determined. Indeed, it is the velocity profile that determines the nature of the instability (Koch (1985)) and not the body itself, with vortex shedding being observed numerically in the absence of a wake producing body (Huerre & Monkewitz (1990)). Nevertheless, it is the body and the Reynolds number which together determine the velocity profile in the first place. This feature enables information to be inferred about the stability characteristics of one wake flow from the results obtained for other bluff bodies. The procedure just outlined allows for two types of instabilities to be found: convective and absolute.

Briggs (1964) describes an absolute instability as one where the response of a system to a pulse disturbance of finite extent is one in which the pulse grows in time without limit at every point in space. He describes a convective instability as one in which the pulse disturbance propagates through space, such that its amplitude diminishes in time at a fixed point in space (although such

a disturbance may grow as it is convected with the velocity field). Briggs (1964) also suggests that an absolute instability may be physically interpreted as a system with internal feedback, such that disturbances can grow without the need for reflections from boundary conditions. Convective instabilities, however, require external feedback or excitation (such as reflections or forcing) in order for disturbances to grow in time at a fixed point in space. Hence convective instabilities are likely to be influenced by the nature of the impulse disturbance, in that such a disturbance is likely to be amplified within the system. Absolute instabilities on the other hand are likely to amplify all disturbances, although some will grow faster than others, and it is these faster growing modes that are likely to dominate. Thus convective instabilities are likely to amplify external noise, while absolute instabilities are likely to produce oscillatory type behaviour of a fixed frequency, or set of frequencies.

Koch (1985) examines the compressible wake behind a blunt edged plate, and notes that the region of linear absolute instability is contained within a zone in the near wake, with Triantafyllou et al. (1986) observing similar behaviour for a circular cylinder. For regions outside of this zone, the wake is convectively unstable, which implies that only the disturbances within the zone of absolute instability will be self excited, while those outside of this zone will be convected away once the external disturbance is removed. As the zone of instability spans a region of finite size, with the extent diminishing with increasing Reynolds number (Triantafyllou et al. (1986)), Koch (1985) proposes a criterion whereby it is the disturbances at the transition point between the zone of absolute and convective instability that controls the downstream shedding process. For further discussion of other mode selection criteria see Oertel (1990). The stability of asymmetric velocity profiles are also considered by Koch (1985), with such profiles of considerably greater relevance to flow past a cylinder close to a free surface. For this case Koch (1985) notes that there exists only a limited range of asymmetry, before no time-harmonic resonance (absolute instability) is possible. Importantly this indicates that wake profiles which exhibit significant asymmetry are more likely to be convectively unstable.

Chomaz et al. (1988) investigate the Ginzburg-Landau equation, which allows for some non-parallel effects to be considered. They find that the zone of absolute instability must reach a finite critical size, which is problem dependent, before self excitation can occur. This implies that the presence of a local absolute instability is not necessarily a sufficient condition for a global mode (term given by Chomaz et al. (1988)) to become self excited. Indeed, Monkewitz (1988) finds that the Reynolds number at which parts of the wake for a circular cylinder first become absolutely unstable, is less than the Reynolds number at which Kármán vortex shedding

is first observed. This result has a number of implications, as it suggests that while stability analysis can give an indication of the shedding frequency for a given Reynolds number and velocity profile, this indication must be viewed only as an estimate; as parts of the non-parallel wake may already be absolutely unstable on a locally parallel basis, at Reynolds numbers well below that at which Kármán vortex shedding is first observed.

The stability characteristics for the interaction of separated flow with a free surface at low Froude number is considered by Triantafyllou & Dimas (1989). The Froude number (u/\sqrt{gd} , where u is the velocity, g is the gravitational acceleration and d is the length scale of the body) arises, as the gravitational acceleration term is required in the momentum (Navier-Stokes equations) for problems involving free surfaces. In this investigation, the authors find that the wake formed behind a floating cylinder (which is half submerged) is convectively unstable at all locations behind the cylinder at low Froude numbers. This suggests that disturbances will tend to be convected out of the recirculation bubble which makes up the wake. They note that two unstable branches of the dispersion relation are found for low Froude numbers: The first one, which they label branch I, occurs at low wavenumbers (large wavelengths) and is close to the antisymmetric stream function mode in an infinite fluid, which according to Triantafyllou et al. (1986) corresponds to a symmetric arrangement of vortices, as opposed to a vortex street. This mode is found to be convectively unstable. The second branch, which they label as branch II, is deemed a hybrid mode, and is in between the symmetric and antisymmetric stream function modes in an unbounded fluid; however this hybrid mode is found to have very small growth rates at low Froude numbers. As the Froude number is increased (beyond a value of 1.77 for a Froude number based on the cylinder diameter), branch I weakens while branch II approaches the sinuous mode (absolute instability), which produces a staggered array of vortices (a Kármán vortex street).

Dimas & Triantafyllou (1994) then go on to investigate the non-linear interaction of inviscid shear flow with a free surface. Their analysis is of most use if the wavelength of the perturbation is much longer than the thickness of the shear, which is potentially the case in the current study. They indicate that at low Froude numbers, the first branch of the dispersion relation (branch I), develops strong oval shaped vortices immediately below the free surface. Furthermore, sharp horizontal shear is noted near the free surface, and this is found to result in sharp small amplitude surface waves. The second branch (branch II), results in weak vortices with dimensions much smaller than their distance from the free surface at low Froude numbers, and they suggest that the free-surface elevation takes the form of a propagating wave. At larger Froude numbers strong

vortices form, that result in significant surface deformation and strong vertical shear near the free surface. They indicate that branch I instability waves are similar to the ones which would develop beneath a non-deformable free-slip wall, while branch II instability waves are more likely to develop considerable vertical velocities near the free surface. Each branch is also observed to result in a different mode of surface wave breaking, with branch I surface wave breaking resulting from significant horizontal but small vertical velocities at the free surface. Branch II surface wave breaking on the other hand, develops from small horizontal velocities but significant vertical ones.

1.3 Wake Control

The behaviour of the wake of a cylinder has been a topic of keen interest to many researchers, primarily for the reason of gaining a better understanding of vortex shedding, while also for the purpose of controlling the forces acting upon the cylinder. To control the wake, various techniques have been employed, such as perturbing the wake via in-line, cross-flow and rotational oscillations, and via the addition of various obstacles or modifications to the ‘cylinder in a continuous medium’ arrangement. Some of these features are described in differing forms by Apelt & West (1975), Griffin & Ramberg (1974, 1976), Ongoren & Rockwell (1988*a*, 1988*b*), Unal & Rockwell (1988*b*), Strykowski & Sreenivasan (1990), and Griffin & Hall (1991). This section now details some of the key findings that are likely to be of relevance to flow past a cylinder close to a free surface.

Apelt & West (1975) note that both the forces and the frequency of vortex shedding could be altered in a dramatic way if a thin plate, referred to as a splitter plate, was attached to the rear of a cylinder. Its presence was found to result in a significant drop in the drag even for short splitter plates, with plates of significant length being sufficient to suppress the instabilities that lead to the formation of the Kármán vortex street. Unal & Rockwell (1988*b*) also examine the influence of a splitter plate on the wake of a cylinder, although they consider the placement of the splitter plate at various distances behind the cylinder (such that there is a variable gap between the plate and the cylinder). Under these circumstances, Unal & Rockwell (1988*b*) note the length at which vortices form behind the cylinder (formation length) and find that the gap ratio required to suppress vortex shedding varies significantly with Reynolds number. They suggest that the strength of the instability may be a function of the Reynolds number, with their observations at a Reynolds number of 142 being the least susceptible to disturbances

produced by the presence of the splitter plate, with either coherent shedding being observed or none at all. This is of relevance here as the presence of vorticity at distances downstream appears to have less of an effect at the lower Reynolds numbers, with smaller gap ratios being required to attenuate vortex shedding. Their results at larger Reynolds numbers indicate that the unstable disturbance growth associated with the vortex shedding frequency is still noted in the separating shear layer. From these results they conclude that the presence of the splitter plate acts only to inhibit the formation of large scale vortices, as opposed to extinguishing the initial instability immediately downstream of the cylinder.

Strykowski & Sreenivasan (1990) modify the wake behaviour via the placement of an additional small circular cylinder at positions in the near wake of the larger cylinder. They find, that they are able to suppress shedding altogether if the smaller cylinder is placed appropriately. While this phenomenon is only observed within a range of low Reynolds numbers, its behaviour is consistent with that predicted by Gerrard (1966) and Green & Gerrard (1993), who indicate that if one can diffuse the shear layer vorticity or prevent the shear layers from interacting with one another (within a critical formation length), then it should be possible to delay or inhibit vortex shedding. Hence, for the low Reynolds number case being examined by Strykowski & Sreenivasan (1990), it would be expected that the diffusion introduced into the shear layer by the additional small cylinder would be sufficient to increase the diffusion length to a point at which shedding ceases. The notion put forward by Gerrard (1966) and Green & Gerrard (1993) is further supported by the fact that the shedding frequency was still reduced at larger Reynolds numbers where shedding was not suppressed. This indicates that by weakening the shear layer, it is possible to lengthen the period of time required for one shear layer to draw its opposite across the wake. This finding is likely to be of particular relevance to flow past a cylinder close to a free surface, as the free surface will tend to preferentially weaken the strength of one of the shear layers.

Fornberg (1985) discusses two-dimensional steady flow past a cylinder (a half cylinder with symmetry condition imposed). He details the growth of the recirculatory wake bubble up to Reynolds numbers of 600. The wake bubble is found to grow linearly with Reynolds number, with the width initially growing as Reynolds number to the power of 0.5, before growing linearly at Reynolds numbers greater than 300. The bubbles formed, extend over significant distances, and depending upon the Reynolds number may also span considerable widths. While at first this may seem completely unrelated to the problem under consideration here, the symmetry condition (which is essentially a free slip condition) is analogous to a non-deformable free-surface boundary

condition, which is considered later in this chapter in the section dealing with free surfaces and vorticity. Hence the possibility exists that large recirculation bubbles may form at small gap ratios.

Sumner et al. (1999) consider the flow behaviour associated with side-by-side circular cylinders in cross flow. This arrangement should share some similarity with the current problem, as potential flow models for free slip boundaries involve considering cases in which the free slip boundary is essentially a mirror plane. Sumner et al. (1999) indicate that there are three differing wake states observed for flow past two cylinders in a side-by-side arrangement. When the cylinders are in contact or are close to one another, single-body type vortex shedding is observed; at intermediate gap (or pitch) ratios biased flow is observed, whereby the flow from between the bodies tends to be drawn towards one of the cylinders. At larger gap ratios each cylinder produces its own vortex street, although some phase locking of the vortex formation is detected. The flow regime of greatest interest for the current problem is the one at intermediate gap ratios where biased flow is observed, and the one at small gap ratios. Williamson (1985) also considers this problem, noting that the bias of the flow from between the cylinders to one side, resulted in harmonic modes of vortex shedding between the two cylinders, such that the shedding frequency as measured on the outer side of one cylinder was a multiple of that on the other cylinder. No reason is given as to why two cylinder system preferentially favours one side, however, the notion that the flow remains attached to the cylinder as a result of the Coanda effect (a phenomenon in which a jet of fluid clings to a curved surface), is ruled out as similar behaviour was also found for flow between two flat plates. For the cylinders in this side-by-side arrangement, Bearman & Wadcock (1973) indicate that there is a net repulsive force acting between the two bodies.

1.4 Flow Past a Cylinder Close to a No-slip Wall

In this section flow past cylinders close to an adjacent no-slip wall will be discussed. It will be shown later, in the chapter dealing with flow past a cylinder close to a free surface at low Froude numbers, that these flows share many common features.

This flow was considered by Taneda (1965), who examined the problem at a Reynolds number of 170 and at gap ratios of 0.60 and 0.10 (where the gap ratio is simply the ratio of the distance between the edge of the cylinder and the wall, to the diameter of the cylinder). To eliminate the influence of the wall boundary layer that develops when a similar problem is considered in a

wind or water tunnel, a towing tank experimental rig was used. At a gap ratio of 0.60, he found that regular vortex shedding was observed. However, at a gap ratio of 0.10, only a single layer of vortices were seen to be shed from the cylinder. For the smaller gap ratio case the wavelength of the vortices was found to increase with downstream distance, and after a few wavelengths the wake became unstable and broke down. It is assumed that this breakdown refers to the coalescence of the vortical structures within the wake.

The lift and drag forces on a cylinder located close to a plane boundary for gap ratios between 0.00 and 6.00 were investigated by Roshko et al. (1975). The boundary layer thickness in their experimental investigation was half a cylinder diameter. They note that at larger gap ratios (i.e. greater than 0.60) the drag had a propensity to increase as the cylinder was moved closer to the wall. However, as the gap ratio was reduced further (i.e. the cylinder was moved closer), a rapid decrease in the drag was observed, with the minimum occurring when the cylinder and the wall were in contact. They attributed this effect partly to the movement of the cylinder into a lower energy wall boundary layer flow. The lift on the other hand was found to increase as the gap ratio was reduced, with its maximum value being observed when the cylinder was in contact with the wall. Similar trends were also observed by Taniguchi & Miyakoshi (1990), who investigated the variation of the forces with boundary layer thickness. For the most part the trends are similar, although they note that the boundary layer can have a significant influence on the forces, particularly at small gap ratios.

Bearman & Zdravkovich (1978) investigate the frequency response of flow past a circular cylinder near a plane boundary. They compared, as an analogy, their results with those of two cylinders in a side-by-side arrangement, which both authors had considered previously and which has a potential flow solution. On the basis of this analogy, they were able to make a number of predictions regarding the directions of the forces acting on the cylinder, as well as the nature of the shedding that would likely be observed. They suggest that for gap ratios larger than half a cylinder diameter, that the flow would continue to shed normally with a mean force directed away from the plane boundary. At smaller gaps they indicate that the wall boundary layer should separate at distances both upstream and downstream of the cylinder. They also discuss the findings of Göktun (1975), whose results largely corroborate those of Roshko et al. (1975). Göktun (1975) also noted that the minimum drag occurred when the cylinder was in contact with the wall, while the maximum drag, (C_d between 1.4 and 1.5) occurred at a gap ratio of 0.50. In addition, it is reported that Göktun (1975) also observed a slight shift in the shedding frequency as the cylinder was moved closer to the wall, such that the Strouhal number

reached a maximum at a gap ratio of 0.50. Bearman & Zdravkovich (1978) do not observe any similar increase in the Strouhal number, although they do find that the Strouhal number drops quite rapidly as the gap ratio is reduced, with the contraction from the gap ratio of 0.30 to 0.20 signifying the point of dramatic change. Bearman & Zdravkovich (1978) also indicate that the separation points were observed to shift with changing gap ratio; however the shift of the separation point closest to the wall in the downstream direction was generally matched by an equal shift in the separation point on the other side of the cylinder in the upstream direction.

The influence of Reynolds number was investigated by Angrilli et al. (1982), who considered Reynolds numbers between 2860 and 7640. They found that the shedding frequency increased when the gap ratio was decreased, with the maximum discrepancy of approximately 10% occurring at a gap ratio of 0.50, which was the smallest they examined. This result compares favourably with that of Göktun (1975), who also observed a maxima in the Strouhal number at this gap ratio. Such agreement is significant, as the Reynolds numbers differ by a factor of approximately 40 (i.e. Göktun (1975) approximately 2×10^5 , Angrilli et al. (1982) roughly 5000), with the formation length for a fully submerged cylinder varying by almost a cylinder diameter over this range (Norberg (1998)). The results of Angrilli et al. (1982) differ somewhat from those of Bearman & Zdravkovich (1978), who found negligible change in the shedding frequency. Angrilli et al. (1982) suggest that the thickness of the boundary layer on the wall may noticeably influence the results (with the smallest gap ratio being more than twice the boundary layer thickness in their findings). Little description of the flow behaviour was offered, although they do note that the presence of the wall, results in an asymmetric flow; with the mean velocity profile indicating that the flow in the near wake is larger on the wall side, while the opposite is true at distances greater than 2.5 diameters downstream.

The influence of boundary layer velocity gradients were investigated by Grass et al. (1984) and Taniguchi & Miyakoshi (1990). In considering the flow arrangement for Reynolds numbers between 2000 and 4000, Grass et al. (1984) found that for gap ratios between 2.00 and 0.75, that shedding was very regular; with only a slight downstream shift in the separation point on the side closest to the wall being observed. For gap ratios smaller than 0.50, it was observed that the vortex shedding was more intermittent and less energetic. From the basis of their visualizations they indicate that small detached separation regions form on the solid wall at positions both upstream and downstream for small gap ratios. This was attributed to the presence of adverse pressure gradients on the wall, that cause the wall boundary layer to separate. Grass et al. (1984) also suggested that the downstream separation zone deflects the fluid passing beneath

the cylinder away from the wall to form a free jet, and that it is this action that helps to inhibit the roll-up of vortices on the wall side of the wake. They also observe that the Strouhal number varies with gap ratio, with changes in the order of 25% observed (although it should be noted that the Strouhal number used by Grass et al. (1984) was based on the approach velocity at the cylinder center position, which is influenced by the boundary layer). The gap ratio at which shedding ceases was also found to vary with boundary layer thickness, with weakened shedding still observed at a gap ratio of 0.25 for the case in which the approach flow is uniform, but no shedding noted at a gap ratio of 0.50 when a roughened wall boundary was used (i.e. thicker boundary layer).

This problem was later investigated numerically by Lei et al. (1998), who considered the behaviour of a two dimensional cylinder close to a no-slip wall at a Reynolds number of 1000. They found a considerable weakening in the shedding for gaps less than 0.30, and suggest that the Strouhal number reaches a minimum, as opposed to a maximum or near maximum seen by others, at a gap ratio of 0.50.

Lei et al. (1999) experimentally consider the effect of a plane boundary on the forces and the vortex shedding of a circular cylinder for Reynolds number between 1.30×10^4 and 1.45×10^4 . They find that the manner in which the boundary layer is developed can have a substantial impact on the subsequent lift forces acting upon the cylinder. With regard to the Strouhal number, they measure some change with gap ratio, and note that the boundary layer plays an important role in the observed changes. Contrary to Grass et al. (1984), they claim that the critical gap ratio at which shedding is suppressed decreases as the thickness of the boundary layer increases.

Price et al. (2000) have also considered the same problem but at a Reynolds number of 1200. They find much larger changes in the Strouhal number (of order 40%), while also observing the presence of additional signal frequencies in the wake velocity, especially at small gap ratios. These additional frequencies are attributed to the motion of the boundary layer as it separates from the wall downstream of the cylinder. Price et al. (2000) suggest that the suppression of the Kármán vortex shedding is not likely to be due to the cross annihilation of the vorticity from the wall and the cylinder, as their PIV results suggest that the oppositely signed vorticity does not cancel out.

1.5 Vorticity and the Free Surface

This section briefly touches on some of issues relating to vorticity and its interaction with a free surface. It is intended that the material presented here be treated only as a commentary on some of the basic principles and mechanisms associated with the production and evolution of vorticity and its interaction with a free surface. The reader is recommended to consult Green (1995), Truesdell (1953), Morton (1984) and Rood (1991, 1994*a*, 1994*a*, 1995) for a more detailed discussion.

1.5.1 What is Vorticity?

The vorticity, ω , is a vector quantity which is simply defined as the curl of the velocity field (\mathbf{u}),

$$\omega = \nabla \times \mathbf{u}. \quad (1.1)$$

Equation (1.1) can then be written in Cartesian component form as follows:

$$\omega_x = \frac{\partial w}{\partial y} - \frac{\partial v}{\partial z} \quad (1.2)$$

$$\omega_y = \frac{\partial u}{\partial z} - \frac{\partial w}{\partial x} \quad (1.3)$$

$$\omega_z = \frac{\partial v}{\partial x} - \frac{\partial u}{\partial y} \quad (1.4)$$

and provided that the velocity field has continuous second derivatives these can be combined to yield the following

$$\nabla \cdot \omega = \frac{\partial \omega_x}{\partial x} + \frac{\partial \omega_y}{\partial y} + \frac{\partial \omega_z}{\partial z} = 0. \quad (1.5)$$

This implies that once two components of the vorticity are known, the third can then be calculated. For cases in which the flow field is assumed to be two dimensional (such that the flow is restricted to, for example, the (x,y) plane), then equation (1.4) clearly illustrates that only the z component of vorticity need be considered.

1.5.2 Why Discuss Phenomena in Terms of Vorticity?

One of the major attractions associated with the discussion of phenomena in terms of vorticity is that it is a quantity that is Galilean invariant, which means that irrespective of the reference frame of the observer, the vorticity field will always appear the same.

1.5.3 What is a Free Surface?

In nature, free surfaces represent interfaces between two fluids of differing physical properties, with a common example being the interface between air and water (the word ‘free’ has been used loosely here, with its more appropriate use clarified shortly). The boundary condition that applies at the interface between the two fluids is that the stresses at the interface be in balance. If one fluid is designated the subscript 1 and the other the subscript 2, then this stress condition implies that

$$stress_1 + stress_2 + stress_{surface} = 0. \quad (1.6)$$

The stress components t_i on a surface element with unit normal vector \mathbf{n} may be written as

$$t_i = T_{ij}n_j, \quad (1.7)$$

where T_{ij} are the elements of a stress tensor. For an incompressible Newtonian fluid, T_{ij} is simply

$$T_{ij} = -P\delta_{ij} + \mu \left(\frac{\partial u_j}{\partial x_i} + \frac{\partial u_i}{\partial x_j} \right), \quad (1.8)$$

where P is the pressure, δ_{ij} is the Kronecker delta, μ is the fluid viscosity, u_k is the k^{th} component of \mathbf{u} and x_k is the k^{th} component of \mathbf{x} (the position vector in Cartesian coordinates). Hence the i^{th} component of the stress is

$$stress_i = - \sum_{j=1}^3 P\delta_{ij}n_j + \sum_{j=1}^3 \mu \left(\frac{\partial u_j}{\partial x_i} + \frac{\partial u_i}{\partial x_j} \right) n_j. \quad (1.9)$$

For a surface normal vector oriented like the one in figure (1.2), the stress on the surface $stress_{surface}$ (which is produced by surface tension), has an i^{th} component of

$$(stress_{surface})_i = \sigma \left(\frac{1}{R_1} + \frac{1}{R_2} \right) (-n_i) + (\nabla\sigma)_i, \quad (1.10)$$

where σ is the surface tension and R_1 and R_2 are the radii of curvature of any two mutually orthogonal lines drawn on the surface (Hughes & Brighton (1991)). As in Rood (1995), the terms in $stress_{surface}$ are defined such that the positive stresses in the interface are a surface normal pressure towards the center of curvature and a surface parallel stress in the direction of increasing surface tension.

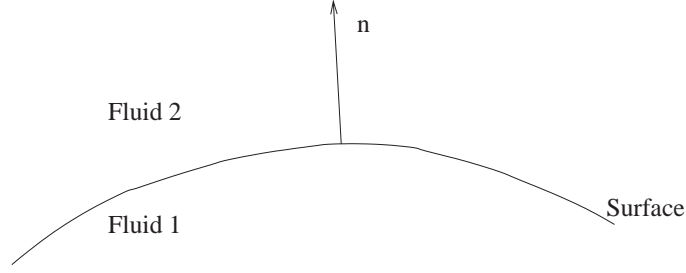


Figure 1.2: Schematic illustrating the interface between $fluid_1$ and $fluid_2$

The stress balance at the surface as given in equation (1.6) yields

$$\begin{aligned}
 & -P_1 \delta_{ij} (-n_j) + \sum_{j=1}^3 \mu_1 \left(\frac{\partial u_j}{\partial x_i} + \frac{\partial u_i}{\partial x_j} \right)_1 (-n_j) - \\
 & P_2 \delta_{ij} (n_j) + \sum_{j=1}^3 \mu_2 \left(\frac{\partial u_j}{\partial x_i} + \frac{\partial u_i}{\partial x_j} \right)_2 (n_j) + \\
 & \sigma \left(\frac{1}{R_1} + \frac{1}{R_2} \right) (-n_i) + (\nabla \sigma)_i = 0,
 \end{aligned} \tag{1.11}$$

where the normal vector is oriented as in figure (1.2).

If it is now assumed that one of the fluids, for example fluid 2, exerts a constant stress normal to the surface, and no stress parallel to the surface, then the surface is said to be ‘free’ (Sarpkaya (1996)). This assumption implies that ρ_1 is substantially greater than ρ_2 , and μ_1 is also significantly larger than μ_2 , such that μ_2 can be considered 0, and that pressure changes in the less dense phase may be ignored (i.e. height changes in the less dense phase will not result in any pressure change at the free surface, hence $p_2 = \text{constant}$). The influence of surface tension is ignored in many theoretical and numerical free surface problems, with this one being no exception. In experiments, surfactant concentrations are often unknown or unreported, and it is often assumed that the free surface is uniformly and repeatedly dirty (Valluri (1996)). More details on the influence of surfactants are discussed later in the section dealing with the interaction of vorticity with a free surface. These assumptions lead to the following free surface boundary conditions in Cartesian coordinates (as stated in Rood (1995))

$$\left(-P + 2\mu \frac{\partial u_{normal}}{\partial x_{normal}} \right)_1 + \text{constant} = 0 \tag{1.12}$$

$$\mu \left(\frac{\partial u_{tangential}}{\partial x_{normal}} + \frac{\partial u_{normal}}{\partial x_{tangential}} \right)_1 = 0. \tag{1.13}$$

In nature, a technical free surface is never observed, but the assumptions made are found to give good approximations to the reported behaviour.

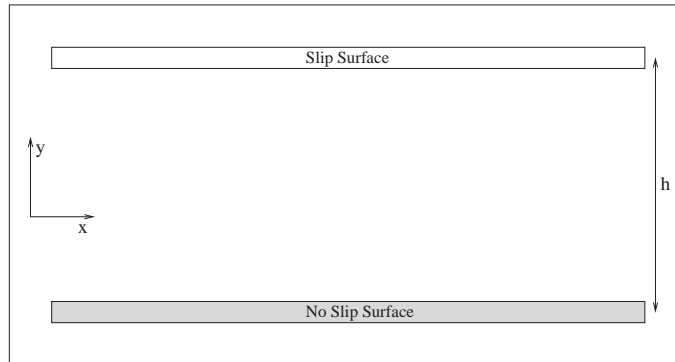


Figure 1.3: Flow schematic for the modified Couette flow problem.

It should be noted at this point that the technical definition of a free surface is equivalent to a zero shear stress boundary condition (free slip boundary) in the absence of surface deformation. This is true for all values of the viscosity (and hence Reynolds number), and it is in no way related to the often made assumption that the viscosity may be ignored at high Reynolds numbers.

Before proceeding to discuss the interaction of vorticity with a free surface, a few issues regarding definitions and the conservation/non-conservation of vorticity will now be considered.

1.5.4 Conservation / Non-Conservation of Vorticity

While equation (1.1) indicates that the components of vorticity are related in the same fashion as the velocity components are in an incompressible fluid, it does not imply that vorticity is conserved. Indeed, it will now be shown that the conservation of vorticity (or lack of it) is dependent upon the boundary conditions.

Morton (1984) discusses in some detail the lack of appropriate boundary conditions for vorticity, however, one may readily show that vorticity is free to vanish from within a computational domain if free slip (zero shear stress) boundary conditions are employed. To illustrate this, consider two dimensional viscous flow between flat plates (in an arrangement similar to Couette flow), but let the problem be modified such that the top boundary is free slip (which is analogous to a non-deformable free surface). This insightful problem is considered by Rood (1994b), and is reproduced here to highlight its message. The problem schematic is shown in figure 1.3, with the assumption that the surfaces extend from $-\infty$ to $+\infty$ in the x direction.

The boundary conditions are $u = u_0$ and $v = 0$ at $y = 0$ and $\frac{\partial u}{\partial y} = 0$ at $y = h$. Due to the periodic nature of the problem, it is clear that u will only be a function of y and t .

Continuity (conservation of mass) dictates that

$$\frac{\partial u}{\partial x} + \frac{\partial v}{\partial y} = 0, \quad (1.14)$$

but since $u = u(y, t)$, continuity tells us that $\frac{\partial v}{\partial y} = 0$ and hence $v = \text{constant} = 0$ everywhere. Thus, the momentum equation (in the absence of an applied pressure gradient) becomes

$$\frac{\partial u}{\partial t} = \nu \frac{\partial^2 u}{\partial y^2}. \quad (1.15)$$

This equation can then be solved analytically using the method of separation of variables, which gives

$$u = u_0 + \sum_{k=0}^{\infty} A_k e^{-\nu t \left(\frac{\pi}{h} \frac{2k-1}{2}\right)^2} \sin\left(\left(\frac{\pi}{h} \frac{2k-1}{2}\right)y\right). \quad (1.16)$$

Evolution of the solution forward in time will yield the familiar Couette flow results for small times, but the eventual solution as $t \rightarrow \infty$ will be one in which the flow throughout the entire domain has a velocity equal to that of the bottom driving wall (u_0).

Hence the vorticity that was present initially will have simply passed out of the domain through the top boundary. Morton (1984), prefers to envisage free slip boundaries as no-slip ones in which there is zero viscosity or as ones in which the vorticity is contained within an infinitely thin layer at the boundary. This assumption is often made for flows at very high Reynolds numbers, and hence under these circumstances the vorticity is still present at the wall, but due to the restriction on the viscosity (i.e. assumed to be zero) it is unable to diffuse away from it.

A non-deformable free surface on the other hand is essentially a free slip boundary without the assumption that the Reynolds number is very high. Hence any vorticity that would be stored in the boundary should be free to diffuse from it, as the free-slip assumption holds at any Reynolds number. What happens to this vorticity is hence a point of contention, with some, such as Lundgren & Koumoutsakos (1999) indicating that the lost vorticity is stored in the surface. However such vorticity cannot be measured directly.

It is thus apparent that for any experimental or numerical measurements in which a technical free surface or free-slip boundary is present, there is no formal requirement that the vorticity be conserved. Rood (1995) discusses the erroneous but often ascribed notion that the vorticity is conserved in much the same manner as the momentum is. He indicates that while the conservation law for momentum is a physical rule which is obtained by the application of Newton's third

law, for vorticity there is no ‘third law of motion’, and hence no requirement that it should be conserved in the same fashion that momentum must be.

If vorticity is not conserved globally, then circulation (which is the integral of the vorticity over a volume) will also not be conserved. To illustrate this, a relationship for the circulation is derived which includes the contribution of the viscous term (it should be noted that this approach largely follows that taken by Green (1995)).

First consider the momentum equation for a Newtonian fluid,

$$\frac{D\mathbf{u}}{Dt} = \frac{-\nabla P}{\rho} + \nabla\phi + \nu\nabla^2\mathbf{u}, \quad (1.17)$$

where \mathbf{u} is the velocity vector, P is the pressure, ν is the kinematic viscosity and $\nabla\phi$ is the body force vector.

Now consider the time rate of change of the circulation about a material loop in the fluid. The circulation is simply given by

$$\Gamma = \oint_c \mathbf{u} \cdot d\mathbf{l}, \quad (1.18)$$

and its time rate of change is

$$\frac{D\Gamma}{Dt} = \frac{D}{Dt} \oint_c \mathbf{u} \cdot d\mathbf{l} = \oint_c \frac{D\mathbf{u}}{Dt} \cdot d\mathbf{l} + \oint_c \mathbf{u} \cdot \frac{D(d\mathbf{l})}{Dt}. \quad (1.19)$$

According to Green (1995), $\frac{D(d\mathbf{l})}{Dt} = d\mathbf{u}$.

Hence equation (1.19) then becomes

$$\frac{D\Gamma}{Dt} = \oint_c \frac{-\nabla P}{\rho} \cdot d\mathbf{l} + \oint_c \nabla\phi \cdot d\mathbf{l} + \oint_c \nu\nabla^2\mathbf{u} \cdot d\mathbf{l} + \oint_c \mathbf{u} \cdot d\mathbf{u}, \quad (1.20)$$

and by using the identities $\nabla P \cdot d\mathbf{l} = dP$, $\nabla\phi \cdot d\mathbf{l} = d\phi$ and $\mathbf{u} \cdot d\mathbf{u} = \frac{1}{2}d(\mathbf{u} \cdot \mathbf{u})$ equation (1.20) becomes

$$\frac{D\Gamma}{Dt} = \oint_c \frac{-dP}{\rho} + \oint_c d\phi + \oint_c \nu\nabla^2\mathbf{u} \cdot d\mathbf{l} + \frac{1}{2} \oint_c d(\mathbf{u} \cdot \mathbf{u}). \quad (1.21)$$

As $d\phi$ and $d(\mathbf{u} \cdot \mathbf{u})$ are scalars, the terms containing their integral around a closed loop are zero. If one assumes P is a function of ρ only, then the term containing the pressure will also involve the integration of a continuous scalar around the loop, which will yield zero (incompressible fluids and gasses may be assumed to possess a polytropic equation of state which satisfies this constraint). This finally results in the following relation

$$\frac{D\Gamma}{Dt} = \oint_c \nu\nabla^2\mathbf{u} \cdot d\mathbf{l}. \quad (1.22)$$

For an infinite fluid, the loop can be chosen such that $\nabla^2 \mathbf{u} \approx 0$ on the boundaries, and hence

$$\frac{D\Gamma}{Dt} = 0, \tag{1.23}$$

which is the standard circulation theorem. However, for cases in which one part of the loop cannot be chosen arbitrarily (i.e. cases in which a surface provides a boundary to the fluid), then the influence of the $\nabla^2 \mathbf{u}$ term is of importance.

This is highlighted by considering the application of this circulation theorem to two simple cases involving the modified Couette flow; with the first having a technical free surface and the second consisting of two fluids of differing densities and viscosities.

Problem One

This simply involves the application of the circulation theorem to the modified Couette problem which was reproduced from Rood (1994b). Without loss of generality, consider a rectangular loop c which is of length L in the x direction. When the lower plate is first set into motion, the circulation is simply uL , however as $t \rightarrow \infty$, it tends towards zero. Hence while the circulation started at a finite value, it ended at zero value, thus implying that circulation is not conserved when one has a technical free surface.

Problem Two

Now consider the same problem as the one above, but this time replace the free (slip) surface with an interface between two immiscible fluids. The aim of this problem will be to show that there is a circulation loss in lower fluid. In the limit as the top fluid approaches a vacuum (i.e. the density and the viscosity of the top fluid approach zero), the result should approach that obtained in problem one. When the lower plate is first started, the circulation in the lower fluid is a maximum and is zero in the upper fluid. At some later time t , in which some of the vorticity present at the lower wall has diffused upward toward the interface between the fluids, it is expected that some or perhaps all of the vorticity will diffuse across the surface. To measure what happens to the circulation, only the loop around which the circulation will be calculated needs to be considered. From equation (1.22), it is clear that rate of circulation change in fluid one will be balanced by the change in fluid two, if $\nu \nabla^2 \mathbf{u}$ on one side of the interface is equal to $\nu \nabla^2 \mathbf{u}$ on the other side. For this simple problem this is obviously the case, as the combination of the momentum equations which indicates that $\frac{\partial u}{\partial t} = \nu \frac{\partial^2 u}{\partial y^2}$ throughout the flow, and the boundary condition that the velocity be continuous at the interface for all times, simplifying to ensure that equation (1.22) is satisfied.

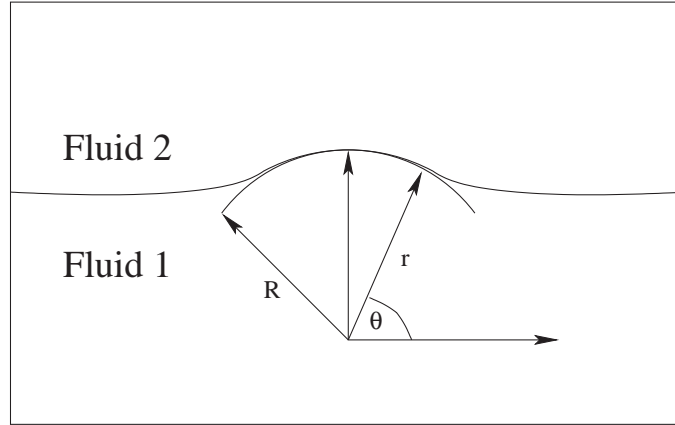


Figure 1.4: Schematic showing a curved surface.

This result implies that there is no requirement for the vorticity or circulation in one fluid (e.g. denser one) to remain conserved. This highlights the difference between the conservation properties of vorticity and momentum, which is emphasized by Rood (1994*b*). It is clearly apparent in the problem considered above that as $t \rightarrow \infty$, the bulk of the momentum will reside in the denser fluid while the bulk of the vorticity will reside in the lighter fluid (with the limiting case of a technical free surface having all of the momentum in the denser fluid, and perhaps all of the vorticity in the lighter fluid (vacuum) or maybe even stored at the interface). Hence the presence of a technical free surface or a numerical free-slip boundary condition implies that vorticity will not be conserved.

1.5.5 Free Surface Vorticity

This section describes the presence of vorticity at a free surface. Lugt (1987), and Rood (1995) both discuss the presence of surface vorticity, which arises as a result of the free tangential stress boundary condition. The derivation of the steady surface vorticity (as discussed by Lugt (1987)) highlights the role that the free tangential stress boundary condition plays, and is briefly discussed below.

Consider two-dimensional flow involving a free surface with a shape shown in figure (1.4).

The vorticity, ω , in cylindrical polar coordinates is given as:

$$\omega = \frac{\partial u_\theta}{\partial r} + \frac{u_\theta}{r} - \frac{1}{r} \frac{\partial u_r}{\partial \theta}, \quad (1.24)$$

where u_θ is the azimuthal velocity, and u_r is the radial velocity. The boundary condition at the

interface between the two fluids (fluid 1 and fluid 2) is that the stresses at the interface must be in balance. This gives at $r = R$ the following set of conditions (Lugt (1987)):

$$(u_r)_1 = (u_r)_2 = 0 \quad (1.25)$$

$$(u_\theta)_1 = (u_\theta)_2 \quad (1.26)$$

$$\mu_1 \left(\frac{\partial u_\theta}{\partial r} - \frac{u_\theta}{r} \right)_1 = \mu_2 \left(\frac{\partial u_\theta}{\partial r} - \frac{u_\theta}{r} \right)_2 \quad (1.27)$$

$$\left(P - 2\mu \frac{\partial u_r}{\partial r} \right)_1 = \left(P - 2\mu \frac{\partial u_r}{\partial r} \right)_2 + \frac{\sigma}{r}, \quad (1.28)$$

where the subscript denotes the fluid and σ is the coefficient of surface tension. A free surface is defined as one in which stresses in one fluid are assumed zero (in this case it is assumed that the stresses in fluid 2 are zero), thus giving at $r = R$:

$$(u_r)_1 = 0 \quad (1.29)$$

$$\mu_1 \left(\frac{\partial u_\theta}{\partial r} - \frac{u_\theta}{r} \right)_1 = 0 \quad (1.30)$$

$$\left(P - 2\mu \frac{\partial u_r}{\partial r} \right)_1 = P_2 + \frac{\sigma}{r}. \quad (1.31)$$

At the free surface $r = R$, equation (1.24) becomes

$$\omega = \frac{\partial u_\theta}{\partial r} + \frac{u_\theta}{r}, \quad (1.32)$$

and when combined with equation (1.30) yields

$$\omega = \frac{2}{R} u_\theta = 2\kappa u_\theta, \quad (1.33)$$

where $\kappa = \frac{1}{R}$ is the curvature. This is the well known expression for the vorticity at a steady curved surface.

For a surface whose position changes with time, Rood (1994a) gives the rate of change of vorticity at the free surface as

$$\begin{aligned} \nu \int_{fs} \mathbf{n} \cdot \nabla \omega ds &= \nu \int_{fs} \nabla \omega \cdot \mathbf{n} ds + \\ \int_{fs} \mathbf{n} \times \left(\frac{\partial \mathbf{u}}{\partial t} + \mathbf{u} \cdot \nabla \mathbf{u} + \frac{\nabla P}{\rho} - \mathbf{g} \right) ds, \end{aligned} \quad (1.34)$$

where $\int_{f_s} ds$ represents integration along the free surface, \mathbf{n} is the unit normal to the free surface and the other quantities are as previously specified. Equation (1.34) relates the flux of vorticity through the free surface to the tangential component of the acceleration of the free surface fluid. Hence it is clearly apparent that the flux of vorticity through the free surface will vary with time for unsteady flows.

Before continuing, it is perhaps best to restate the key points noted by Rood (1994*b*) with regard to the physics associated with free-surface vorticity.

1. Vorticity appears spontaneously on free-surface boundaries. The appearance is related to surface parallel velocity of the free-surface fluid and surface curvature.
2. The flux of vorticity through a free surface depends on the viscous acceleration of the free-surface fluid in the direction tangential to the free surface.
3. The vorticity flux can be equated to the sum of the inertial, pressure, and gravitational accelerations, tangential to the free surface.
4. Vorticity is not conserved. Hence it is acceptable for vorticity to vanish entirely from the flow.
5. In the presence of a free surface, initially irrotational flow can become rotational and rotational flow can become irrotational without external stress on the fluid.
6. Vortex lines initially connected in the flow interior, can break at the free surface.
7. Vortex interactions with a deformable free surface are not generally represented by image vortex interactions.

1.5.6 Interaction of Vorticity with a Free Surface

Now that some of the issues relating separately to free surfaces and vorticity have been discussed, previous studies involving the interaction of vorticity with a free surface may be considered. It should be noted at this point that some of the following investigations have assumed that the flow could be treated as being inviscid. Such an assumption will have a significant influence near the free surface, with no secondary vorticity being produced as a result of the induced curvature. This will tend to limit their usefulness to situations in which the surface curvature is neither sharp nor substantial. In the following discussion all investigations are assumed to include viscosity unless stated otherwise.

Tryggvason (1988) numerically examines shear flow beneath a free surface. He assumes that the flow is two dimensional and inviscid, and suggest that depending upon the depth and strength of the vortex sheet, that varying levels of surface deformation can be observed. For some cases, wave breaking is noted and the shape of the surface profile for others suggests that some form of entrainment is likely to occur. Yu & Tryggvason (1990) also investigate the free surface signature of unsteady two-dimensional vortex flows using a numerical approach. Their examination is based on the assumption that the fluid may be treated as inviscid and that for most cases surface tension may be ignored. However, they do consider the effect of surface tension in two cases, and conclude that its main effect is that it reduces the surface deformation in regions of high surface curvature. Their major finding is that the dominant parameter governing the surface deformation is the Froude number, and they claim that the surface/vortex interaction can be classified as either high or low Froude number motion. At small Froude numbers the vortices interact with the free surface as if it were a rigid wall, with minimal surface deformation being detected. At larger Froude numbers however, the vortices have sufficient strength to cause marked surface deformation. Yu & Tryggvason (1990) also note that the time scale over which a vortex develops has an influence on the resultant surface deformation.

These observations are largely corroborated by the findings of Ohring & Lugt (1991), and Lugt & Ohring (1992), who also numerically investigate the interaction of a two-dimensional vortex pair with a free surface, however, their investigation includes both viscous effects and the influence of surface tension. For intermediate Froude numbers and low Reynolds numbers, the authors indicate that the vortices were observed to rebound away from the free surface, with the degree of rebounding diminishing with increasing Reynolds number. The inclusion of viscosity gives a much clearer picture of what is happening near the free surface, with significant levels of surface vorticity being generated in the regions of high curvature. The presence of this secondary vorticity is found to have a pronounced effect on the subsequent evolution of the primary vortex, such that the shedding of vorticity from the region of significant surface curvature results in a considerable weakening of the primary vortex after the two interact.

The influence of surface tension is further investigated numerically by Tryggvason et al. (1991), who considers spatial variations in the surface tension. In these instances, the subsequent behaviour of the colliding vortices changes considerably, with the non-uniform surface tension altering the vorticity generated at the free surface.

Sarpkaya (1996) reports on the finding of Wang & Leighton (1991), who indicate that the presence of surfactants can alter the surface boundary condition, so that it lies somewhere

between no slip and free slip. Furthermore, Tryggvason et al. (1991) notes that the surface motion is often sufficient to produce an uneven contaminant distribution, which in turn gives rise to surface shear. Such gradients in the surface tension are often sufficient to alter the evolutionary behaviour of the vorticity as it interacts with a free surface. This is described to some extent by Anthony et al. (1991).

1.6 Flow Past a Body Close to a Free Surface

This section will now discuss some of the previous work pertaining to flow past a cylinder close to a free surface. While Lamb (1924) gives a potential flow solution for this problem, the absence of viscosity is likely to alter the behaviour in a significant manner. The results of Ohring & Lugt (1991) and Lugt & Ohring (1992) illustrate the impact that surface generated vorticity has on evolutionary characteristics of the vorticity field. Hence the absence of a wake in the potential solution, which otherwise indicates that a train of waves of wavelength $\frac{2\pi U^2}{g}$ form downstream of the cylinder (here U is the free stream velocity and g is the gravitational acceleration), is unlikely to give a true indication of the actual behaviour.

It is perhaps best to begin the discussion that details the findings of previous investigations, by considering the work of Valluri (1996) who examined flow past a flat circular disk (placed normal to the flow) close to a free surface. While this geometry is obviously three-dimensional, it is expected that it may share some common features with flow past a cylinder. Valluri (1996) notes that the wake can exhibit two basic modes with differing stabilities, with some degree of hysteresis also observed. The first mode involves the attachment of the fluid passing over the disk to the free surface, while the second involves this fluid separating from the free surface (with the flow associated with the second mode being strongly recirculatory). Valluri (1996) claims that the first mode (mode 1) displays some time-dependent behaviour, while the second mode (mode 2) is largely steady. He also finds that the transitions between the two states are found to be hysteretic, such that the depth at which the flow changes from mode-1 to mode-2 as the disk is raised towards the free surface, is different to the depth at which the flow changes back from mode-2 to mode-1 as it is moved away from the surface.

Valluri's (1996) measurements indicate that the drag initially increases as the disk is moved toward the surface, before reaching a maximum and then decreasing again, in much the same manner that the drag on the cylinder close to a no-slip wall varied in the experiments of Roshko et al. (1975). Valluri's (1996) comparison of the drag results for the disk placed adjacent to

both a plane no-slip wall and a free surface, indicate that similar trends are observed. However, the drag on the disk near a free surface is considerably larger over most of the range in which deviations away from the fully submerged case are noted. Indeed, Valluri (1996) claims that the magnitude of the drag increase experienced near a no-slip surface is about 25% of that experienced near the free surface. The depth at which the peak in the drag is noted also appears to have shifted slightly, with the peak for the free-surface case occurring at smaller submergence depths (gap ratios).

With regard to the surface profiles and the general behaviour of the wake, Valluri (1996) indicates that once the fluid from above the disk separates from the free surface, further alteration of the depth was found to change the angle that the separated fluid makes with the free surface.

Flow past a circular cylinder beneath a free surface is investigated by Miyata et al. (1990) with their experimental and numerical examination conducted at a Reynolds number of 4.96×10^4 and at a Froude number (based on cylinder diameter) of approximately 0.24. They note a number of step changes in the flow behaviour as the submergence depth (gap ratio) of the cylinder is reduced from a value of 0.35. In particular, a sharp reduction in drag and sharp increase in the Strouhal number was observed. The large jump in the Strouhal number occurs in conjunction with a notable weakening in the intensity of the lift spectra (spectra of the lift forces), along with the occurrence of a broader range of frequencies, and they suggest that the shedding at the smaller gap ratio is less remarkable (which is assumed to mean weaker). While their visualization at this gap ratio suggests that the flow changes with time, there is no explicit evidence that shedding was observed. With regard to the forces acting upon the cylinder, Miyata et al. (1990) found an increase in the lift with decreasing submergence depth. They suggest however, that the drag is predominantly bimodal, in that it attains an almost steady value at larger gap ratios and another value at smaller gap ratios. The variation of the lift has much in common with the observations of Roshko et al. (1975), with the same trend noted. The trend for the drag on the other hand differs somewhat, with Roshko et al. (1975) observing a continuous reduction in drag with decreasing gap ratio, while Miyata et al. (1990) note a step-like reduction in the drag as the gap ratio is reduced below 0.35.

The flow behaviour of a cylinder close to a free surface at a Froude number of 0.60 and a gap ratio of 0.45 was considered by Sheridan et al. (1995), who indicate that at a this fixed point in parameter space, two admissible wake states were observed. Each state was found to possess limited stability such that transformations from one state to the other occurred in a time-dependent manner (with this behaviour labelled as being metastable). The two states

bear considerable resemblance to those observed by Valluri (1996), with the fluid passing over the cylinder remaining attached to the free surface in one state and separating from it in the other. No clear periodicity in the switching between states was measured, with Sheridan et al. (1995) indicating that transformations between the two states occur spontaneously at a non-dimensionalized frequency of the order of 10^{-3} . Hysteretic behaviour was also observed by Sheridan et al. (1995), with the artificial piercing of the free surface being sufficient to induce a state change. The deflection of the fluid from above the cylinder, which in the forgoing will often be referred to as a ‘jet’, appears to share common flow features with those observed by both Valluri (1996) and Grass et al. (1984). In each investigation a jet-like structure was observed at small gap ratios. Such observations tend to invalidate the idea of a resonance condition for wave generation which is mentioned in Sheridan et al. (1995). The observation of a free-jet by Grass et al. (1984) suggests that the reported behaviour is more likely due to geometrical constraints, as opposed to being purely a function of the free surface.

A broader spectrum of the parameter space (i.e. gap ratio and Froude number) is mapped out by Sheridan et al. (1997), with a wide variety of wake behaviour noted. The fluid from above the cylinder (i.e., the ‘free jet’) was observed to exhibit a number of states which range from: attachment to the free surface, separation from the free surface such that the ‘jet’ occupies a region in between the free surface and the cylinder, and attachment to the rear of the cylinder. The metastable characteristics observed by Sheridan et al. (1995) are also observed at a number of other gap ratios and Froude numbers.

Both Sheridan et al. (1995) and Sheridan et al. (1997) primarily focus upon mapping out the the wake states, and as a consequence they provide only limited details with regard to the shedding frequency and no details with respect to the forces acting on the cylinder. As a result comparison is limited to being almost purely pictorial (i.e. based on flow visualization).

This problem is also investigated by Warburton & Karniadakis (1997) at a Reynolds number of 100 using a two-dimensional numerical model. They suggest from the basis of their findings that the flow features observed by Sheridan et al. (1997) are largely two dimensional, while also giving some detail with regard to the time dependent forces acting upon the cylinder.

Hoyt & Sellin (2000) confirm some of the findings of Sheridan et al. (1997), and provide a few limiting details about the flows time dependence. Their major finding is that the Kármán vortex shedding is observed at some gap ratios, and that the flow field thus varies in a time-dependent manner.

1.7 Scope of the Present Investigation

As the prior discussion indicates, flow past a cylinder close to a free surface is likely to involve the amalgamation of a considerable number of complex physical phenomena. It is hoped that the behaviour observed by others can be elucidated by the findings presented here.

The major aims of the current investigation are as follows:

1. To confirm that the wake behaviour observed by Miyata et al. (1990), Sheridan et al. (1995), Sheridan et al. (1997) and Hoyt & Sellin (2000) is largely two dimensional as suggested by Sheridan et al. (1997).
2. To map out a larger region of parameter space and to examine the forces and shedding frequencies associated with flow past a cylinder close to a free surface, which to the author's knowledge is largely uncharted.
3. To provide a mechanism that describes the observed transformations in the wake, such that it may be eventually possible to predict, and hence modify, the wake behaviour. It is hoped that the identification of this mechanism may also shed some light on the problem of flow past a cylinder close to an adjacent no-slip boundary.
4. And finally, to infer some details with regard to the nature of the instability associated with the wake over a range in parameter space.

It is anticipated that this problem will be governed by two primary mechanisms: with the first being the supply of fluid into the near wake and the second involving the degree by which the wake is skewed from being parallel.

This thesis is organized as follows: Chapter 2 details the numerical method and its validation while also providing some discussion on the post processing of data, Chapters 3, 4 and 5 then consider the flow at low, intermediate and large Froude numbers respectively, with chapter 6 containing some concluding remarks and suggestions for future work.

Chapter 2

Numerical Method, Validation, Problem Setup and Post Processing

2.1 Foreword

Initially I had hoped to investigate the problem of flow past a cylinder close to a free surface with a numerical technique called Smooth Particle Hydrodynamics (SPH). This technique, which has its origins in astrophysics, is Lagrangian and as a consequence no grid is required. In the past it has been used to study the collapse of gas clouds and a review of SPH can be found Monaghan (1992). It has only relatively recently been applied to engineering type flows (i.e. not astrophysical) with Monaghan (1994), Takeda et al. (1994), Thompson et al. (1994), Reichl et al. (1997*a*), Reichl et al. (1997*b*), Reichl et al. (1998*a*) and Reichl et al. (1998*b*) all considering near incompressible flows with SPH. After spending approximately 18 to 24 months writing and developing an SPH code, it became apparent that this was not an appropriate technique for the flow problem being considered here. One of its major drawbacks was the difficulty in using variable resolution in the near incompressible limit, which meant that in order to resolve the boundary layer, one had to use fine resolution throughout the entire domain. Another drawback was that the SPH formulation used for free surfaces (see Monaghan (1992) for a discussion of the different formulations) had difficulty handling high shear, with the particles making up the fluid tending to move away from one another in these regions.

It was at this point that an alternative method, the Volume Of Fluid (VOF) method (as contained within the commercial computational fluid dynamics software Fluent 5) was employed.

2.2 Free-Surface Flows

Free surface flows occur in a wide variety of situations in both industry and the environment. However, due to the difficulties associated with the implementation of boundary conditions on a surface whose position is constantly changing, such flows often require special techniques to be modelled numerically. Tsai & Yue (1996), and Yeung (1982) consider some of many techniques which have been employed to model free surface behaviour. This chapter is split into three parts, the first part deals with the numerical method, the second part with its validation, and the third part with the problem setup and the post processing of data.

2.3 Numerical Method

To the author's knowledge, little research has been undertaken with regard to flow past a cylinder close to a free surface and the work that has been done has been predominantly experimental. It is thus of great importance that any numerical investigation must show that it can adequately model similar problems, and in particular problems containing the same underlying physics and requiring similar resolution. The Reynolds number for the majority of the cases considered within this study is 180 (unless otherwise stated), and the flow field is assumed to be two dimensional. These assumptions are entirely consistent for a fully submerged cylinder, as the flow field is two dimensional for Reynolds numbers below approximately 180.

The numerical experiments in the current investigation were performed using the commercial computational fluid dynamics software Fluent 5, which utilizes a finite-volume approach to numerically solve the Navier-Stokes equations. This software has a wide range of models available to simulate various physical phenomena, such as combustion, solidification of materials, porous flows and free surface flows. As a consequence of this versatility it is not optimized for any particular flow and tended to require considerable amounts of CPU time to yield solutions.

A brief commentary on the solution approach will now be presented along with discretization and accuracy tests. The specifics regarding the Volume Of Fluid (VOF) scheme and the interface tracking will then be discussed. The details of the technique used here are briefly described below, but the reader is recommended to consider Versteeg & Malalasekera (1995) for an excellent discussion on the finite-volume method.

The fluid studied in this investigation is assumed to be incompressible and Newtonian (i.e. it cannot be compressed, and the viscous stresses are assumed to be proportional to the rate of

deformation), and as such the governing equations are:

$$\rho \frac{\partial \mathbf{u}}{\partial t} + \rho(\mathbf{u} \cdot \nabla)\mathbf{u} = -\nabla P + \mu \nabla^2 \mathbf{u} + \rho \mathbf{g}, \quad (2.1)$$

subject to the constraint,

$$\nabla \cdot \mathbf{u} = 0. \quad (2.2)$$

Where ρ is the fluid density, \mathbf{u} is the velocity vector, P is the pressure, μ is the dynamic viscosity, and g is the body force (or gravity) vector.

Equation (2.1) is simply the Navier-Stokes equation (momentum equation for a Newtonian fluid), and equation (2.2) is simply the continuity equation (i.e. the mass conservation equation for an incompressible fluid).

The governing equations (equations (2.1)) and (2.2) have two outstanding features which make them non-trivial to solve, the first is their non-linearity, while the second is the lack of an equation for pressure. This problem is overcome in Fluent by the use of an iterative solution strategy which is similar to the SIMPLE (Semi-Implicit Method for Pressure-Linked Equations) algorithm of Pantankar & Spalding (1972). The SIMPLE algorithm is basically a guess and correct procedure in which the pressure is calculated and the velocities updated in an iterative fashion until continuity is satisfied. In the current investigation a variant of the SIMPLE algorithm is used. The actual method adopted is the PISO (Pressure Implicit with Splitting of Operators) algorithm of Issa (1986), which is similar to SIMPLE, although it uses an additional correction step which tends to speed up convergence.

The finite-volume technique used essentially involves converting the governing equations into algebraic expressions which can then be solved numerically. This conversion is achieved by integrating the governing equations over each control volume (cell), with this integration then yielding the discretized equations which conserve each quantity on a control volume basis. As Versteeg & Malalasekera (1995) show, the general transport equations for any quantity ϕ (where ϕ can be u , v , or any other scalar quantity such as the volume fraction) is:

$$\frac{\partial(\rho\phi)}{\partial t} + \nabla \cdot (\rho\phi\mathbf{u}) = \nabla \cdot (\Gamma_d \nabla \phi) + S_\phi, \quad (2.3)$$

where Γ_d is the diffusion coefficient (which is simply μ for the momentum equations), and S_ϕ is the source term (which for the momentum equations are the terms containing the pressure gradients and the body forces).

The general transport equation (2.3) can be integrated over each control volume to yield the following:

$$\int_{CV} \frac{\partial(\rho\phi)}{\partial t} dV + \int_{CV} \nabla(\rho\phi\mathbf{u})dV = \int_{CV} \nabla(\Gamma_d\nabla\phi)dV + \int_{CV} S_\phi dV, \quad (2.4)$$

where $\int_{CV} dV$ signifies integration over a control volume.

Gauss' divergence theorem can then be applied to convert to convert the second and third terms into integrals over the surface of the volume, with the result being

$$\frac{\partial}{\partial t} \int_{CV} (\rho\phi)dV + \int_A \mathbf{n} \cdot (\rho\phi\mathbf{u})dA = \int_A \mathbf{n} \cdot (\Gamma_d\nabla\phi)dA + \int_{CV} S_\phi dV, \quad (2.5)$$

where \int_A signifies integration over the surface of the control volume, and it should be noted that the order of the differentiation and integration has been swapped in the first term. Equation (2.5) then states that: the rate of increase in ϕ + the net rate of decrease in ϕ due to convection across the boundaries = the rate of increase in ϕ due to diffusion across the boundaries + the net rate of creation of ϕ (Versteeg & Malalasekera (1995)).

Hence for a two-dimensional control volume with center (x,y) (as shown in figure (2.1)), the rate of increase in ϕ will depend upon the source, as well as the convective and diffusive fluxes across the north, south, east and west boundaries. This balance then yields an algebraic expression for

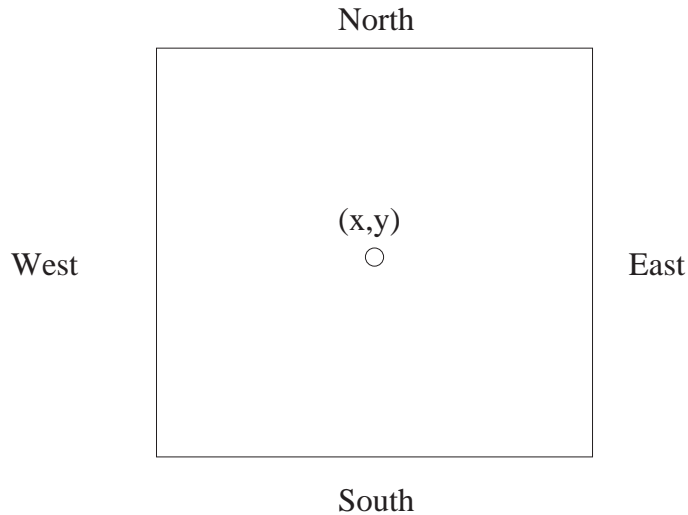


Figure 2.1: Schematic showing a two dimensional control volume.

the changes in the quantity ϕ , with the form of the algebraic expression then determined by the discretization scheme adopted.

In Fluent all quantities are stored at the cell centers, however as the finite-volume scheme requires values on cell faces, interpolation must be used.

The current investigation uses a segregated or segmented solver. In this approach the governing momentum equations are solved sequentially (i.e. uncoupled from one another). However, as the governing equations are non-linear and interdependent, several sweeps or iterations through the solution procedure need to be undertaken for a converged solution to be obtained. The solution procedure can be described in the form of an algorithm, which is basically as follows:

1. Update fluid properties based on the current solution.
2. Solve the momentum equations for u and then v using the current values for the pressure and face-mass flux, to get an estimate of the velocity field.
3. As the velocity estimates from the previous step will not generally satisfy continuity locally, a ‘Poisson-type’ equation is then constructed for the pressure correction from both the continuity equation and the linearized momentum equations. This pressure correction equation is then iteratively solved, and the pressure and velocity is updated.
4. Update flow scalars (which for the current case includes the volume fraction).
5. Check for convergence.

These 5 steps are then repeated until a predefined convergence criteria is satisfied.

As the numerical technique just described iteratively solves for the flow variables, one must assign a criteria, which is commonly referred to as a convergence criteria, at which point the iterative process stops. Such a criteria effectively determines how close the numerical solution approaches the imposed analytic constraint (i.e. the true solution of the discretized conservation equations). At each point, the difference between the numerical solution and the solution of the discretized equations, is referred to as a residual. The sum of these residuals over all the cells in the entire domain is defined here to be the global residual, and its value was used to determine when to cease iterating. The actual values used for the residuals are discussed shortly in section (2.4.6)

2.3.1 Spatial Discretization

The terms in the momentum equations which contain spatial gradients were discretized using the Quadratic Upstream Interpolation for Convective Kinetics (QUICK) scheme of Leonard (1979). The QUICK scheme which is discussed by Versteeg & Malalasekera (1995), and by Fletcher (1991), is a weighted combination of both the standard second-order upwind scheme

and the central-difference scheme (both of which are second order accurate and are described in Fletcher (1991)). This approach which is $\frac{1}{8}$ central-difference and $\frac{7}{8}$ second-order upwind, generally produces results which are more accurate than either the standard central-difference or second-order upwind schemes, as the weighted combination minimizes the truncation error. For non uniform meshes, QUICK will generally yield results which are some where in between second and third order accurate.

2.3.2 Temporal Discretization

Temporal discretization is achieved by the use of the standard implicit backward difference (or backward Euler) scheme as discussed in Smith (1985), and Chapra & Canale (1991), which is unconditionally stable in the Lax-Richtmyer sense. It produces results which are first-order accurate in time (it should be noted that this was the only time stepping scheme available within Fluent for modelling free surface flows when using VOF).

2.3.3 Spatial and Temporal Accuracy Tests

The spatial accuracy was tested by considering Poiseuille flow (i.e. flow between two flat plates), which has an analytic solution. The steady-state velocity profile obtained for a series of grids of differing resolution was then compared with the analytical result. Figure (2.2) shows a comparison, while figure (2.3) shows the variation of the logarithm of the L2 norm (i.e. the square root of the average of the square of the differences) with the logarithm of Δy . The gradient of the line in figure (2.3) indicates that the spatial discretization has an accuracy of order 2.55.

To test the temporal accuracy, Couette Flow (i.e. flow between two flat plates in which the bottom plate is impulsively started) was examined with the analytical and numerical velocity profiles compared at the time $t = 1.00$. Figure (2.4) shows a comparison, while figure (2.5) shows the variation of the logarithm of the L2 norm with the logarithm of the time-step. It should be noted that the result for the L2 norm at a time step of $dt = 0.001$ was then subtracted from the other results, so as to remove the error associated with the spatial discretization. Figure 2.5 indicates that the scheme has an accuracy of order 1.025 in time.

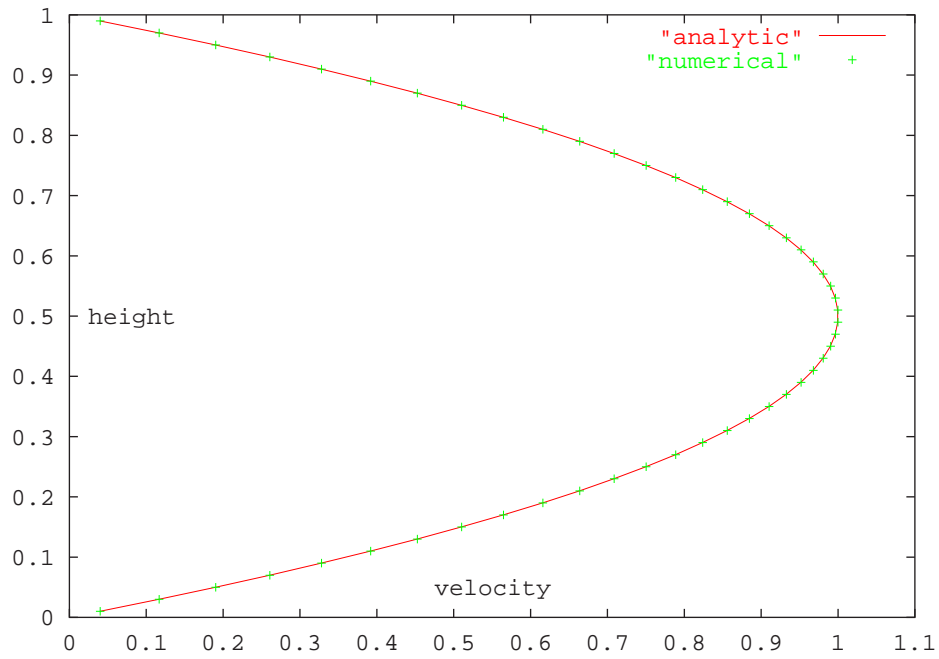


Figure 2.2: Plot showing the comparison between the analytical and numerical results for Poiseuille flow, for a grid with $\Delta y = 0.02$.

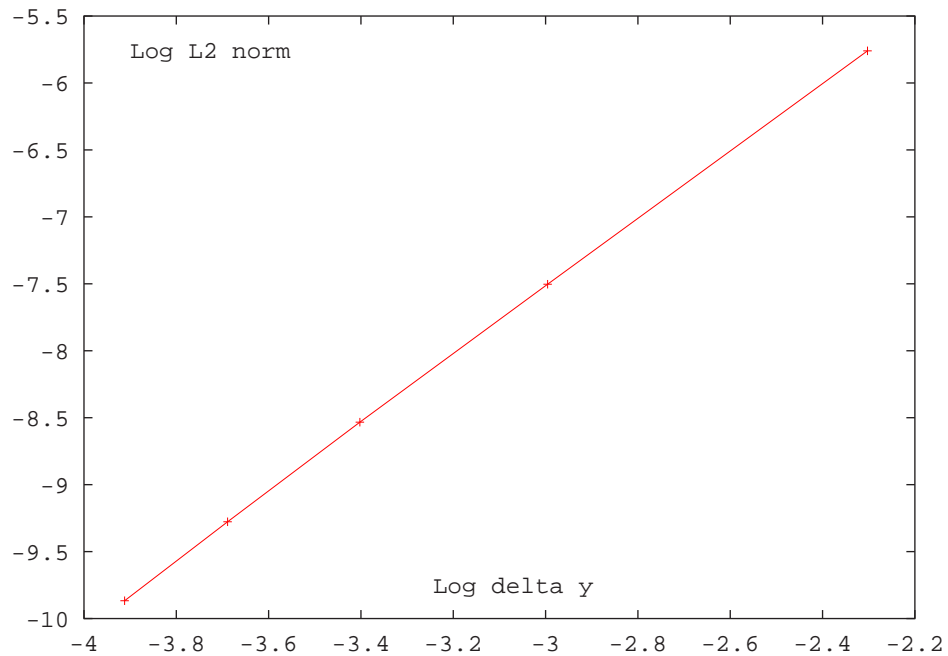


Figure 2.3: Plot showing the variation of the logarithm of the L2 norm with the logarithm of Δy for Poiseuille flow.

2.3.4 Modelling the Free Surface

The free surface, or more appropriately the fluid-fluid interface, was modelled using the volume-of-fluid method as incorporated within Fluent. The variant of the volume-of-fluid method used

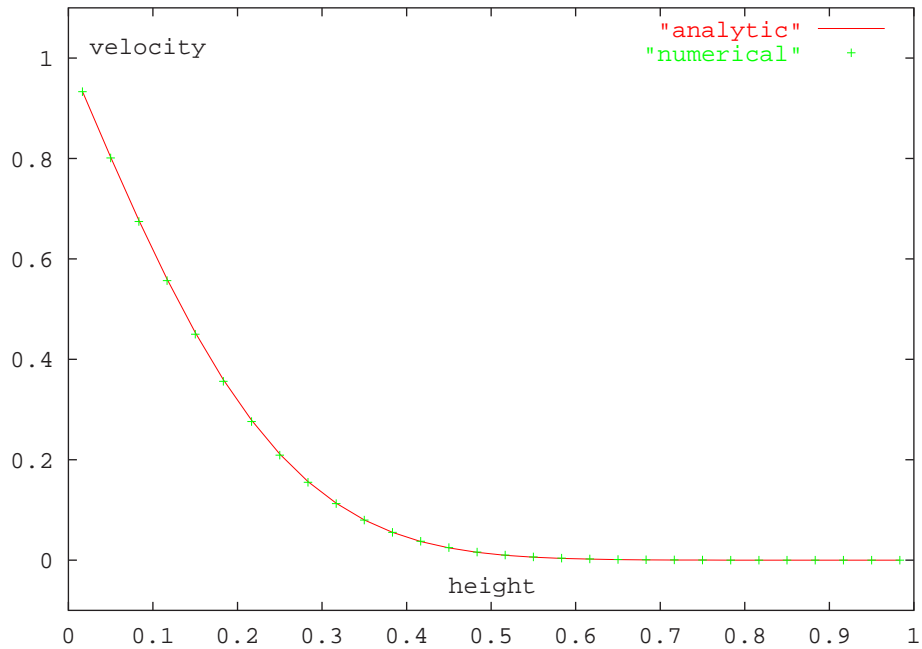


Figure 2.4: Plot showing the comparison between the analytical and numerical results for Couette flow, for a time step of 0.01.

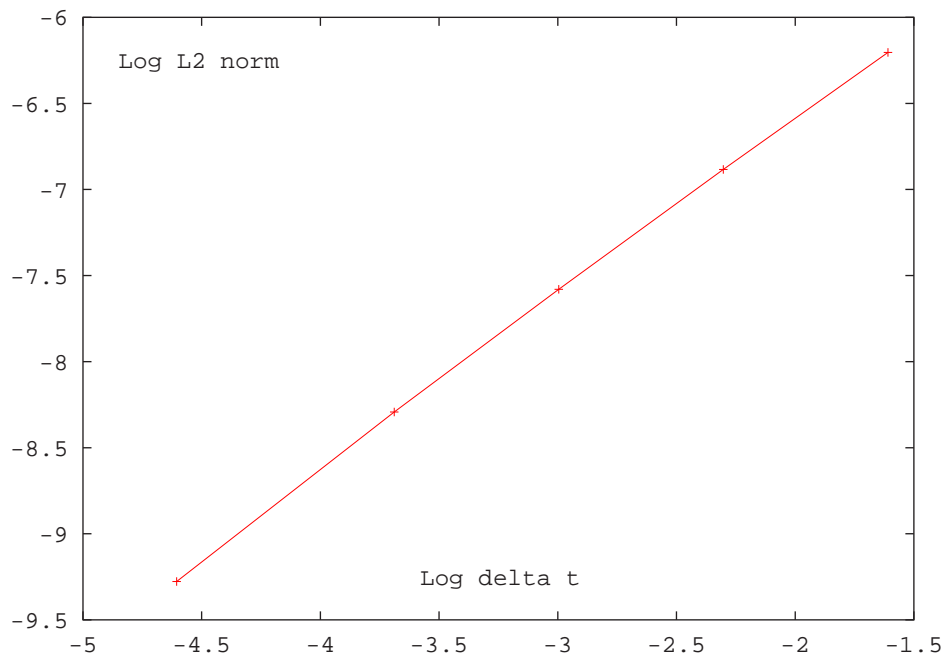


Figure 2.5: Plot showing the variation of the logarithm of the L2 norm with the logarithm of Δt for Couette flow.

by Fluent is similar that discussed by Hirt & Nichols (1981), and the reader is referred to their paper for a more detailed description. However, because of its importance to the simulations, some of the details concerning this model will be presented here. The volume-of-fluid, or VOF

method as it will now be referred to, relies on the fact the two fluids (for example air and water) do not interpenetrate (i.e. the two fluids are immiscible). While this is not always the case, to the degree of accuracy required for the simulations considered here, this assumption is acceptable. The validity of this assumption is to some extent borne out in the test problem which is considered in section (2.4.1), in which a container of fluid is spun and the free-surface profile measured. The VOF method essentially operates by assigning physical properties to a cell based upon the volume fraction of each fluid (or phase) within that cell. The tracking of the interface is then accomplished by solving the volume fraction equation, which seeks to ensure that the amount of each fluid is conserved. The equation solved, is the transport equation for the volume fraction, which is as follows:

$$\frac{\partial \alpha_1}{\partial t} + \mathbf{u} \nabla \alpha_1 = 0, \quad (2.6)$$

where α_1 is the volume fraction of phase (fluid) 1. Clearly by definition, it follows that,

$$\alpha_1 + \alpha_2 = 1. \quad (2.7)$$

The physical properties (i.e. density and viscosity) for each cell are then calculated by

$$\phi = (1 - \alpha_2)\phi_1 + \alpha_2\phi_2, \quad (2.8)$$

where ϕ in this case can represent either the density ρ or the viscosity μ . A single momentum equation is solved throughout the entire domain, resulting in a shared velocity field amongst the phases. The major drawback associated with this shared fields approach is that if large velocity differences exist between the two fluids, the velocities calculated near the fluid-fluid interface become less certain, although this can be overcome by increasing the resolution in these areas.

2.3.5 Interpolation Near the Interface

The finite-volume approach employed by Fluent, requires that convective and diffusive fluxes into a cell be balanced. For cases in which the cell is occupied partly by one fluid and partly by another, it is necessary to apply interpolation to ensure that this balance is maintained. In the current study the *Geometric Reconstruction Scheme* is used. It represents the interface using a piecewise linear approach. This process begins by firstly calculating the position of the interface relative to the center of each partially filled cell based on local volume fraction information. It then calculates the amount of fluid convected through each cell face using the above interface

positions and cell velocity field. Finally it then computes the volume fraction in each cell using the face fluxes from the previous step.

2.4 Validation

To test the ability of this technique to model free-surface flows, two simple test problems are considered: that of a breaking dam, and a spinning (or rotating) bowl. For the breaking dam problem the numerical results for the height of the fluid and surge-front locations at various times, are analyzed and compared with the experimental results of Martin & Moyce (1952). It is hoped that this comparison will give some estimate of the capabilities and accuracy of the numerical method employed. For the spinning bowl problem, the calculated surface position is compared with the steady-state analytical result. To test the ability of Fluent to model relevant viscous flows, flow past a fully submerged cylinder was also examined, as this is directly related to the problem under consideration here, and also because it has been extensively reported on in the literature, with Williamson (1991), Williamson (1996), Barkley & Henderson (1996) and Thompson et al. (1996) being just a few examples.

2.4.1 Spinning Bowl

The problem of a spinning bowl has been used by others such as Hirt & Nichols (1981) as a validation problem, and has the additional advantage in that an analytic solution also exists. It should be noted that the analytic solution only exists if one assumes that the acceleration is constant (constant with time) such that each fluid particle has no motion relative to its immediate neighbor. When this is the case, one may assume that only pressure differences are responsible for balancing the centripetal acceleration experienced by the fluid. The analytic solution to this problem is given by Hughes & Brighton (1991), and it indicates that the free surface position is described by a paraboloid of revolution, which has the following form:

$$z = z_0 + \omega^2 \frac{r^2}{2g}. \tag{2.9}$$

This problem was setup by considering an axisymmetric container which initially contained two fluids at rest. The top boundary condition was one in which the pressure was prescribed and it allowed the lighter of the two fluids to either enter or leave the domain. The side walls were given a prescribed velocity which, through the action of viscous shear, resulted in the gradual

acceleration of the interior fluid. This was evolved forward in time until a steady-state solution was obtained. The grid used for this test problem was relatively crude, in that it contained only 20 cells across the radius, and 100 over the height of the tank. The heavier fluid was initially set to a height of 2.25 radii, and the entire tank height was 5 radii.

A number of tests were performed with this problem to establish the effect of changing the relative densities and viscosities of the two phases (fluids). The comparison between the theoretical predictions and the numerical results for a range of different density and viscosity ratios is shown in table (2.1). The accuracy was estimated by calculating the L2 norm. This simply involves calculating the sum of the square of the differences between the numerical and the analytical results, and then averaging this result before finally taking the square root. It should be noted that no scaling was employed.

For the cases in which the density ratio was largest, the results were obtained using the $\frac{\rho_1}{\rho_2} = 100$ and $\frac{\mu_1}{\mu_2} = 100$ case (which was run from the zero velocity initial condition) as the starting conditions. It should be noted that as the density ratio between the two fluids was increased, the level of computation also increased markedly, and some difficulty was experienced in obtaining converged solutions at very large ratios.

$\frac{\rho_1}{\rho_2}$	$\frac{\mu_1}{\mu_2}$	$\frac{\nu_1}{\nu_2}$	l2norm
10	100	10.00	2.745914986093020E-003
100	100	1.000	4.334047508819092E-004
100	60	0.600	4.157280855137843E-004
811	60	0.074	3.851848721180833E-004
811	500	0.617	3.910692863397731E-004

Table 2.1: Variation of the L2norm (comparing analytic and numeric results) with differing density and viscosity ratios.

These results indicate that a good level of agreement is observed between the numerical and analytical results throughout the domain for a density ratio of both 811 and 100 (with the result for a density ratio of 100 and a viscosity ratio of 100 shown in figure (2.6)). For a density ratio of 10 however the agreement is poorer, with notable regions of both under and over prediction for the surface location (see figure (2.7)). This behaviour is not surprising as the analytic result assumes that the lighter fluid is a vacuum, and hence provides no resistance to the movement of the denser fluid.

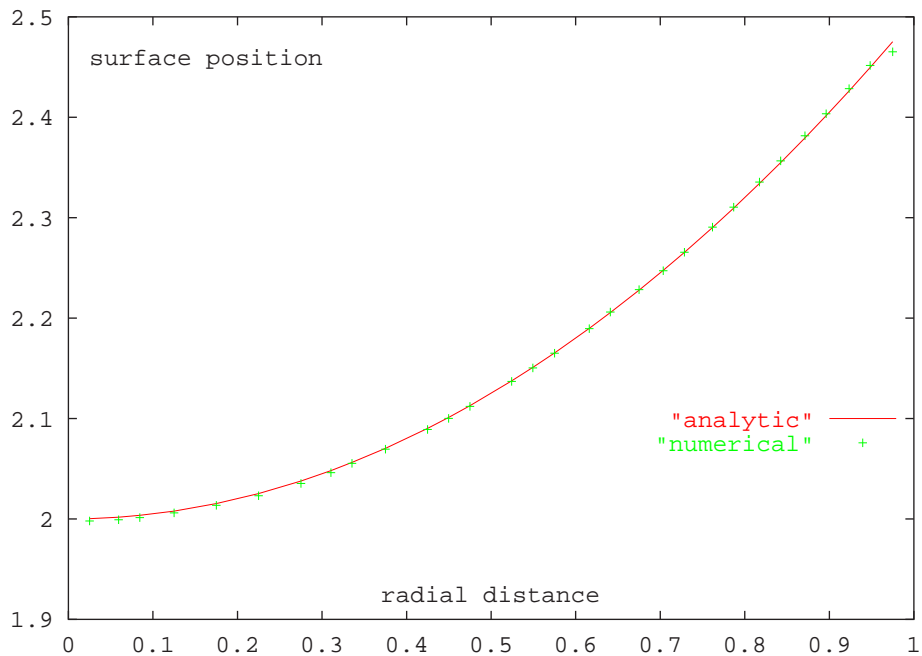


Figure 2.6: Plot showing the comparison between the analytical and numerical results for a spinning bowl, $\frac{\rho_1}{\rho_2} = 100$, $\frac{\mu_1}{\mu_2} = 100$.

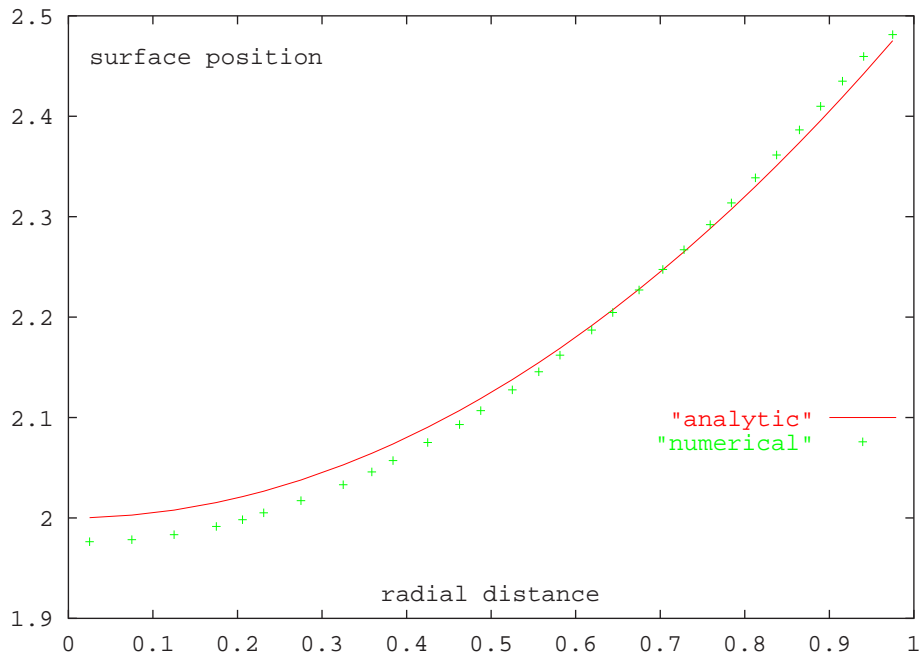


Figure 2.7: Plot showing the comparison between the analytical and numerical results for a spinning bowl, $\frac{\rho_1}{\rho_2} = 10$, $\frac{\mu_1}{\mu_2} = 100$.

For density ratios of both 811 and 100, it should be noted the the level of agreement tended to diminish somewhat toward the outer edge of the bowl, as shown in figure (2.6). This is

expected as the codes ability to interpolate for the surface position within the cell, will fall away as the level of fluid within each cell and in the neighbouring cells lessens. Changing the viscosity ratio appears to have little impact on the solution, as table (2.1) indicates. The density and viscosity ratios for air and water are 811 and 60 respectively, and the kinematic viscosity ratio is approximately 0.076. Since the behaviour of the lighter phase (air) is not of concern in the present study, it is reasonable to suggest that provided the densities are sufficiently different (i.e., 100 or greater), that the impact of the lighter phase is almost negligible. In the current investigation for flow past a cylinder close to a free surface, the density and viscosity ratios used were 100 and 100 respectively. The viscosity ratio of 100 was chosen so that the model would approach a technical free surface (i.e. the viscosity of the lighter phase would approach 0).

2.4.2 Breaking Dam

For the breaking dam problem, both the surface height and the surge-front location are measured as a function of time and are compared with the experimental results of Martin & Moyce (1952). The basic setup for this problem is illustrated in figure (2.8). While figure (2.9) shows that fluids location as a function of time. For this experiment the density and viscosity ratios were both 100. It should be noted that these early experimental results have a fairly large error associated with them. This uncertainty (in the time at which the various locations are recorded) is illustrated by the error bars on the graphs. It should be noted that the experimental results have been shifted to the left slightly, so as to match the shift Martin and Moyce themselves used in their comparison with theory. It is clear that all the numerical results lie within the bounds of the experimental error.

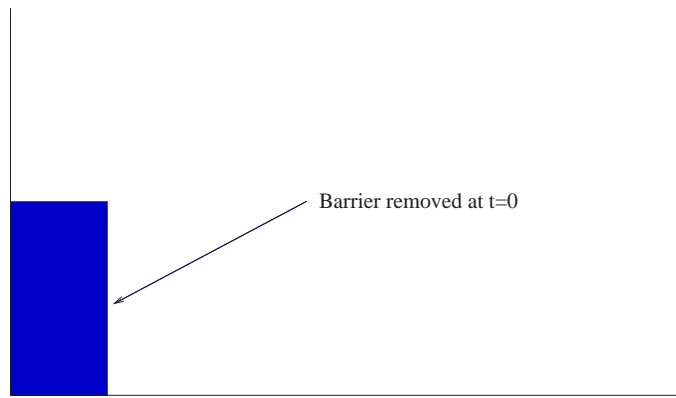


Figure 2.8: Schematic showing the setup of the breaking dam problem.

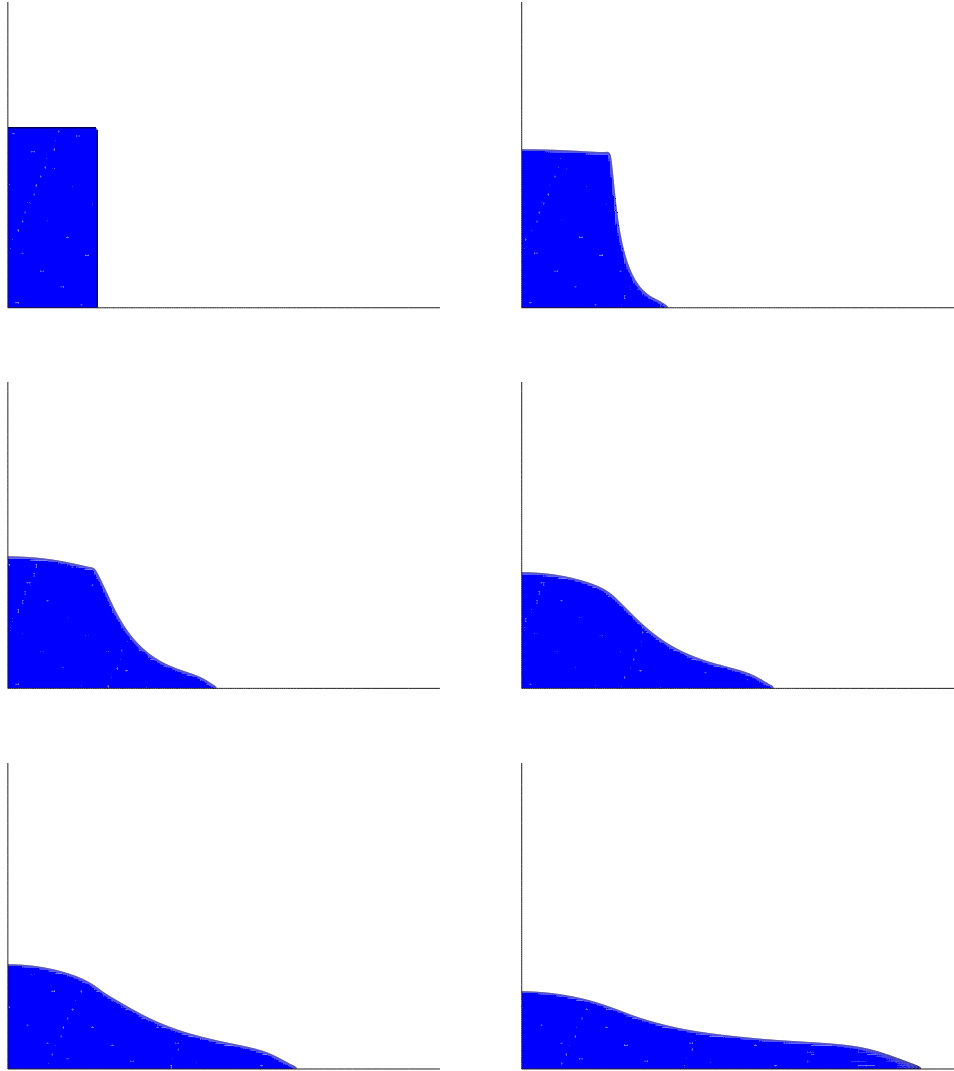


Figure 2.9: Evolution of the breaking dam.

2.4.3 Fully Submerged Cylinder

To validate the ability of the code to model bluff body viscous flows, flow past a fully submerged cylinder was investigated. As changes in lift, drag, and Strouhal number will all be measured for the cylinder near the surface, it is imperative that measurements of such quantities are both accurate and comparable with the results of other authors, for example Williamson (1996). It should be noted that all the tests within this section were performed with a time step of 0.025 unless otherwise stated.

Table (2.2) shows the comparison of the non-dimensionalized shedding frequency (Strouhal number fd/v) with the experimental results of Williamson (1989) and the numerical findings of Barkley & Henderson (1996), at a Reynolds number of 190 (this value was used as Barkley

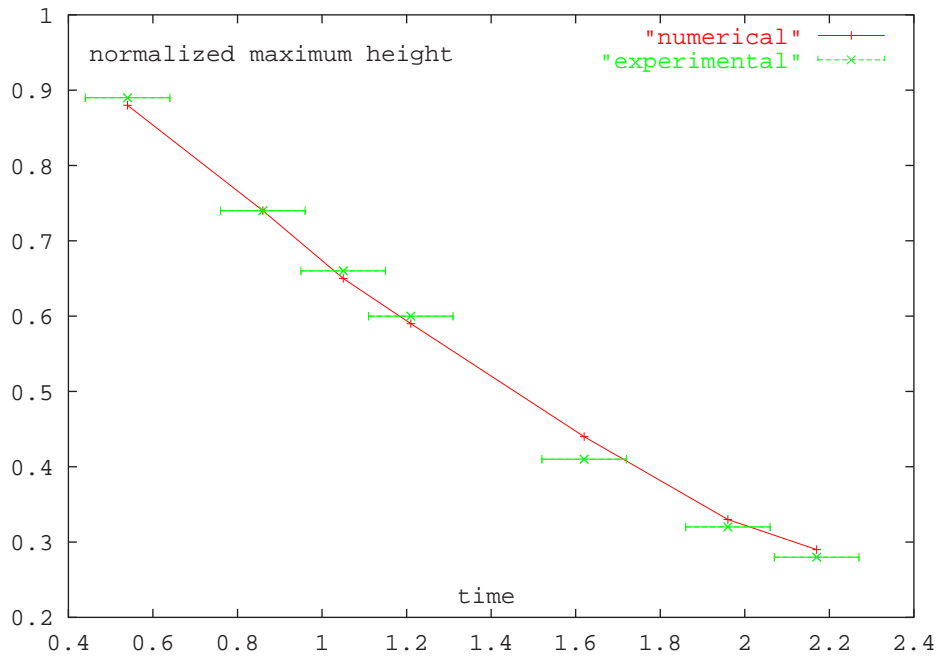


Figure 2.10: Comparison of the numerical results and those of Martin and Moyce (1952) for the breaking dam. This plot shows the variation of the normalized surface height with time ($\frac{\rho_1}{\rho_2} = 100, \frac{\mu_1}{\mu_2} = 100$).

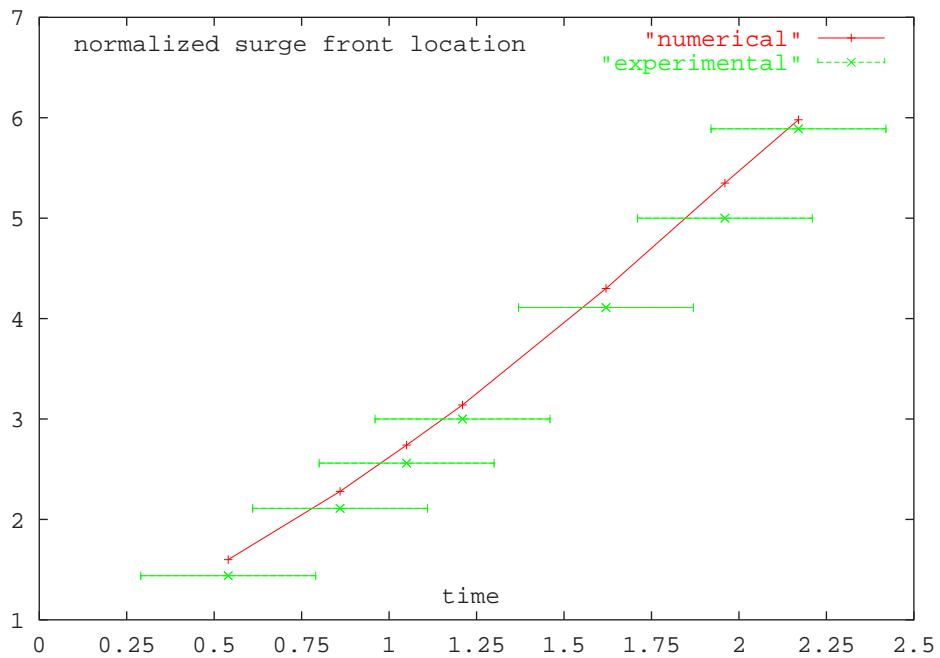


Figure 2.11: Comparison of the numerical results and those of Martin and Moyce (1952) for the breaking dam. This plot shows the variation of the surge-front location with time ($\frac{\rho_1}{\rho_2} = 100, \frac{\mu_1}{\mu_2} = 100$).

& Henderson (1996) only give results at a Reynolds number of 190). The results of the current study are slightly smaller (approximately 2%) than those of both Williamson (1989), and Barkley & Henderson (1996). It is believed that this slight discrepancy may be due to the artificial numerical diffusion introduced by the relatively low-order scheme used in the current investigation. Such numerical diffusion will typically result in the flow behaving as if it were at a slightly lower Reynolds number (which is consistent with the smaller value observed here).

Present Study	Williamson (1989) experimental	Barkley & Henderson (1996) numerical
0.191	0.194	0.195

Table 2.2: Comparison of the Strouhal number with the results of other authors for a fully submerged cylinder (Reynolds number 190).

The behaviour of the mean and root mean square (RMS) components of both the lift and drag coefficients are also considered, with table (2.3) showing the comparison between the current results and those of Barkley & Henderson (1996). The RMS values were obtained by squaring all the values then taking the average of squares, before finally taking the square root of the average.

	C_d	C'_d	C'_l	$-C_{pb}$
Present study	1.335	0.0262	0.435	0.8963
Barkley & Henderson (1996)	1.344	0.0293	0.465	0.9326

Table 2.3: Comparison of the mean and RMS components of the lift and drag acting on the cylinder with the results of Barkley and Henderson (1996) for a Reynolds number of 190.

The discrepancy between the RMS results is bordering on being significant, with the difference in the RMS lift being of order 6% while the RMS drag differs by 10% (albeit from a small base value). It should be noted that Barkley & Henderson (1996) give the fluctuating lift and drag, which one assumes to mean the RMS component. Williamson (1996) on the other hand suggests that the mean base pressure coefficient ($-C_{pb}$) is a sensitive measure of vortex formation, and as this varies by roughly 4%, the agreement is deemed to be acceptable.

2.4.4 Testing Domain Sizes

To obtain an estimate of the domain size required for the full development of the flow field for flow past a cylinder close to a free surface, a number of domain sizes were tested. The domain size tests were all conducted at a gap ratio of 0.25 and a Froude number of 0.20. The gap ratio (h/d) and the Froude number (u/\sqrt{dg}) are most clearly defined with reference to the schematic in figure (1.1). The Reynolds number for all of the tests was 180.

This region in parameter space was chosen as deviations in either the gap ratio or Froude number were found to have a significant effect on the Strouhal number, as well as the lift and drag (a point which will be discussed in later chapters). The domain size is expected to be important in this investigation as initial tests indicate that a restricted domain can lead to an artificial alteration in the height of the fluid above the cylinder. Such height changes will influence the measurements of the mean lift acting upon the cylinder, as the lift calculation involves subtracting the buoyancy force. This matter is discussed further in the section dealing with the lift and drag forces.

A basic schematic of the domain is shown in figure 2.12. The influence of L1 (inlet distance), L2 (outlet distance) and L3 (blockage) is shown in tables (2.4) to (2.6).

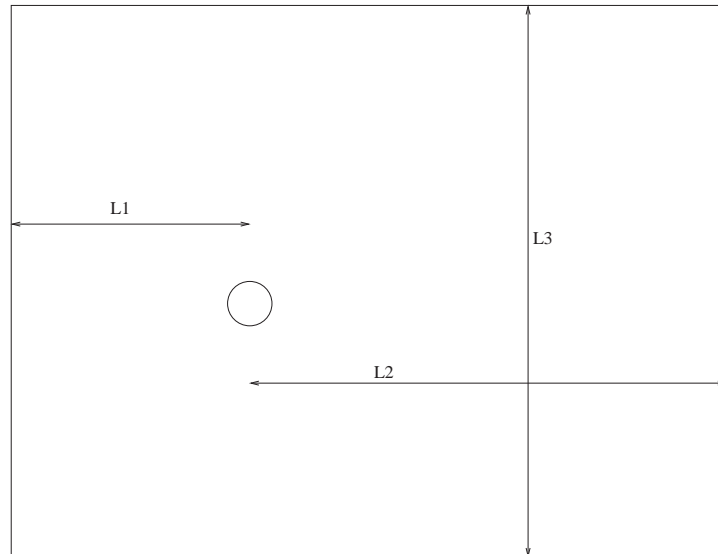


Figure 2.12: Schematic for the flow domain showing the critical parameters used for constructing the mesh.

These tests indicate that a mesh with the following parameters, L1=10, L2=30 and L3=30 will yield results which are accurate for Strouhal numbers to about 3% and for the mean lift to about 5% and the RMS lift to about 7%. This level of accuracy is considered appropriate for

L1	mean C_l	C'_l	St
10	-0.476	0.338	0.1635
15	-0.459	0.318	0.1598
20	-0.452	0.313	0.1585

Table 2.4: Comparison of the mean and RMS components of the lift and Strouhal numbers for differing inlet distances (L1). (Reynolds number 180, gap ratio 0.25 and Froude number 0.20).

L2	mean C_l	C'_l	St
30	-0.476	0.338	0.1636
40	-0.481	0.342	0.1654

Table 2.5: Comparison of the mean and RMS components of the lift and Strouhal numbers for differing outlet distances (L2). (Reynolds number 180, gap ratio 0.25 and Froude number 0.20).

L3	mean C_l	C'_l	St
30	-0.476	0.338	0.1635
40	-0.475	0.343	0.1633

Table 2.6: Comparison of the mean and RMS components of the lift and Strouhal numbers for differing domain widths (L3). (Reynolds number 180, gap ratio 0.25 and Froude number 0.20).

the current investigation, which seeks to characterize the physical behaviour of each of the flow regimes, as opposed to obtaining highly accurate (and hence expensive) results for a limited number of cases.

2.4.5 Resolution

To examine the effect of changing the resolution, two grids having the same domain size were tested. The grid resolution test was conducted at a gap ratio of 0.40 and Froude number of 0.20. Two grids of differing resolution were used: the first grid (which is shown in figure (2.13)) had 52960 cells, while the second grid which is shown in figure (2.14)) had 88670 cells.

Table (2.7) shows the comparison between the two grids and it indicates that the approximately 66% increase in the number of cells has little effect on any of the quantities measured. The maximum change recorded in each value was of order 1%.

On the basis of the results in table (2.7), one can use Richardson extrapolation to get an estimate

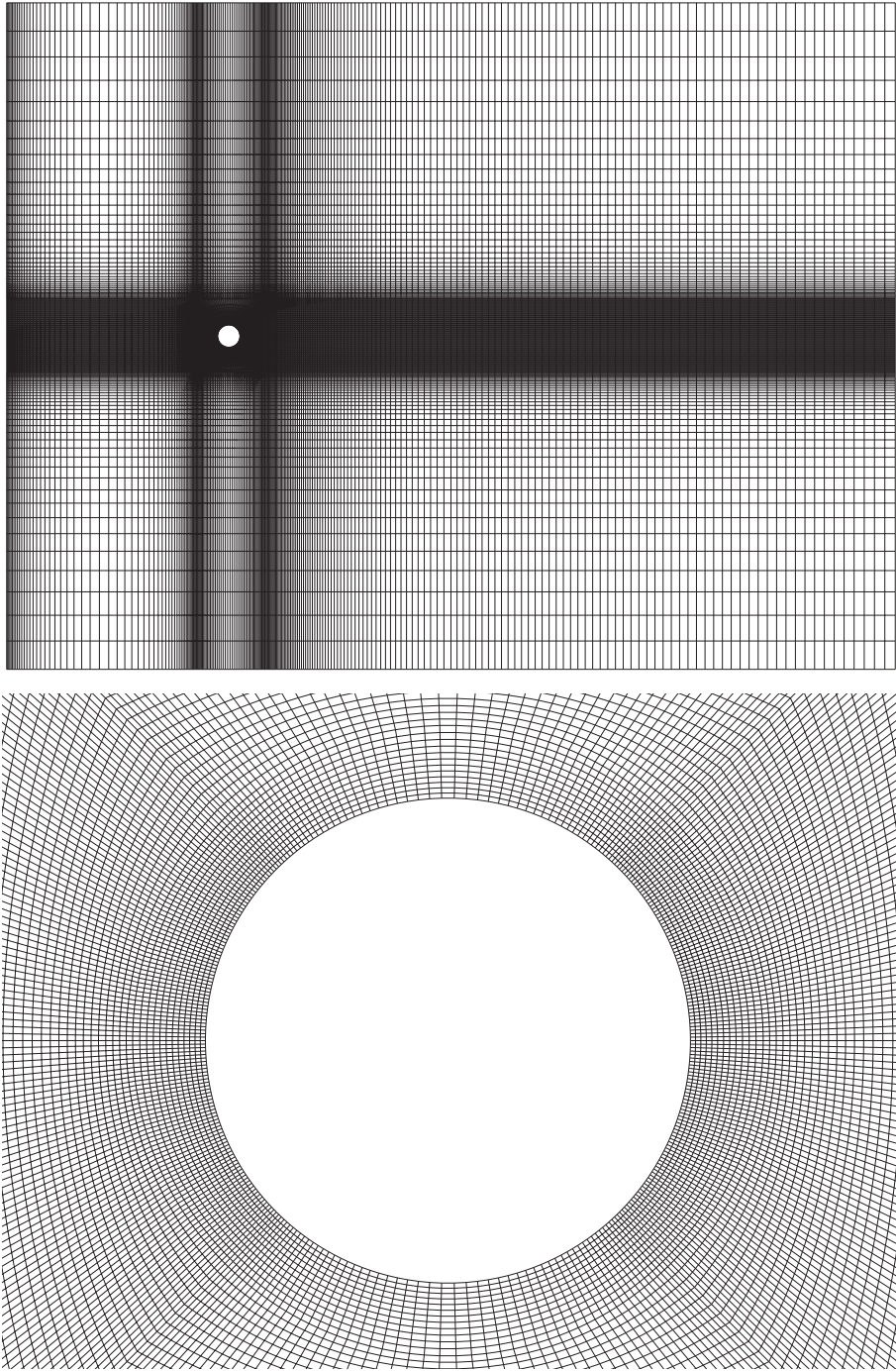


Figure 2.13: Grid 1 (55960 cells)

of the asymptotic error. This process is as follows:

$$\phi_{true} = \phi(h_r) + \alpha(h_r)^2 \tag{2.10}$$

$$\phi_{true} = \phi(\beta h_r) + \alpha(\beta h_r)^2 \tag{2.11}$$

where ϕ is the quantity being measured and which is a function of the resolution h_r . β is the

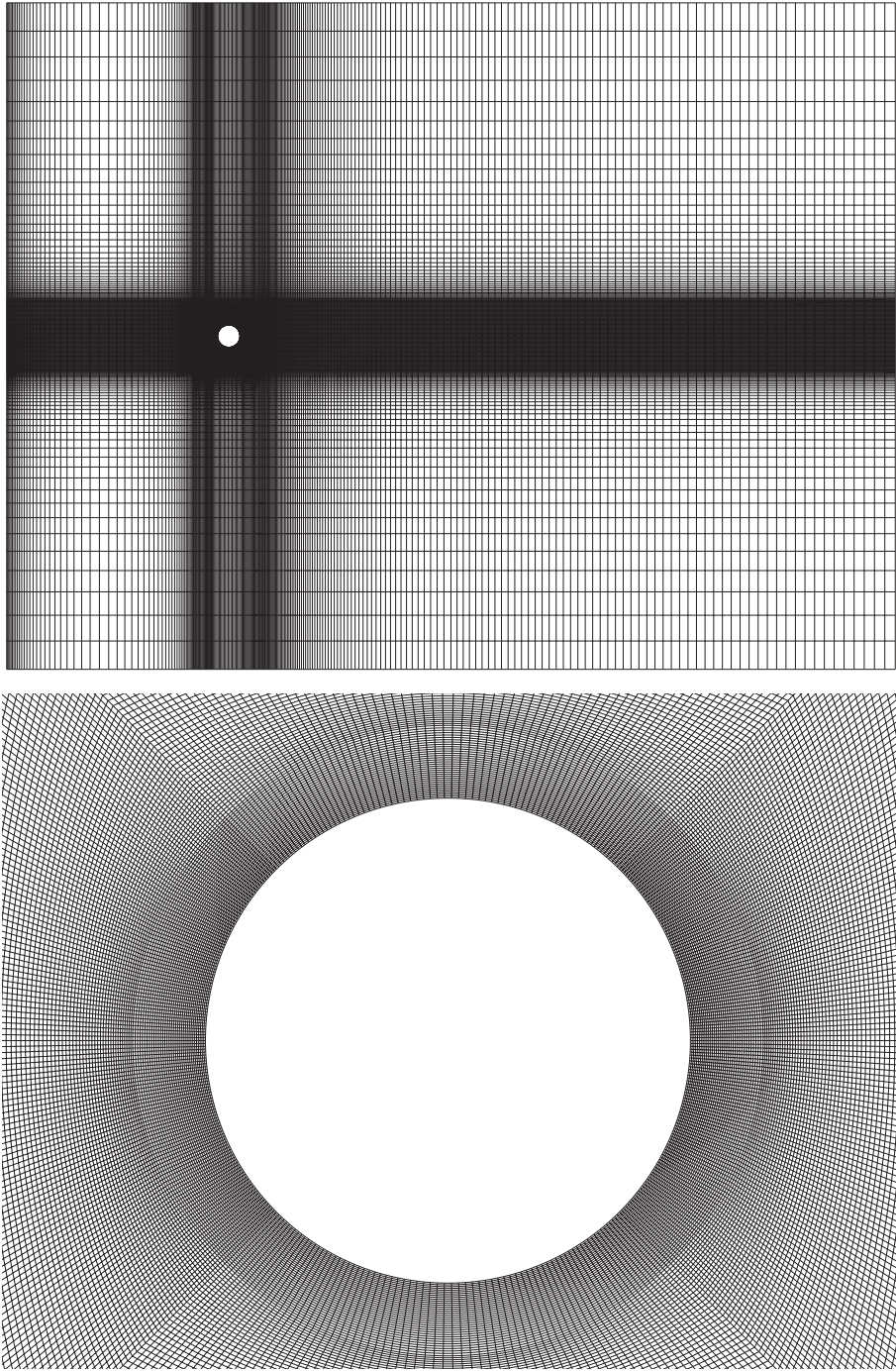


Figure 2.14: Grid 2 (88670 cells)

factor by which the resolution in each direction was reduced, α is an estimate of the truncation error coefficient and ϕ_{true} is the true value of the quantity ϕ . It should be noted that this approach is only really valid for situations in which the grids are geometrically similar, which is the case here. The result of this extrapolation suggests that the ‘true’ values of the quantities are as shown in table (2.8).

Number of Grid cells	Strouhal number	C_d	C'_d	C_l	C'_l
52960	0.1969	1.6225	0.1526	-0.3245	0.5366
88670	0.1972	1.6209	0.1507	-0.3268	0.5229

Table 2.7: Comparison of the Strouhal number and the mean and RMS components of the lift and drag for differing resolutions (Reynolds number 180, gap ratio 0.40, Froude number 0.20).

	Strouhal number	C_d	C'_d	C_l	C'_l
Grid (52960)	0.1969	1.6225	0.1526	-0.3245	0.5366
Extrapolated result	0.1976	1.6185	0.1479	-0.3302	0.5026
% difference	0.3543	0.2471	3.1778	1.7262	6.7648

Table 2.8: Table showing the asymptotic values (from Richardson extrapolation), those obtained using the grid with 52960 cells, and the percentage difference (Reynolds number 180, gap ratio 0.40, Froude number 0.20).

Table (2.8) indicates that the solution for a grid of 52960 cells should yield results for all quantities except the RMS lift which lie within approximately 3% of that expected on an grid of infinite resolution (with the RMS lift varying by 6.76%). For the current investigation this is deemed to be an acceptable compromise between accuracy and allowing for a sufficient number of simulations to be performed to adequately cover the parameter space.

2.4.6 Convergence

As mentioned earlier the numerical technique used here iteratively solves for the flow variables, and as such it is necessary to determine the point at which the iterative process stops. At each point, the difference between the numerical solution and the solution of the discretized equations, is referred to as the residual. The sum of these residuals over all the cells in the entire domain is referred to as the global residual, and it was this value that was used to determine when to cease iterating.

The actual values used for the residuals, were determined according to what fractional discrepancy of the total flux of both momentum and mass was deemed acceptable. The residual used here allowed for a global fractional discrepancy of approximately 0.0002 in the mass flux, and 0.001 in the momentum flux.

To test that an adequate level of convergence for the flow field at each time step was achieved,

a test which varied the convergence criteria was performed. This involved simulating the same problem, but with convergence criteria which differed by a factor of 10 (i.e. the one used in the preceding calculations, and one 10 times smaller). Table (2.9) shows how the measured quantities compare at both these residuals.

Residual	Strouhal number	C_l	C'_l
standard	0.1635	-0.476	0.338
standard/10	0.1634	-0.476	0.337

Table 2.9: Comparison of the Strouhal number and the mean and RMS components of the lift for differing convergence criteria. (Reynolds number 180, gap ratio 0.25, Froude number 0.20).

Again it is clearly seen that only very minor differences are recorded, with the maximum difference in any quantity less than 0.03%. This suggests that the convergence criteria used here was adequate.

2.4.7 Time Step

To test the influence of the size of the time step, two identical cases were again considered, but time steps of differing sizes were used. The time-step tests were performed at a larger Froude number, as the surface variation is typically greater and hence is more likely to impact upon the results. The comparison is shown in the table (2.10).

Time step	Strouhal number	C'_d	C'_l	$-C'_{pb}$
0.0250	0.1886	0.2168	0.5161	0.3936
0.0125	0.1916	0.2103	0.5272	0.4147

Table 2.10: Comparison of the Strouhal number and the mean lift and drag for differing time steps (Reynolds number 180, gap 0.40, $Fr = 0.30$).

It is expected that at higher Froude numbers, (where local wave breaking can occur), that the size of the time step will be more important. However, as almost infinite resolution in both time and space would be required to predict the nature of the breaking wave, with its influence upon the flow expected to be only slight, a compromise had to be made. It was decided (based largely upon the available resources and time constraints) that a time step of 0.025 would be used. This time step was found to give results which were deemed acceptable for the tests illustrated in table (2.10) (i.e. all results vary within about 3% except for the RMS component of the

base pressure coefficient which is within 5.4%), and while a smaller time step may improve the capture of the wave breaking process, it is still unlikely to be able to predict the intricacies associated with it.

It should be noted that the availability of resources was an influencing factor in the choice of the larger time step. As the actual time taken to evolve the flow field forward 100 time units, required approximately 2 days on a Intel Pentium III 500, which was the fastest machine available at the time during which the majority of the simulations were performed. Having said this, it is estimated that all of the simulations undertaken in this study would have required in excess of 2.75 years of continuous run time if performed on a single computer with an Intel Pentium III 500 processor.

2.5 Problem Setup and Post Processing

It has been shown by Sheridan et al. (1997) that the problem of flow past a cylinder close to a free surface has two major governing parameters, namely the gap ratio (or dimensionless submergence depth) and the Froude number (with the Reynolds number being less important). This section will now define these parameters while also discussing how they were altered, and the boundary conditions used.

With reference to figure (1.1), table (2.11) lists some of the important quantities.

Symbol	Definition
u	free stream flow velocity
d	cylinder diameter
h	submergence depth
ρ	fluid density
μ	dynamic fluid viscosity
g	gravitational acceleration

Table 2.11: Table detailing the nomenclature used (also see figure (2.12)).

The dimensionless quantities were then defined as follows:

- Reynolds number, $Re = \frac{\rho du}{\mu}$: It represents the ratio between the inertial and viscous forces. The Reynolds number was varied by altering the viscosity μ .

- Froude number, $Fr = \frac{u}{\sqrt{dg}}$: It represents the ratio between the inertial and gravitational forces. The Froude number was varied independently of the Reynolds number by altering the gravitational acceleration g .
- Gap ratio, or dimensionless submergence depth, $h^* = \frac{h}{d}$: It represents the ratio of between the submergence depth (as measured between the free surface and the top of the cylinder) and the cylinder diameter.

The boundary conditions used were as follows:

- At the inlet : prescribed constant velocity with both phases entering the domain at the same speed. The submergence depth was set by altering the height at which each phase enters the domain.
- On the cylinder : no-slip boundary condition.
- At the top and bottom walls : zero shear stress (free slip).
- At the outlet : prescribed pressure at the outlet boundary. This boundary condition permits both inflow and outflow. All other conditions are extrapolated from those in the interior of the domain. A hydrostatic pressure gradient was prescribed at the outlet, as was the height at which each phase left the domain.

Many of the quantities obtained that are discussed in the later chapters, involved the extraction and analysis (such as integration) of raw data. This section will discuss the procedure used to obtain the relevant data, as well as defining any sign conventions used.

2.5.1 Lift and Drag Forces

The lift and drag forces on the boundary are calculated by integrating the dot product of the stress vector with the force vector around the cylinder. (where the stress vector as given in Acheson (1990) is $\mathbf{t} = -p\mathbf{n} + \mu(2(\mathbf{n} \cdot \nabla)\mathbf{u} + \mathbf{n} \times (\nabla \times \mathbf{u}))$, and the force vector is simply the unit vector in the direction one wishes to calculate the force). With regard to the lift acting upon the cylinder, the presence of gravity in the governing equations implies that there will be a buoyancy force acting upon the cylinder (i.e. the pressure varies around the cylinder as a consequence of the hydrostatic pressure gradient). As such, any measurement of the lift force will naturally include a hydrostatic contribution, and one must subtract this component to

obtain the flow induced lift force acting upon the cylinder. Thus, the lift induced by the flow will simply be

$$L_{actual} = L_{measured} - L_{noflow}, \quad (2.12)$$

where L is the lift force.

2.5.2 Moment

The moment acting on the body is calculated by summing the product of the force vectors for each face with the moment vector. For a cylinder the moment is simply the integral of $t \cdot \mathbf{e}_\theta R d\theta$ from 0 to 2π (where t is the stress vector which was defined previously, R is the radius, and \mathbf{e}_θ is the unit vector in the theta direction). Both the moment vector and the vorticity are defined to be positive if they have a counter-clockwise sense of rotation.

2.5.3 Force and Moment Coefficients

The forces and moments are usually most useful when expressed as non-dimensionalized coefficients. The lift and drag were both non dimensionalized by dividing the respective forces by $1/2\rho u^2 A$, where ρ is the fluid density, u is the free-stream velocity, and A is the area projected in the appropriate direction (which is simply the cylinder diameter for the case being considered here). The moment is non dimensionalized by dividing by $1/2\rho u^2 A d$, where all the quantities are as previously stated and d is the cylinder diameter.

2.5.4 Separation and Stagnation Points

Rosenhead (1963) and Blackburn & Henderson (1995) indicate that in the frame of reference of the body, the separation and attachment points occur at locations of zero surface vorticity. These points were then found via linear interpolation of the vorticity in the cell just outside of the cylinder.

2.5.5 Vortex Paths and Convective Speeds

The paths and speeds of individual vortices as they are convected downstream is of interest as they give an indication of the of the altered conditions in wake.

The paths taken by the vortices was determined by firstly dividing part of the domain into a series of small intervals or bins. At each time step the position of the local maximum and minimum of the vorticity within each bin was recorded. This process was then repeated over a number of time steps with the result yielding the locus of points (or path) traced out by the vortex cores. The convective velocities of the vortices were then calculated by simply dividing the distance traveled by the vortex core, by the time it took to travel that distance.

2.5.6 Time Averaged Flow and Standard Deviation

The time-averaged flow field was obtained for cases in which the flow was periodic by averaging the velocity at each point within the flow field over one or more periods. The standard deviation about the mean was then determined at every point by summing the squares of the residuals between the data at each time step and the mean at the corresponding points, and then dividing that by the $n - 1$, where n is the number of time intervals used to determine the standard deviation. This approach is consistent with standard statistical sampling theory, and is discussed in Chapra & Canale (1991).

2.5.7 Strouhal Number

The Strouhal number (or dimensionless frequency fd/u , where f is the response frequency, d is the cylinder diameter, and u is the free stream velocity) was determined via two different methods. The first, which is only applicable when the flow is periodic in time, involved determining the time difference between successive peaks or troughs in the lift cycle via fitting a cubic polynomial to the four closest points, and then analytically determining the maximum or minimum. In general this method gave accurate results for data spanning only a few periods (with its accuracy less affected by the number of available data points). The second approach is perhaps the most standard, and is applicable to all data types (as opposed to purely periodic ones), as it simply involved calculating the Fourier transform of the lift signal (see Chapra & Canale (1991) for more details with regard to Fourier transforms). The Fourier transform yields the frequency spectra and from this the dominant frequencies are determined. It should be pointed out that the first approach is often used in numerical investigations, where the collection of a large numbers of data points is often expensive, as the second approach requires data over many periods to achieve reasonable frequency resolution, and as such it is more commonly used in experiments.

2.5.8 Particle Transport Plots/Videos

To enhance ones understanding of the flow behaviour, inert tracer particles were released into the flow. These particles which did not influence the flow field, were modelled as small spheres, with their trajectory being determined via the integration of the force balance for each particle. This force balance is as follows,

$$\frac{du_{part}}{dt} = F_D(u - u_{particle}) + g \frac{(\rho_{particle} - \rho)}{\rho_{particle}}, \quad (2.13)$$

where $F_D(u - u_{particle})$ is the drag force per unit particle mass and $F_D = \frac{18\mu}{\rho_{particle}D_{particle}^2} \frac{C_D Re}{24}$ and $Re = \frac{\rho D_{particle} |u_{particle} - u|}{\mu}$.

Here u is the fluid velocity, $u_{particle}$ the particle velocity, μ the fluid viscosity, ρ the fluid density, $\rho_{particle}$ the particle density, $D_{particle}$ the particle diameter, g the gravitational acceleration, Re the relative Reynolds number and C_d the Drag coefficient. The value of C_d is determined from the following relationship

$$C_D = a_1 + \frac{a_2}{Re} + \frac{a_3}{Re^2}, \quad (2.14)$$

which applies to spherical particles over a range of Reynolds numbers, with the constants a_1, a_2 and a_3 being given by Morsi & Alexander (1972). The inert particles used in the current investigation had a mass of 5.23599×10^{-19} , and as such have almost negligible inertia associated with them.

The particles were released at a locations 8 diameters upstream of the cylinder, and are colored according to the height at which they were injected, which ranged from -0.50 up to the surface height in 0.05 increments. In many instances this involved releasing particles exactly on the surface (i.e. for cases in which the gap ratio is an integer multiple of 0.05). Hence any fluctuation, even very slight in the surface height at positions upstream, may result in particles being released on the other side of the free surface. When this occurs the particles typically follow the free surface up until the point at which significant surface curvature is noted, at which point they then tend to follow the flow structures associated with the lighter phase. This behaviour was more prevalent at larger Froude numbers in which small scale wave breaking was observed, and while such particles could have been removed (i.e. never injected) they serve as an effective means of determining height variations at positions upstream of the cylinder.

It should be noted that all of the particle transport plots contained within this written document have had the particles in the lighter phase removed, while all of the videos contained on the

accompanying compact disk have not.

For the plots that show the particles coloured by residence time, the more red the particle the longer it has been in the flow.

2.5.9 Vorticity Plots/Videos

As it is the behaviour of the denser fluid which is of primary importance (with the lighter phase possessing only roughly 1% of the momentum), most of the plots showing the vorticity are only concerned with the denser phase. The vorticity within the denser phase was obtained by calculating the volume fraction weighted vorticity, which is found by multiplying the vorticity at each point by the local volume fraction (which is 1 in the denser phase, and 0 in the lighter phase). The vorticity contours plots were obtained by first contouring the negative vorticity and then overlaying the contours for the positive vorticity. As a red to blue colour map was used to contour both the positive and negative vorticity (with red representing the maximum value and blue the minimum value) the vorticity close to the body will generally possess the most extreme colour. When using this colour map the lighter the shade of the red the more negative the vorticity and the lighter the shade of blue the more positive the vorticity. Unless otherwise stated the vorticity contours are between -35 and -0.35 for the negative vorticity between 0.35 and 35 for the positive vorticity.

2.5.10 Free-Surface Position

The volume of fluid (VOF) approach used by Fluent prescribes characteristics to the fluid within each cell according its volume fraction (with the volume fraction also being solved for as part of the solution process). Hence the interface between the two fluids occurs where the volume fraction rapidly changes from 1 to 0. This change will generally occur over a range of finite thickness, and as such, the location of the free surface is smeared somewhat over this distance. The thickness of the interface is largely determined by the spatial resolution in the region where the interface exists, and hence the accuracy of the surface position is dependent upon the spatial resolution. As the resolution tests above indicate, little variation (less than 1%) was observed when the spatial resolution was altered (with the resolution in the region where the surface lies being altered by 20%). The resolution in the region of the free surface, varied slightly with horizontal location, and at its worst (near the inlet and the outlet) the cell height was 0.03 of a cylinder diameter. While the geometrical reconstruction scheme used within Fluent calculates

the location of the interface within each cell (hence improving the accuracy somewhat), one must assume that the accuracy of the surface position (at its worst point) is of order 0.03 which is slightly larger than the 0.02 of a cylinder diameter claimed experimentally by Sheridan et al. (1997).

Plots showing the surface position were obtained by finding the location where the volume fraction was equal to 0.50. This procedure involved interpolating within a cell to find this location. Figure (2.15) shows a schematic that illustrates the estimated surface location found using this piecewise linear approach (geometric reconstruction).

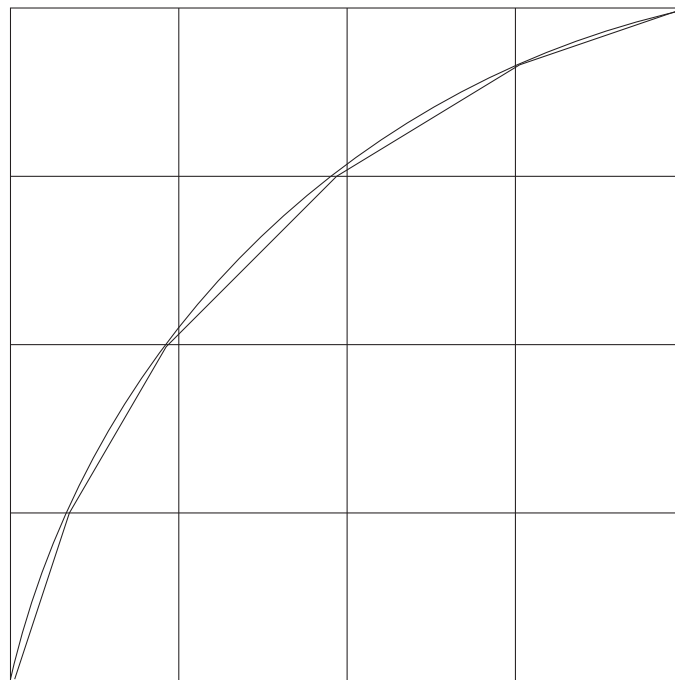


Figure 2.15: Actual free surface position (curved line) and the piecewise linear reconstruction (straight lines) used to reconstruct the position of the free surface.

2.5.11 Pressure Plots

As mentioned earlier, the presence of the gravitational acceleration term in the y momentum equation, results in the establishment of a hydrostatic pressure gradient. As also mentioned earlier, the Froude number was altered independently of the Reynolds number by varying the magnitude of the gravitational acceleration. Hence the hydrostatic component of the pressure was different for each gap ratio, and each Froude number. As it is the changes in pressure on top of the hydrostatic component which are of interest, its influence was removed by subtracting

an imposed hydrostatic pressure field from the calculated pressure field (i.e. subtracting ρgh from the pressure field, where h is chosen arbitrarily provided it is greater than the maximum surface height). This approach allows the underlying relative variation in the pressure field to be examined, but at the cost of losing information regarding the magnitude of the pressure. As such, one must be careful when comparing the pressure fields between different gap ratios and different Froude numbers. However having said that, it is the relative pressure differences which are present in the Navier-Stokes (momentum) equations, and hence it is these relative differences between different points in the flow field which are of interest, as opposed to the actual values.

2.6 Videos

The compact disk accompanying this thesis contains videos which illustrate the time dependent behaviour of the vorticity field, the transport of particles, and the free surface position. These videos are all in an animated gif format and should be viewable on most web browsers (i.e. Netscape Navigator or Microsoft Internet Explorer), or via other gif animation software. It is recommended that the reader consider these videos especially when reading the sections which discuss the mechanism.

The naming convention used for the videos is as follows:

- The first part of the name indicates the gap ratio (so for example H_0.25, will indicate that the gap ratio is 0.25).
- The second part of the name denotes the Froude number (so for example FR_0.25, indicates that the Froude number is 0.25).
- The third part of the name then indicates the quantity being measured. The three quantities are: ‘part’ for particles, ‘vort’ for vorticity, and ‘surf’ for surface.
- The fourth part of the name then indicates the viewable area. ‘ex’ indicates a larger viewing area, while ‘cl’ indicates a closer view.
- And finally the last part of the file name indicates the background colour, with ‘b’ denoting black and ‘w’ denoting white.

Hence the file with the name H_0.16_FR_0.20_part_ex_b.gif will contain the video which shows an extended view of the particle transport plots with a black background for a gap ratio of 0.16 and a Froude number of 0.20.

Most of the videos are all of a consistent size and colour, although some of the videos are only available with a white background and the image size may also be smaller.

2.7 Summary

A brief description of the numerical method and its validation has been provided. As this problem contains a number of complicated physical phenomena, all of which require assumptions to be made before they can be modelled, it is hoped that predictions which are accurate to within approximately 10% of the ideal case can be obtained.

Chapter 3

Free Slip and Froude Number 0.20

The problem under investigation is that of a cylinder close to a free surface. As to the author's knowledge little work has been done in this area to date, with the exceptions being Miyata et al. (1990), Sheridan et al. (1995), Sheridan et al. (1997), Warburton & Karniadakis (1997), and Hoyt & Sellin (2000), comparison with the more widely investigated and related case of flow past a cylinder close to a plane no-slip boundary will be sought. Such a comparison is considered as it is envisaged that this problem may highlight some of the distinct similarities and key differences between itself, and the case of a cylinder close to a free surface at low Froude numbers. For the interaction of vortices with a free surface it has been shown by Yu & Tryggvason (1990), Ohring & Lugt (1991), and Lugt & Ohring (1992) that the free surface at low Froude numbers behaves remarkably like a rigid surface, with little or no large scale surface deformation being observed. To investigate the similarities between the two cases, both flow past a cylinder close to a free-slip boundary (which approximates a free surface in the limit as the surface deformation tends towards zero), and flow past a cylinder close to a free surface at a Froude number of 0.20 are considered.

Before proceeding it is perhaps best to briefly re-examine some of the behaviour for flow past a cylinder close to a no-slip wall, and to discuss the likely implications for flow past a cylinder close to a free surface. For the case of a free surface, it is expected that the pressure gradients on the adjacent wall that were observed by Bearman & Zdravkovich (1978), Grass et al. (1984) and Price et al. (2000), will manifest themselves as surface deformations. As these separation zones correspond to regions of adverse pressure gradient, it is expected that the surface is likely to curve or deform upwards in these regions. Hence it is anticipated that the surface will rise in the regions just upstream and downstream of the cylinder, with the size of the height changes

being dependent upon the Froude number. However, the lack of wall vorticity and the presence of self induced surface vorticity may alter the results in a potentially significant manner. The comparison between the solid surface results and those for a free surface at low Froude numbers (including the limiting case of zero Froude number which gives a flat non deformable free-slip surface) are now considered.

3.1 Scope and Layout of the Chapter

The findings of Yu & Tryggvason (1990), Ohring & Lugt (1991), and Lugt & Ohring (1992) suggest that the level of surface deformation is largely dependent upon the Froude number, with the Froude number representing the ratio between the inertial forces and the gravitational forces acting upon the fluid. Hence for cases in which the Froude number is small, gravitational forces will dominate and the level of surface deformation will remain negligible. For these cases it is envisaged that the flow will remain largely parallel, and it is to this portion of the parameter space that this chapter will be largely restricted.

The Froude numbers considered here are 0.00 and 0.20. The limiting Froude number of 0.00 is obtained by assuming that the free surface acts like a non-deformable free-slip surface, which is approximately the case in the limit as $g \rightarrow \infty$, and hence the Froude number $Fr \rightarrow 0$. The Froude number 0.20 case is also considered as only limited surface deformation is observed at this value. It is expected that these cases will share many common features with flow past a cylinder close to a plane no-slip wall, for which there exists a wider variety of experimental results, as the geometrical arrangement is almost identical.

Trends for the behaviour of the Strouhal number, the mean and root mean squared (RMS) components of both the lift and the drag and the mean moment acting upon the cylinder will all be considered. In addition, the behaviour of the pressure distribution, the position of both the stagnation and separation points, and the paths traced out by the vortices as they are convected downstream, will also be examined. The gap ratios (or dimensionless submergence depths) investigated at both Froude numbers are as follows: 0.10, 0.13, 0.16, 0.19, 0.22, 0.25, 0.40, 0.55, 0.70, 0.85, 1.00, 2.50 and 5.00.

The earlier parts of this chapter will largely present the results, with some comment being provided on how this material relates to the work of others. The later part of the chapter will then be devoted to a discussion of a mechanism which explains the observed behaviour.

3.2 Strouhal Number

One of the minor aims of the current investigation is to determine whether or not changes in the Strouhal number exist as the proximity of the cylinder to the surface is altered. Miyata et al. (1990), Angrilli et al. (1982), Grass et al. (1984), Lei et al. (1999) and Price et al. (2000) all note that the Strouhal number does vary with gap ratio, while Taniguchi & Miyakoshi (1990) detect only a slight change and Bearman & Zdravkovich (1978) observe no change at all.

For the authors that did observe changes in the Strouhal number with gap ratio there is some degree of spread in their results, both with regard to the magnitude of the changes and with respect to the asymptotic behaviour of the Strouhal number with gap ratio. Angrilli et al. (1982) found that the normalized Strouhal number approached unity for gap ratios of approximately 5 or 6. However, Grass et al. (1984) and Lei et al. (1999) both observed the asymptote to occur over a much shorter distance, with values approaching unity being observed at gap ratios of approximately 1 or 2. This discrepancy is likely to be a function of the wall boundary layer thickness and may also be a function of Reynolds number. Hence it is expected that a cylinder close to a free surface at low Froude number should also display similar behaviour.

Table (3.1) and figure (3.1) show the numerically predicted asymptotic behaviour of the normalized Strouhal number with gap ratio (with the Strouhal number for the reference cylinder being 0.1893). It is clear from these results that the changes in Strouhal number are only of order 1% when the gap ratio is greater than or equal to 2.50, which is largely as expected. It should be noted that no shedding was observed at some of the smaller gap ratios, with the flow behaviour for these cases discussed in more detail later in this chapter.

The asymptotic behaviour of the Strouhal number shows good agreement with the results of Angrilli et al. (1982) who gives the finest detail with regard to such behaviour. This agreement is even more remarkable when one considers that there is almost a 20 fold difference in Reynolds number between the two cases, with the current investigation being conducted at a Reynolds number of 180. This agreement may be partially due to the roughly comparable formation length of a fully submerged cylinder at both Reynolds numbers (see Norberg (1998) for details on formation length). Comparison with the results of other authors is made more difficult, as the scaling used on their plots is usually large (i.e. the data is plotted for values between 0 to 0.3, even though the changes in Strouhal number normally lie within the range of 0.20 to 0.28). It is tentatively suggested that the asymptotic distance may vary with Reynolds number, or more appropriately formation length, as the portion of the shear layer exposed to interference

gap ratio	St	normalized St	St	normalized St
h/D	$Fr = 0.00$	$Fr = 0.00$	$Fr = 0.20$	$Fr = 0.20$
REF	0.1893	1.0000	0.1893	1.0000
0.10	no shedding	no shedding	no shedding	no shedding
0.13	no shedding	no shedding	0.4031 pseudo shedding	2.1294
0.16	0.1292	0.6825	0.1243	0.6566
0.19	0.1441	0.7612	0.1350	0.7132
0.22	0.1604	0.8478	0.1491	0.7876
0.25	0.1738	0.9181	0.1635	0.8637
0.40	0.1988	1.0502	0.1969	1.0396
0.55	0.2054	1.0851	0.2052	1.0840
0.70	0.2064	1.0903	0.2071	1.0958
0.85	0.2054	1.0850	0.2067	1.0914
1.00	0.2037	1.0761	0.2054	1.0845
1.50	0.2000	1.0565	0.2010	1.0618
2.50	.0.1950	1.0301	0.1955	1.0338
5.00	0.1909	1.0084	0.1913	1.0106
7.67	NA	NA	0.1898	1.0026

Table 3.1: Variation of Strouhal number for both the free slip (Froude number 0.00) and Froude number 0.20 cases. The Reynolds number for each case is 180.

from the adjacent surface will vary in accordance with this length.

As figure (3.1) illustrates, the rises in the Strouhal number observed in the current investigation are less than 10% and compare well with those found by Angrilli et al. (1982). However, others such as Price et al. (2000) have noted changes in the Strouhal number of order 40%, while Miyata et al. (1990) observed a change of approximately 50%.

For the no-slip cases, all authors noted that the maximum increase in Strouhal number occurred for gap ratios in between 0.40 and 0.75, while Miyata et al. (1990) (who looked at flow past a cylinder close to a free surface) observed that the change occurred at a gap ratio of about 0.35. It is suggested here that the results of Miyata et al. (1990) for gap ratios less than 0.35 are in the range at which limited or no shedding occurs, and hence the frequency detected from their spectra is not a shedding frequency but a frequency of flow structure adjustment. This assertion

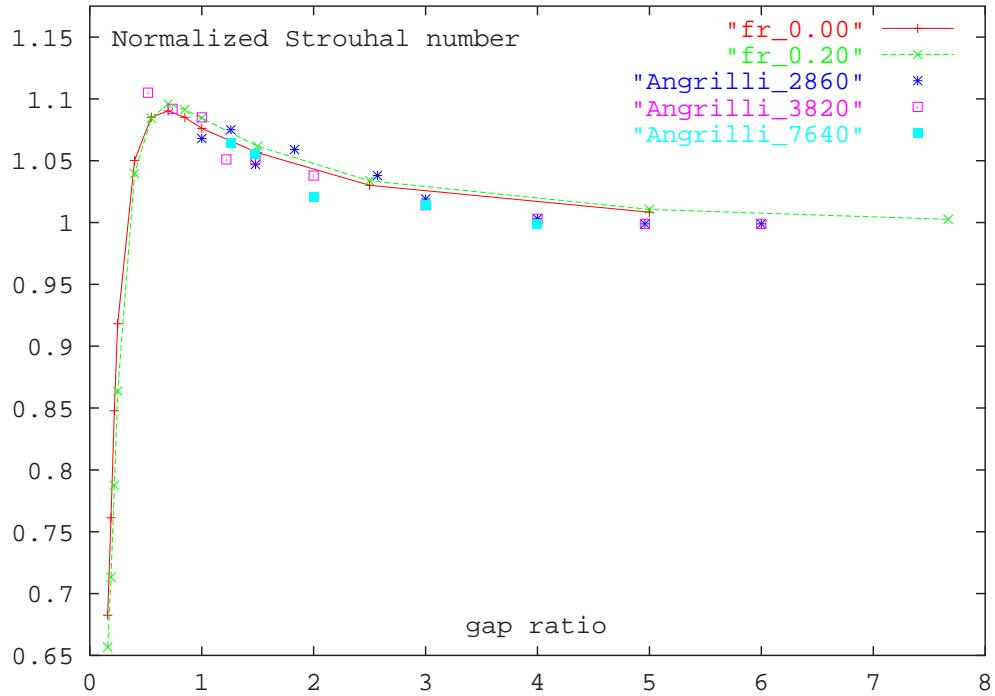


Figure 3.1: Plot showing the variation of normalized Strouhal number (normalized with respect to Strouhal number of the reference cylinder i.e. $\frac{St}{St_0}$) with gap ratio for Froude numbers of 0.00 and 0.20. The Reynolds number for each case is 180. The labels *Angrilli_2860*, *Angrilli_3820* and *Angrilli_7640*, refer to the results of Angrilli *et al.* (1982) at three different Reynolds numbers, namely 2860, 3820 and 7640.

will be discussed later in the section dealing with the suppression of vortex shedding.

One of the key points to note is the similarity between the results at the two different Froude numbers, with a good agreement being observed over the entire gap ratio range. This suggests that the almost negligible surface curvature (which is illustrated later in the chapter) has little effect on the period of vortex shedding.

3.3 Lift, Drag and Moment Coefficients

The forces and moments acting upon the cylinder are of interest as they have direct relevance to the design and construction of a variety of offshore structures and vehicles. They are also important as they provide a point of comparison between the current results and those of others.

3.3.1 Lift Coefficient

Miyata et al. (1990) find that the mean lift coefficient increases as the gap ratio decreases, with the maximum lift being measured when the cylinder just pierces the surface (i.e. at a gap ratio of 0.00). Their observation that the lift continuously increases as the gap ratio decreases is consistent with the results of Roshko et al. (1975), and Lei et al. (1999). Such trends are also observed here, with the mean lift coefficient obtaining its maximum value at the smallest gap ratio considered, namely 0.10. The favourable comparison between the current results and those of Miyata et al. (1990), Roshko et al. (1975), and Lei et al. (1999) are shown in figure (3.2). The results of Lei et al. (1999) suggest that the boundary layer plays an important part in the determination of the lift, with their results for boundary layers generated using cylinders, producing negative lift (positive in the orientation used here) at some gap ratios. Roshko et al. (1975) also notes that the shape of the body has a notable impact on the behaviour of the lift coefficient, with a triangular section producing different lift behaviour.

3.3.2 Root Mean Square (RMS) Lift Coefficient

Lei et al. (1999) suggest that the onset or suppression of vortex shedding is more clearly illustrated if the behaviour of the Root-Mean-Square (RMS) lift coefficient is considered. Figure (3.3) illustrates the agreement in the trend between the current results and those of Lei et al. (1999) for their thinner boundary layer (boundary layer 1) case, although a notable horizontal shift is observed. This shift is likely due to the changes in the adjacent boundary condition, which for the case of the no-slip boundary effectively moves the surface closer. In other words, if one assumes that the boundary layer for the no-slip case only exerts an influence extending over its own boundary layer thickness, then the free surface and no-slip surface results should be comparable when a quantity resembling this boundary layer thickness is subtracted from the gap ratio.

The major differences between the current findings and those of Lei et al. (1999) are all observed for the cases in which the cylinder is close to the adjacent surface. In this region, Lei et al. (1999) note that the RMS lift drops to a point and then stays relatively constant, with a slight increase noted as the gap ratio is further reduced. For the free slip and free surface cases considered here, this plateauing of the RMS lift coefficient is not observed and it is the altered boundary conditions at the surface that are believed to be responsible for this difference.

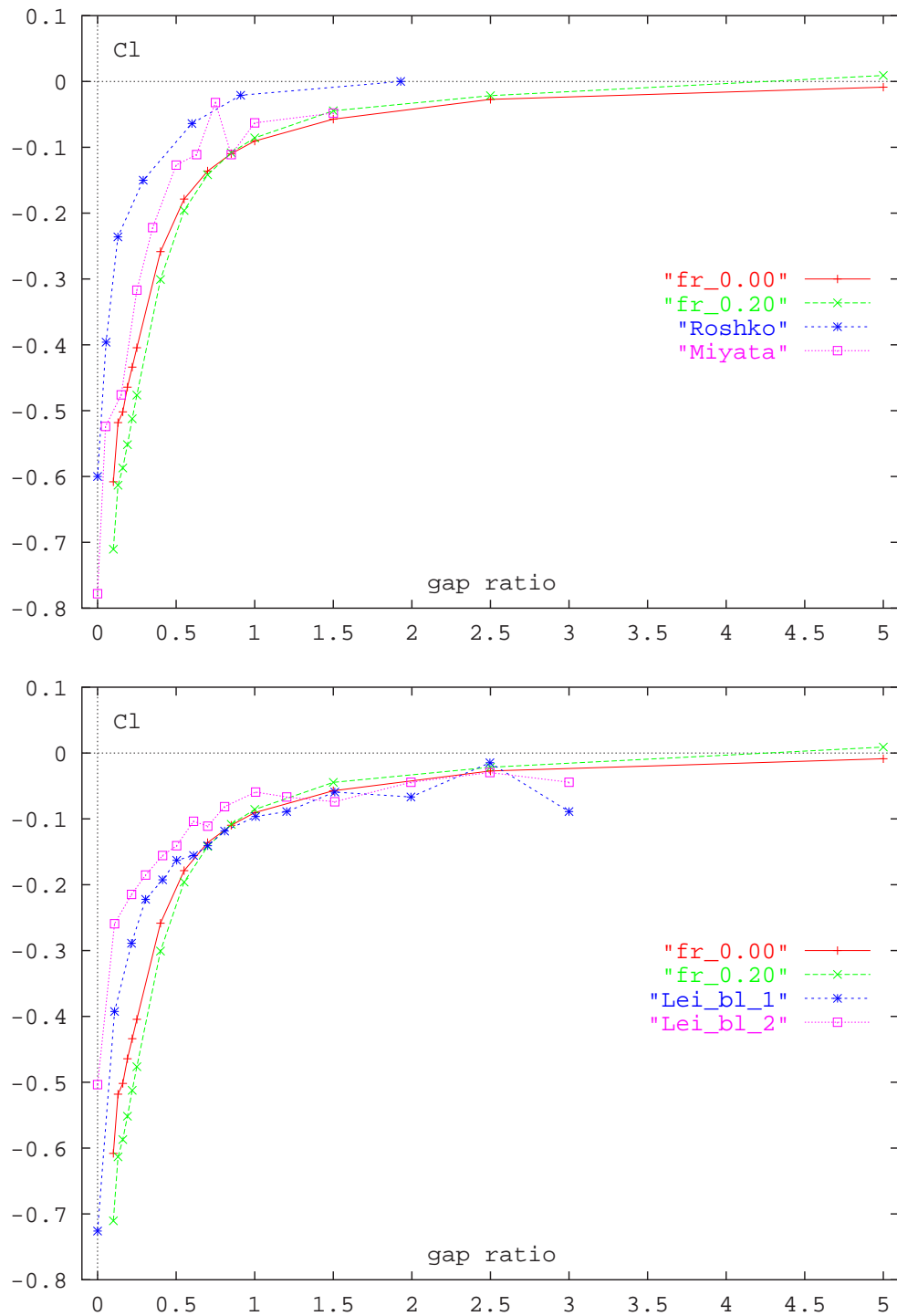


Figure 3.2: Plots showing the variation of the mean lift coefficient with gap ratio for the free slip (Froude number 0.00) and Froude number 0.20 cases. The Reynolds number for each case is 180. Also plotted are the results of Roshko *et al.* (1975), Miyata *et al.* (1990) and Lei *et al.* (1999) (the results from Lei *et al.* (1999) are for their boundary layers 1 and 2).

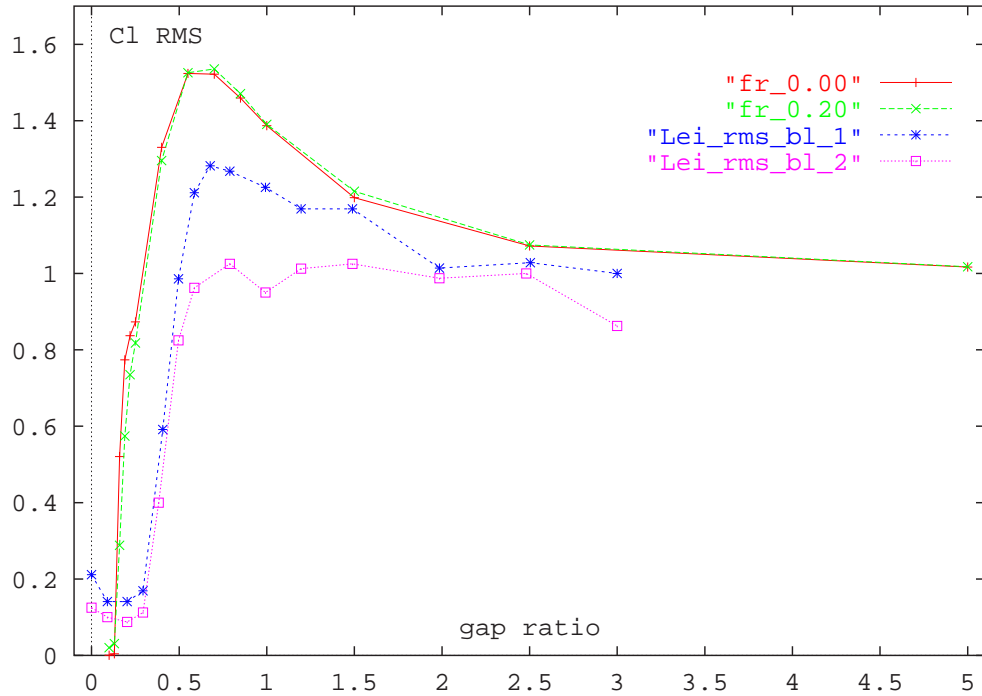


Figure 3.3: Plot showing the variation of RMS lift coefficient with gap ratio for the free slip (Froude number 0.00) and Froude number 0.20 cases. The Reynolds number for each case is 180. Also plotted are the results of Lei *et al.* (1999) (for their boundary layers 1 and 2).

3.3.3 Drag Coefficient

The variation of the normalized drag coefficient with gap ratio and its comparison with the results of Lei *et al.* (1999), Miyata *et al.* (1990) and Roshko *et al.* (1975) are shown in figure (3.4). The current results differ from those observed by Miyata *et al.* (1990) with regard to both magnitude of the drag changes and with respect to the trend in its behaviour at smaller gap ratios. The current study suggests that the drag continues to decrease as the cylinder is moved closer to the free surface, while the results of Miyata *et al.* (1990) suggest that the drag drops to a point, and then it gradually decreases from that point onward. The general trends observed here do however, compare more favourably with those of Lei *et al.* (1999) and Roshko *et al.* (1975), with the drag in all of these cases exhibiting a peak at a gap ratio close to 0.50.

It should be noted that the drag values of the other authors were normalized with respect to the drag at the largest gap ratio they considered. Hence some degree of vertical translation may have been introduced, although this will not effect the trends in the behaviour. The differences observed in the trends are again for the cases in which the cylinder is at close proximity to the surface, so the altered boundary condition will play a larger role in this region. Although this

does not explain the differences between the current results and those of Miyata et al. (1990). An interesting point to note from the results of Lei et al. (1999) is the slight reversal of the trend in drag coefficient for the thinner boundary layer cases as the cylinder gets very close to the surface. This alteration in the behaviour is likely to be due to the influence of the wall boundary layer.

The magnitude of the forces acting upon the cylinder are also significantly larger here, than those observed for flow past a no-slip wall. Such differences in the magnitude appear to be related to the free surface, with other free surface investigations such as the one conducted experimentally by Valluri (1996) also displaying this behaviour. Valluri (1996) considers flow past a flat circular disk placed close to a free surface, and notes that the change in the normalized drag for the case near a free surface, is significantly larger than that near a no-slip wall. The size of this magnitude difference is substantial, with Valluri (1996) finding the peak normalized mean drag being of order 1.25 for the free surface, while for the no-slip surface it was approximately 1.08. The trends observed by Valluri (1996) are reproduced here in figure (3.5).

3.3.4 RMS Drag Coefficient

The behaviour of the normalized RMS drag coefficient is shown in figure (3.6). The first point to note is the significant increase in the time varying drag force acting upon the cylinder, with the results at both Froude numbers indicating an increase of roughly 600% (i.e. the RMS drag measured for the cylinder close to the free surface is 600% larger than that for a fully submerged cylinder). It is believed that these changes may in part be attributed to the time-dependent shift in the position of the stagnation and separation points, with the larger angular shift associated with the front stagnation point during the course of one shedding cycle, exposing a larger portion of the cylinder to the front stagnation pressure. Thus increasing the time-dependent magnitude of the drag experienced by the cylinder.

3.3.5 Mean Moment Coefficient

The moment acting upon the cylinder is also of interest, as the tendency for the cylinder to spin could have a large impact on the behaviour of an unrestrained cylinder close to a free surface. The moments behaviour may also provide some assistance in explaining the observed vorticity distribution and its relationship to the lift and drag forces acting upon the cylinder (as the moment is due solely to viscous effects and it is thus likely to illustrate changes in

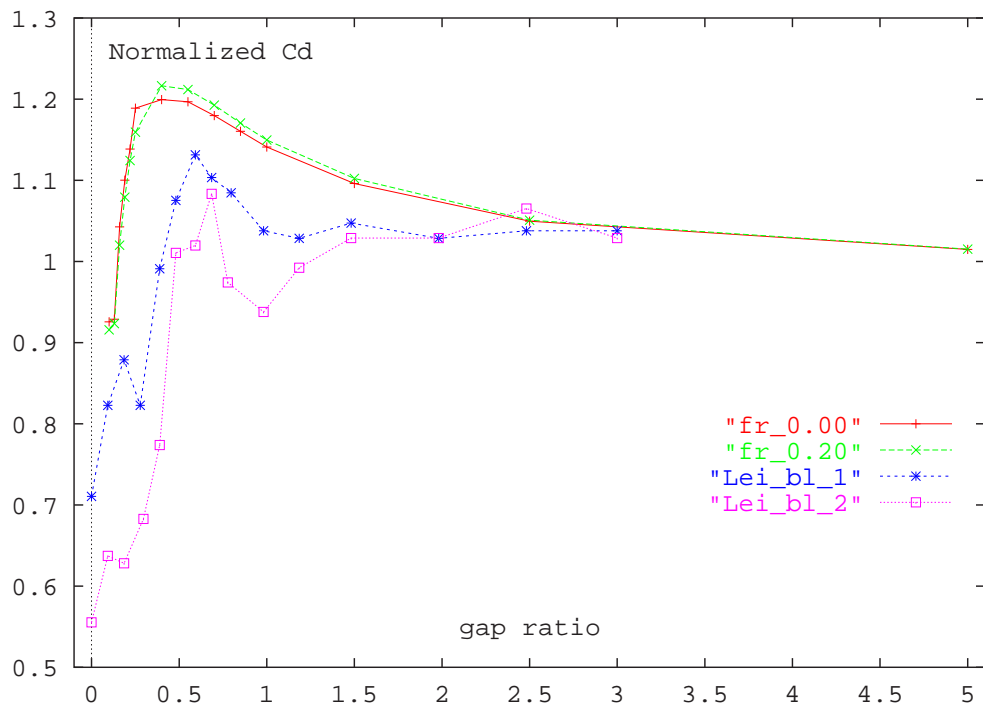
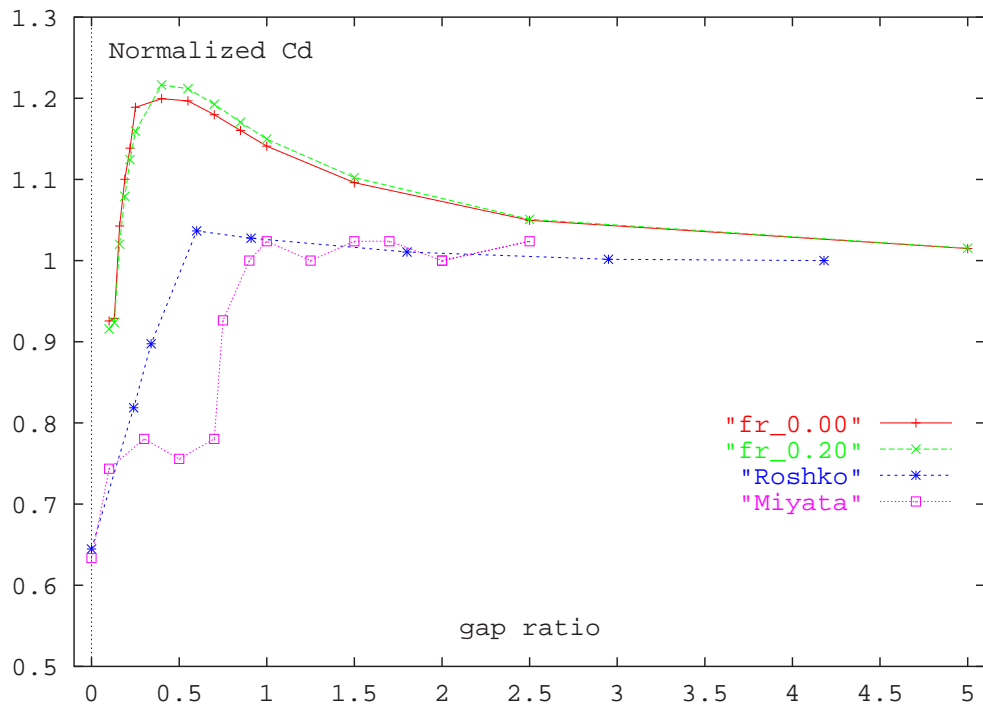


Figure 3.4: Plot showing the variation of normalized mean drag coefficient with gap ratio for the free slip (Froude number 0.00) and Froude number 0.20 cases. The Reynolds number for each case is 180. Also plotted are the results of Roshko *et al.* (1975), Miyata *et al.* (1990) and Lei *et al.* (1999) (for their boundary layers 1 and 2).

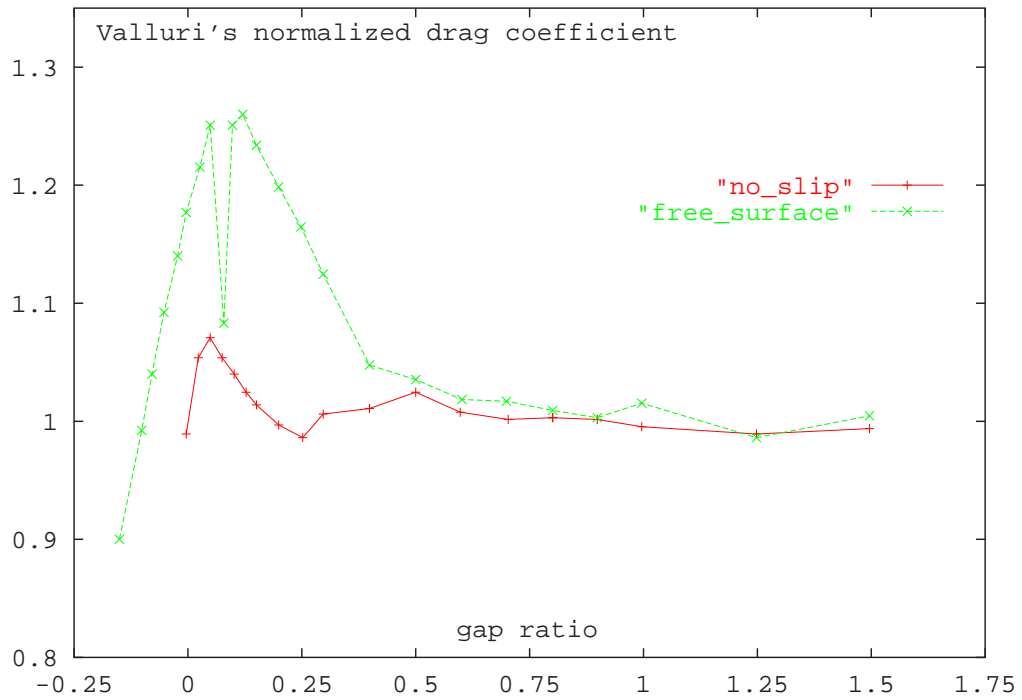


Figure 3.5: Valluri's (1996) normalized drag data for flow past a flat disk close to both a no-slip and free surface.

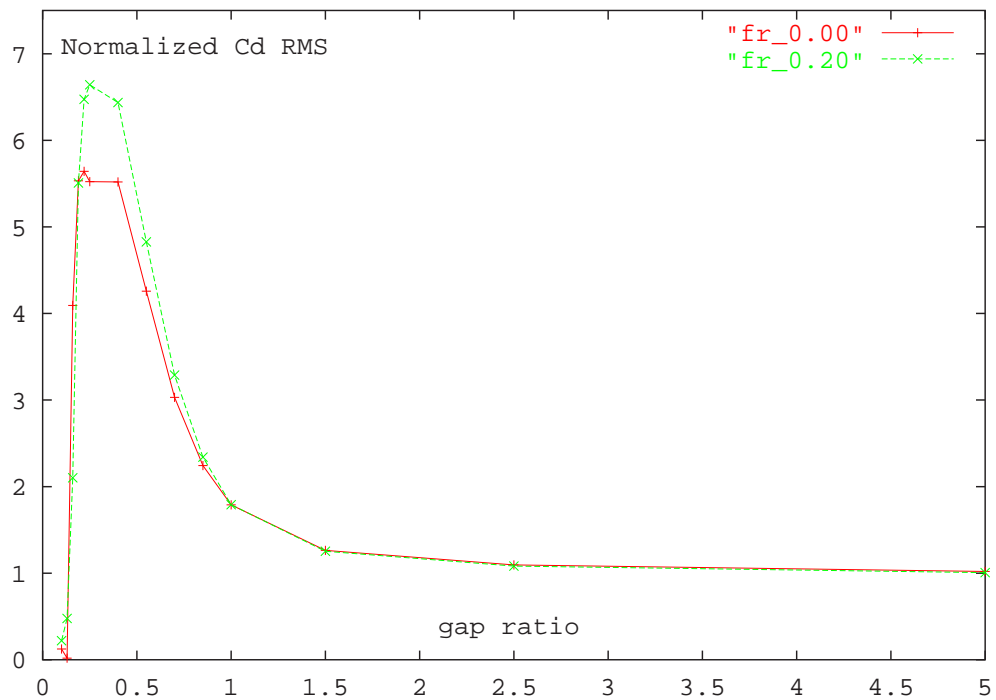


Figure 3.6: Variation of the normalized RMS drag coefficient with gap ratio for the free-slip (Froude number 0.00) and Froude number 0.20 cases. The Reynolds number for each case is 180.

the position of the separation points). White (1994) has shown using potential theory, that a spinning cylinder will produce a non zero mean lift. Thus it would seem plausible that a flow field which results in a non zero mean lift, will also result in a non zero mean moment. The variation of the mean moment coefficient with gap ratio for both Froude numbers is shown in the figure (3.7).

While the magnitude of the moments measured are expected to change with Reynolds number, it is the sign and the trends which are important here. What is clearly discernible from figure (3.7), is the tendency for the cylinder to possess a positive mean moment coefficient when the cylinder is close to the surface. This result and the potential result in White (1994) compare favourably with the observations, in that the theory suggests that there should exist a mean force directed away from the surface (i.e. there should exist a negative mean lift) when there is a positive mean moment. While the potential flow results cannot support the possibility of separation, as the influence of viscosity is ignored, they do suggest that the angular distance between the stagnation and separation points is likely to vary, as the angle between the two ideal stagnation points (those at the front and rear of the cylinder) become unequal. Hence one would expect changes in the moment to be related to changes in both the positions of the stagnation and separation points.

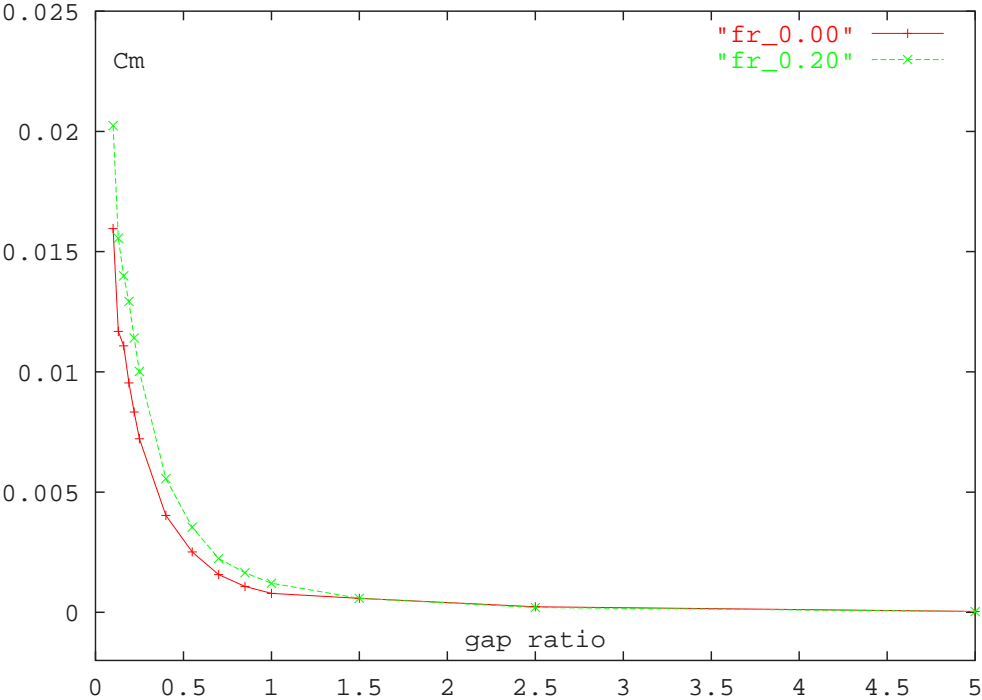


Figure 3.7: Variation of the mean moment coefficient with gap ratio for the free-slip (Froude number 0.00) and Froude number 0.20 cases. The Reynolds number for each case is 180.

3.4 Pressure Distribution, and the Stagnation and Separation Points

The presence of the adjacent surface will in general result in a redistribution of the pressure field, with such a redistribution coinciding with a shift in both the stagnation and separation points. These shifts are intrinsically tied to the changes observed in both the lift and drag, as the pressure profiles on the surface of the cylinder in figures (3.8) and (3.9) indicate.

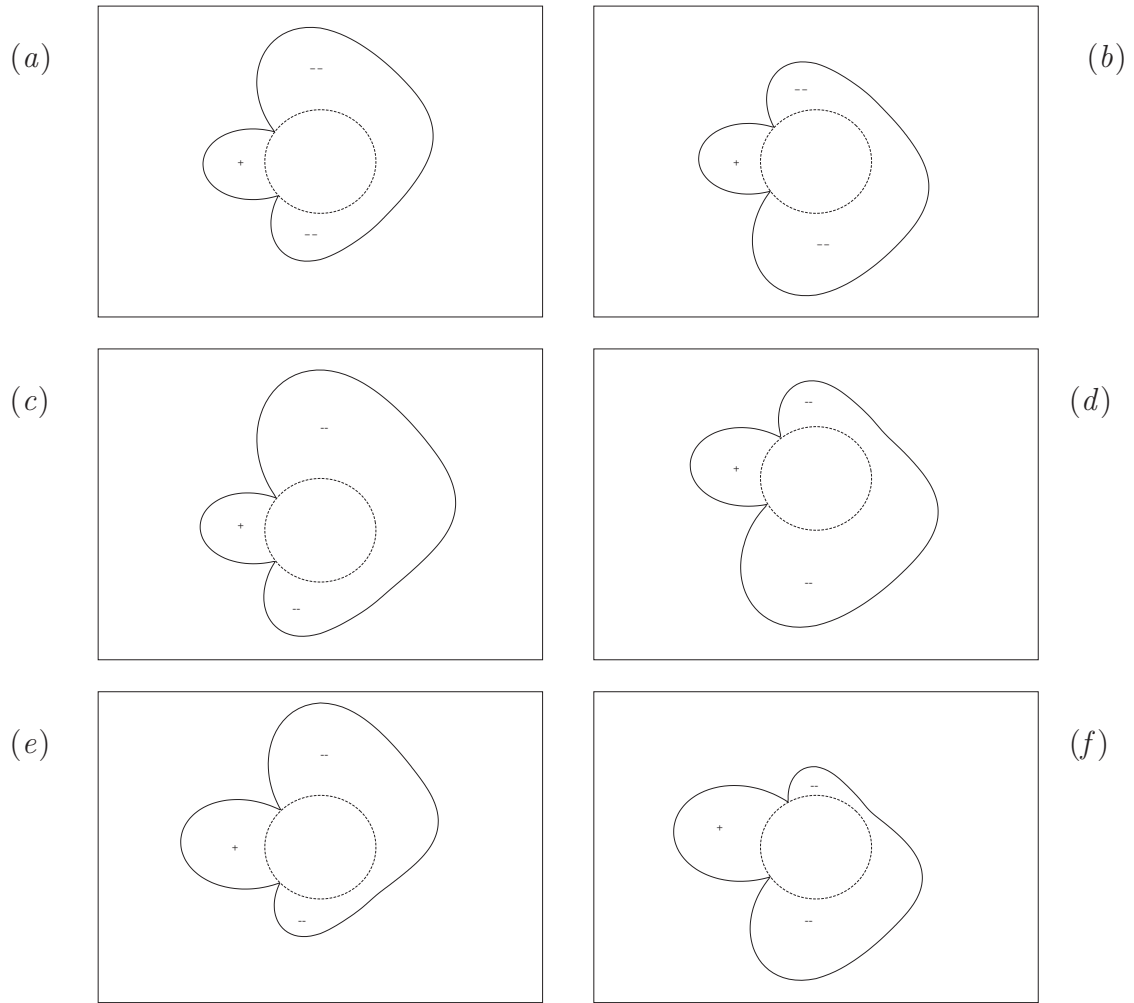


Figure 3.8: Plot showing the pressure distributions around the cylinder. All figures on the left are at maximum lift while those on the right are at minimum lift. The cases shown from top to bottom are: the reference cylinder (fully submerged) (a and b), and the cylinder at a gap ratio of 0.70 for the slip (Froude number 0.00) (c and d) and free surface (Froude number 0.20) (e and f) cases. The Reynolds number for each case is 180.

What also becomes clearly apparent are the changes in the relative magnitude of the pressure

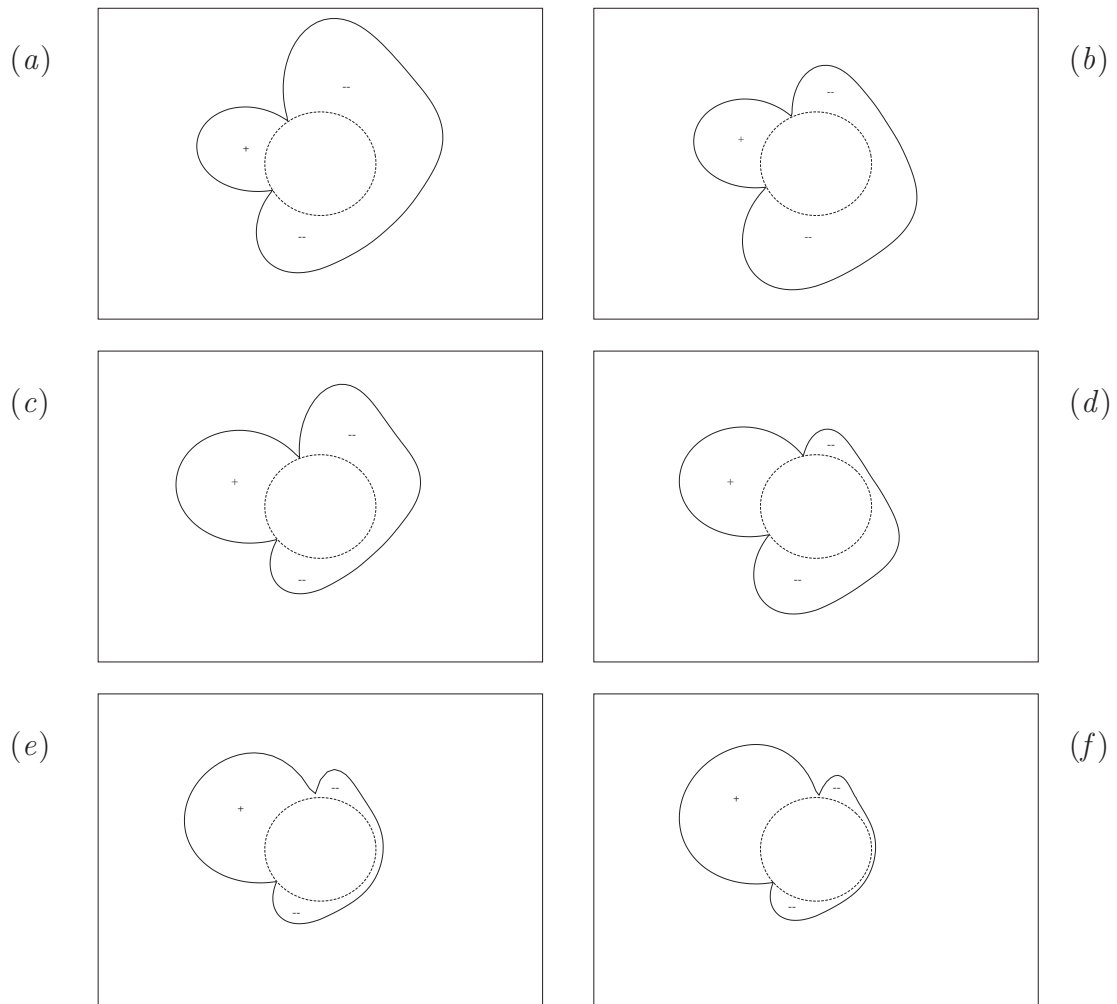


Figure 3.9: Plot showing the pressure distributions around the cylinder. All figures on the left are at maximum lift, while those on the right are at minimum lift, except for the cases in which no shedding was observed (e and f). Cases shown are: free slip (Froude number 0.00) at a gap ratio of 0.25 (a and b), free surface (Froude number 0.20) at a gap ratio of 0.25 (c and d), and the free slip (e) and free surface (f) cases at a gap ratio of 0.10. The results shown are all for a Reynolds number of 180.

distribution around the cylinder with gap ratio. For the smaller gap ratio cases (particularly those in which shedding has ceased) there is dominant high pressure region in the upper section at the front of the cylinder and relatively small pressure differences everywhere else. This suggests that the increasing lift and decreasing drag observed as the gap ratio is reduced is primarily due to the rotation of the front stagnation point. For these conditions the stagnation region now contributes more to lift and less to drag, than would otherwise be the case for a fully submerged cylinder.

For the cases involving the free surface, it should be noted that the pressure distribution was

obtained via direct measurement of the pressure around the cylinder, including the component due to the body forces. A cylinder subject to the same body force but with no flow, was used as a point of reference to then remove the body force contribution. It is expected that this approach will have a tendency to highlight regions in which the surface deformation is non-negligible.

The behaviour of the separation and stagnation points is also of interest, as these values shift with the cylinders proximity to the surface. Before proceeding to measure the angular shift in both the stagnation and separation points with gap ratio, it is first necessary to compare the results obtained for a fully submerged cylinder with those observed by others. Both Dimopoulos & Hanratty (1968) (experimental investigation) and Shariff et al. (1991) (numerical investigation) give details with regard to the position of these points. The findings of Dimopoulos & Hanratty (1968) indicate that the position of the top separation point for a cylinder at a Reynolds number of 180 is approximately 115 to 116 degrees (with these values being read from a graph in which a line of best fit was drawn). This agrees reasonably well with the value measured here, in which the top separation point shifts between a value of 109 and 117 degrees. Shariff et al. (1991) also study a cylinder at a Reynolds number of 180 (which is the same value used in the current investigation) and indicate that the angular difference between the two separation points is approximately 132 degrees (a result which was also measured from a graph). The present study gives 135 degrees for the angle between the two separation points, which indicates agreement to within 2.27%. The angular convention used for the measurement of the stagnation and separation points is shown in figure (3.10), while tables (3.2) and (3.3) show the variation of these points with gap ratio.

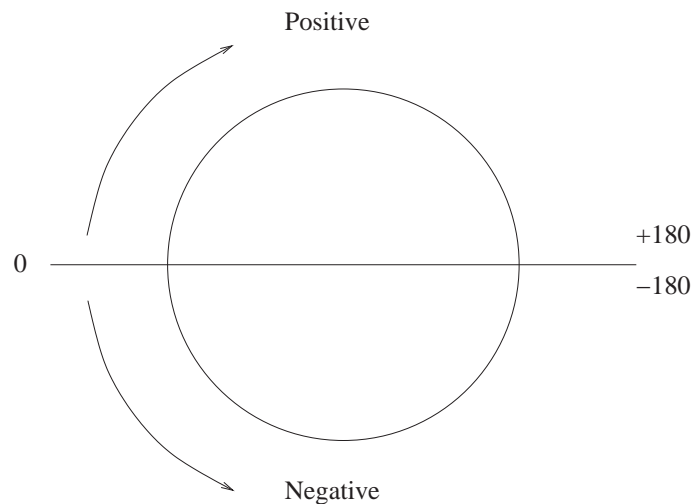


Figure 3.10: Schematic showing the angular convention used for the measurement of the stagnation and separation points.

gap ratio	θ_{1max}	θ_{2max}	θ_{3max}	θ_{4max}	θ_{1min}	θ_{2min}	θ_{3min}	θ_{4min}
0.10	25.03	125.00	-98.32	-167.42	25.03	125.00	-98.32	-167.42
0.13	22.09	123.32	-98.78	-168.72	22.09	123.32	-98.78	-168.72
0.16	18.28	122.16	-100.22	-136.73	20.67	122.88	-101.65	157.72
0.19	15.77	121.84	-101.44	-135.31	19.24	122.56	-103.53	152.38
0.22	13.98	121.65	-102.63	-135.67	17.68	122.15	-104.58	151.11
0.25	12.55	121.49	-103.54	-135.91	16.30	121.74	-105.35	150.40
0.40	7.20	120.31	-105.32	-134.48	12.38	119.64	-109.65	145.06
0.55	4.33	119.76	-106.14	-134.05	9.93	117.80	-112.37	141.98
0.70	2.79	119.70	-106.73	-134.55	8.19	116.42	-113.51	140.39
0.85	1.85	119.55	-107.20	-135.11	6.82	115.13	-114.17	139.66
1.00	1.25	119.47	-107.39	-135.79	5.73	114.06	-114.61	139.52
1.50	0.42	118.48	-108.13	-137.37	4.16	112.31	-114.84	139.61
2.50	-0.54	117.05	-108.90	-138.59	2.72	110.75	-115.32	140.09
5.00	-1.24	116.30	-109.53	-139.19	1.96	110.13	-115.72	139.91
REFERENCE	-1.57	115.79	-109.50	-139.59	1.59	109.56	-115.72	139.53

Table 3.2: Angular variation of the stagnation and separation points with gap ratio at the point of both maximum and minimum lift for a Froude number of 0.00. The Reynolds number for each case is 180.

The tables also show the shift in these values as the proximity of the cylinder to the surface is altered. As discussed by Rosenhead (1963) and Blackburn & Henderson (1995), the separation and attachment points must always occur in pairs. Thus it is expected that there will be at least two attachment and two separation points at both the point of maximum and minimum lift (with three pairs being seen at some other stages in the shedding cycle). The trends for the behaviour of these points are shown graphically in figures (3.11) to (3.13).

With regard to the angular difference between the front stagnation point and the separation points, clear differences are seen between the current work and that of Bearman & Zdravkovich (1978), who mention that the angle between the two separation points remained constant as the cylinder was moved closer to the boundary. The current study indicates that the size of the wake varies slightly with gap ratio while also varying with time. This variation is illustrated in figures (3.14) to (3.16) and while the difference angles do remain constant at larger gap ratios, at smaller ones they vary quite significantly. An interesting point to note at a gap ratio of 0.25,

gap ratio	θ_{1max}	θ_{2max}	θ_{3max}	θ_{4max}	θ_{1min}	θ_{2min}	θ_{3min}	θ_{4min}
0.10	28.88	125.97	-98.07	-167.30	28.88	125.97	-98.07	-167.30
0.13	24.26	123.56	-99.20	-168.29	24.26	123.56	-99.20	-168.29
0.16	21.80	123.29	-99.25	-146.09	22.68	123.96	-99.47	176.69
0.19	18.83	123.25	-100.64	-135.77	21.18	123.69	-101.89	155.05
0.22	16.69	123.29	-101.65	-135.17	19.31	123.67	-103.43	151.45
0.25	14.70	123.16	-102.69	-135.31	17.76	123.53	-104.29	150.09
0.40	8.70	122.05	-104.72	-134.55	13.22	121.59	-108.56	144.64
0.55	5.33	120.96	-105.87	-133.93	10.62	119.33	-111.66	141.70
0.70	3.54	120.34	-106.41	-134.49	8.79	117.55	-112.97	140.09
0.85	2.49	119.92	-106.83	-135.17	7.36	115.88	-113.76	139.33
1.00	1.78	119.45	-107.19	-135.79	6.29	114.58	-114.09	139.21
1.50	0.53	118.03	-107.97	-137.27	4.29	112.26	-114.49	139.32
2.50	-0.52	116.71	-108.62	-138.54	2.78	110.60	-114.93	139.88
5.00	-1.22	116.02	-109.23	-139.22	1.96	109.86	-115.44	139.86
REFERENCE	-1.57	115.79	-109.50	-139.59	1.59	109.56	-115.72	139.53

Table 3.3: Angular variation of the stagnation and separation points with gap ratio at the point of both maximum and minimum lift for a Froude number of 0.20. The Reynolds number for each case is 180.

is that the angular difference between the front stagnation point and the top separation point at maximum lift approaches a value close to that of the reference cylinder at the opposite extreme of the lift cycle. That is, the angle between stagnation and top separation point at maximum lift at a gap of 0.25, is similar in magnitude to the difference between front stagnation and the top separation point for the reference cylinder at the point of minimum lift.

3.5 Surface Deformation

Another point of interest is the relation between the surface curvature and the gap ratio. The problem being considered here is predominantly distinguished from that of a standard cylinder by the interaction or feedback between the free surface and the instability associated with the cylinder wake. For the most part, bluff body flows may be loosely characterized as follows: the bulk flow sets up a boundary layer, the boundary layer then adjusts the bulk flow field, which

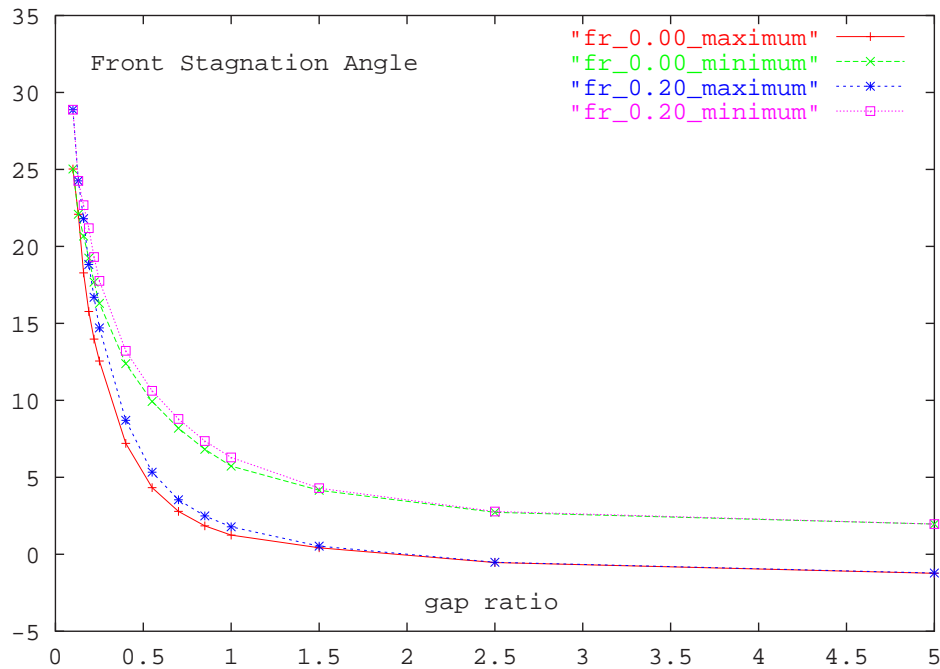


Figure 3.11: Plot showing the variation in the stagnation angle with gap ratio for Froude numbers of 0.00 and 0.20. The Reynolds number for each case is again 180.

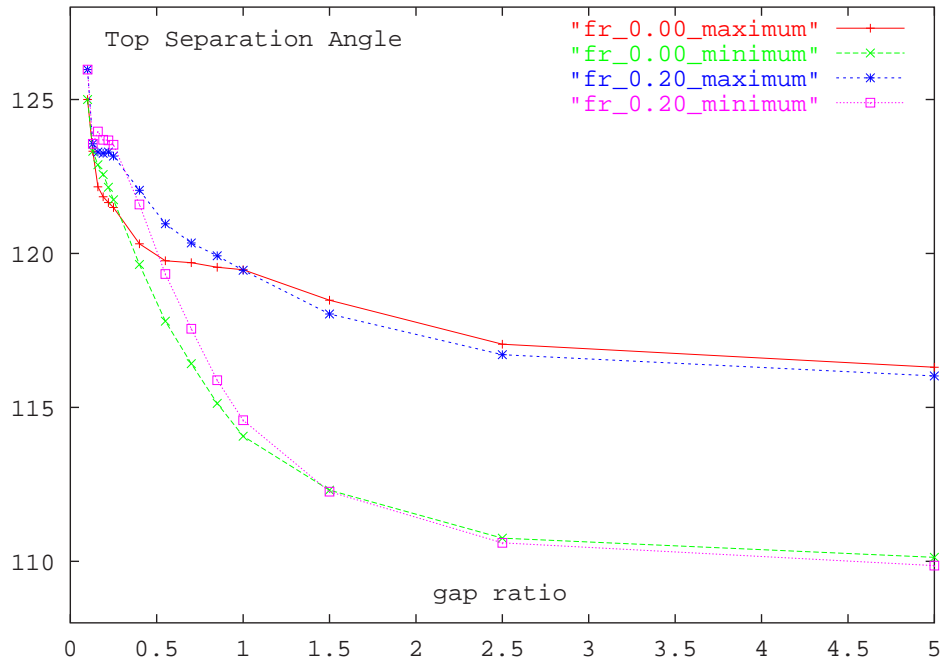


Figure 3.12: Plot showing the variation in the top separation angle with gap ratio for Froude numbers of 0.00 and 0.20. The Reynolds number for each case is again 180.

in turn alters properties such as the lift and drag acting upon the body. For the case in which a free surface is present, the adjustment stage is more complex as the surface acts in a manner

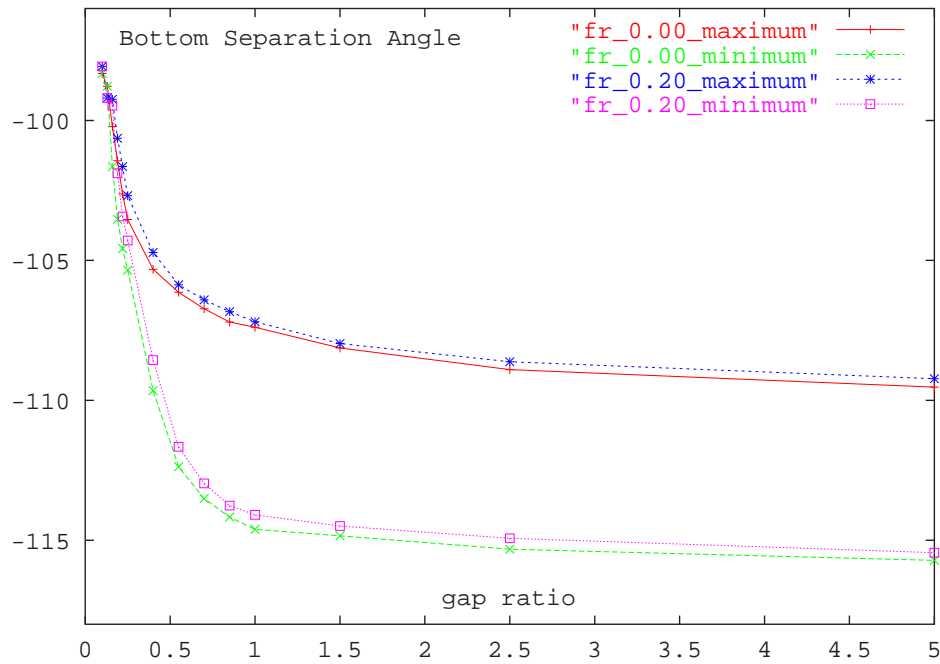


Figure 3.13: Plot showing the variation in the bottom separation angle with gap ratio for Froude numbers of 0.00 and 0.20. The Reynolds number for each case is 180.

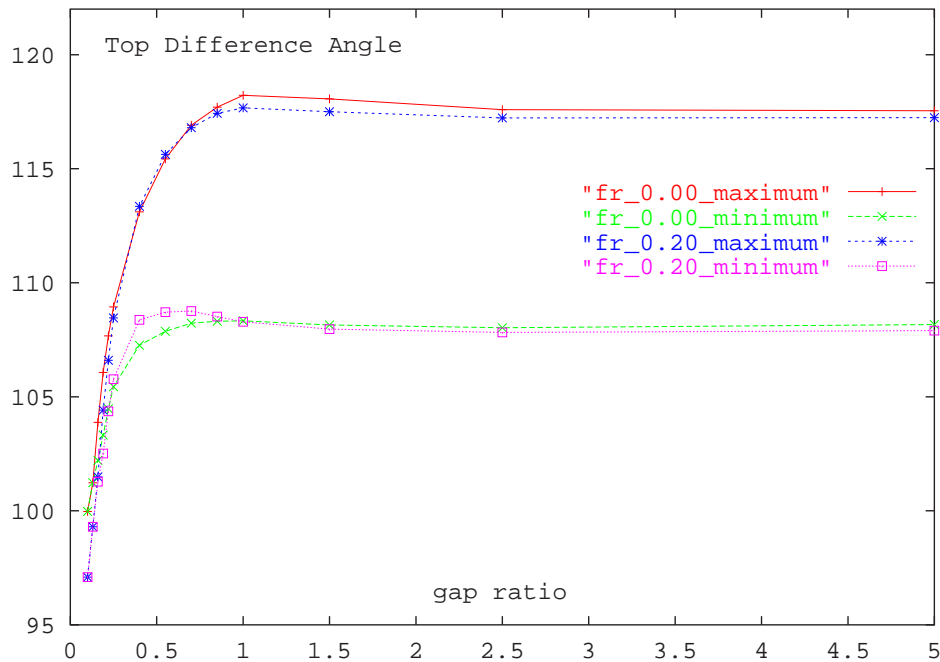


Figure 3.14: Plot showing the angular difference between the front stagnation point and the top separation point for Froude numbers of 0.00 and 0.20. The Reynolds number for each is 180.

similar to the boundary layer in that it exerts a controlling influence on the flows behaviour. The influence of the free surface is then governed by an additional parameter set, namely the

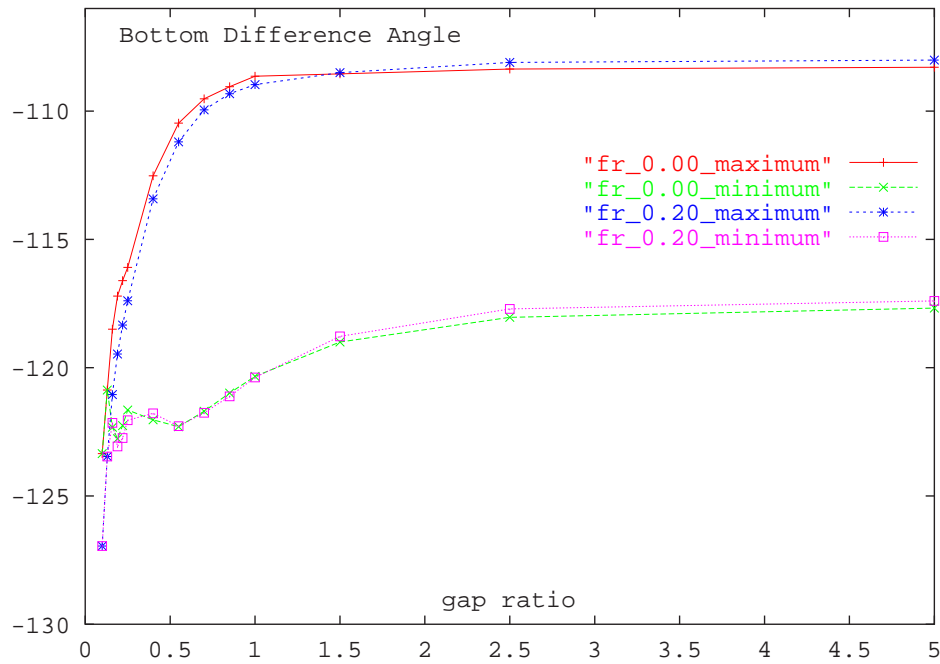


Figure 3.15: Plot showing the angular difference between the front stagnation point and the bottom separation point for Froude numbers of 0.00 and 0.20. The Reynolds number for each case is 180.

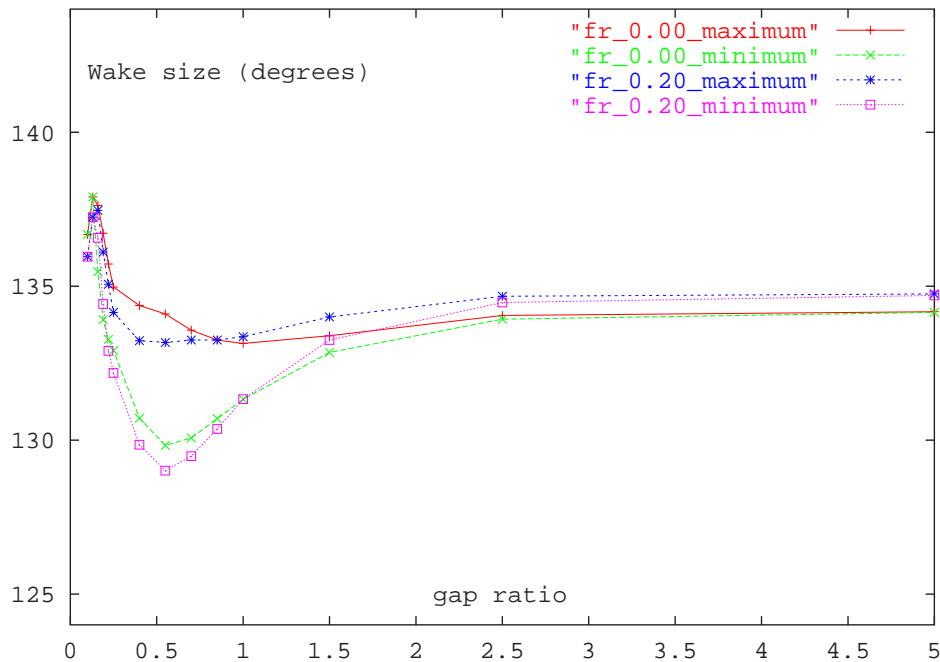


Figure 3.16: Plot showing the angular difference between the two separation points (i.e. wake size) for Froude numbers of 0.00 and 0.20. The Reynolds number for each case is 180.

Froude number. However, as figure (3.17) indicates, for the Froude numbers considered here the surface remains relatively flat and this interaction is limited.

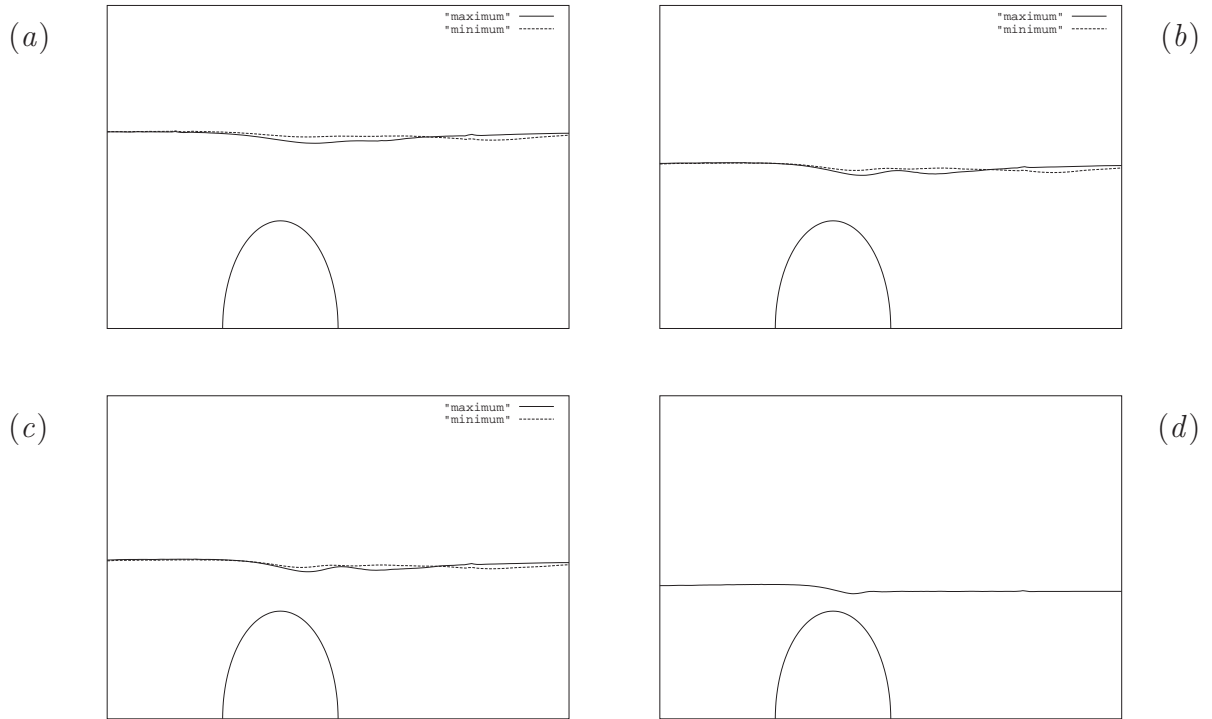


Figure 3.17: Rescaled surface profiles for gap ratios of 0.40 (a), 0.25 (b) and 0.22 (c) at both the point of maximum and minimum lift. The surface position at a random instant in time for a gap ratio of 0.10 is shown in (d). The Reynolds number for each case is 180.

3.6 Formation Length

The behaviour of the formation length may help to explain why the RMS components of the lift and drag all initially increase as the gap ratio is reduced, but later decrease as it is reduced further. Traditionally for bodies in which the flow field is predominantly symmetric, the formation length was estimated by considering the point along a line of symmetry at which the standard deviation in the vertical velocity was a maximum (see Griffin (1995) for a more detailed discussion of the calculation of the formation length). As the flow field considered here has an inherent asymmetry introduced by the presence of the free surface, there is no obvious line of symmetry and hence a larger region of the flow must be considered. To estimate the formation length three different approaches were used. The first simply involved calculating the standard deviation of the vertical velocity component at every point in the flow field and then locating

the point at which this was a maximum. The second approach was similar, but it involved calculating the point of the maximum standard deviation in the velocity azimuthal to the cylinder. The third method was slightly different as it involved calculating the point (away from the body) at which the standard deviation in the vorticity was a maximum. The first two methods yielded similar positions, while the third produced points closer to the cylinder. However, it is the trending behaviour which is the most important and this was found to be similar for all the techniques. The results for the standard deviation in vertical velocity and vorticity are shown in figure (3.18).

It is clear that the increase in RMS components of the lift and drag coincide with the forward movement of the formation length. With regard to the standard deviation of vorticity plot, it is clear that as the gap ratio is reduced the formation length decreases. At submergence depths of 0.85, 0.70 and 0.55 it attains its shortest value, where the closer proximity of the forming vortices (and thus regions of lower pressure) correlate well with the subsequent increase in the magnitude of the time-varying forces acting on the cylinder. As the gap ratio is reduced further, the formation length begins to grow and the RMS components of the forces decrease. At a gap ratio of 0.25 the strength of the vortex shedding weakens quite rapidly and from this gap ratio onward the position of the formation location begins to shift vertically away from the surface. Furthermore, the position of the formation length for the gap ratio 0.16 case, essentially highlights the location at which the positive vortices from the underside of the cylinder roll-up.

It is expected that the formation length observed in the current investigation will differ somewhat from that observed by Sheridan et al. (1997), as the difference in Reynolds number has a significant affect on the formation length of a fully submerged cylinder. For the fully submerged cylinder the behaviour of the formation length initially grows at Reynolds numbers between roughly 200 and 2000, before decreasing again as the Reynolds number is increased further (as discussed by Unal & Rockwell (1988*a*), Lin et al. (1995) and Norberg (1998)).

3.7 Flow Fields

It is perhaps best at this point to examine the behaviour of the flow fields for the range of gap ratios considered.

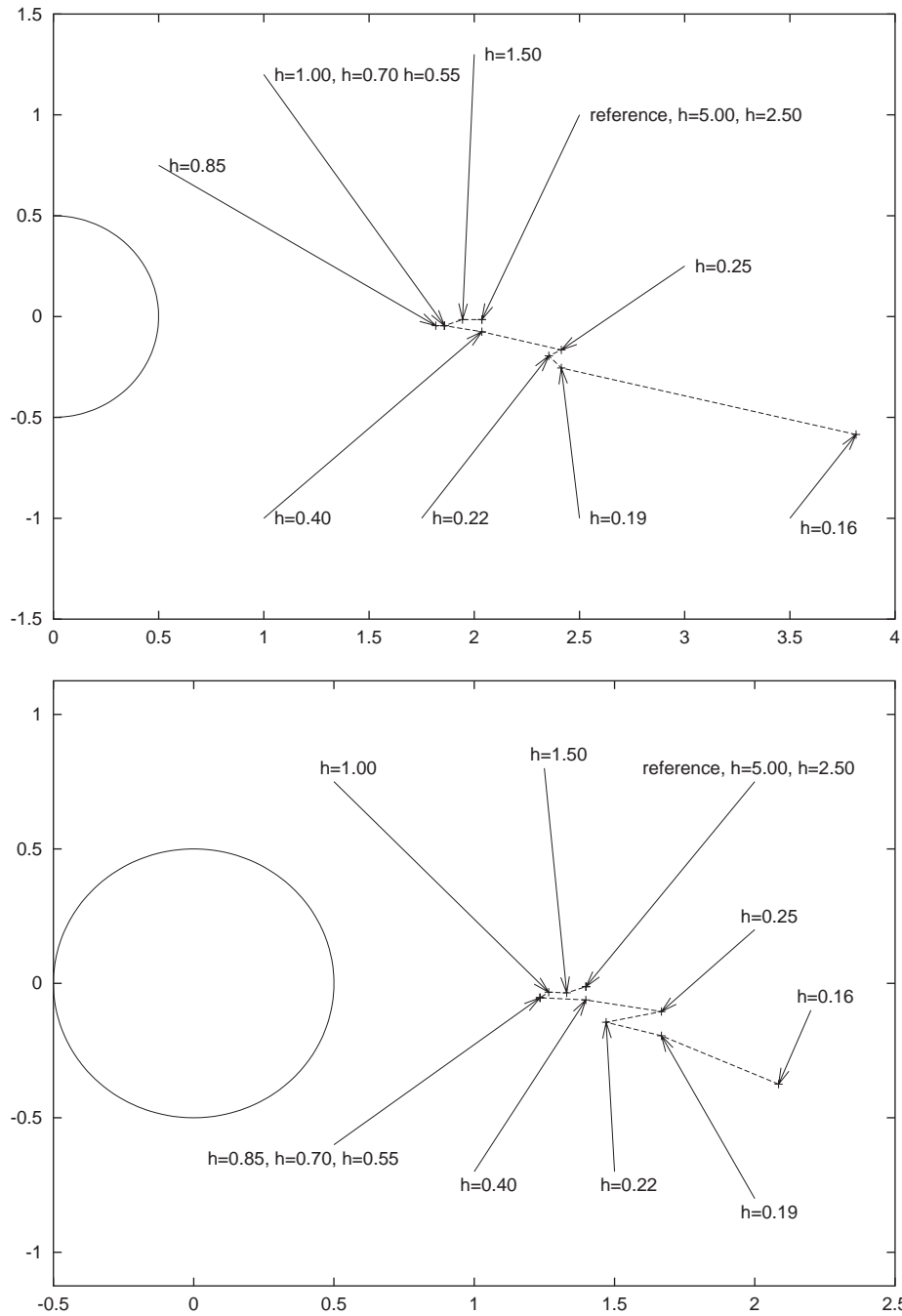


Figure 3.18: Position of the formation length calculated using the standard deviation in the vertical velocity (top) and vorticity (bottom), for a Froude number of 0.20. The Reynolds number for each case is 180.

3.7.1 Gap Ratios 5.00, 2.50, 1.50

At these depths no discernible surface deformation is noted with the lift, drag, moment, Strouhal number, stagnation and separation points and formation length, all tending towards the fully submerged case. The results at these gap ratios were primarily included so as to allow an estimate

of the range over which the observed changes occur. For the most part the measured quantities usually lie within a couple of percent of that of the reference cylinder. This is expected, as depending upon the quantity measured most asymptote towards the reference cylinder values within the ranges suggested by Lei et al. (1999) and Angrilli et al. (1982) (i.e. within two to seven diameters).

3.7.2 Gap Ratios 1.00 to 0.10

This section will now deal with the cases for gap ratios between 1.00 and 0.10 as it is within this range that most of the interesting and significant changes take place. A series of lift plots in figures (3.19) and (3.20) show the progressive influence of the adjacent surface. In particular, the continuous shift in the mean lift which is denoted by the dashed horizontal lines and the variation of the amplitude of the lift trace should be noted. The results shown in these figures are for a Froude number of 0.20, although similar behaviour was also observed for the free-slip case.

It is perhaps best at this point to examine the behaviour of the vorticity field, as it is expected that these plots will highlight the viscous transport of vorticity across the free surface. Figures (3.22) to (3.32) show the vortex street at the point of maximum lift, for both the free slip and free surface case (i.e. Froude number 0.00 and 0.20 cases respectively). As a point of comparison figure (3.21) shows the vorticity field for the reference cylinder at the point of maximum lift. The reader is recommended at this point to examine the videos showing the evolutionary behaviour of the vorticity field, that are contained on the compact disk accompanying this thesis.

It should be noted that very slight surface curvature is observed for some of the free surface cases, and that this curvature typically gives rise to small patches of oppositely signed vorticity near the free surface (as shown in figures (3.28) to (3.32)).

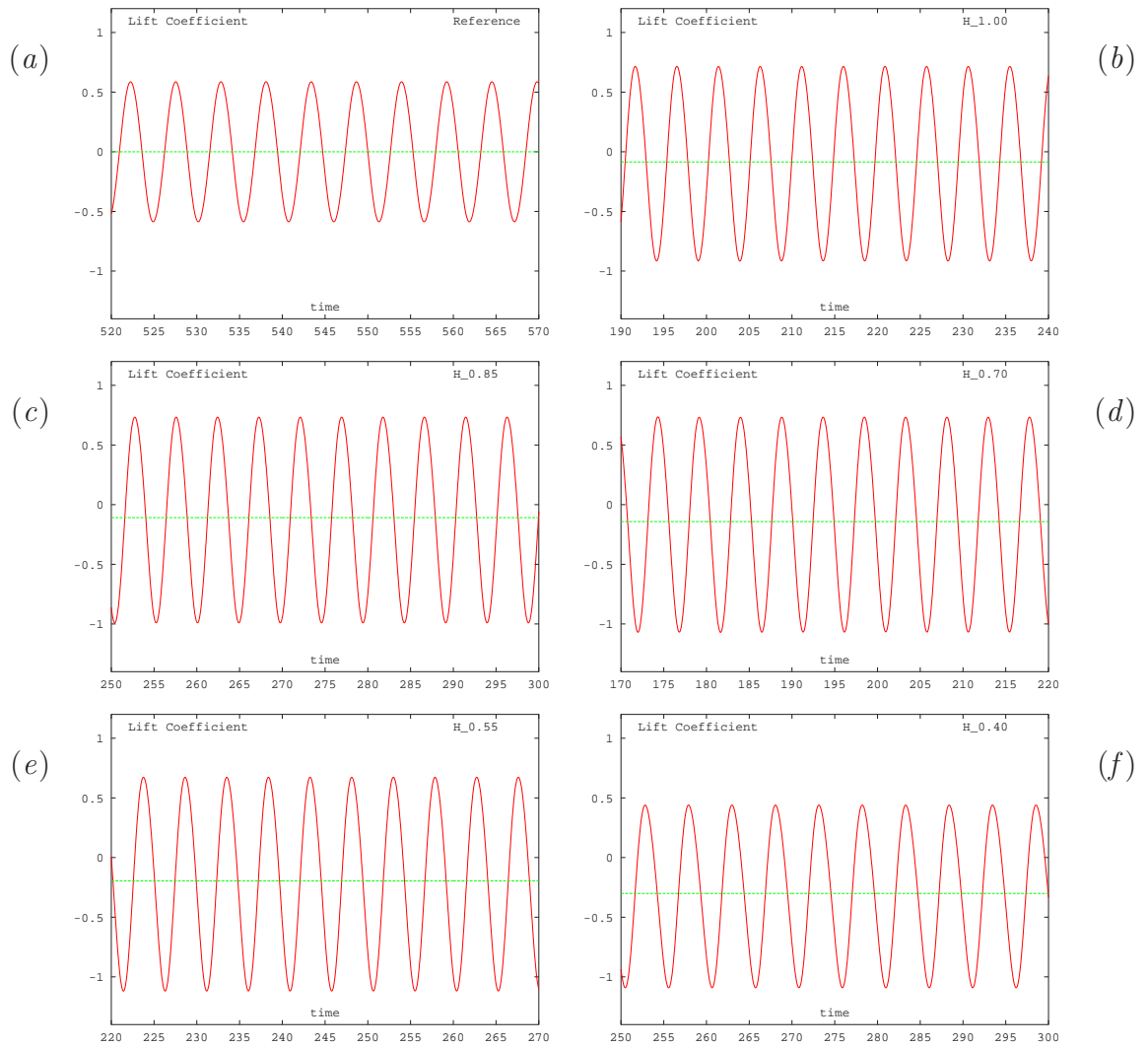


Figure 3.19: Plots showing the variation of the lift coefficient with time for the reference cylinder (a), and gap ratios of 1.00 (b), 0.85 (c), 0.70 (d), 0.55 (e) and 0.40 (f). The Froude number in all cases is 0.20 and the Reynolds number is 180.

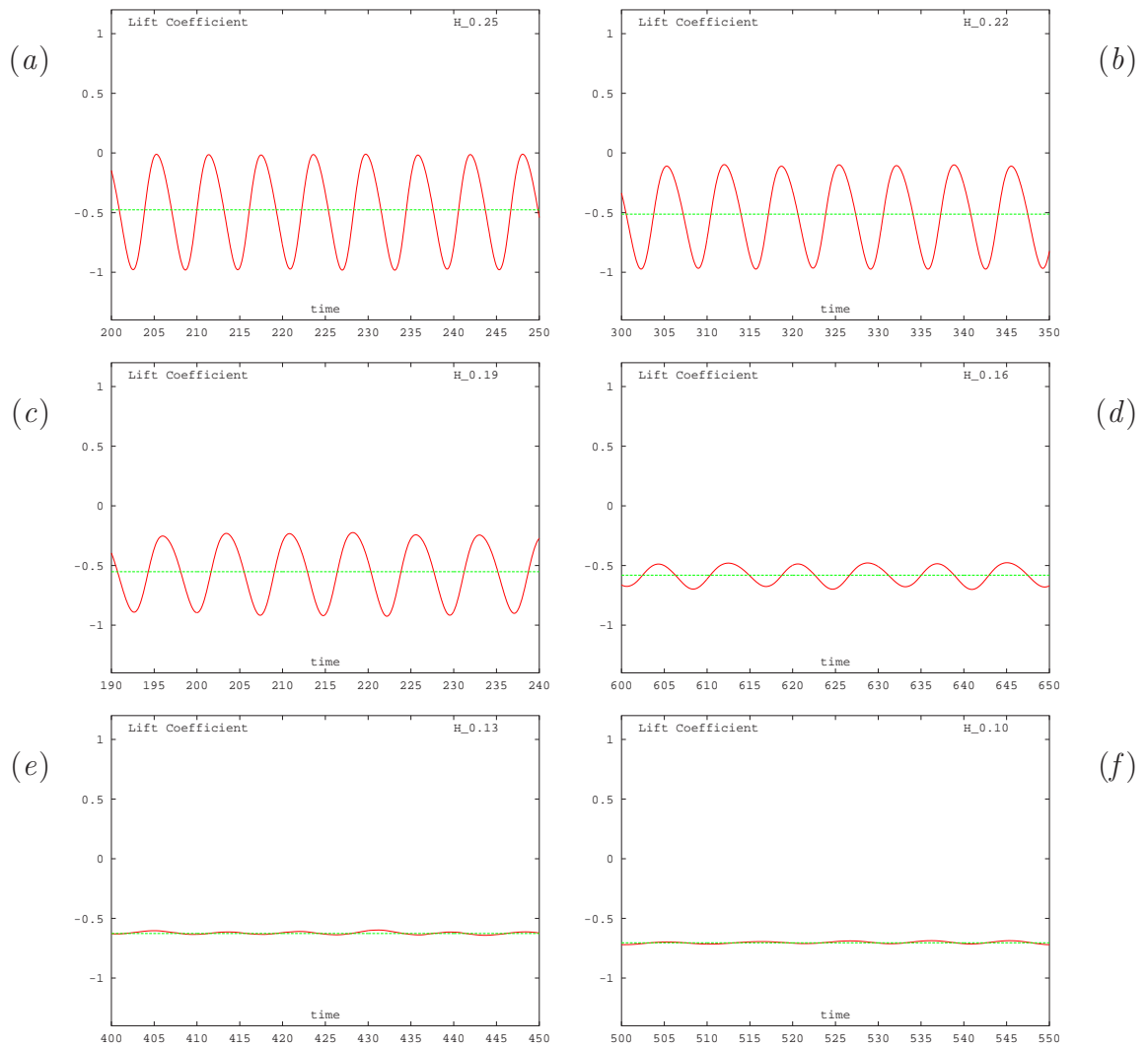


Figure 3.20: Plots showing the variation of the lift coefficient with time for gap ratios of 0.25 (a), 0.22 (b), 0.19 (c), 0.16 (d), 0.13 (e) and 0.10 (f). The Froude number in all cases is 0.20 and the Reynolds number is 180.

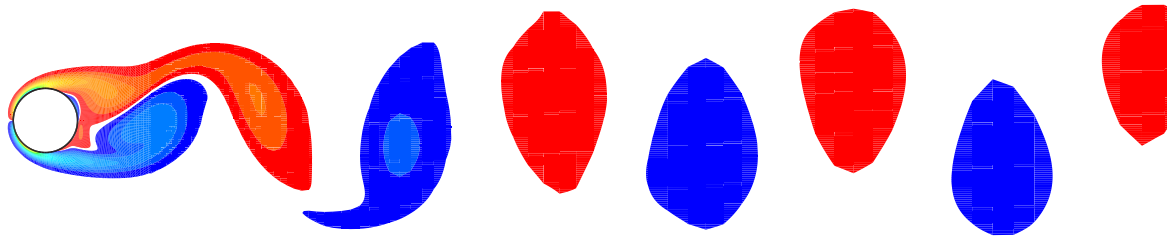


Figure 3.21: Vortex street for fully submerged (reference) cylinder at a Reynolds number of 180 at the point of maximum lift.

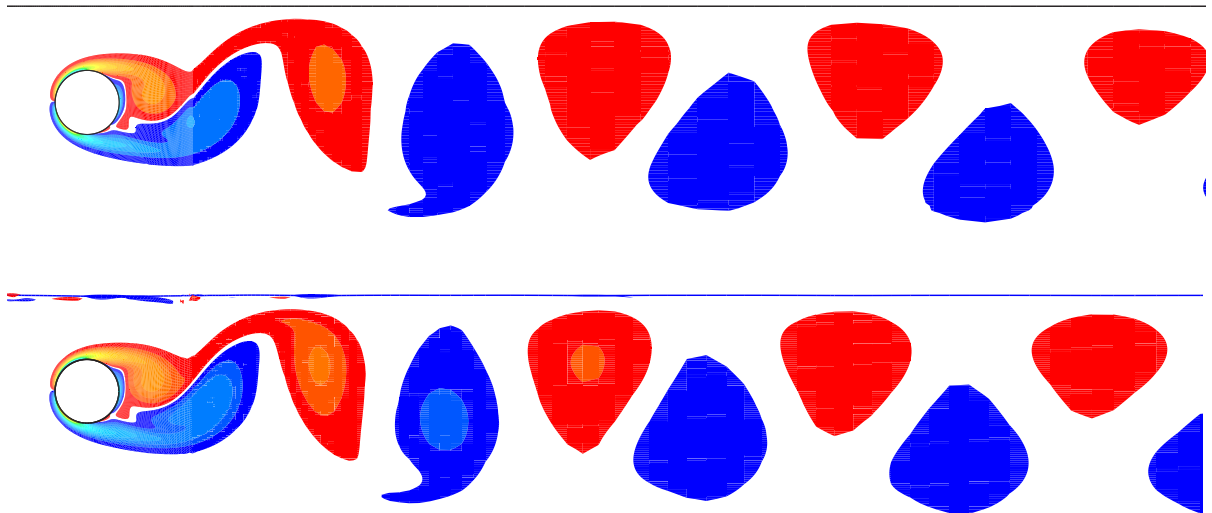


Figure 3.22: Vortex street for the gap ratio 1.00 case at the point of maximum lift for Froude numbers of 0.00 (top) and 0.20 (bottom). The Reynolds number in each case is 180.

For many of the larger gap ratios within this range (i.e. 1.00 and 0.85), only minor changes in the flow field were observed as the gap ratio was reduced. One of the more notable changes was that observed in the Strouhal number, which appears to be strongly related to the position of the formation length (as discussed earlier). At these depths the flow fields look similar to those obtained for a fully submerged cylinder. Although the negative vortices are restricted in their upward movement by the free surface and this tends to result in the reorientation of the shed vortices. As the gap ratio is further reduced, the restricted flow conditions tend to bring the vortices closer together (as illustrated in figures (3.22) to (3.32)), with the closer proximity of the vortices increasing the amount of cross annihilation. The increasing level of skew in the wake with decreasing gap ratio is shown in figure (3.33), which illustrates the time-averaged velocity fields for gap ratios between 0.85 and 0.16.

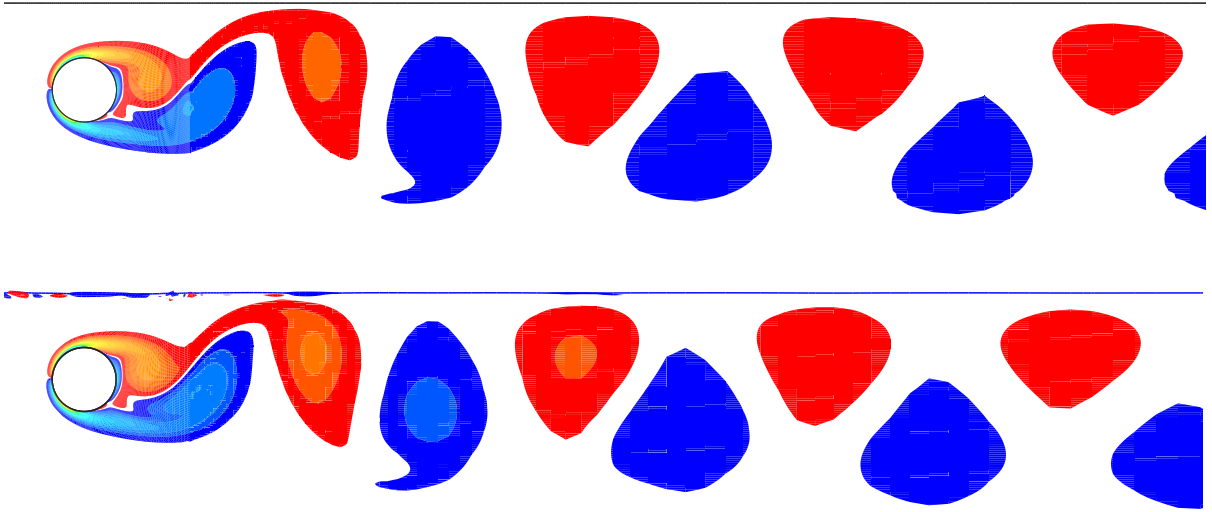


Figure 3.23: Vortex street for the gap ratio 0.85 case at the point of maximum lift for Froude numbers of 0.00 (top) and 0.20 (bottom). The Reynolds number in each case is 180.

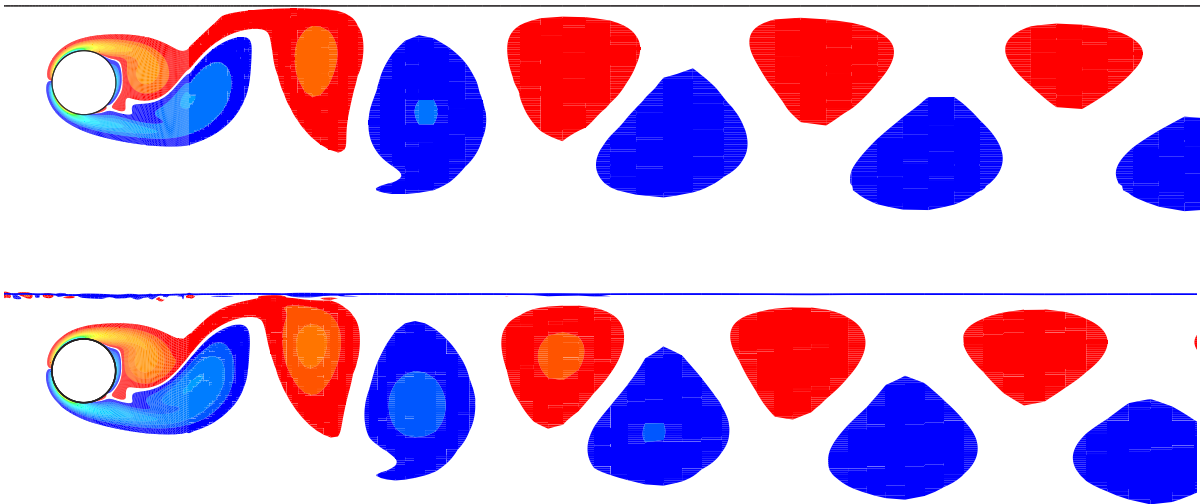


Figure 3.24: Vortex street for the gap ratio 0.70 case at the point of maximum lift for Froude numbers of 0.00 (top) and 0.20 (bottom). The Reynolds number in each case is 180.

One of the key points to note from figure (3.33) is the increasing asymmetry in the time averaged velocity as the gap ratio is reduced. The variation of the maximum velocity for the time-averaged flow in the gap directly above the cylinder, is shown in figure (3.34). The extent of this asymmetry is a crucial point that is considered later in this chapter in the section discussing the mechanism.

It should be noted that there is some uncertainty near the free surface in the time-averaged

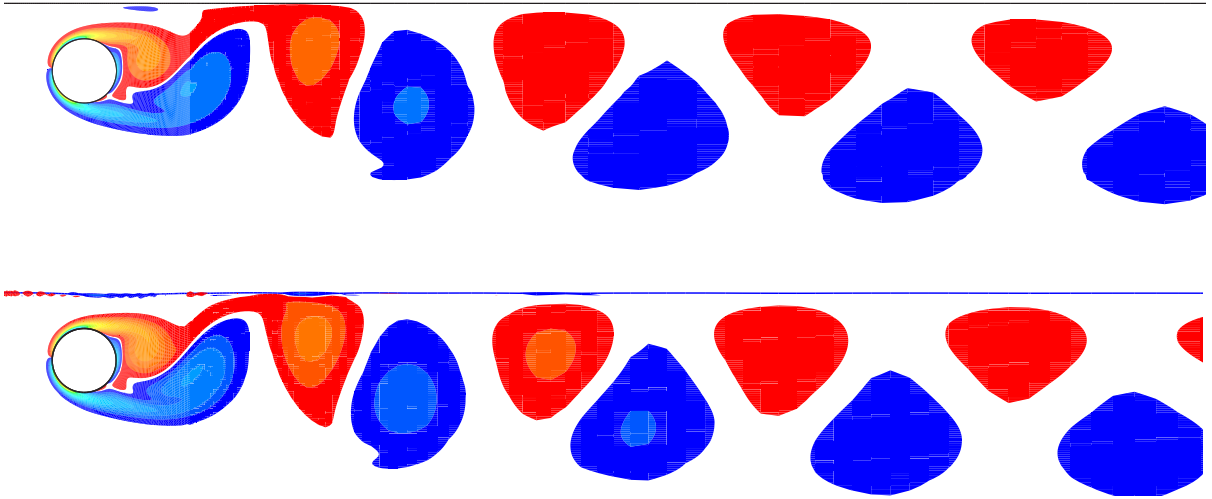


Figure 3.25: Vortex street for the gap ratio 0.55 case at the point of maximum lift for Froude numbers of 0.00 (top) and 0.20 (bottom). The Reynolds number in each case is 180.

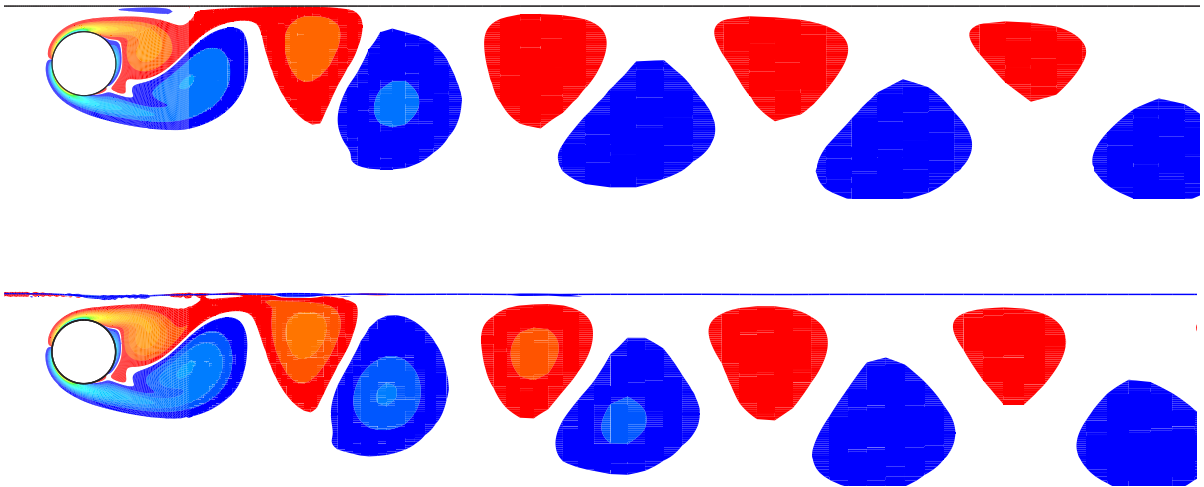


Figure 3.26: Vortex street for the gap ratio 0.40 case at the point of maximum lift for Froude numbers of 0.00 (top) and 0.20 (bottom). The Reynolds number in each case is 180.

velocity plots, as the interface may shift slightly (from one cell to either the one above or below it) with time and hence any time averaging may involve occasionally counting one cell which contains the less dense fluid and then one which contains the denser fluid. Thus some anomalous results may be recorded in this region purely as a result of the time-averaging process. However, it is expected that these will be limited to small band near the free surface.

As the gap ratio is reduced the wake shows further signs of the influence of the free surface,

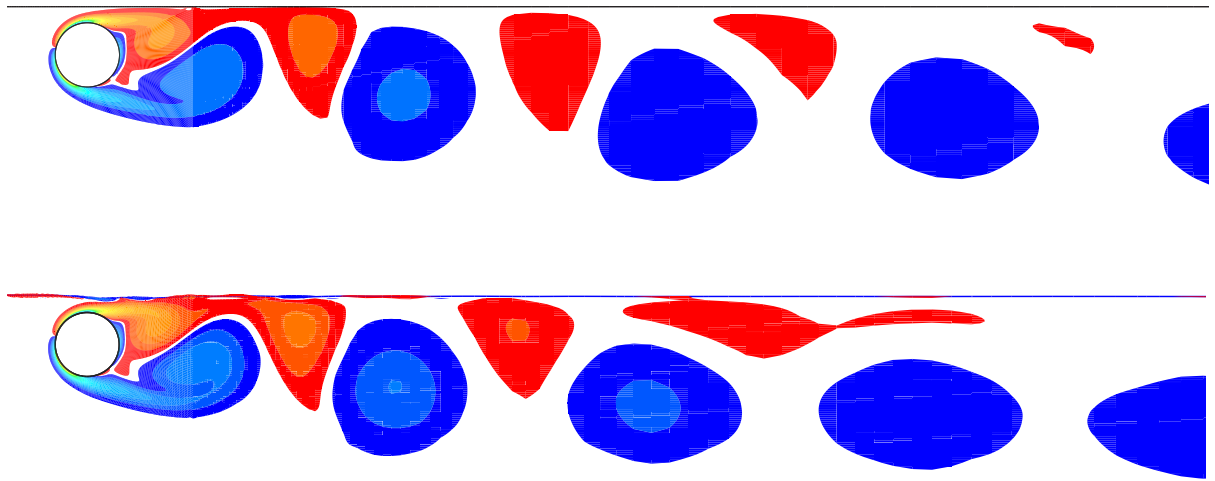


Figure 3.27: Vortex street for the gap ratio 0.25 case at the point of maximum lift for Froude numbers of 0.00 (top) and 0.20 (bottom). The Reynolds number in each case is 180.

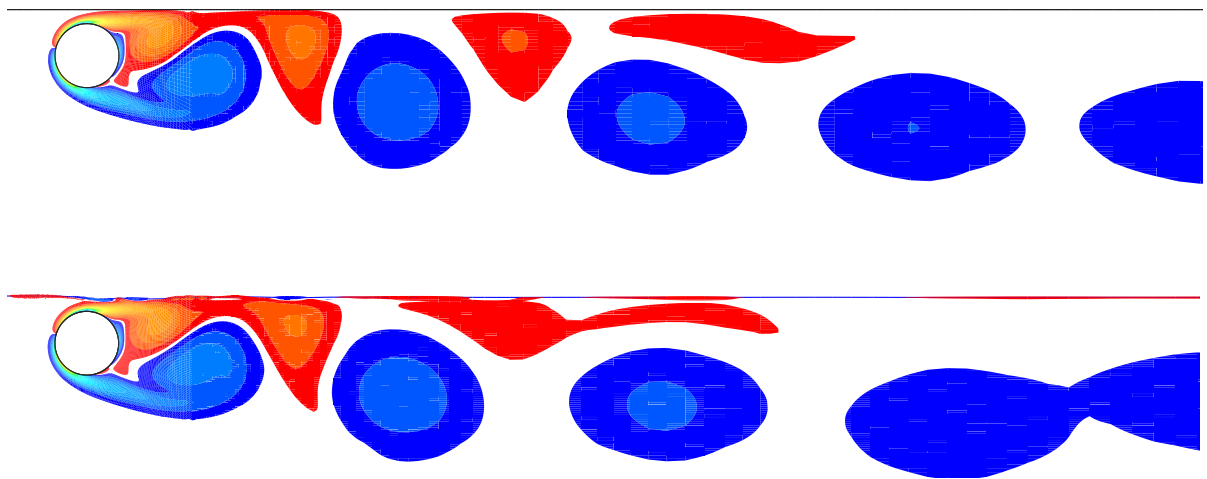


Figure 3.28: Vortex street for the gap ratio 0.22 case at the point of maximum lift for Froude numbers of 0.00 (top) and 0.20 (bottom). The Reynolds number in each case is 180.

with the vortices becoming more confined or cramped as they move downstream. The cramped conditions then alter both the shape and strength of the vortices such that they become more oval shaped, with their major axis no longer lying perpendicular to the free surface (see for example the vortex street for a gap ratio of 0.70 in figure (3.24) and vortex street at a gap ratio of 0.22 in figure (3.28)). At the smaller gap ratio (i.e. 0.22), the positive vortices take on a more oval appearance such that their major axis is now parallel to the free surface, which is in

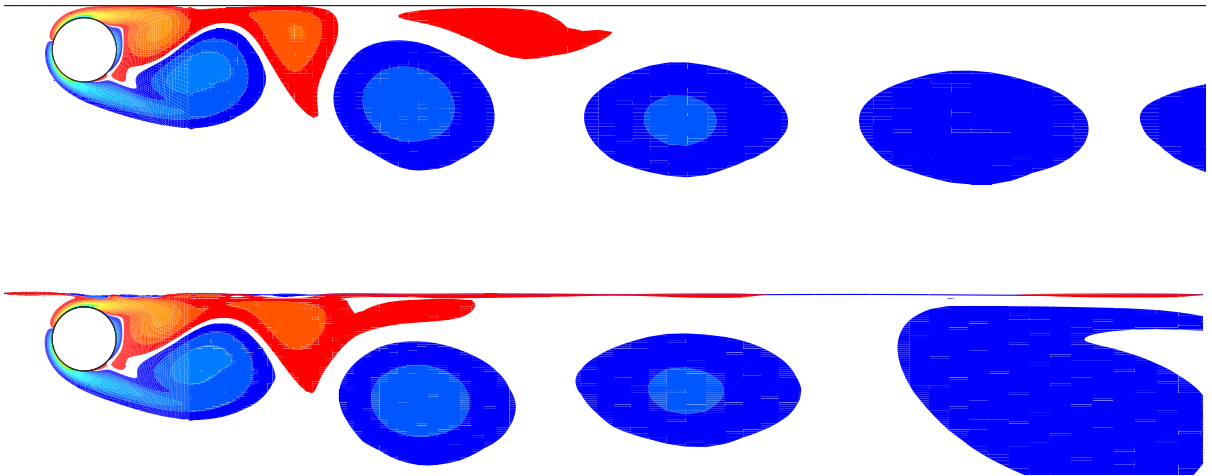


Figure 3.29: Vortex street for the gap ratio 0.19 case at the point of maximum lift for Froude numbers of 0.00 (top) and 0.20 (bottom). The Reynolds number in each case is 180.

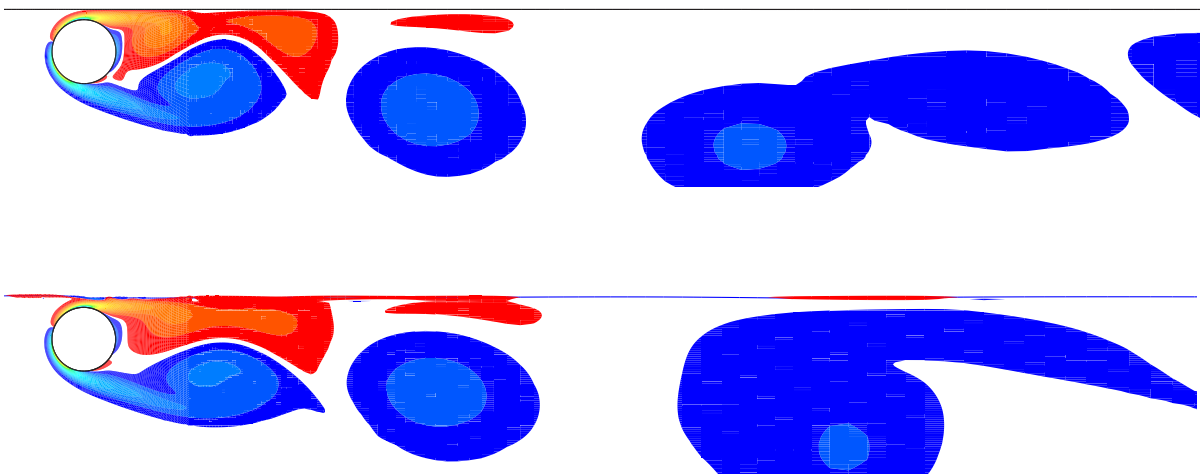


Figure 3.30: Vortex street for the gap ratio 0.16 case at the point of maximum lift for Froude numbers of 0.00 (top) and 0.20 (bottom). The Reynolds number in each case is 180.

agreement with the observations of Dimas & Triantafyllou (1994).

The ability of the vortices to diffuse across the interface also becomes more important as the cylinder approaches the free surface. As the flux of vorticity across the free surface depends upon the viscous acceleration of the surface fluid (which varies throughout the shedding cycle), the presence of the adjacent surface allows for the viscous transport of vorticity across it. However, as the convective speed of the vortices is considerably greater than their diffusive speed, it is

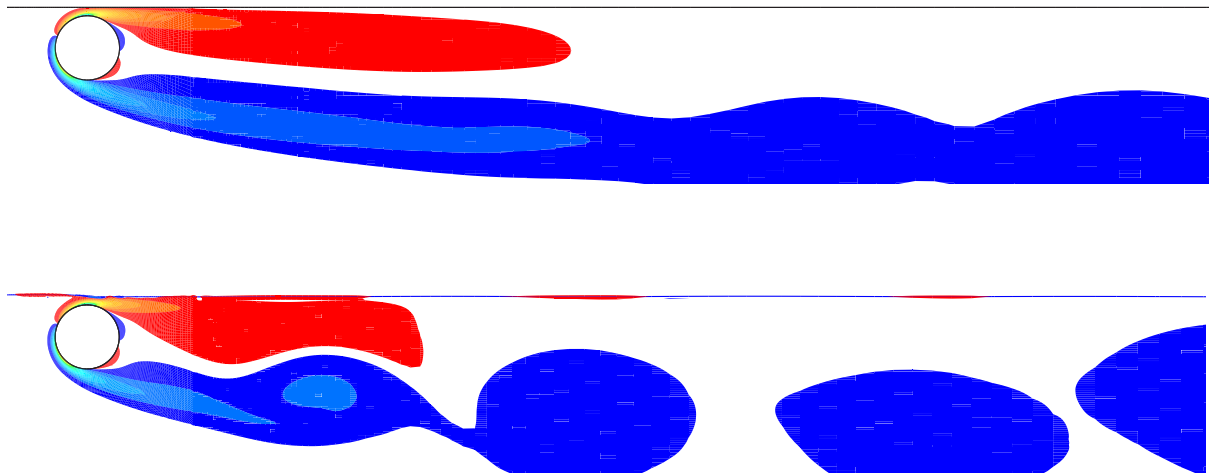


Figure 3.31: Vortex street for the gap ratio 0.13 case at the point of maximum lift for Froude numbers of 0.00 (top) and 0.20 (bottom). The Reynolds number in each case is 180.

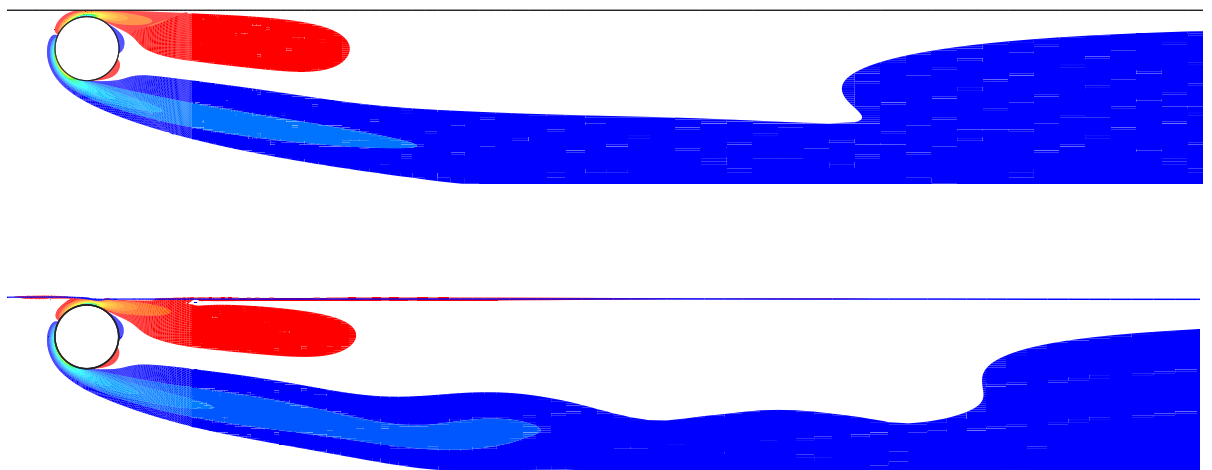


Figure 3.32: Vortex street for the gap ratio 0.10 case at the point of maximum lift for Froude numbers of 0.00 (top) and 0.20 (bottom). The Reynolds number in each case is 180.

expected that the vortices near to the free surface will behave as if they were suddenly exposed to the free surface boundary condition. According to Rood (1995), this would imply that the flow in the vicinity of the free surface should accelerate and that a jump in the velocity derivative may be seen. Such acceleration should produce vorticity of the opposite sign in the lighter fluid on the other side of the interface and hence patches of counter signed vorticity should form in the lighter phase. And this is indeed what is observed, with figure (3.35) showing the vorticity

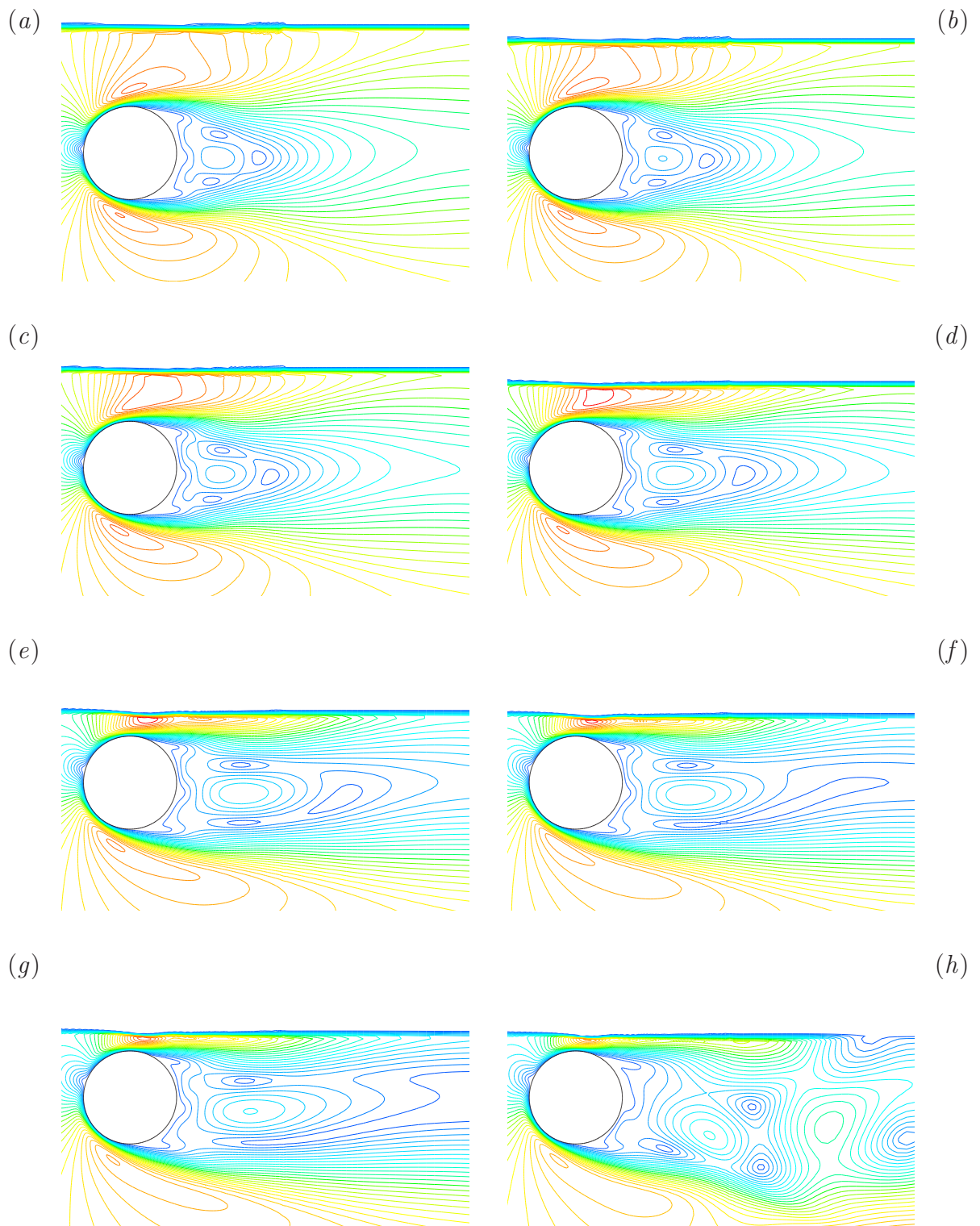


Figure 3.33: Plots showing the time-averaged velocity contours for gap ratios of 0.85 (a), 0.70 (b), 0.55 (c), 0.40 (d), 0.25 (e), 0.22 (f), 0.19 (g) and 0.16 (h). The Froude number in each case is 0.20 and the Reynolds number is 180.

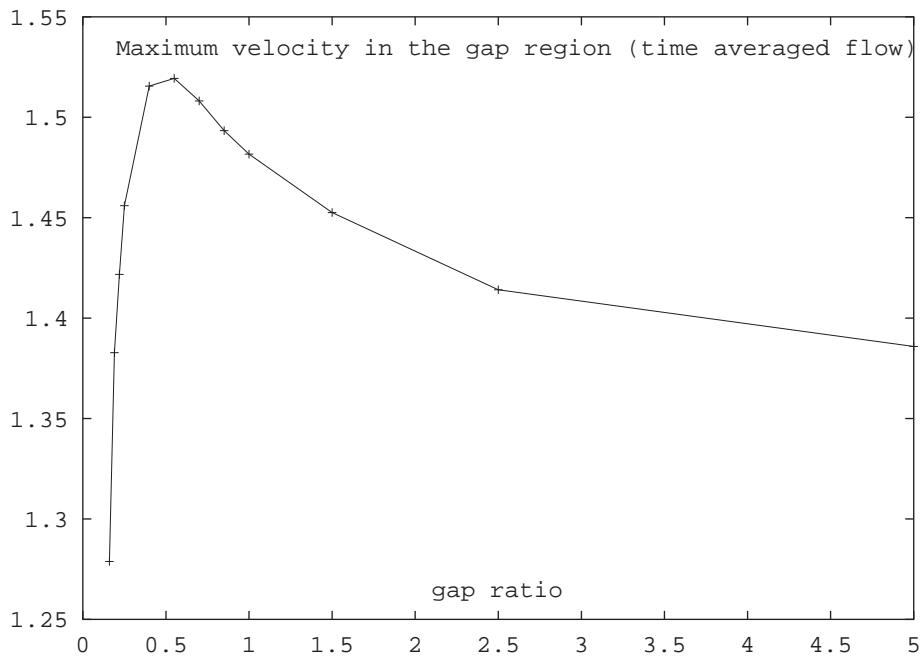


Figure 3.34: Variation of the maximum time-averaged velocity in the gap directly above the cylinder with gap ratio for a Froude number of 0.20. The value of the Reynolds number for each case is 180.

field in both phases.

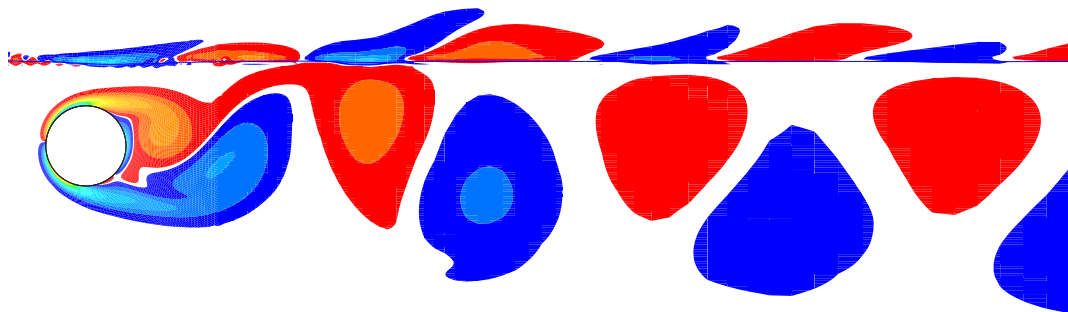


Figure 3.35: Vorticity distribution in both phases for a gap ratio of 0.55 and for a Froude number of 0.20. The Reynolds number for this case is 180.

This behaviour suggests that the free surface acts in a fashion both similar to, and distinctly different from, a no-slip surface. The similarity is that both act in a manner to remove the existence of locally present vorticity. So while a no-slip surface will generate oppositely signed vorticity (which then often cross annihilates with the vorticity which was its progenitor), a free surface will allow local surface acceleration that results in a flux of vorticity across the interface

and hence in its subsequent removal from the fluid. The difference, apart from the fact that the free surface is able to deform, is in the way in which the vorticity transport and generation occurs.

For gap ratios below 0.25, the wake behaviour tends to vary more significantly, and it is perhaps best at this point to consider each of the smaller gap ratio cases separately.

gap ratio 0.25

At this gap ratio the shedding strength as measured by the RMS lift reduces considerably. The shear layer from above the cylinder is now forced into closer contact with the free surface, and hence it allows for a greater level of vorticity to be transported across the interface. The removal of this negative vorticity is highlighted by its limiting presence at locations further downstream. Both the movie of the vorticity field and figure (3.27) indicate that no discernible negative vorticity is observed at distances greater than approximately 16 diameters downstream.

gap ratio 0.22

As the gap ratio is reduced, the shedding strength continues to weaken and the negative vortices decay more rapidly. The absence of negative vorticity at positions downstream results in the wake at these distances becoming dominated by positive vortical structures. Such structures are largely recirculatory in that they rotate in a counter clockwise manner (i.e. they tend to direct fluid upstream at locations close to the free surface).

gap ratio 0.19

At a gap ratio of 0.19, the shedding strength weakens further and the absence of negative vorticity moves upstream such that it is no longer observed after a mere 9 diameters. The lack of negative vorticity tends to result in the wake becoming more recirculatory, with larger scale positive vortical structures forming from the coalescence of previous shed positive vortices (the reader is recommended at this point to view the video showing the evolution of the vorticity field for this case).

gap ratio 0.16

As the gap ratio is reduced even further, the shedding strength continues to weaken and the close proximity of the free surface facilitates an even greater flux of vorticity across the interface. There is now almost no negative vorticity in the wake, apart from the shear layer which is still attached to the cylinder. This behaviour is shown in both the movie on the attached compact disk and in figure (3.30). The location at which the positive vortices coalesce also moves upstream and the wake is observed to become increasingly recirculatory as it is now largely dominated by positive vortical structures.

gap ratio 0.13

At a gap ratio of 0.13 shedding is no longer observed and the wake consists of large recirculation bubble that is dominated by positive vorticity. This behaviour is shown both in figure (3.31) and in the movie showing the evolution of the vorticity field. The negative shear layer shows no signs that it is attempting to roll-up and the flow field becomes considerably less time-dependent.

gap ratio 0.10

At a gap of 0.10 (the smallest gap considered in the current study), the flow largely resembles that at a gap of 0.13 with the wake again being dominated by a large recirculation bubble. The bubble is larger at this smaller gap as the influence of the negative shear layer from above the cylinder is diminished.

It is interesting to note that the recirculation bubble observed here at the small gap ratios is considerably larger than that observed for a similarly dimensioned backward facing step. The large discrepancy between the current case and that observed for a backward facing step, arises as a result of the free surface boundary condition. The free surface boundary condition more easily facilitates the reversal of flow near the free surface (while the no slip boundary for a backward facing step does not), and as a consequence it allows the recirculating bubble to grow.

The cessation of vortex shedding and the formation of a large scale recirculation bubble, immediately suggests that there is some form of analogy between this problem and that of two side-by-side cylinders in cross flow. Sumner et al. (1999) indicates that when the gap (or pitch) ratio between the cylinders is small, that the two side-by-side cylinders then produce single body vortex shedding (i.e. the two bodies act like one larger body). However, as there is no second

body in the current problem, single body shedding is not permitted and the flow resembles that of a half body with a symmetry condition imposed. Fornberg (1985) considers symmetric flow past a cylinder (i.e. flow past a half cylinder with a symmetry condition imposed along the centerline) and notes that for Reynolds numbers less than 600 (the maximum value he considered), large recirculation bubbles form. Such bubbles are then found to extend over considerable distances and span significant widths.

The fact that similar structures are observed here is not surprising when one considers that the symmetry condition and a non deformable slip boundary condition (or weakly deformable free-surface condition) are essentially identical. A discussion of the stability characteristics of the wake when in this form, is deferred until the chapter dealing with the flow at larger Froude numbers (i.e. Chapter 5).

3.8 Comparison with Experiment

While most of the results of Sheridan et al. (1997) lie outside of the Froude number range considered in this chapter, one of their results is within its scope. The flow at a gap ratio of 0.40 and a Froude number of 0.22 is considered by Sheridan et al. (1997), with figures (3.36) and (3.37) showing the pictorial comparison between their results and those from the current study at a gap ratio of 0.40 and a Froude number of 0.20. To obtain agreement between the results, it is necessary to consider them both at the same point in the shedding cycle. To make such a comparison easier, videos of the numerically predicted solution that show the evolution of both the vorticity field and the transport of fluid were produced. The comparison between the two cases is not particularly favourable at this Froude number, with the vorticity field of Sheridan et al. (1997) not showing any indication of discrete vortices in the near wake. The results do, however, compare much more favourably with those of Miyata et al. (1990), with the comparison at a gap ratio of 0.25 shown in figures (3.38) and (3.39).

The difference between the current results and those of Sheridan et al. (1997) may be to be due to differences in the Reynolds number and perhaps more importantly its influence upon the formation length. The latter is asserted, as the match up between the current results and those of Miyata et al. (1990) are particularly good, despite the more the 250 fold difference in Reynolds number. However, it is anticipated that the formation length will tend to be shorter at both the smaller and larger Reynolds numbers, while it is likely to be longer for the Reynolds numbers considered by Sheridan et al. (1997).

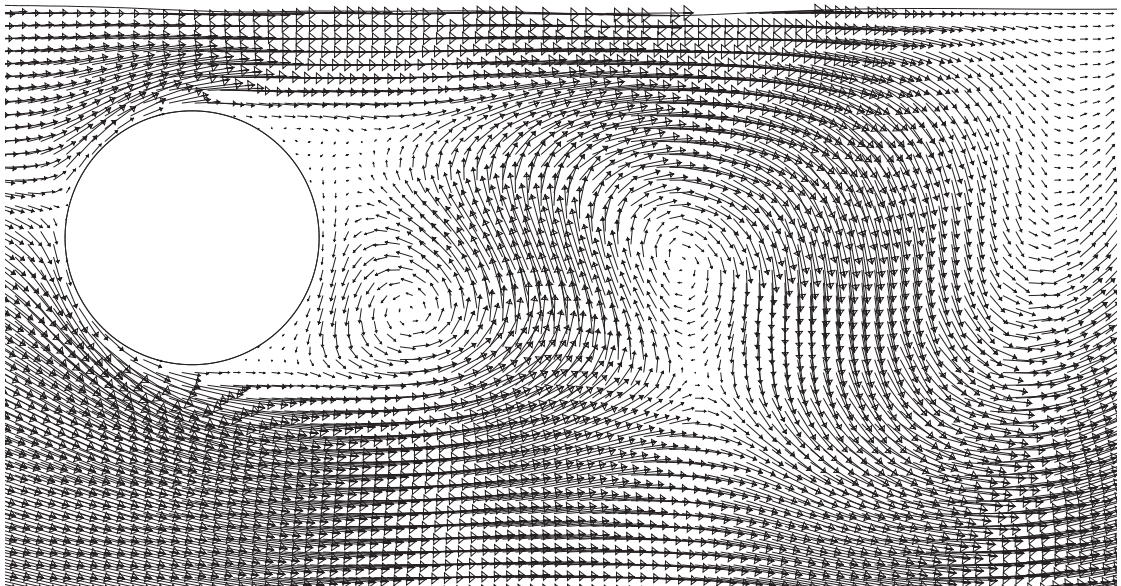
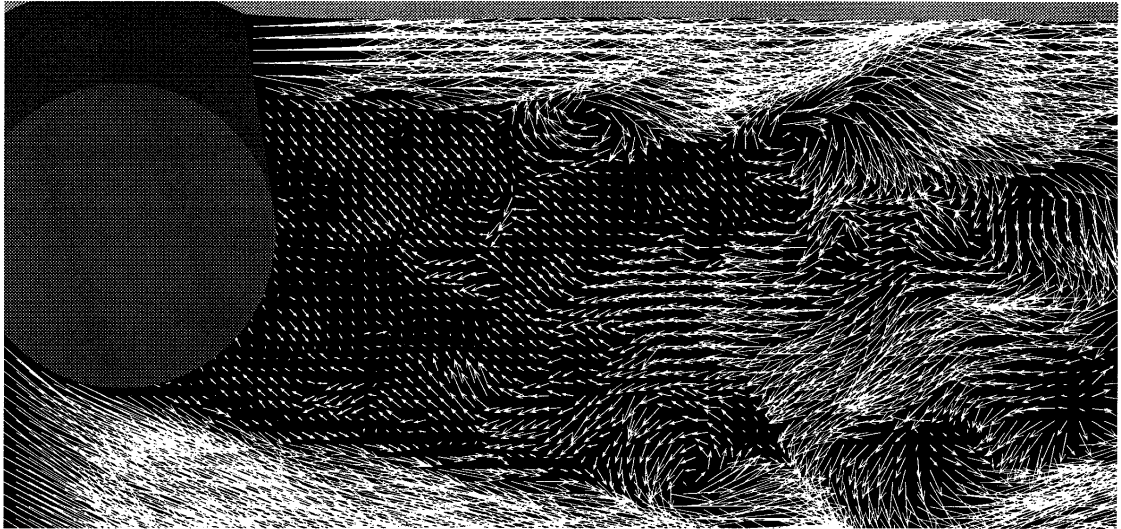


Figure 3.36: Velocity vector field from Sheridan *et al.* (1997) (top), and the current numerical prediction at the point of minimum lift (bottom). The result from Sheridan *et al.* (1997) is for a gap ratio of 0.40, a Froude number of 0.22 and for a Reynolds number between 5990 and 9120, while the numerical prediction is for a gap ratio of 0.40, a Froude number of 0.20 and a Reynolds number of 180.

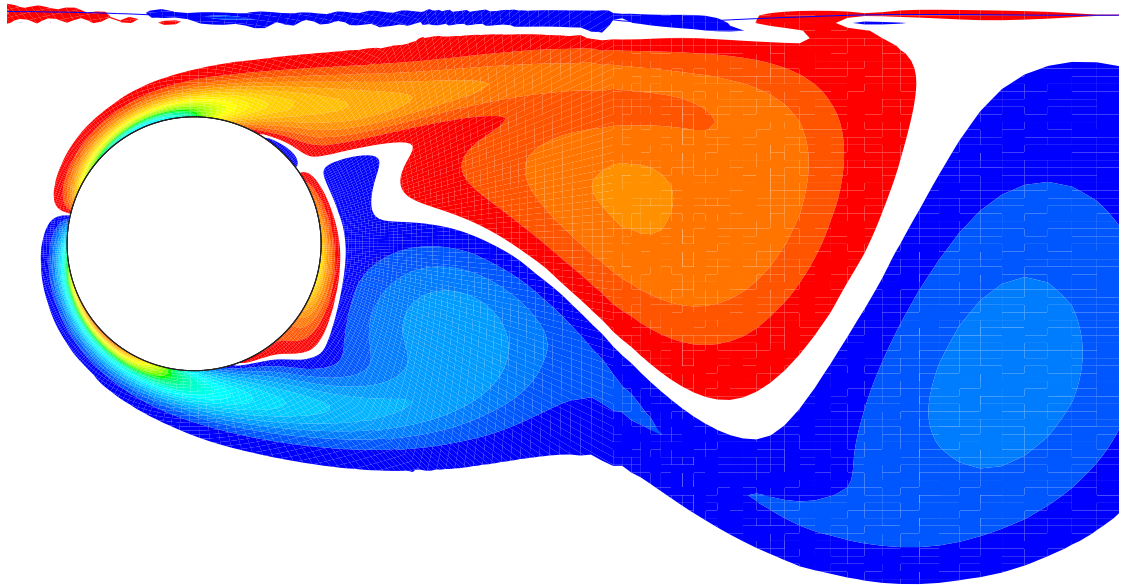


Figure 3.37: Vorticity field from Sheridan *et al.* (1997) (top), and the current numerical prediction at the point of minimum lift (bottom). The result from Sheridan *et al.* (1997) is for a gap ratio of 0.40, a Froude number of 0.22 and for a Reynolds number between 5990 and 9120, while the numerical prediction is for a gap ratio of 0.40, a Froude number of 0.20 and a Reynolds number of 180.

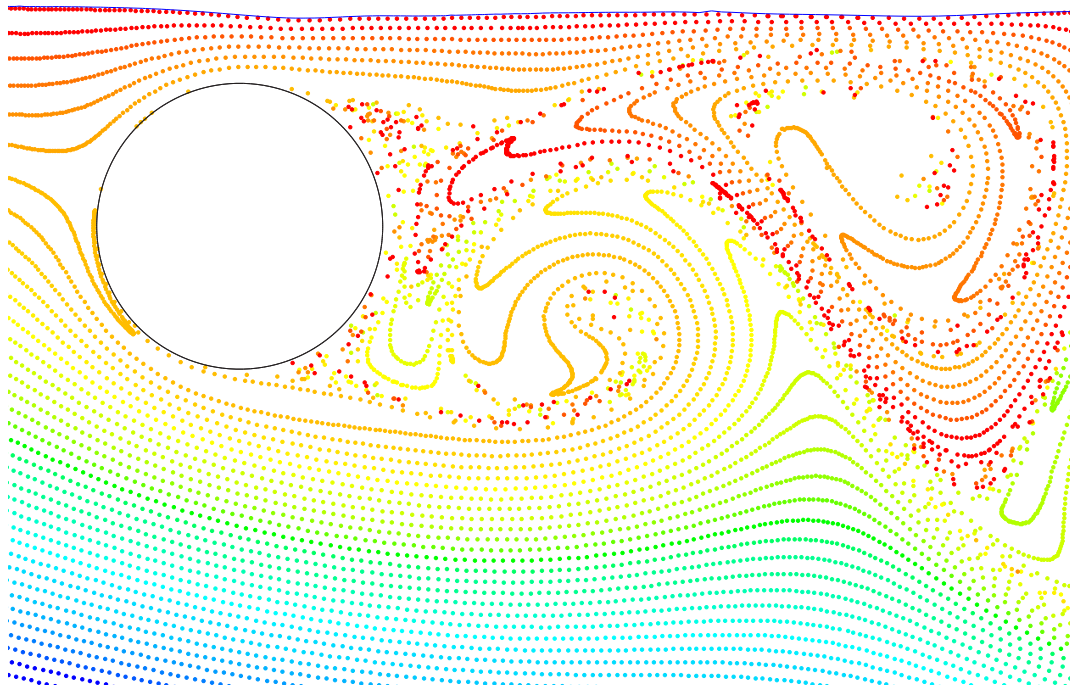
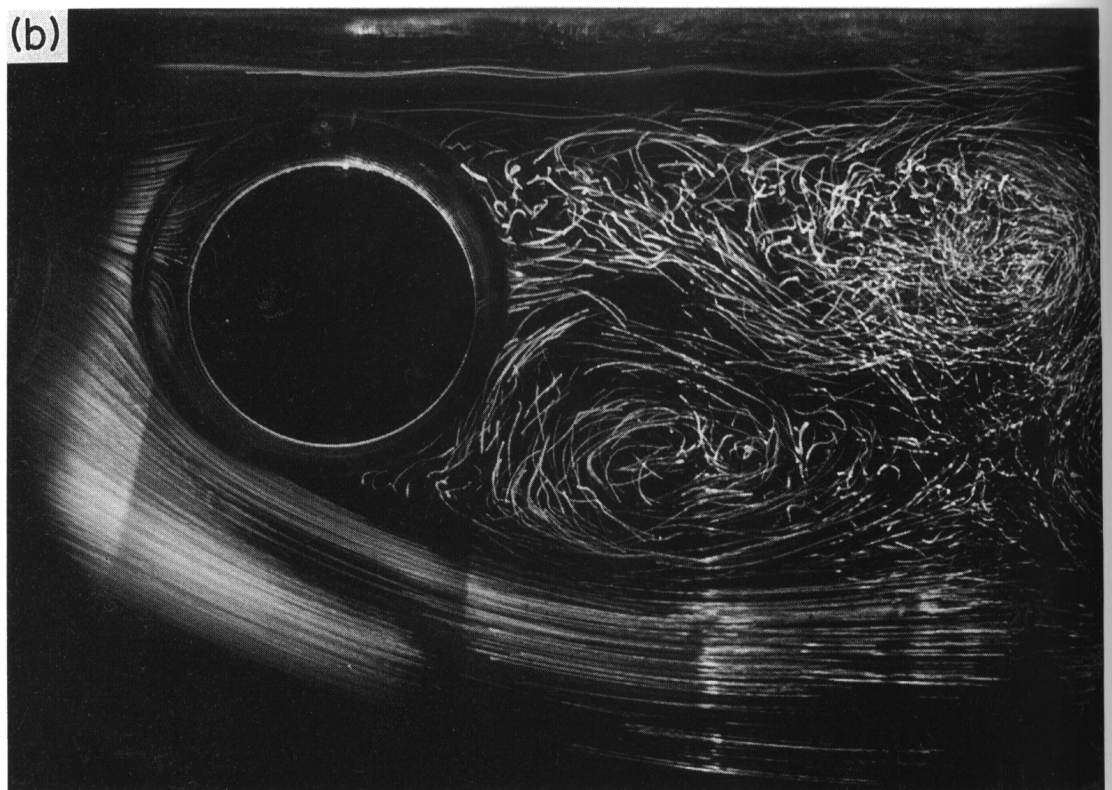


Figure 3.38: Visualized flow field of Miyata *et al.* (1990) and the current numerical prediction at a similar instant in time. The result from Miyata *et al.* (1990) (top) is for a gap ratio of 0.25 and for a Froude number of 0.24, while the numerical prediction (bottom) is for a gap ratio of 0.25 and for a Froude number of 0.20.

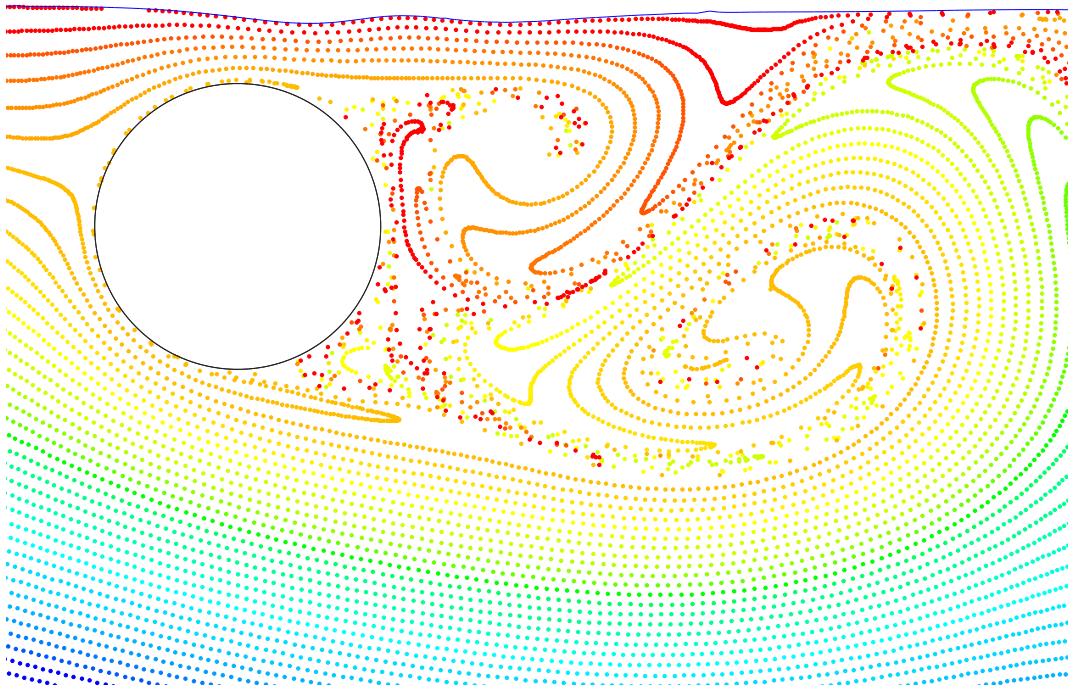
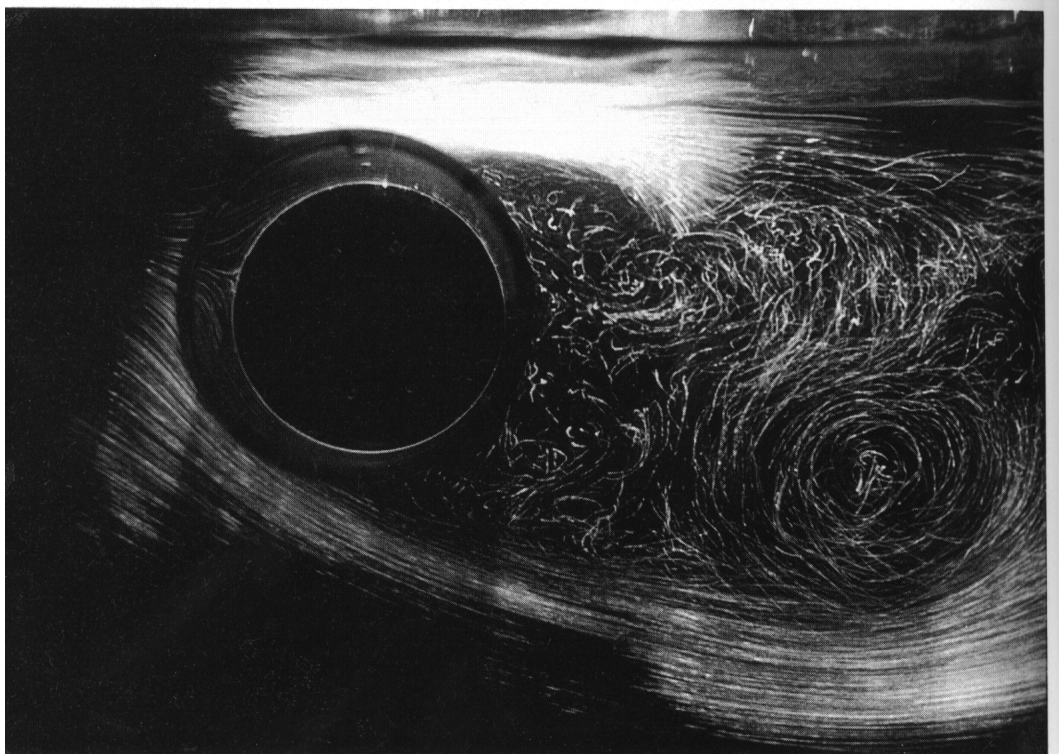


Figure 3.39: Visualized flow field of Miyata *et al.* (1990) and the current numerical prediction at another instant in time. The result from Miyata *et al.* (1990) (top) is for a gap ratio of 0.25, a Froude number of 0.24 and a Reynolds number of 49600, while the numerical prediction (bottom) is for a gap ratio of 0.25, a Froude number of 0.20 and a Reynolds number of 180.

3.9 Suppression of Vortex Shedding

The gap ratio at which vortex shedding is first suppressed is of interest as it represents the critical depth at which the global instability is extinguished, while also being a value which can be compared with the results of others. Before comparing the critical gap ratios, it is first necessary to highlight the different ways in which the critical gap has been measured. Most authors such as Bearman & Zdravkovich (1978), Angrilli et al. (1982), Grass et al. (1984), and Price et al. (2000) all consider the spectra of the fluctuating velocity as measured at a number of positions in the wake (usually using hot wire probes). Others such as Miyata et al. (1990) measure the spectra associated with the lift force, while Lei et al. (1999) suggests that the RMS component of the lift is a more appropriate method. All approaches are expected to yield similar results, although Lei et al. (1999) indicates that the hot-wire method is not likely to be systematic. In the current investigation, three approaches have been adopted: the first involves measuring the lift spectra, the second the RMS lift, and the third required a consideration of the vorticity field (such that the presence of discrete vortices of both signs was deemed to constitute shedding). The third method is more subjective, but it allows for a more physical insight into the wake structures and it is the method used in the proceeding section.

For the current investigation, vortex shedding was observed down to a gap ratio of about 0.16 when using all of the methods just described. Although a significant drop in the spectra was noted for gap ratios of 0.25 and below. This gap ratio is smaller than that observed by others, such as Miyata et al. (1990) (free surface, ceases at gap 0.35), Bearman & Zdravkovich (1978) (no slip, ceases at gaps between 0.20 and 0.30) and Grass et al. (1984) (no slip, ceases for gaps below 0.25). One possible explanation for the difference is the altered boundary condition on the adjacent surface. However, while this may explain the difference between the current results and those for a no-slip boundary, it does not explain the difference between the current findings and those of Miyata et al. (1990).

While differences in the Froude numbers may play a part, with the difference being roughly 20% (which is not insignificant), the step increase in Strouhal number reported by Miyata et al. (1990) at a gap ratio of 0.35 cannot be reasonably explained. As mentioned earlier, it is believed that the significant drop in the magnitude of the spectrum for the vertical lift force observed by Miyata et al. (1990), indicates that shedding is close to or may have even ceased. This suggests that their frequencies measured at the smaller gap ratios are not frequencies associated with the weakened shedding, but rather those associated with the structural adjustment of the flow. The

small amplitudes associated with their spectra support this, and it is at this point that one can more fully appreciate the suggestion by Lei et al. (1999) that the RMS lift is a better measure of the suppression of vortex shedding.

The displacement thickness (i.e. the distance by which the external flow is displaced by the slower moving flow inside the boundary layer) is expected to have some influence on the depth at which shedding is suppressed, as it gives an approximation for the range of influence of the cylinders boundary layer. Thus it is expected that the depth at which shedding is suppressed may be in part a function of Reynolds number. For the cases in which a no-slip wall boundary is considered, the wall boundary layer and cylinder boundary layer will interact, hence suggesting that a combination of the two may be more important.

To test the influence of the displacement thickness in the current study, simulations at two different Reynolds numbers were performed for cases at shallow submergence depths (where shedding was found to cease). The simulations indicate that shedding is suppressed at a gap ratio of approximately 0.13 at a Reynolds number of 180, while at a Reynolds number of 500, weak shedding (or a form of flapping) was observed to persist down to a gap ratio of 0.10 (ceasing at 0.07). In order to get a crude estimate of the displacement thickness, it is assumed that the boundary layer on the cylinder will behave roughly like a flat plate for short sections along the cylinder. Hence the displacement thickness should be roughly $\delta^* = s \frac{1.721}{Re_s^{\frac{1}{2}}}$.

For the cases examined here at a Reynolds number of 180, $\delta^* \approx 0.129$ when one assumes that the length s is distance from stagnation point to separation point (roughly 2.00 radians). At a Reynolds number of 500 the displacement thickness is then roughly $\delta^* \approx 0.077$. This result (albeit being very crude) is in good agreement the numerical simulations (i.e. shedding should experience some changes at a gap ratio of approximately 0.13 for a Reynolds number of 180, and at 0.077 for a Reynolds number of 500). Hence it is expected that the gap ratio at which shedding ceases, may show some Reynolds number dependence. However, it is anticipated that the trends observed in Strouhal number, lift, drag and moment should be all be maintained, although the gap ratios at which they occur may be shifted slightly.

3.10 Vorticity Distributions

For a fully submerged cylinder, the pressure gradient and hence the vorticity generating regions on the cylinder are symmetric when averaged over one shedding cycle. However, this is not

obviously the case for a cylinder close to a free surface, where the deformable free surface may introduce asymmetries in the pressure field and hence in the regions of vorticity generation upon the cylinder. To examine what effect such asymmetries are likely to have, it is necessary to consider the net flux density of vorticity.

A derivation of the flux density of vorticity for a general cylinder is now presented, with the intention that the result will yield information pertaining to the net generation of vorticity. This approach largely follows that of Morton (1984), who considered the flux density of vorticity for a flat plate.

The derivation begins by first considering the azimuthal component of the two dimensional Navier-Stokes equations in cylindrical polar coordinates.

$$\begin{aligned} \frac{\partial u_\theta}{\partial t} + u_r \frac{\partial u_\theta}{\partial r} + \frac{u_\theta}{r} \frac{\partial u_\theta}{\partial \theta} + \frac{u_r u_\theta}{r} = \frac{-1}{\rho r} \frac{\partial P}{\partial \theta} + \\ \nu \left(\frac{1}{r} \frac{\partial}{\partial r} \left(r \frac{\partial u_\theta}{\partial r} \right) + \frac{1}{r^2} \frac{\partial^2 u_\theta}{\partial \theta^2} + \frac{2}{r^2} \frac{\partial u_r}{\partial \theta} - \frac{u_\theta}{r^2} \right) + g e_\theta. \end{aligned} \quad (3.1)$$

Its application on a stationary cylinder of radius R_0 is then considered, so that $u_r = 0$ and $u_\theta = 0$ at $r = R_0$. Equation (3.1) then simplifies to yield the following

$$\frac{-1}{\rho r} \frac{\partial P}{\partial \theta} + \nu \left(\frac{1}{r} \left(\frac{\partial u_\theta}{\partial r} \right) + r \frac{\partial^2 u_\theta}{\partial r^2} \right) + g \cos(\theta - \theta_0) = 0. \quad (3.2)$$

The vorticity in cylindrical polar coordinates is given by

$$\omega = \frac{1}{r} \left(u_\theta + r \frac{\partial u_\theta}{\partial r} - \frac{\partial u_r}{\partial \theta} \right) e_z, \quad (3.3)$$

and this indicates that the flux density of vorticity is

$$\nu \frac{\partial \omega}{\partial r} = \nu \left(-\frac{u_\theta}{r^2} + \frac{1}{r} \frac{\partial u_\theta}{\partial r} + \frac{1}{r^2} \frac{u_r}{\partial \omega} + \frac{\partial^2 u_\theta}{\partial r^2} - \frac{1}{r} \left(\frac{\partial^2 u_r}{\partial \theta \partial r} \right) \right). \quad (3.4)$$

From equation (3.2), it can be seen that

$$r \frac{\partial^2 u_\theta}{\partial r^2} = r \left(\frac{1}{\nu \rho r} \frac{\partial P}{\partial \theta} - \frac{g \cos(\theta - \theta_0)}{\nu} \right) - \frac{\partial u_\theta}{\partial r}, \quad (3.5)$$

which upon substitution into the flux density of vorticity equation (equation (3.4)) yields,

$$\nu \frac{\partial \omega}{\partial r} = \frac{1}{\rho r} \frac{\partial P}{\partial \theta} - g \cos(\theta - \theta_0) - \nu \frac{1}{r} \frac{\partial^2 u_r}{\partial r \partial \theta}. \quad (3.6)$$

If equation (3.6) is then integrated around the cylinder the result is

$$\int \nu \frac{\partial \omega}{\partial r} d\theta = 0, \quad (3.7)$$

which indicates that the net flux density of vorticity is zero.

While this finding does not reveal which regions of the cylinder are responsible for most of the vorticity generation, it does indicate that equal levels of oppositely signed vorticity are being produced. As stated by Morton (1984), Lighthill (1963) identifies $-\nu \frac{\partial \omega}{\partial z}$ as the diffusive flux density (or flow per unit area per unit time) of positive vorticity from a plane flat boundary, as the local boundary source of vorticity (with z being aligned normal to the plane boundary). The extension to a cylinder implies that at any instant in time the flux density of vorticity on the cylinder must be zero. This suggests that there must be a balance in the flux density of vorticity throughout the vortex shedding cycle, such that the vorticity flux of both positive and negatively signed vorticity is always in balance. This result is crucial as it indicates that the presence of an excess or a deficit in one sign of vorticity in the general flow field, can not be attributed to an uneven generation of a particular sign of vorticity on the body.

As indicated in Chapter one, the vorticity and hence the circulation within one fluid that is bounded by a free surface need not be conserved (with the flux of vorticity across the interface being governed by the local tangential acceleration of the free surface fluid (Rood (1994b))). Hence one must be cautious when attempting to ascribe meaning to vorticity distributions.

The presence of the free slip boundaries at the top and bottom of the computational domain ensure that global circulation is not conserved, however, it was measured anyway so as to get an indication of the circulation associated within each fluid. For a gap ratio of 0.40 and a Froude number of 0.20, figure (3.40) illustrates the variation of the circulation with time for the entire domain, while figures (3.41) and (3.42) show the variation of the circulation with time for each fluid. While it is possible to relate forces to vorticity distributions for a single fluid (for example see Lin & Rockwell (1996) and Noca et al. (1997)), it is not obvious how such an approach could be extended to cases in which more than one fluid is present. This makes quantitative estimates of the forces from the vorticity distribution difficult.

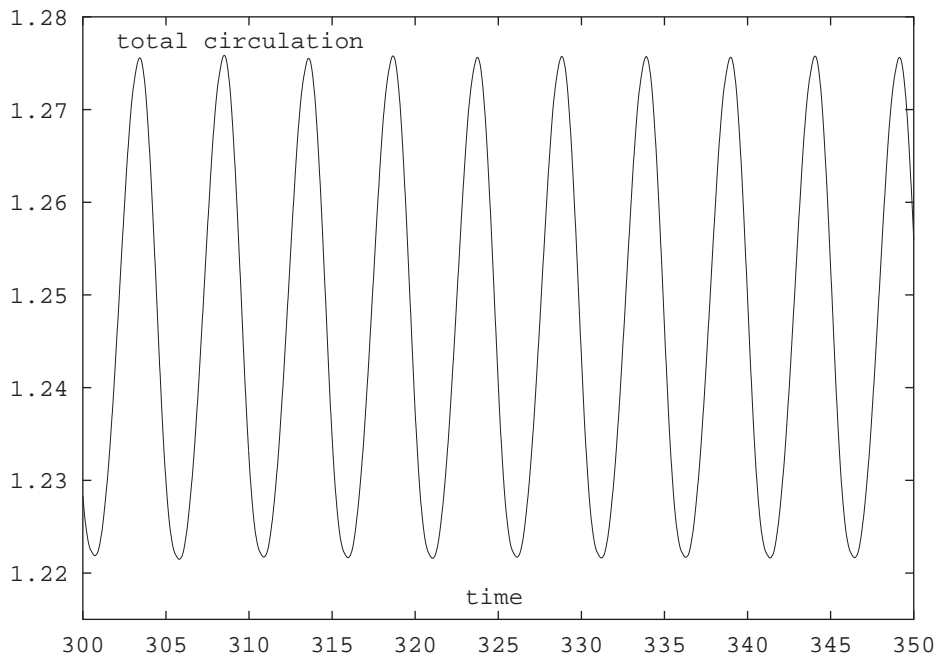


Figure 3.40: Variation of the total circulation with time for a gap ratio of 0.40, a Froude number of 0.20 and a Reynolds number of 180.

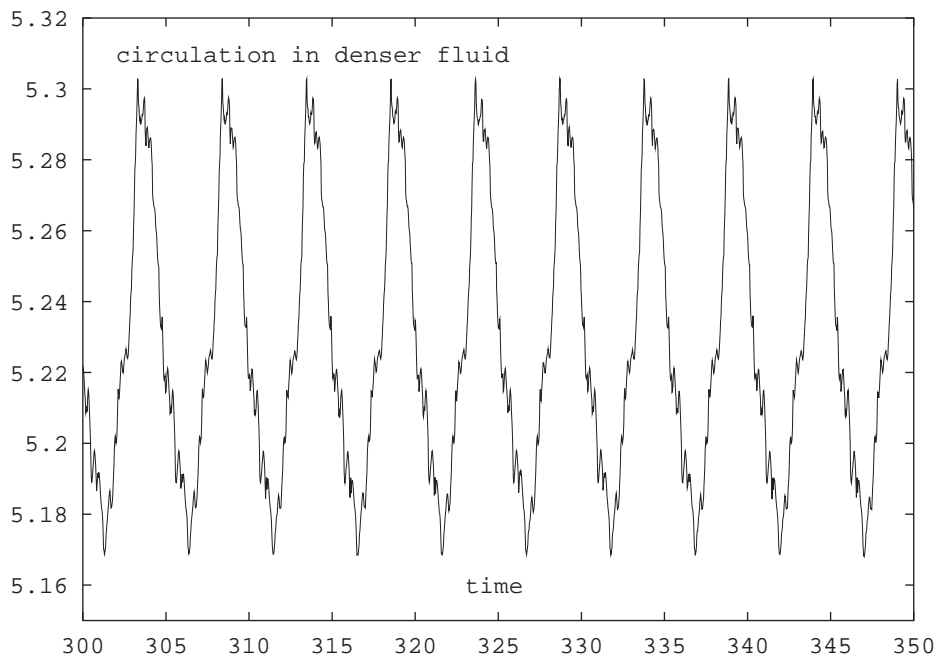


Figure 3.41: Variation of the circulation in the denser fluid with time for a gap ratio of 0.40, a Froude number of 0.20 and a Reynolds number of 180.

3.11 Vortex Paths

The path traced out by the vortices as they move downstream is also of interest as it should illustrate the influence of the free surface upon their motion. Three cases are considered, namely

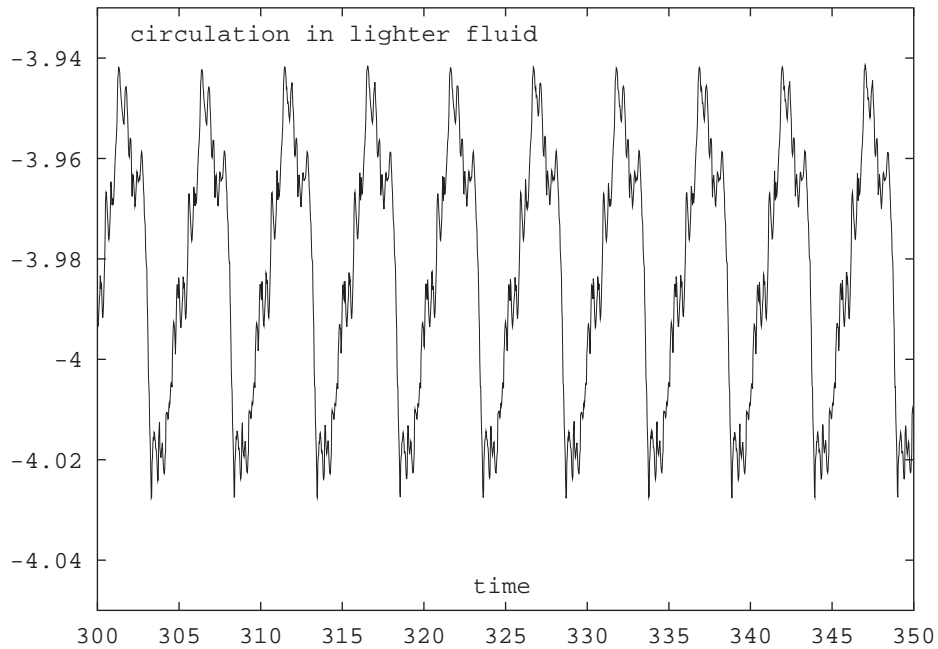


Figure 3.42: Variation of the circulation in the lighter fluid with time for a gap ratio of 0.40, a Froude number of 0.20 and a Reynolds number of 180.

the case of the fully submerged reference cylinder and the free surface cases at a gap ratios of 0.70 and 0.25 respectively. At a gap of 0.70, the path traced out by the vortices shows some degree of rebound, with the negative vortex initially approaching the surface and the bouncing or moving away. This bouncing phenomenon ties in well with what was observed by Ohring & Lugt (1991), where they find vortex rebounding at low Reynolds numbers. However, as Ohring & Lugt (1991) noted, the degree of rebounding is likely to vary somewhat with Reynolds number. The convection speed of the vortices as they travel downstream also changes with submergence depth and this is likely to be related to the confined conditions in the wake cavity. Estimates of the convective speeds of the positive vortices are as follows: reference cylinder 0.8656, gap ratio of 0.70 and Froude number of 0.20, 0.7534 and gap ratio of 0.25 and Froude number 0.20, 0.6352. The observed slowdown in the convection speed with decreasing gap ratio appears to be related to the ease via which fluid may enter the wake cavity. Figures (3.43), (3.44) and (3.45) show the paths traced out by both the positive and negative vortices as they are convected downstream.

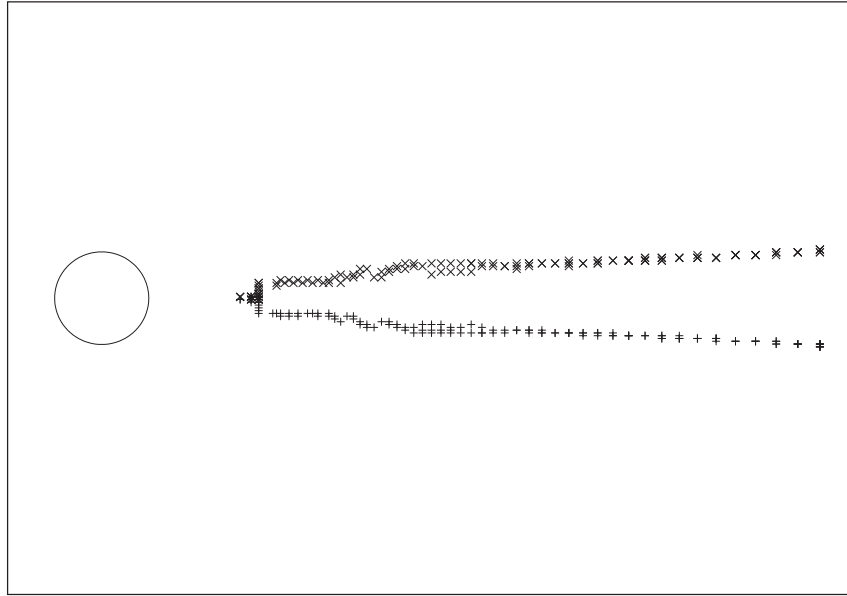


Figure 3.43: Locus of the vortex cores over an number of periods for the fully submerged cylinder at a Reynolds number of 180.

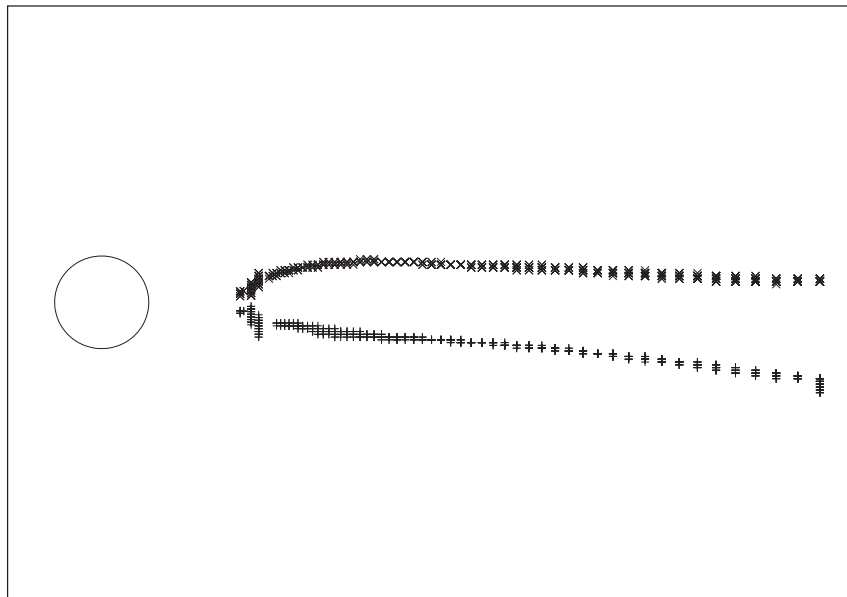


Figure 3.44: Locus of the vortex cores over an number of periods for the gap ratio 0.70, Froude number 0.20 case. The Reynolds number is 180.

3.12 Mechanism for the Cessation of Vortex Shedding

All of the discussion so far has primarily focused on observations, but ideally one would like to know why the observed changes in the wake behaviour occur. To get an idea as to why vortex shedding is suppressed, it is perhaps desirable to know where the fluid making up a vortices

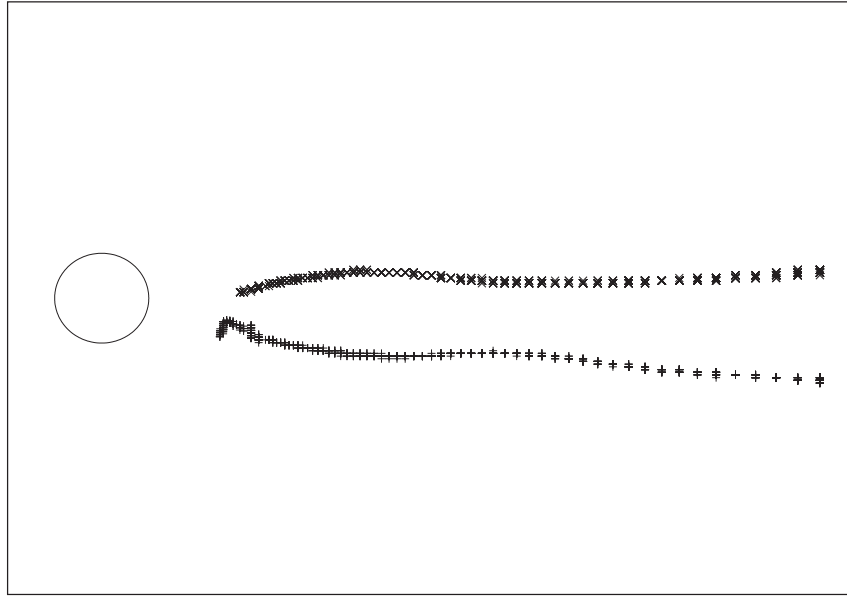


Figure 3.45: Locus of the vortex cores over an number of periods for the gap ratio 0.25, Froude number 0.20 case. The Reynolds number is 180.

comes from. To this end, inert tracer particles were injected into the numerical simulation so that one could observe which regions of fluid make up the forming vortices. As a starting point, this was done for the reference cylinder so as to enable a point of comparison to be obtained. The particle transport videos for the reference cylinder are of considerable worth, as they highlight the extent of the entrainment observed in the wake of the fully submerged cylinder. In particular, it is interesting to note that particles from more than 1.5 cylinder diameters on either side of the cylinder are drawn into the forming vortices. It is also interesting to note that the fluid that vertically spans only 2 diameters at a position 8 diameters upstream of the cylinder, expands such that it vertically spans roughly 6 diameters at locations approximately 12 diameters downstream. This behaviour shown is figure (3.46). By simply watching the video for this case it is clearly visible that the presence of an adjacent surface (be it no slip, free slip or free surface) will severely alter the entrainment process and hence the overall dynamics of the wake.

The fact that similar behaviour is observed in the free slip, the low Froude number free surface, and the no-slip boundary cases, suggests that the governing mechanism for the cessation of vortex shedding with decreasing gap ratio must be common to all situations. Hence it appears as if this problem is primarily governed by a geometrical constraint as opposed to one peculiar to a given set of boundary conditions.

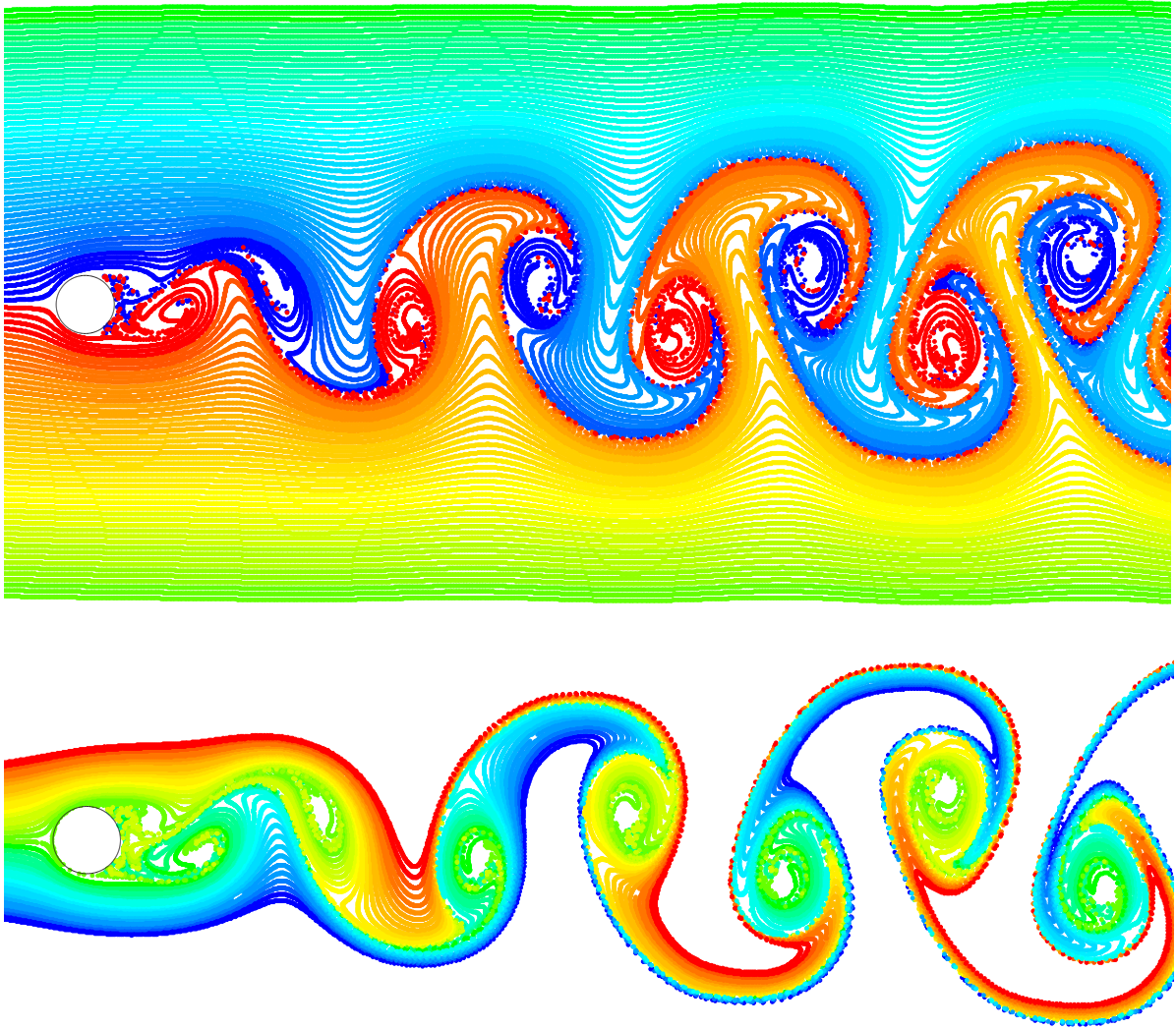


Figure 3.46: Particle transport plots for flow past a fully submerged cylinder at a Reynolds number of 180.

Figure (3.47) shows the particle tracer plot for a gap ratio of 0.40 and a Froude number of 0.20. It is clear from figure (3.47) that the surface blocks the upward movement of fluid, and in doing so forces the vortices into closer contact with one another. It is also apparent that fluid released from below the cylinder is being drawn up toward the surface. The presence of a significant number of the particles that originated above the cylinder within the vortex cores of vortices formed from beneath the cylinder, highlight the entrainment of the fluid which previously made up the negative vortices into the positive vortices.

The particle tracer plots for the smaller gap ratio cases (see figures (3.48), (3.49) and (3.50) and the movies for each case) allude to what may be the underlying mechanism governing the suppression of vortex shedding. In particular, figure 3.50 (for a gap ratio of 0.22 and a Froude

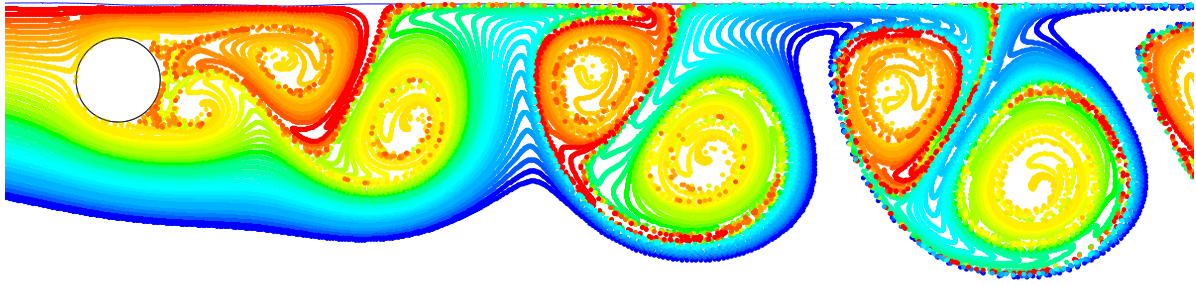


Figure 3.47: Particle transport plot for a gap ratio of 0.40 and for a Froude number of 0.20. The Reynolds number is 180.

number of 0.20), shows the vortex formed from beneath the cylinder almost touching the free surface. The movement of this fluid towards the surface restricts the avenue for entrainment, of both the vortex formed from beneath the cylinder and the vortex forming at the top of the cylinder. It also has the effect of slowing the flow at locations close to the free surface, as the positive vortex from beneath the cylinder will tend to establish a velocity gradient which assists in the slowing/reversal of fluid close to the surface.

The close proximity of the surface also limits amount of fluid available to facilitate the formation of vortices. It is believed that it is the time taken to acquire such fluid, that explains the increasing period (of vortex shedding) observed as the gap ratio is reduced. Such a lengthening in the period is akin to the process suggested by Green & Gerrard (1993), who indicate that the period for a fully submerged cylinder depends upon the time taken for sufficient vorticity to accumulate outside of the region of high shear stress (i.e. in a region from which it can be shed).

For many of the cases in which the gap ratio is small, the fluid required by the forming vortex must be entrained upstream, from downstream. In these cases the fluid from further downstream is forced to flow upstream in order to satisfy the entrainment demands, and this process tends to preferentially strip fluid from the previously shed negative vortices (as they tend to constitute regions of higher pressure). The reader is recommended at this point to view the particle transport videos for the smaller gap ratio cases, as such videos highlight the upstream entrainment of fluid.

When the vortex from beneath the cylinder pinches off the supply of fluid from further downstream, the only fluid available to be entrained into each of the vortices making up the wake cavity is the fluid making up the vortices themselves. This generally leads to a more significant

portion of the fluid passing over the cylinder being pulled down and entrained into the positive vortex which formed beneath the cylinder and hence the flow becomes considerably more skewed. As the gap ratio is decreased the entrainment of the fluid making up one vortex into the other, becomes more severe, until eventually most of the downstream transport of the fluid passing over the cylinder is via entrained into the vortex from beneath the cylinder. And it is at this point that shedding ceases. The reader is recommended to consider the particle transport video for the gap ratio of 0.13, Froude number 0.20, case (in which there is almost no transport of fluid downstream near the free surface).

The notion that the fluid from downstream is drawn upstream to feed the forming vortex at small gap ratios also explains to some extent the rapid decay of the negative vorticity with downstream distance. Consideration of the vortex street images (figures (3.22) to (3.32)) clearly show the negative vortices from above the cylinder diminishing at successively shorter distances as the gap is reduced. This may in part be due to the drawing of the fluid making up these vortices upstream, so as to satisfy the entrainment demands of the later shed vortices. It is this cannibalization or recycling of the fluid which made up the vortices shed earlier, that assists in the premature demise of the negative vortices with downstream distance. This is highlighted when one considers that the structures resembling discrete negative vortices have vanished after progressively shorter distances with decreasing gap, leaving only larger scale positive vortices at greater distances.

It may be advantageous at this point to look at this same phenomenon in terms of the local pressure field, which makes up part of the actual solution and hence may perhaps provide greater insight. Examination of the pressure field indicates that vortices constitute regions of low pressure and hence will tend to draw fluid towards them (entrainment process), as fluid will flow in the direction of decreasing pressure gradient. This applies equally to both the negative vortex formed from above and the positive vortex formed from beneath the cylinder. As the most recently formed vortices tend to have the highest concentrations of vorticity, they also tend to have the lowest pressures associated with them. Hence, fluid will be drawn to these vortices. For the case of a fully submerged cylinder there is a ready supply of fluid which can be attracted to each vortex, however, for the case considered here in which the surface limits the amount of fluid available, both vortices are forced to compete for fluid. The bias in available fluid created by the adjacent surface then results in the establishment of a pressure gradient which facilitates a reduction (and in some cases a reversal) in the convective velocity of the fluid close to the free surface.

The reduction or reversal of the flow in this region introduces fluid upstream from previously shed vortices (and in particular previously shed negative vortices, due to their location closer to the surface). The free-surface boundary condition clearly facilitates the upstream movement of fluid, whereas the no-slip condition would tend to hinder the reverse flow and this may explain why shedding was observed down to smaller gap ratios in the current study. One may observe that the pressure just above the vortex from beneath the cylinder tends to increase as it is pushed upward (against the surface which is fairly rigid at this Froude number), and that this assists with the upstream movement of some of the fluid which made up the last shed negative vortex. It is also apparent that the pressure associated with the vortex core is significantly lower in the downstream region for the shed vortices from beneath the cylinder as opposed to those from above. This seems to be in part due to the fact that the negative vortices are being ‘squashed’ against the almost rigid free surface. The pressure field for a gap ratio of 0.22 and a Froude number of 0.20 is shown in figures (3.51) and (3.52).

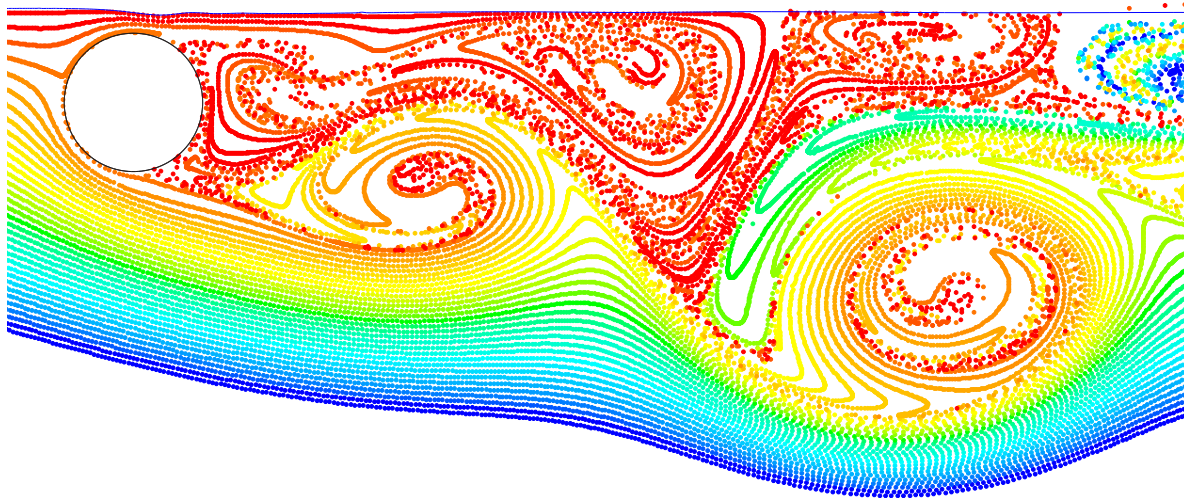


Figure 3.48: Particle transport plot for a gap ratio of 0.16 and for a Froude number of 0.20. The Reynolds number is 180.

The suggestion by Koch (1985) that an asymmetric wake can not support an absolute instability implies that the cessation of shedding is likely to be due to an asymmetry in the velocity profile. It is believed that it is the reduction in the velocity near the surface, which is largely brought about by the close proximity of the positive vortices, that introduces this asymmetry. This notion is supported at least in part, by the rapid reduction of the maximum time-averaged velocity in the region just above the cylinder with gap ratio, as shown in figure (3.34). Thus it appears as

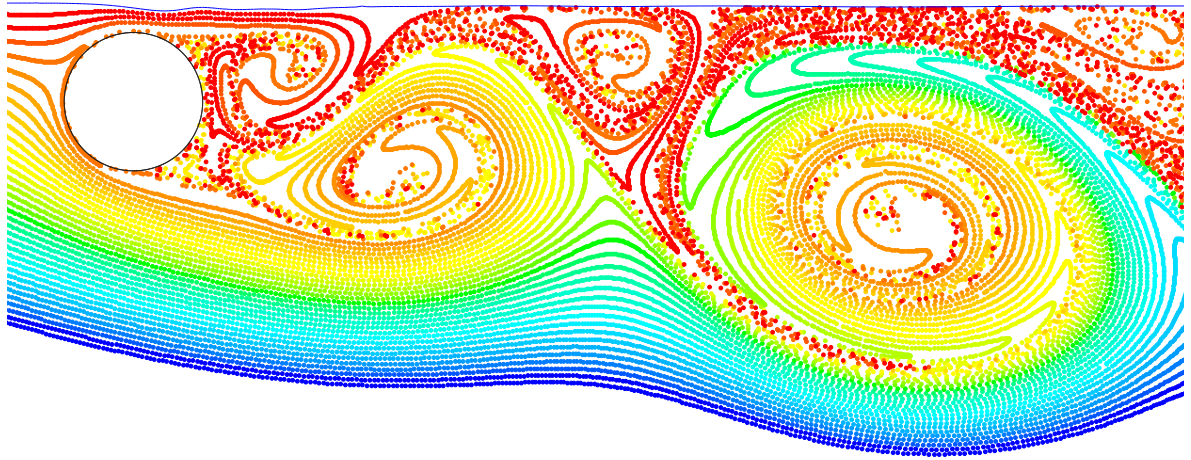


Figure 3.49: Particle transport plot for a gap ratio of 0.19 and for a Froude number of 0.20. The Reynolds number is 180.

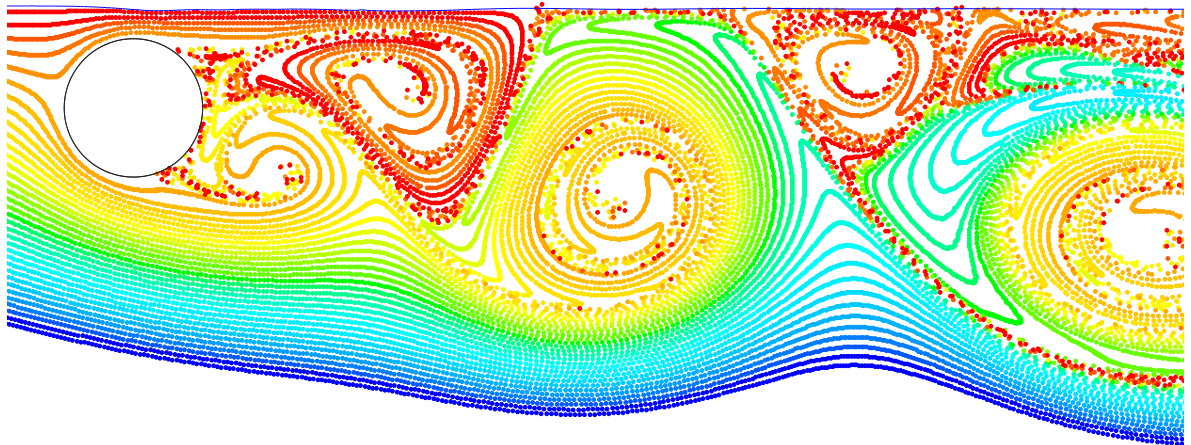


Figure 3.50: Particle transport plot for a gap ratio of 0.22 and for a Froude number of 0.20. The Reynolds number is 180.

if it is the close proximity of the positive vortices from beneath the cylinder, in conjunction with the lack of available fluid for discrete vortex formation, that leads to the cessation of shedding. To reiterate, the mechanism which results in the cessation of vortex shedding is believed to be as follows. The roll-up of the positive vortex from beneath the cylinder pushes the fluid directly

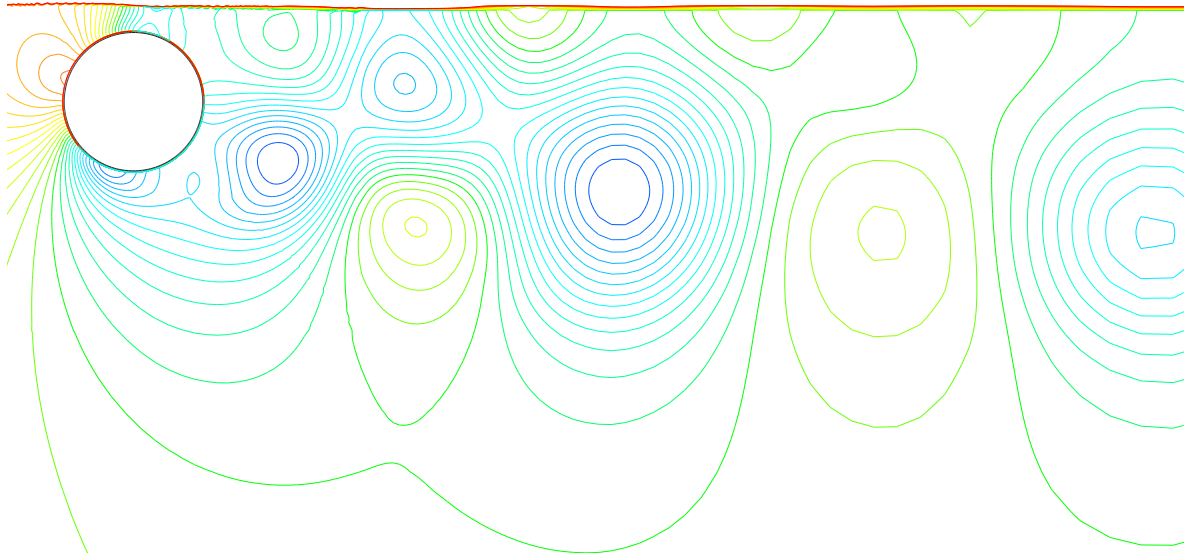


Figure 3.51: Plot showing the pressure field at the same instant as the particle transport plot in figure (3.50) (gap 0.22, Froude number 0.20, Reynolds number 180).

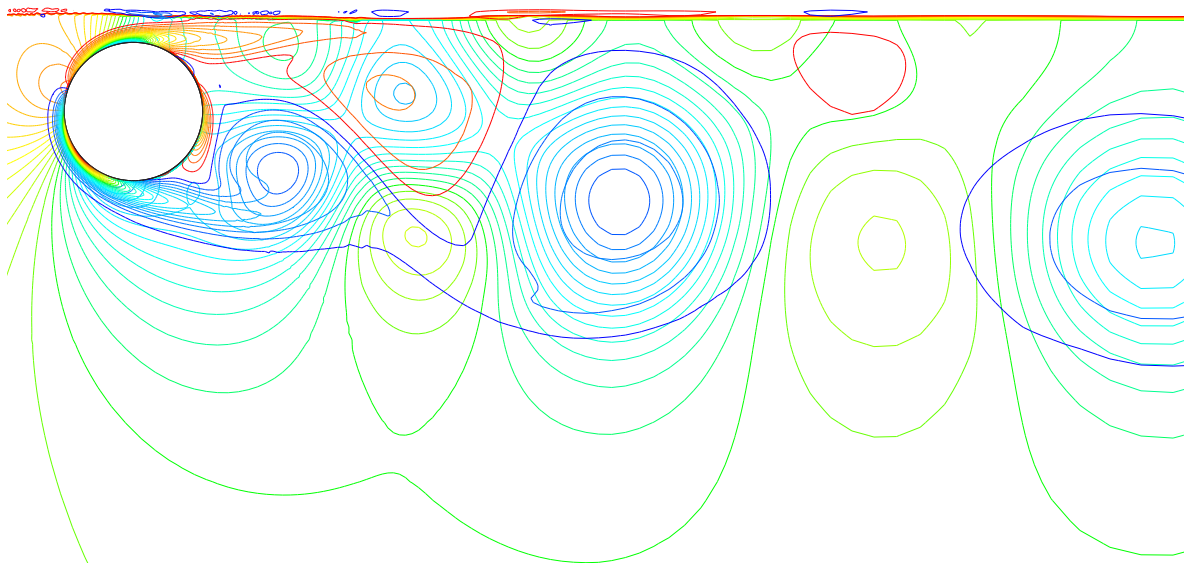


Figure 3.52: Plot showing the pressure plot with vorticity overlaid at the same instant as the particle transport plot in figure (3.50) (gap 0.22, Froude number 0.20, Reynolds number 180).

above it upwards and the rigid nature of the adjacent surface (in the case of a free surface, the surface is only rigid at low Froude numbers) results in the surface remaining relatively flat. Hence the pressure associated with the fluid located above the vortex from beneath the cylinder increases. This pressure rise results in the establishment of a pressure gradient that helps to

promote the movement of the fluid close to the surface upstream toward the region of lower pressure. Now as the most recently formed vortices correspond to the regions of lowest local pressure, the fluid located above the positive vortex will tend to accelerate towards the vortex cores. The restricted flow conditions and in particular those at smaller gap ratios, ensure that the previously shed vortices from the upper half of the cylinder always possess a greater pressure than those from the lower half of the cylinder. This is the case, as all of the fluid closer to the surface is to some extent being pushed upward. The sign of the vortices (i.e. their direction of spin) will then determine the path taken by the fluid as it moves towards these regions of lower pressure.

The establishment of these pressure gradients imply that the flow close to the surface should be slowed and in some cases reversed at positions just above the positive vortices. The closer the cylinder is to the surface the stronger the pressure gradient created and hence the greater the impact of positive vortices from beneath the cylinder on the local flow. This phenomenon will tend to draw in fluid from previously shed negative vortices (as they are being pushed against the surface, thus increasing the local pressure in the regions above the positive vortices), which will subsequently result in the premature decay of these negative vortices with downstream distance.

The intromission of fluid upstream from downstream into the forming vortex, is likely to occur for free-slip, free-surface and no-slip boundary conditions. However, the ease via which this intromission of fluid upstream from downstream occurs will depend on the boundary condition. Indeed, for the free-slip and free-surface (at low Froude number in which the surface barely deforms) cases, it is expected that this intromissive process will be assisted by the zero tangential surface stress condition. For the no-slip case on the other hand, the nature of the local wall boundary layer is likely to influence this behaviour.

As the gap ratio is reduced the avenue through which fluid from downstream may move upstream is increasingly restricted. However, the fluid near the surface is still drawn upstream due to the pressure gradient and at small gap ratios most of the fluid making up the negative vortex shed in the last cycle, is intromitted upstream (with this process best observed via consideration of the particle transport videos for the gap ratio 0.16, Froude number 0.20 case). The stripping of fluid from previously shed negative vortices appears to take on the form of ‘vortex swallowing’, in which much of the fluid from a previously shed vortex is ‘swallowed’ or intromitted upstream, into the vortex of the same sign shed during the following cycle (with this process again best illustrated in the video). This ‘swallowing’ coincides with formation of larger scale positive vortical structures that arise from the coalescence of previously shed positive vortices.

At a gap ratio of 0.19 and a Froude number 0.20, this is observed to occur at the second most recently shed negative vortex (see the video). In this case the fluid making up the third most recently shed vortex is ‘swallowed’ or intromitted into the second most recently shed vortex. This is not entirely surprising, as the presence of the positive vortices from beneath the cylinder will tend to force the fluid above them to move upstream while also becoming partly entrained into the more dominant positive vortices.

The ‘vortex swallowing’ process tends to move further and further upstream with decreasing gap ratio, until it eventually moves to the rear of the cylinder. The lack of negative vorticity at locations downstream of the cylinder at the smaller gap ratios, results in a slowdown in the convection of the positive vortices as there is little mutual induction or propulsion to assist their downstream convection. Under these circumstances there is a tendency for the positive vortices to move up into the lower energy part of the wake (i.e. the region behind the cylinder and closer to the surface), thus leading to the formation of large scale positive vortical structures.

The larger scale positive vortical structures typically form when one positive vortex moves upward slightly and in doing so it pushes the fluid above it both upstream and downstream. The next shed positive vortex will then have more fluid above it and hence it will not move as far upward. This creates a situation in which one positive vortex is closer to the surface than the one shed after it. The slight height difference results in the positive vortex closer to the free surface having a slower convective velocity. When the later shed positive vortex eventually catches the one shed prior to it the two vortices are observed to coalesce.

This degeneration of the vortex street may be what Taneda (1965) referred to (for the case of a cylinder close to a no-slip wall), when he mentioned that the wavelength of the vortices increased with downstream distance and that the wake broke down after a few wavelengths. The formation of these large structures is also consistent with the comments of Angrilli et al. (1982), who indicate that the flow is slower on the wall side at locations downstream of the cylinder.

The coalescence of the positive vortices assists in the transport of fluid upstream, as the upper slowly moving positive vortex revolves around the one shed later, in a process that is again best illustrated in the videos (see videos for gap ratios of 0.16 and 0.19). At gap ratios approaching the depth at which shedding ceases completely, for example gap 0.16 Froude number 0.20, much of the fluid located above and behind the cylinder simply oscillates backwards and forwards, with little actually being removed (i.e. much of the fluid is being recycled) with entrainment into the positive vortices dominating its downstream transport. For these cases the residence

time of the fluid located in this region is high, with figures (3.53) and (3.54) showing particles colored by residence time, for the free surface case at gap ratios of 0.16 and 0.19 respectively.

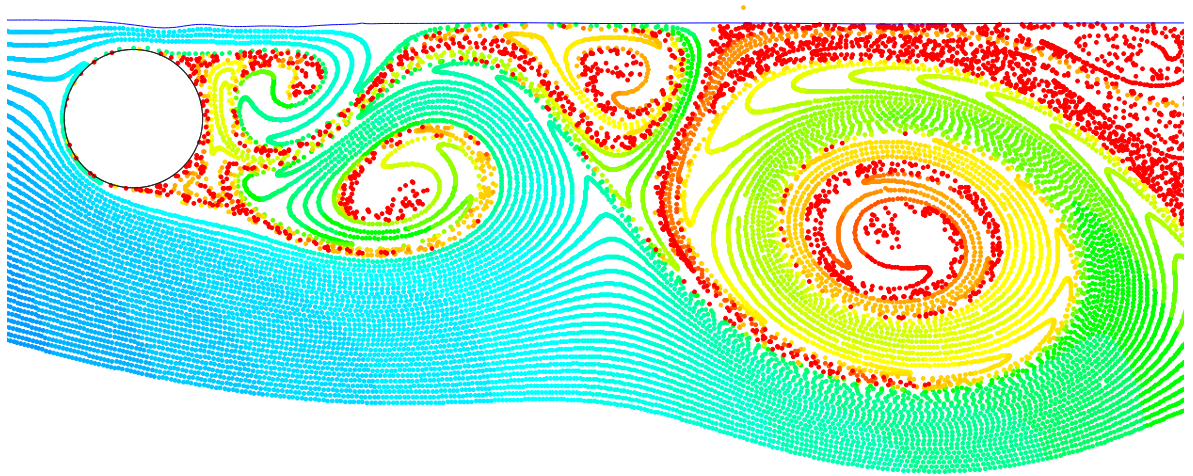


Figure 3.53: Particles colored by residence time for a gap ratio of 0.19 and for a Froude number of 0.20. The Reynolds number is 180.

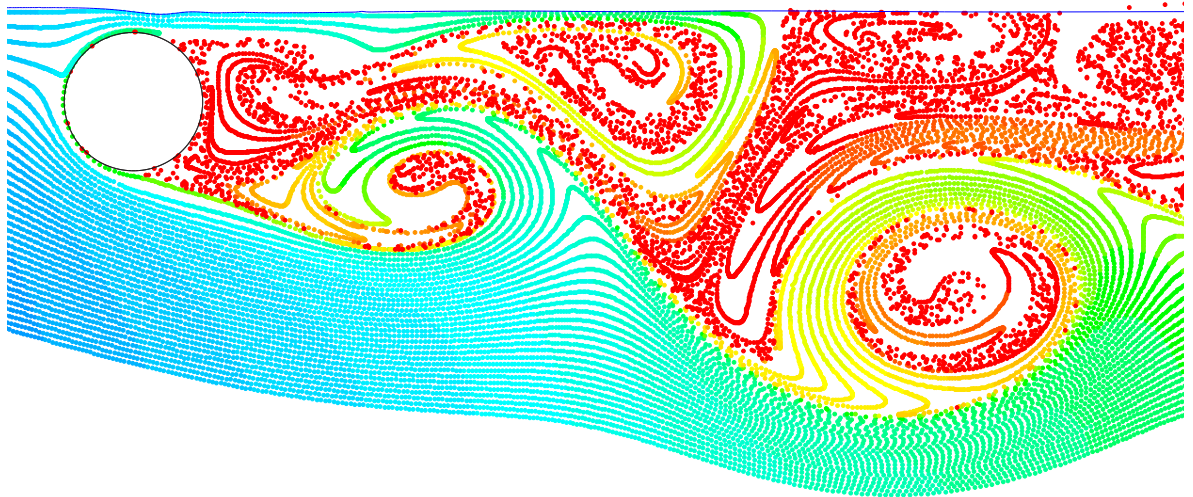


Figure 3.54: Particles colored by residence time for a gap ratio of 0.16 and for a Froude number of 0.20. The Reynolds number is 180.

When the gap ratio is reduced even further much of the fluid from above the cylinder will be pushed against surface, resulting in an increase in the local pressure in this entire region. When

this is coupled with an insufficient intromission of fluid into the forming negative vortex, the two most recently formed/forming vortices are forced closer together with each attempting to entrain fluid from the other. As the positive vortex from beneath the cylinder will tend to be stronger having not had to interact with the free surface as well as not having its fluid supply limited, it will constitute the region of lower pressure. Much of the fluid that would have been entrained into the negative vortex is now drawn toward the positive vortex and at this point shedding ceases. Aspects of this phenomenon are shown in figure 3.55, which shows the particle transport plot for a gap ratio of 0.16, and a Froude number of 0.20. However the reader is recommended to view the video for this case which more clearly illustrates the entire process.

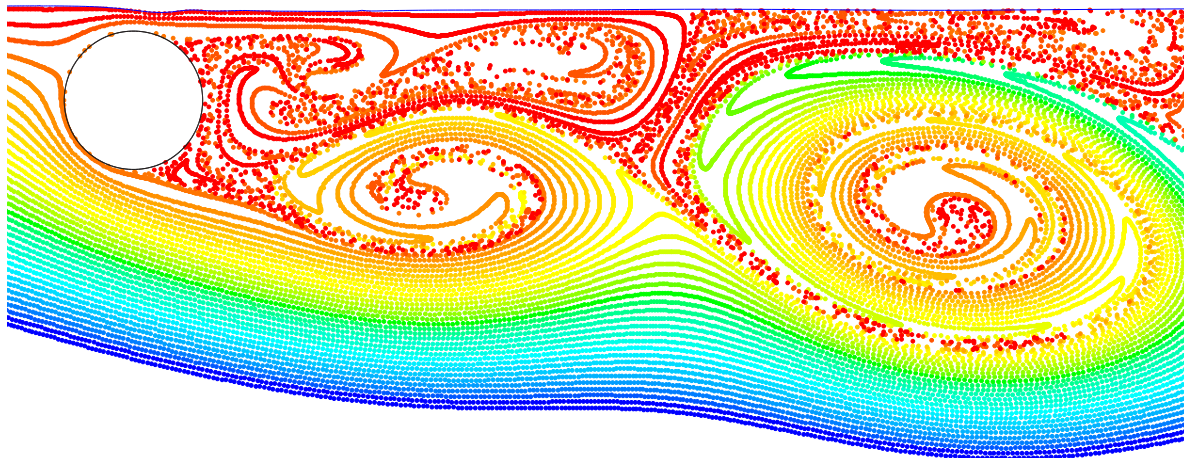


Figure 3.55: Particle transport plot for a gap ratio of 0.16 and for a Froude number of 0.20. The Reynolds number is 180.

The next question that arises is: what influence does a more readily deformable free surface have on the events described above? This question will be considered in the next chapter which looks at the flow at larger Froude numbers.

3.13 Summary

It is clear that the free-slip surface and the free surface at low Froude number, share similar characteristics with flow past a cylinder close to a no-slip boundary. The agreement in the trending behaviour of most quantities, suggests that the problem is largely governed by geometrical constraints. A mechanism which describes the cessation of vortex shedding is proposed, and it

is envisaged that this mechanism should be applicable to the free-slip, free-surface, and no-slip cases.

Chapter 4

Froude Numbers 0.25, 0.30, 0.35 and 0.40

In this chapter the flow in the region of parameter space in which the wake begins to shift away from being parallel is examined, such that the influence of skew is now more prevalent. Although this discussion will be largely limited to the cases in which the fluid from above the cylinder remains attached to the free surface, it will illustrate the impact that significant surface curvature has on the wake. The first part of this chapter will examine the results with key points being noted as they arise, while the latter part will again be dedicated to a discussion of the mechanism which is believed to be responsible for the observed behaviour.

The study will primarily focus upon changes in Strouhal number as well as the mean and RMS components of both the lift and drag. In addition, the mean moment acting upon the cylinder is examined, as is the behaviour of the stagnation and separation points, the pressure distribution, the mass flux over the cylinder, the formation length, the local Froude number (Froude number based on the submergence depth) and the path and velocity of the vortices as they are convected downstream.

To the author's knowledge, little work on flow past a cylinder close to a free surface has been conducted within this Froude number range, with the exceptions being Miyata et al. (1990) (at a Froude number of 0.24), and one result from Sheridan et al. (1997) (at a Froude number of 0.35). Hence comparisons with the results of Miyata et al. (1990), the previous chapter, and with those of Sheridan et al. (1995), Sheridan et al. (1997) and Hoyt & Sellin (2000), (with the last three studies all looking at predominantly larger Froude numbers) have been made.

The influence of the Froude number on the surface deformation is discussed by Yu & Tryggvason (1990), Ohring & Lugt (1991), and Lugt & Ohring (1992). In each of these investigations, the interaction of vortices with a free surface were considered, and it was noted that the level of surface deformation was largely dependent upon the Froude number (with the length scale in the Froude number used by Ohring & Lugt (1991) being the initial vortex separation). The definition of the Froude number used in the current investigation follows this approach, with the cylinder diameter being used as the length scale. Some free surface behaviour is described in terms of a Froude whose length scale is the submergence depth (with hydraulic jumps being one example). To allow for a discussion that includes both definitions, the latter one (i.e. the one based on the submergence depth) has been deemed to be the local Froude number.

Ohring & Lugt (1991) indicate that at intermediate Froude numbers (approximately 0.40), some degree of vortex bouncing (or rebounding) was observed, whereby the path of the primary vortex center describes a loop. This bouncing occurs as a consequence of the presence of secondary vorticity formed by the interaction of the primary vortex with the free surface. However, this rebounding was found to be a function of Reynolds number (with its influence tending to be stronger at lower Reynolds numbers), and hence this phenomenon may have some slight impact in the current investigation.

Ohring & Lugt (1991) also note that although the level of surface deformation is greater at larger Froude numbers, it is the sharpness of the scar (region in which surface curvature changes sign) that determines the amount of surface vorticity present (which is largely as expected, as the surface vorticity for a steady surface is $2\kappa v_\theta$, where κ is the surface curvature, and v_θ is the component of the velocity tangential to the free surface).

Before proceeding further, it is beneficial to consider what effect the increasing Froude number is likely to have upon the flows behaviour so that key points can be sought out in advance. Firstly, it is expected that the gap ratio at which shedding ceases is likely to grow with increasing Froude number, as the greater levels of time varying surface curvature should increase the flux of negative vorticity (vorticity from the upper side of the cylinder) across the interface. This assumption follows directly from the statement by Rood (1994*b*) that the flux of vorticity through a free surface depends on the viscous acceleration of the free surface fluid in the direction tangential to the free surface. Hence, the acceleration associated with a free surface whose position is constantly changing (largely in response to the underlying time dependent vorticity field) will permit a flux of vorticity across the interface. The removal of this vorticity is then expected to result in the wake being dominated by positive vortical structures, particularly at smaller gap

ratios, and it is thus anticipated that the wake will become skewed at progressively larger gap ratios with increasing Froude number.

To observe the influence of the surface curvature upon the wake, a series of simulations at Froude numbers of 0.25, 0.30, 0.35 and 0.40 were considered. The change in Froude number was facilitated by the modification of the body force (g) present in the simulations. This was achieved by using the solutions from the Froude number 0.20 case and slowly ramping the body force until the desired Froude number was obtained. Such an approach was adopted to ensure that the Froude number could be changed independently of both the Reynolds number and fluid properties. The submergence depths considered here were the same as those examined in the previous section, namely; 0.10, 0.13, 0.16, 0.19, 0.22, 0.25, 0.40, 0.55, 0.70, 0.85, 1.00, 1.50, 2.50 and 5.00. The behaviour of the flow over this range of parameters is now considered.

4.1 Flow Behaviour and Surface Deformation

For the most part the flow field at the lower Froude numbers (i.e. 0.25 and 0.30) largely resembled that in the previous chapter, with the flow from above the cylinder following the free surface, and only slight surface curvature being noted. At the larger Froude numbers (i.e. 0.35 and 0.40), the surface curvature was more pronounced and a flux of positive vorticity into the flow was observed, with some small scale wave breaking noted at gap ratios between 0.40 and 0.70. Much of the flow behaviour is best illustrated in the videos, which are contained on the compact disk accompanying this thesis. However, the vortex streets for a selection of the gap ratios spanning the range of Froude numbers considered here are shown in figures (4.1) to (4.4).

An interesting point to note in figures (4.1) to (4.4) is the rapid decay of the negative vorticity with distance downstream. This appears to be due to two major effects: the first is the flux of vorticity across the free surface, while the second is the cannibalization of the fluid making up these vortices by the more recently shed negative vortices. This cannibalization process is again best illustrated via consideration of the videos on the attached compact disk.

To gain an understanding of what the surface looks like in the region close to the cylinder, the position of the free surface was examined. The surface position was defined by locating the point at which the volume fraction was equal to 0.5 (which yields the location of the interface position within a grid cell, hence giving better accuracy near the cylinder where the grid is finer and more inaccurate results at positions away from the cylinder, where the vertical grid spacing

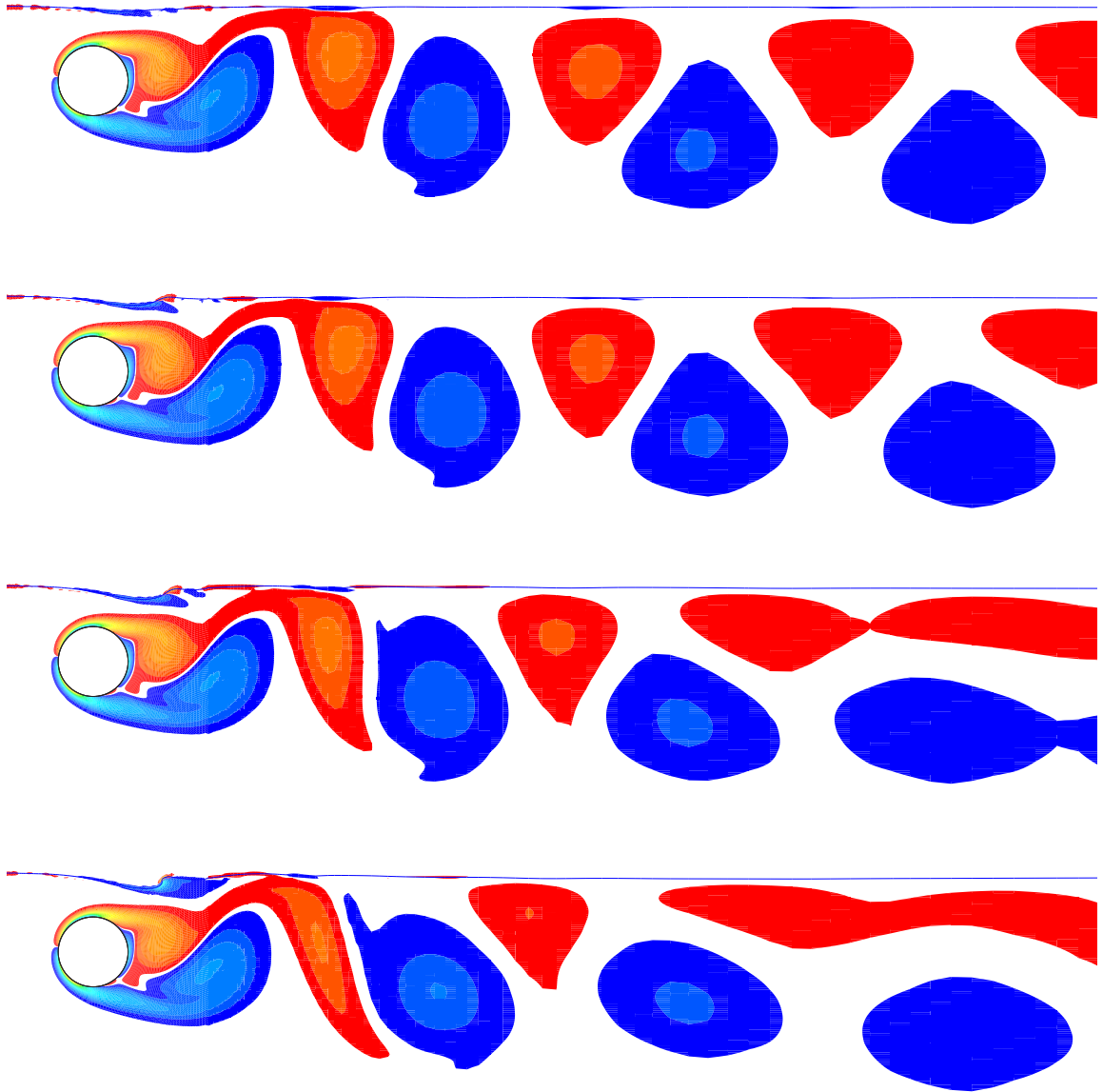


Figure 4.1: Vortex streets for a gap ratio of 0.55 and for Froude numbers of 0.25, 0.30, 0.35 and 0.40 (top to bottom). The Reynolds number for each case is 180.

is larger). For cases in which the shedding was close to ceasing, had ceased, or was modulated (i.e. the lift trace showed some degree of modulation), changes in the behaviour of the wake had the capacity to produce small alterations in the surface position which could travel upstream. For most cases, these were transient, and they tended to die down with time. However, in some instances in which the wake was continuously changing in a non purely periodic manner, these changes congregated near the inlet in the form of a mild undulation. Such an undulation appears to result from the changes in the wake (i.e. changes in the wake associated with the cessation

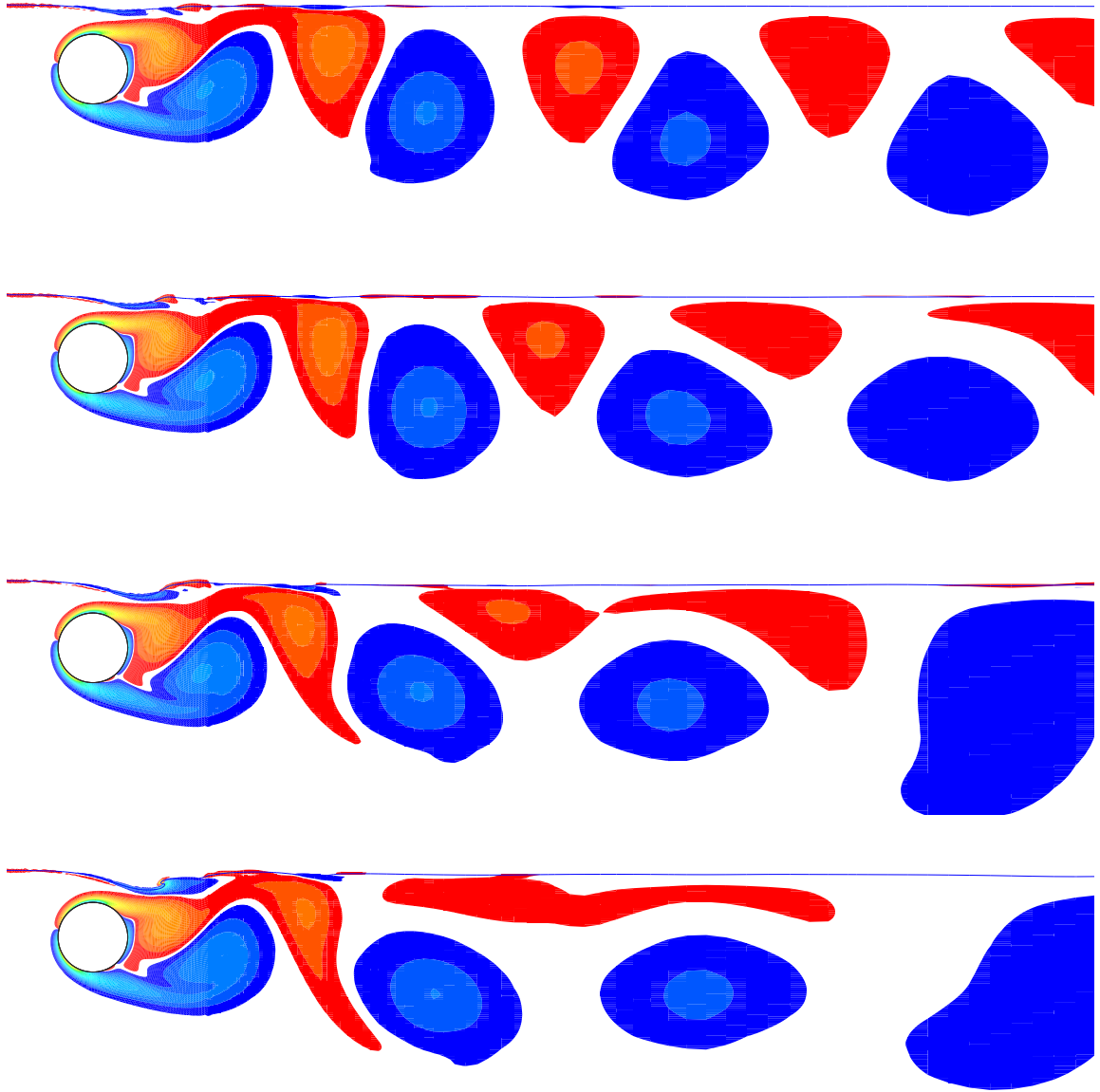


Figure 4.2: Vortex streets for a gap ratio of 0.40 and for Froude numbers of 0.25, 0.30, 0.35 and 0.40 (top to bottom). The Reynolds number for each case is 180.

of shedding or by its weakening tended to result in the increase in the surface elevation near the inlet). It should be noted that no trapped wave was observed (i.e. there was no evidence to suggest that there was a wave that was being continuously reflected from the ends of the domain). These height changes were in the order of the height of one grid cell near the inlet which was 0.03, and in the worst cases the height of 2 grid cells (0.06).

The variation of the surface height near the inlet is shown in figures (4.5) and (4.6), which illustrate one of the more extreme cases at the points of both maximum and minimum lift. As

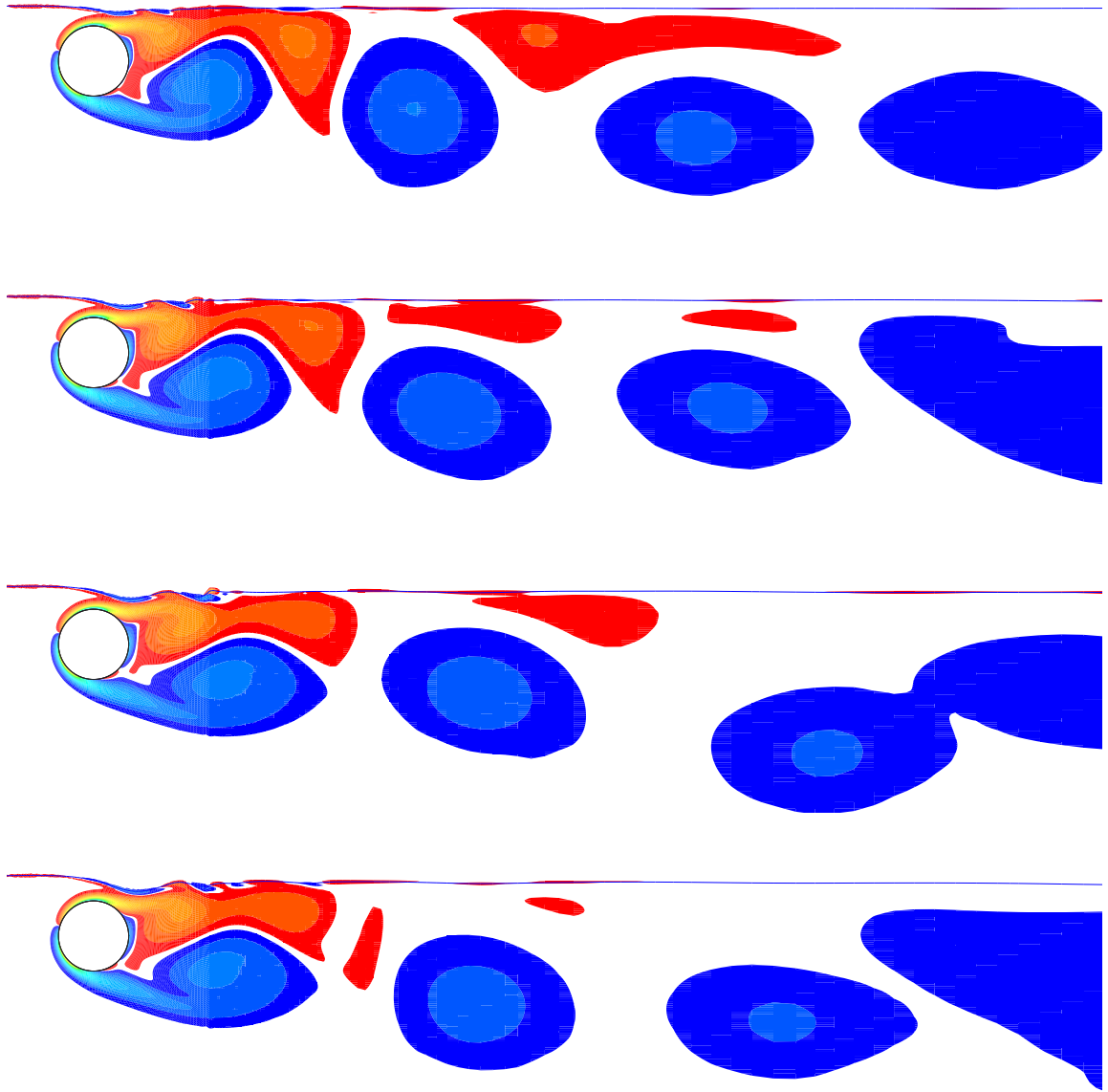


Figure 4.3: Vortex streets for a gap ratio of 0.25 and for Froude numbers of 0.25, 0.30, 0.35 and 0.40 (top to bottom). The Reynolds number for each case is 180.

previously mentioned, these changes did vary slightly in conjunction with the wake behaviour, but are believed to have little impact on the overall flow results. It should be stressed that the surface position at distances further from the inlet varied little, with the variation in height between the results at different Froude numbers at a distance of 5.9 diameters upstream (i.e. the position at which the surface height was measured by Sheridan et al. (1997)) varying by at most the height of one grid cell.

The plots of surface positions near the cylinder in figure (4.7) show the rise in the level of

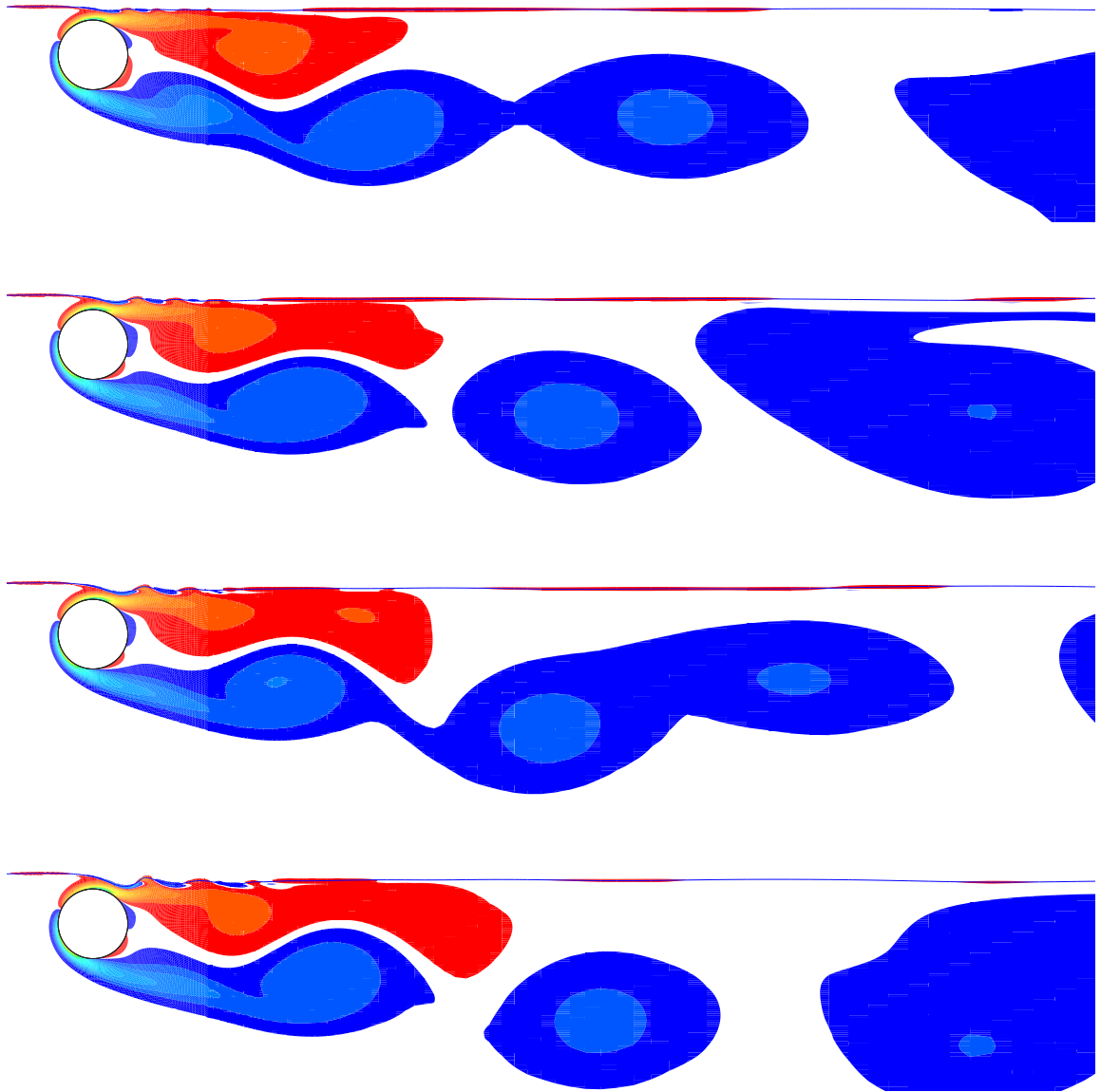


Figure 4.4: Vortex streets for a gap ratio of 0.16 and for Froude numbers of 0.25, 0.30, 0.35 and 0.40 (top to bottom). The Reynolds number for each case is 180.

surface deformation with increasing Froude number. The variation in the surface position with time is also much greater at the larger Froude numbers, with the level of surface distortion experienced during one shedding cycle becoming more significant. It is also important to note where the surface has been distorted at each of the extremes in the shedding cycle. At lower Froude numbers, the level of distortion was small and the surface was smooth with only gentle undulations being noted (i.e. minimal surface distortion was observed at both of the extremes in the shedding cycle). At larger Froude numbers the surface distortions became more marked,

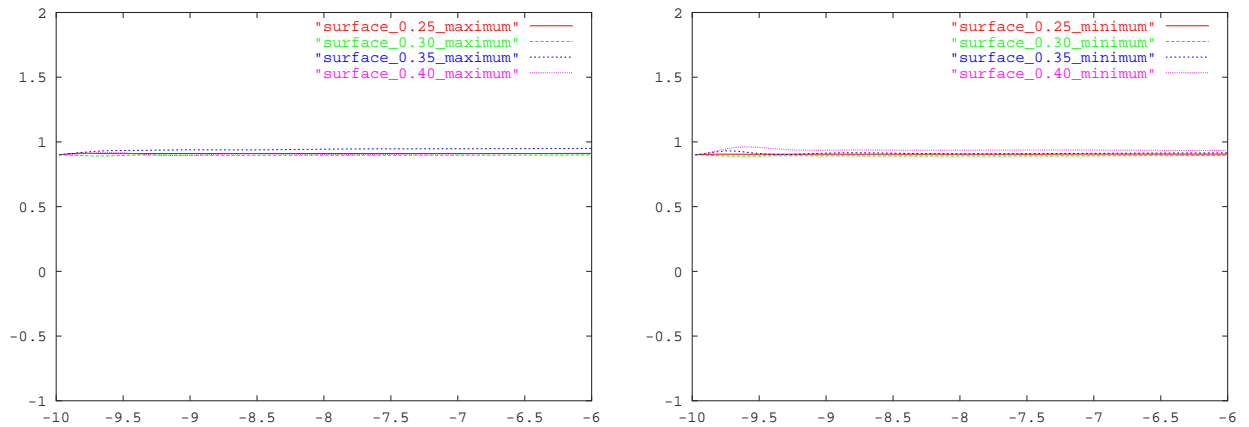


Figure 4.5: Plots showing the variation in the surface position near the inlet at the point of maximum (left) and minimum (right) lift, for Froude numbers of 0.25, 0.30, 0.35 and 0.40 at a gap ratio of 0.40. The Reynolds number in each case is 180.

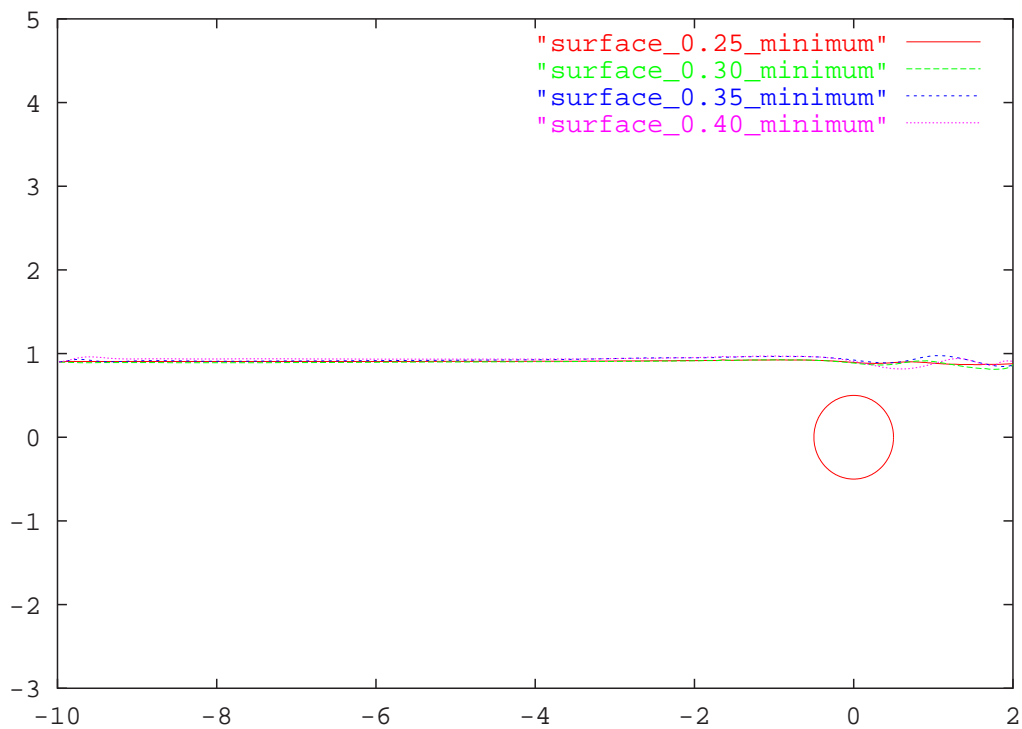


Figure 4.6: Plot showing the variation in the surface position near the inlet at the point of minimum lift but this time over a larger range to give perspective. The gap ratio is again 0.40 and the Froude numbers considered are 0.25, 0.30, 0.35 and 0.40. The Reynolds number in each case is 180.

and there was a notable difference between the levels of deformation at the two extremes in the lift cycle. Typically the surface deformation was more severe at the point of maximum lift, and it tended to occur at positions closer to the cylinder. However, it should be noted that the level surface deformation varied with both Froude number and gap ratio. The Froude

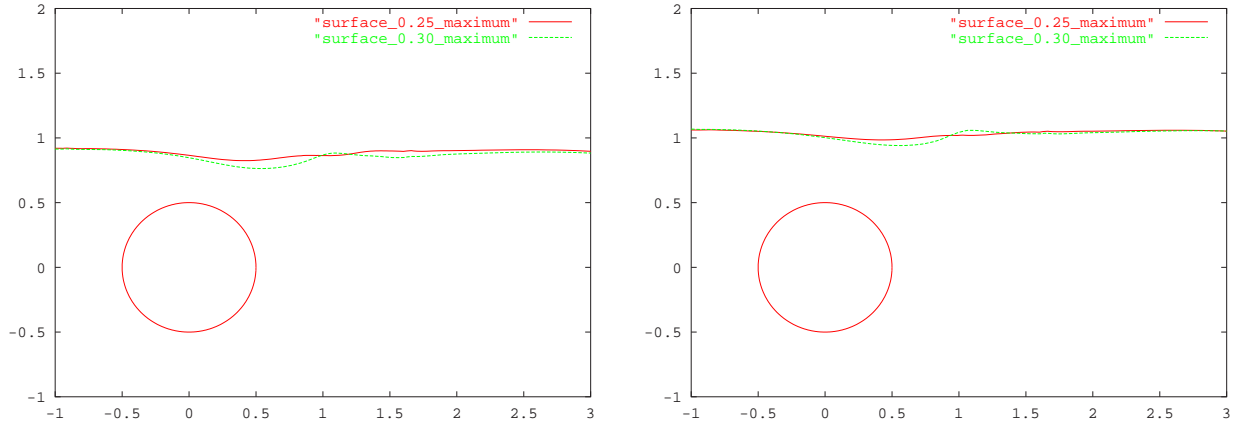


Figure 4.7: Variation of the surface position with Froude number for gap ratios of 0.40 and 0.55 and Froude numbers of 0.25 and 0.30. The Reynolds number in each case is 180.

number dependence of the distortion is best illustrated by considering the surface positions at two different gap ratios for two different Froude numbers. Figure (4.8) illustrates the influence of the Froude number on the surface distortion. It was interesting to note that the surface scar was generally sharper at the point of minimum lift at a Froude number of 0.35, while at a Froude number of 0.40 it tended to be sharper at the point of maximum lift. The variation of the surface position with time was in general accord with the comments of Hoyt & Sellin (2000), who note that the surface oscillates with the Kármán frequency.

The position at which the sharpened surface and small scale wave breaking occurred also varied with gap ratio. At a gap of 0.25, it was observed at locations between 1 and 1.5 diameters downstream of the rear of the cylinder. However, at gaps of 0.40 and 0.55, it tended to occur at roughly half a cylinder diameter downstream. It is expected that this shift is related to the change in the formation length which is considered later in section (4.6).

An examination of the vorticity fields in figures (4.1) to (4.4), and in particular those for the smaller gap ratios, clearly indicates that there is a bias in the vorticity distribution. Such a bias is consistent with the observations of Sheridan et al. (1997) and to some extent Warburton & Karniadakis (1997), and it is believed that that this arises as a result of the viscous transport of negative vorticity across the interface (free surface). Rood (1994*b*) states, that the flux of vorticity through a free surface depends on the viscous acceleration of the free surface fluid in the direction tangential to the free surface. Hence for the cases in which the free surface is close to the cylinder, it is expected that the negative vorticity will be removed from the fluid via both diffusion and cross-annihilation.

The bias in the vorticity distribution tends to result in the wake being dominated by positive

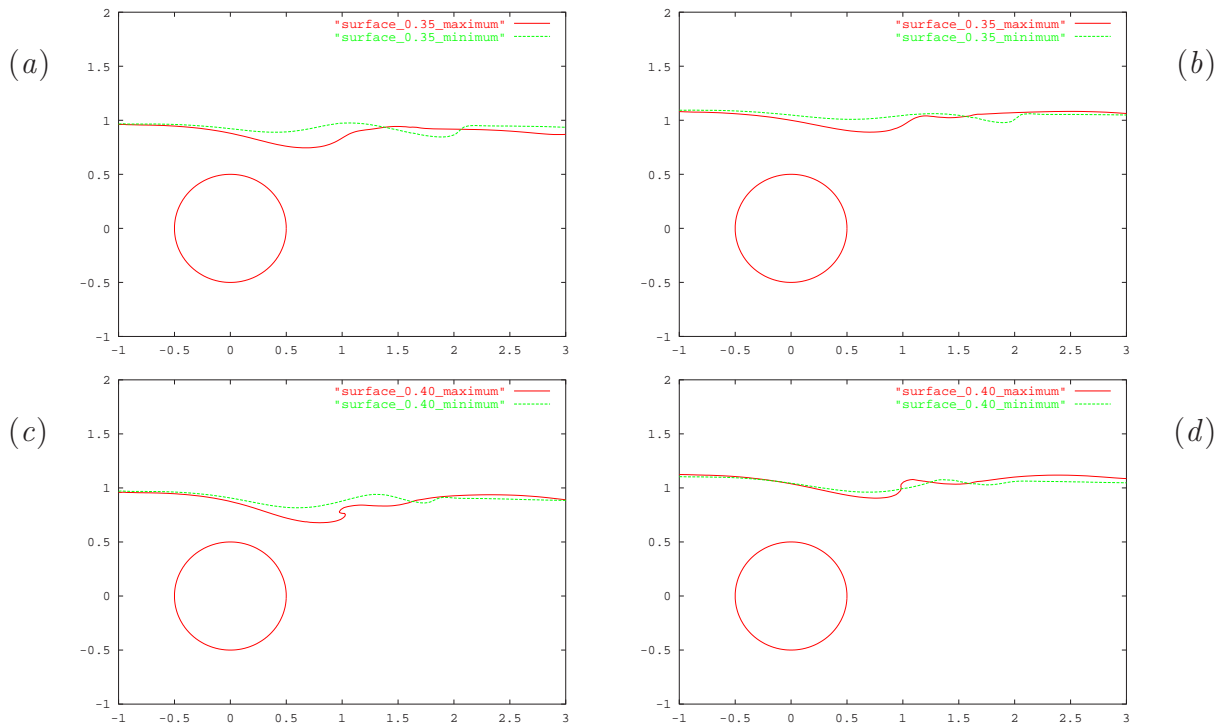


Figure 4.8: Surface position at the two extremes in the lift cycle, for Froude numbers of 0.35 and 0.40 and for gap ratios of 0.40 and 0.55. (gap ratio 0.40, Froude number 0.35 (a), gap ratio 0.55, Froude number 0.35 (b), gap ratio 0.40, Froude number 0.40 (c), gap ratio 0.55, Froude number 0.40 (d)). The Reynolds number in each case is 180.

vortical structures. Such structures arise as the absence of negative vorticity in the wake allows the previously shed positive vortices to coalesce, with this process tending to slow the fluid at locations close to the surface (as the positive vortices tend to rotate in a counter-clockwise manner).

4.2 Strouhal Number

The behaviour of the Strouhal number is shown in table (4.1) and in figure (4.9). It reveals a trend similar to that seen at lower Froude numbers (i.e. 0.00 and 0.20). However, there is a slight shift in the depths at which shedding starts to attenuate and also in the depths at which the peak in the Strouhal number was noted. All of the shifts in the Strouhal number with increasing Froude number were comparatively small, except at the smaller gaps where the critical depth at which shedding ceases progressively grows. For some of these cases, namely the ones at smaller gaps and larger Froude numbers (such as gap 0.22 and Froude number 0.35), the

level of surface deformation becomes quite significant and hence the height varies considerably across the cylinder as shown in figure (4.10).

Gap ratio G/D	$Fr = 0.25$	$Fr = 0.30$	$Fr = 0.35$	$Fr = 0.40$
REF	1.0000	1.0000	1.0000	1.0000
0.10	no shedding	no shedding	no shedding	no shedding
0.13	no shedding	no shedding	no shedding	no shedding
0.16	0.6445	no shedding	no shedding	no shedding
0.19	0.6947	0.6852	no shedding	no shedding
0.22	0.7570	0.7327	no shedding	no shedding
0.25	0.8209	0.7750	0.7638	0.7528, 0.3235
0.40	1.0322	1.0100	0.9725	0.9424
0.55	1.0856	1.0829	1.0708	1.0639
0.70	1.0961	1.0983	1.1025	1.0988
0.85	1.0940	1.0956	1.1046	1.1162
1.00	1.0887	1.0893	1.0961	1.1083
1.50	1.0666	1.0644	1.0676	1.0798
2.50	1.0348	1.0333	1.0333	1.0370
5.00	1.0106	1.0106	1.0106	1.0106

Table 4.1: Variation of the Strouhal number with gap ratio for Froude numbers of 0.25, 0.30, 0.35 and 0.40. The Reynolds number in each case is 180.

The no shedding labels in table (4.1) indicate that no clear periodic or semi periodic response was observed with regard to the lift forces acting upon the cylinder. It should be noted that some time dependent behaviour was still detected, however the fluctuations were generally weak and were found to possess no clearly discernible frequency. It has been noted by Price et al. (2000) that a number of distinct frequencies unrelated to those associated with Kármán vortex shedding can be observed at small gap ratios for flow past a cylinder close to a no-slip surface. Price et al. (2000) detect up to 4 frequencies for a gap ratio of 0.125. Of the frequencies they observe, they attribute the smallest frequency to the separation of the wall boundary layer from the adjacent surface (wall), with the next frequency (which is also the most dominant) associated with vortex shedding. The remaining higher frequencies were then described as coming from the addition of the two lower frequencies, and the second harmonic of the shedding frequency.

With regard to the free surface case, the observed separation from the adjacent wall is likely to

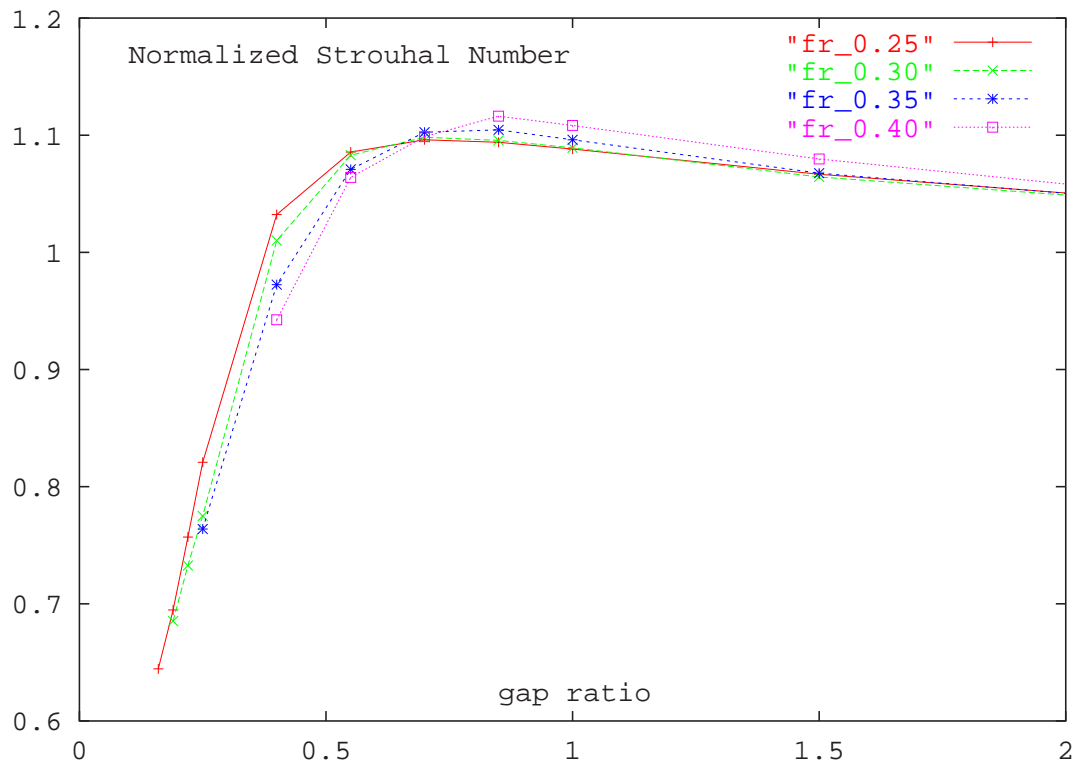
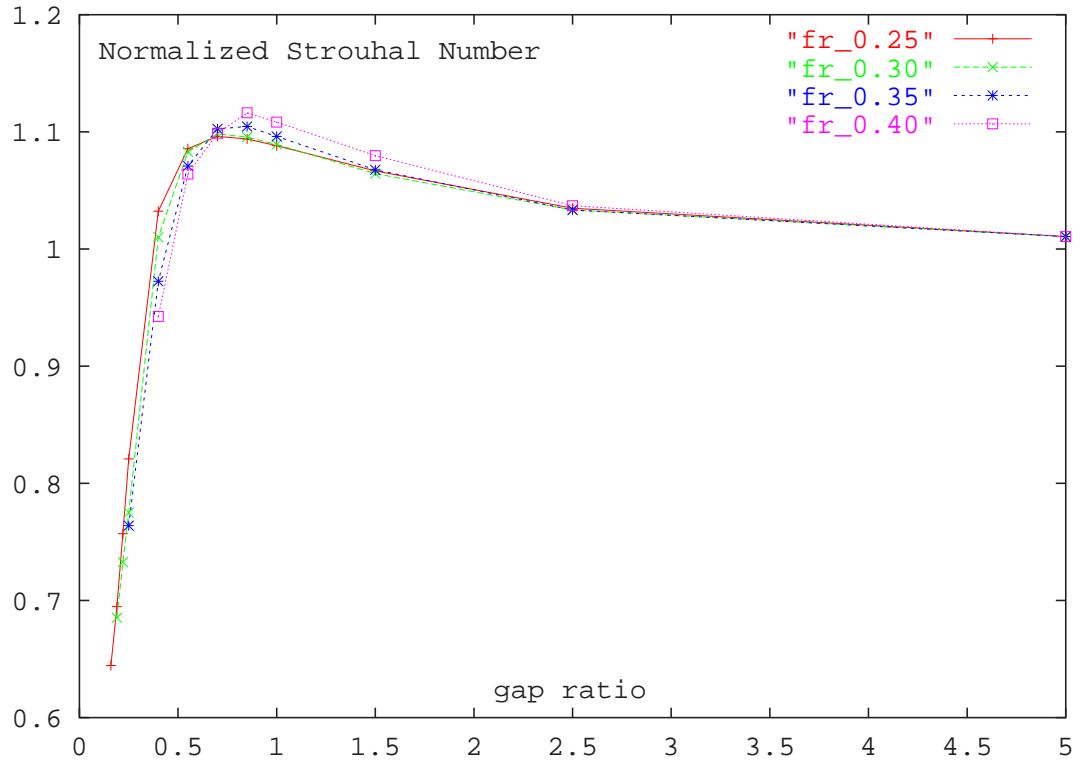


Figure 4.9: Variation of Strouhal number (normalized with respect to Strouhal number of the reference cylinder (i.e. $\frac{St}{St_0}$)) with gap ratio for Froude numbers of 0.25, 0.30, 0.35, and 0.40. The Reynolds number in each case is 180.

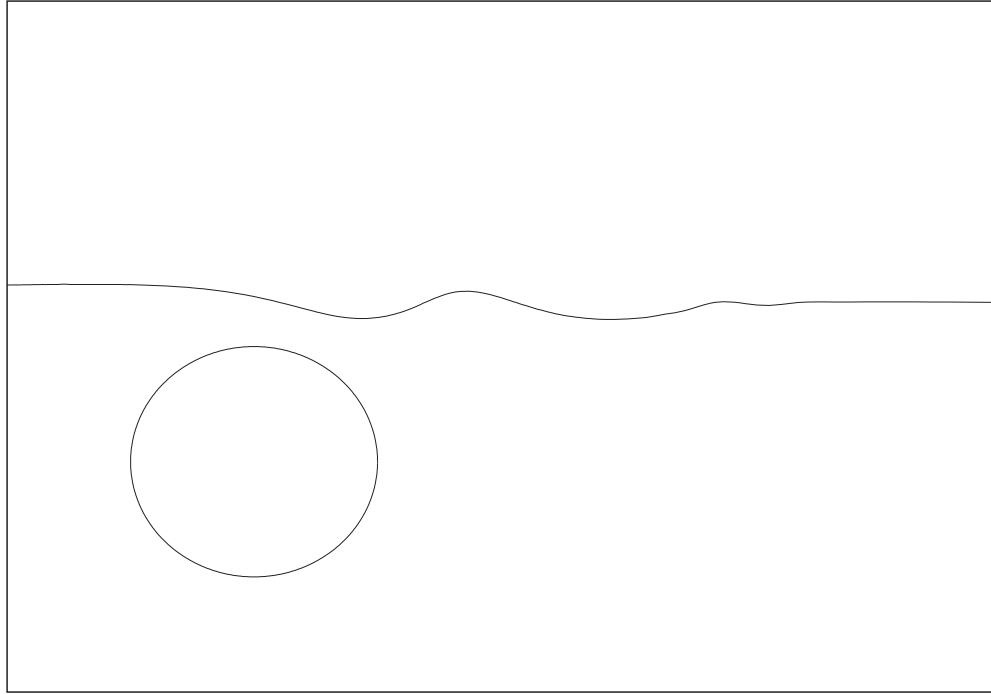


Figure 4.10: Surface position at a random instant in time for a gap ratio of 0.22 and a Froude number of 0.35. The Reynolds number is 180.

first manifest itself as increased surface curvature for low Froude numbers, and at higher Froude numbers with small scale localized wave breaking. Strictly speaking, some form of shedding is still observed at the smaller submergence depths (for example gap 0.25, Froude number 0.40), however, the lift pattern was irregular and was found to display some degree of modulation, making the determination of a shedding frequency difficult. For this case the two most dominant frequencies (as determined by the Fourier transform of the lift signal) are given.

The gap 0.25, Froude number 0.40 case is somewhat special and is considered in greater detail later in this chapter as it is believed to represent a precursor to some of the altered wake states observed by Sheridan et al. (1995), Sheridan et al. (1997) and Hoyt & Sellin (2000).

Figures (4.11) to (4.13) show the variation in lift coefficient and the spectra for a few limiting submergence depths as a function of Froude number. The strength of the signals is of particular importance, as it is often the criterion used in many of the experimental investigations (such as that of Bearman & Zdravkovich (1978)), to determine the gap ratio at which shedding ceases.

While the trend in the Strouhal number is interesting in itself, the goal is to know why the observed changes occur. The assertion of Green & Gerrard (1993), which suggests that the period of vortex shedding is largely determined by the time taken for a sufficient vorticity to

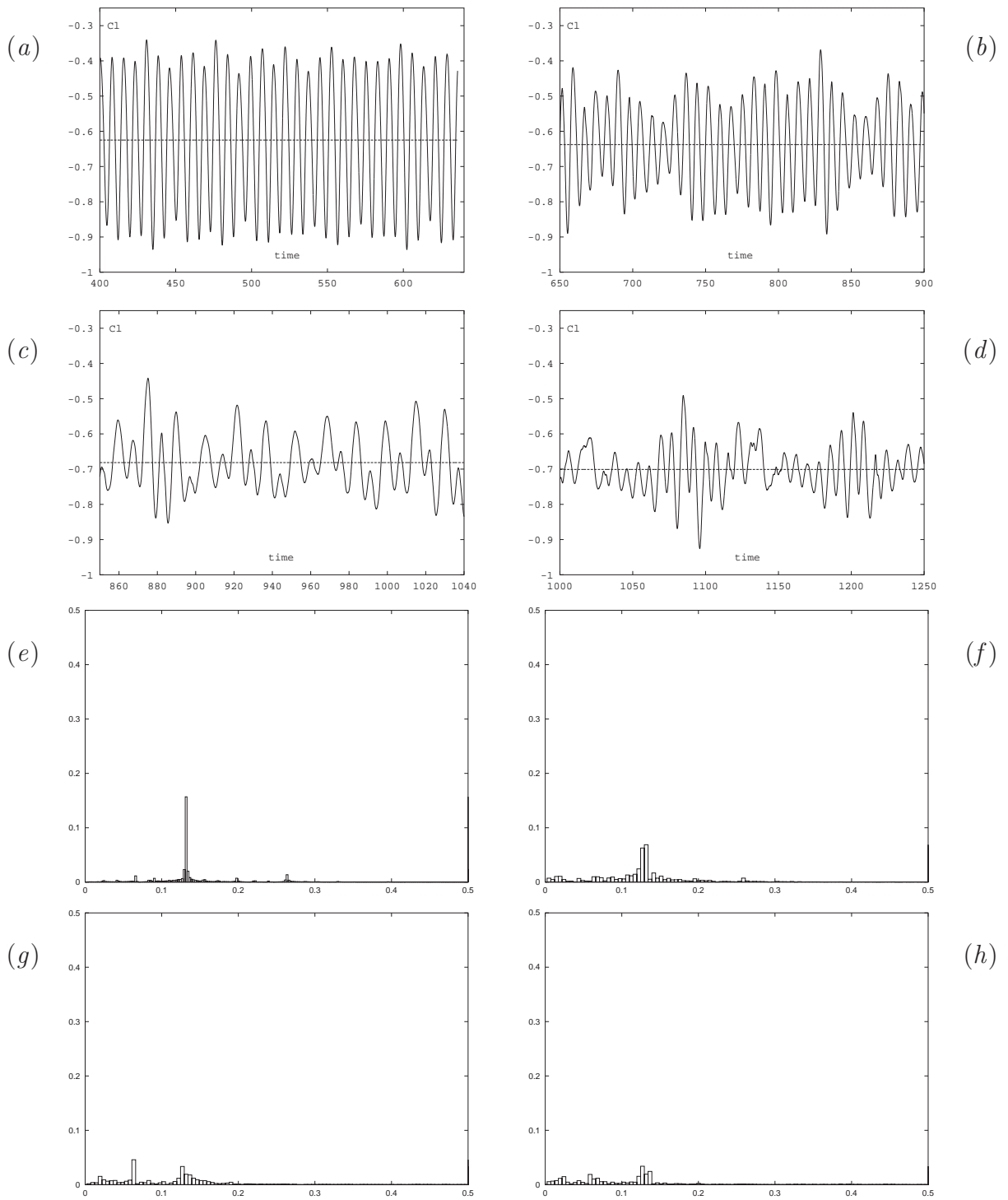


Figure 4.11: Lift traces and spectra for a gap ratio of 0.19 for Froude numbers of 0.25 (a,e), 0.30 (b,f), 0.35 (c,g) and 0.40 (d,h). The Reynolds number for each case is 180.

accumulate outside a region of high shear stress, may provide some insight. Their model was found to largely explain the attenuation of the shedding observed by Strykowski & Sreenivasan (1990) for a small cylinder placed close to a larger one. For this problem, the supply of fluid into

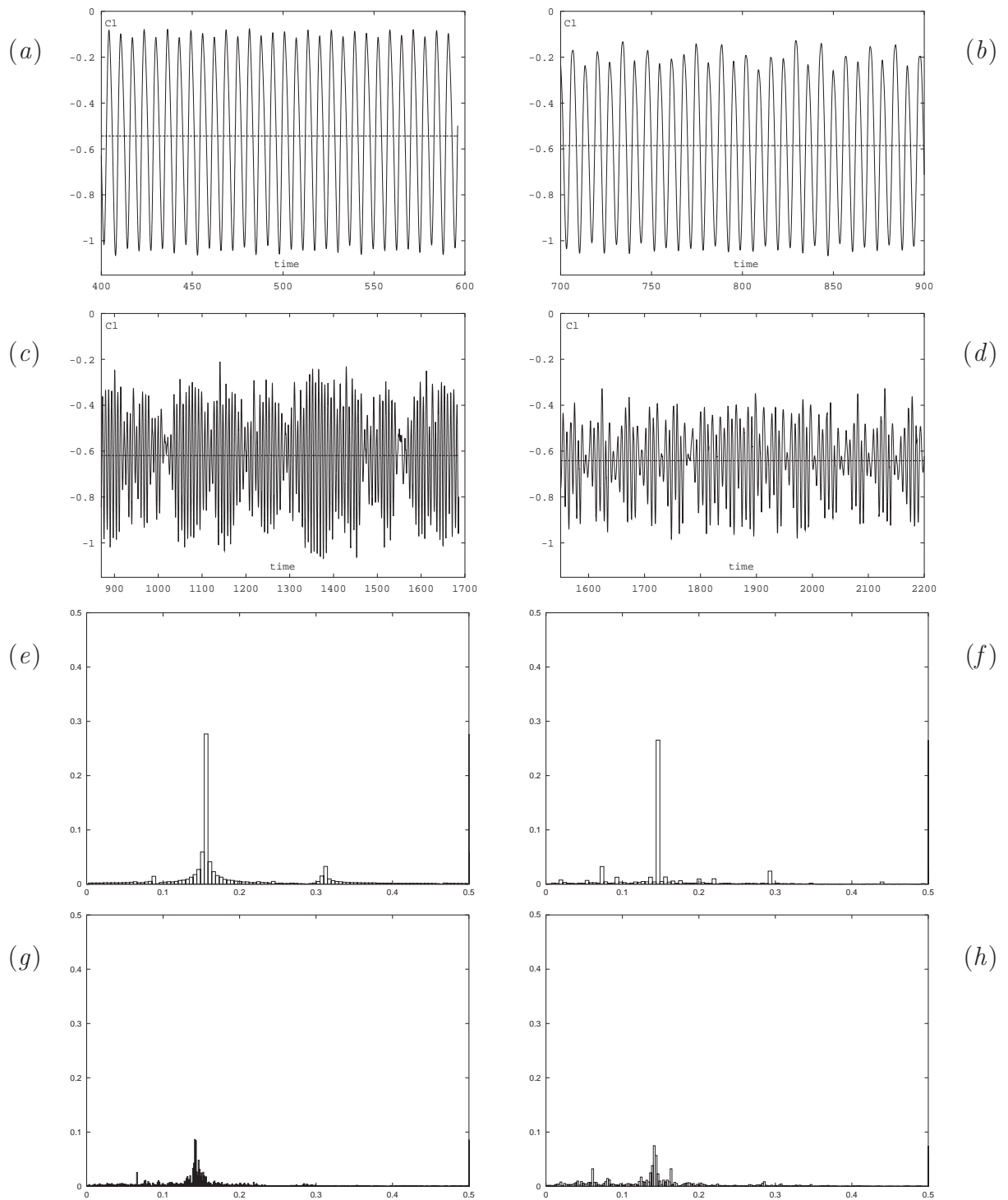


Figure 4.12: Lift traces and spectra for a gap ratio of 0.25 for Froude numbers 0.25 (a,e), 0.30 (b,f), 0.35 (c,g) and 0.40 (d,h). The Reynolds number for each case is 180.

the wake cavity is also an issue and as such both factors are likely to contribute to the variation of the Strouhal number with gap ratio. Indeed, it is hypothesized that the increase in the period of the vortex shedding observed as the cylinder gets close to the surface is in response to the

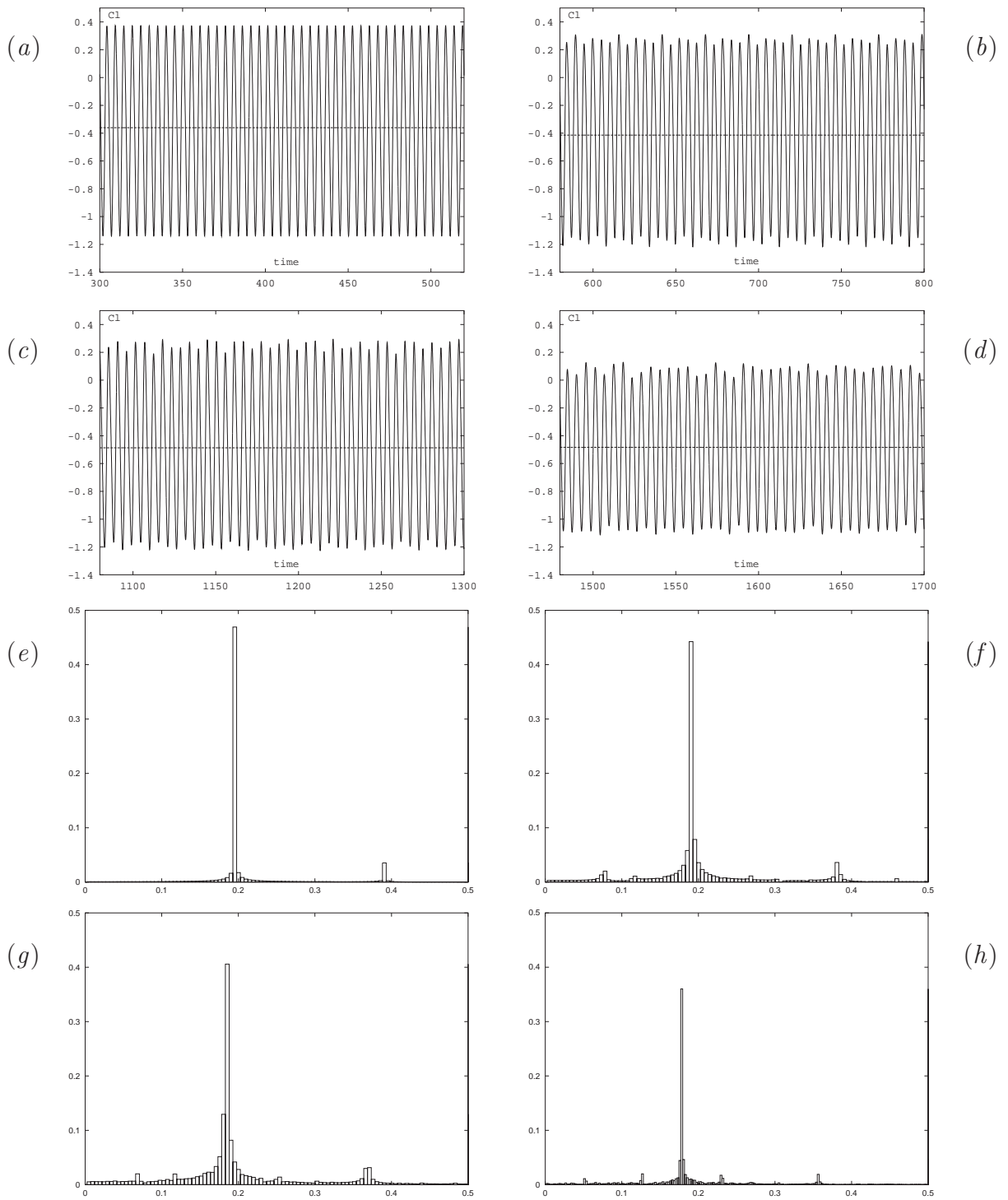


Figure 4.13: Lift traces and spectra for a gap ratio of 0.40 for Froude numbers of 0.25 (a,e), 0.30 (b,f), 0.35 (c,g) and 0.40 (d,h). The Reynolds number for each case is 180.

time taken for sufficient fluid and vorticity to enter the wake cavity, and hence to permit the formation of discrete vortices. For the current problem, the time taken for sufficient vorticity to accumulate will be largely determined by both the proximity and time-dependent nature of the

free surface. Hence, as it is both the supply of fluid and vorticity that is likely to influence the Strouhal number, the flux of fluid above the cylinder is of interest and it will now be examined.

4.3 Mass Flux

To gain some insight into what is happening with regard to the supply of fluid into the wake, the flux of fluid per unit gap height (or spatially averaged velocity) in the region directly above the cylinder was measured. This was undertaken for each Froude number and gap ratio at the two extremes in the lift cycle. For the cases in which no periodic shedding was observed, the average velocity was measured close to a point of maximum lift, while for those gaps below the critical gap ratio (i.e. gap ratio at which shedding is still observed) the flow field at a random instant in time was used. Such a selection of the velocity is unlikely to greatly influence the results as the change in the magnitude of the lift with time at these depths tended to be small. The trend for the average velocity in the gap region at the point of maximum lift for all Froude numbers and at the point of minimum lift for some (0.25, 0.30, and 0.35), was found to correspond well with the trend observed in the Strouhal number. This suggests that the period of the vortex shedding is related to the average velocity in the region just above the cylinder, and hence to the time required for both fluid and vorticity to accumulate. At a Froude number of 0.40, the trend in the behaviour of the average velocity at the point of minimum lift begins to alter somewhat, with the slight drop in the velocity occurring at the gap ratios at which small scale wave breaking was observed. This change appears to be related to the increasing level of surface deformation, and is possibly related to the local Froude number that controls the degree of feedback upstream.

The variation of the average velocity (flux divided by height), and the flux divided by the flux through an equivalent height for the reference cylinder at the same point in the shedding cycle is shown in figures (4.14), (4.15), (4.16) and (4.17). While these flux measurements take into account the slight changes in the height of the fluid as it passes over the cylinder, they are all measured in a vertical plane from the top of the cylinder to the free surface. Hence comparison with the reference cylinder at small gap ratios may highlight the fact that the separation and stagnation points have shifted (which would account for the slight jumps observed in the plots which contain the comparison in fluxes, especially at small gap ratios).

The trends observed for both the mass flux and the Strouhal number are similar in that as the gap ratio is reduced, the average velocity increases up to a point and then decreases rather rapidly as it is reduced further. At the point of maximum lift, the depth at which the maximum

velocity occurs increases with increasing Froude number, while at the point of minimum lift the behaviour was slightly more erratic, with the flux ratio illustrating that the flow changes rather significantly between a Froude number of 0.30 and 0.35. This variation reflects the more pronounced surface curvature and the flux of positive vorticity into the flow that occurs during parts of the shedding cycle.

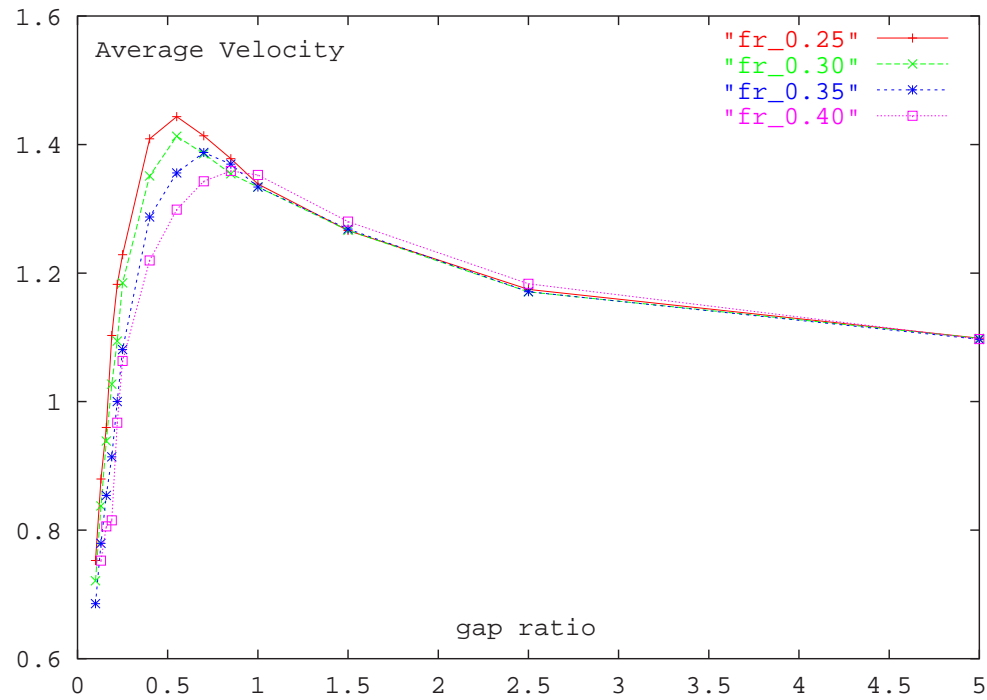


Figure 4.14: Plot showing the average velocity in the region directly above the cylinder as a function of gap ratio at the point of maximum lift, for Froude numbers of 0.25, 0.30, 0.35 and 0.40. The Reynolds number in each case is 180.

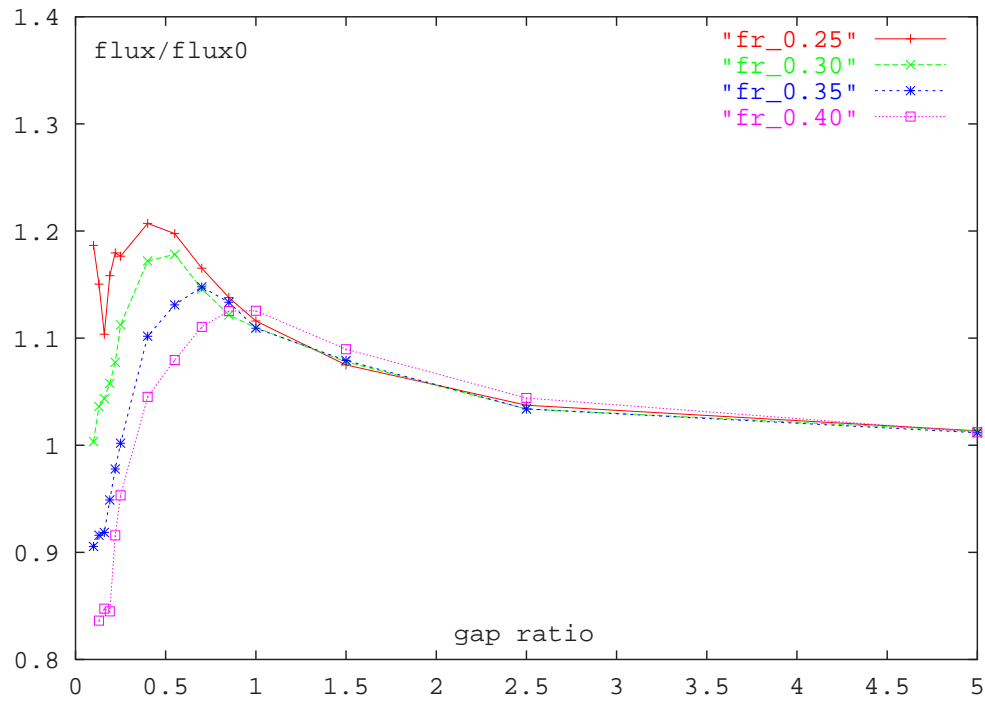


Figure 4.15: Plot showing the flux in the region directly above the cylinder divided by the flux through the same height for the reference cylinder as a function of gap ratio at the point of maximum lift, for Froude numbers of 0.25, 0.30, 0.35 and 0.40. The Reynolds number in each case is 180.

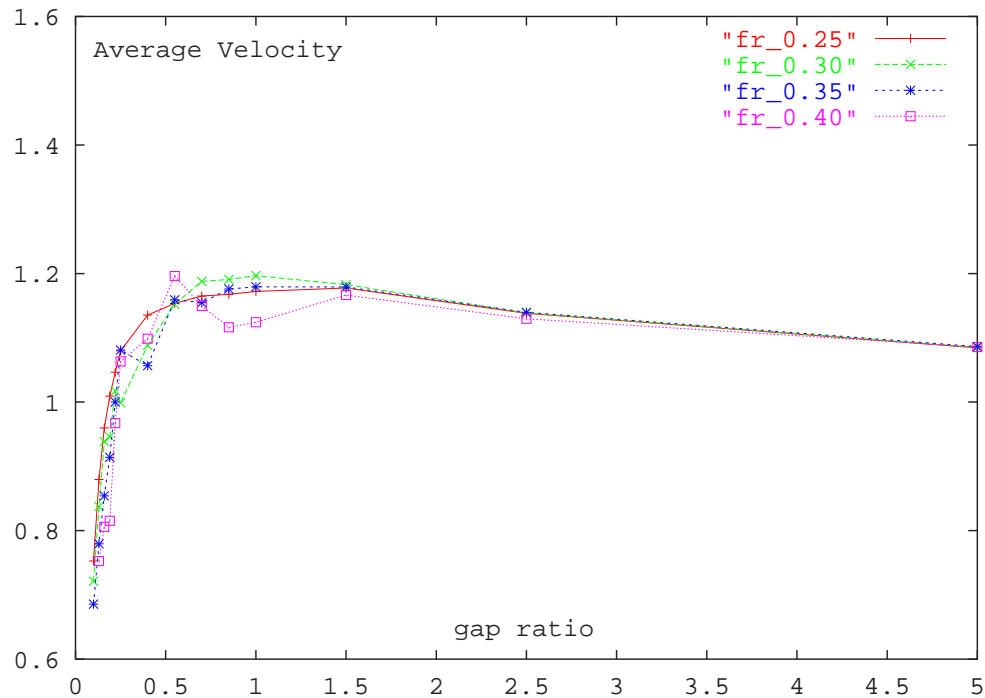


Figure 4.16: Plot showing the average velocity in the region directly above the cylinder as a function of gap ratio at the point of minimum lift, for Froude numbers of 0.25, 0.30, 0.35 and 0.40. The Reynolds number in each case is 180.

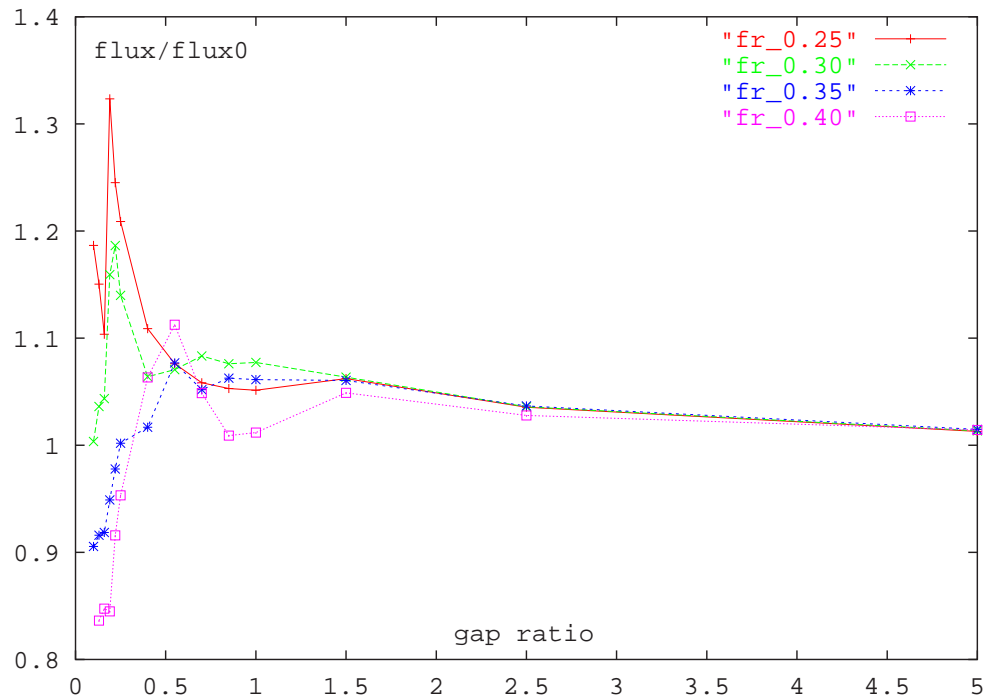


Figure 4.17: Plot showing the flux in the region directly above the cylinder divided by the flux through the same height for the reference cylinder as a function of gap ratio at the point of minimum lift, for Froude numbers of 0.25, 0.30, 0.35 and 0.40. The Reynolds number for each case is 180.

4.4 Lift, Drag and Moment Coefficients

It is useful at this point to consider the forces acting upon the cylinder, as the lift, drag and moment are all of considerable importance in industrial applications. Such quantities are also useful in that they constitute a point of reference from which this study may be compared with that of others. The behaviour of the lift, drag and moment coefficients are now considered.

4.4.1 Lift

Figure (4.18) shows the trends in the behaviour of the mean lift with both gap ratio and Froude number. It is clear that for all but the largest Froude number (i.e. 0.25, 0.30 and 0.35, but not 0.40), the mean lift varies little from that observed in the previous chapter. However, as the Froude number is increased to 0.40, a slight change in the trend is observed, with the magnitude of the lift now increasing at larger submergence depths. Miyata et al. (1990), also investigate this flow at a Froude number of 0.24, and note that the lift grows quite rapidly as the gap ratio is reduced from a value of approximately 0.75. A similar trend was also observed in the current

investigation, with the magnitude of the lift first exceeding 0.10 at a gap ratio of 1.00, and then growing rapidly as the gap was reduced further.

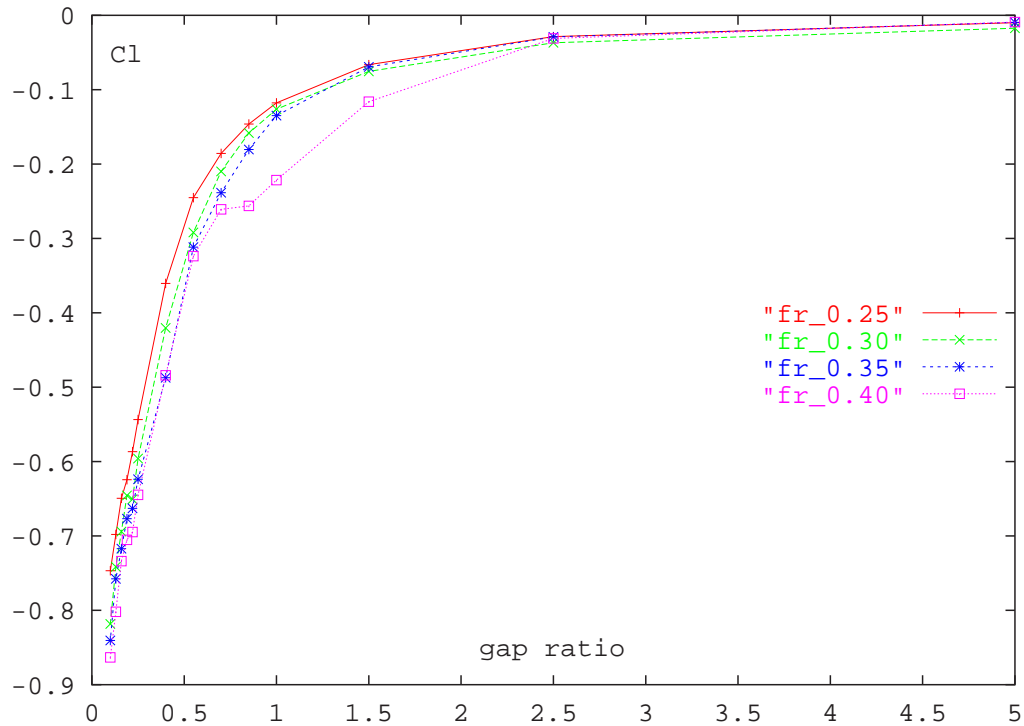


Figure 4.18: Variation of the mean lift coefficient with gap ratio for Froude numbers of 0.25, 0.30, 0.35 and 0.40. The Reynolds number for each case is 180.

4.4.2 RMS Lift

The trend in the behaviour of the RMS lift is similar to that observed in the previous chapter, although there is a slight shift in the results to the right with increasing Froude number. This shift indicates that as the Froude number is increased, the gap ratio at which the strength of the vortex shedding both begins to weaken, and reaches its peak, grows. Such a change is reflected in the gap ratio at which the peak value was observed, with a shift from 0.70 at a Froude number of 0.25, to 1.00 at a Froude number of 0.40 being detected. Again, all of the values of the RMS lift continue to drop with gap ratio in the region where shedding is suppressed, which largely supports the suggestion by Lei et al. (1999) that the RMS lift is a better indicator than the spectra for determining whether or not vortex shedding is observed.

Lei et al. (1999) indicate that shedding ceases for gaps between 0.20 and 0.30 for flow past a cylinder close to a no-slip wall, with the RMS lift for their results falling to between 0.09 and 0.41 within this range. Similar behaviour was also observed here, and while one can confidently

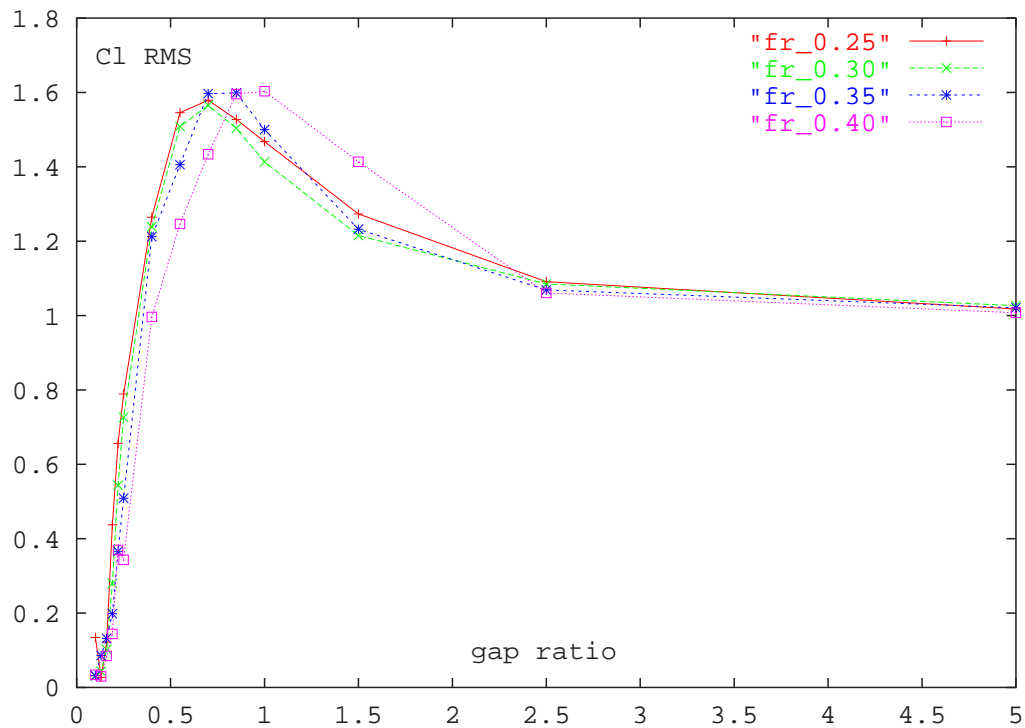


Figure 4.19: Variation of the normalized RMS lift coefficient with gap ratio for Froude numbers of 0.25, 0.30, 0.35 and 0.40. The Reynolds number for each case is 180.

say that no shedding is observed for RMS lift values below 0.09, some shedding was noted at larger values, particularly at lower Froude numbers.

4.4.3 Drag

The variation of the drag (which is normalized with respect to the drag of the reference cylinder) with both gap ratio and Froude number is shown in figure (4.20). Once more, the pattern is similar to that seen at the lower Froude numbers, and for the case of a cylinder close to an adjacent no-slip wall. Increasing the Froude number again has the effect of shifting the results to the right, with little change in the peak magnitude being observed. This shift is largely consistent with that observed for the lift, with only the results at a Froude number of 0.40 showing any real deviation.

4.4.4 RMS Drag

The normalized RMS drag is also examined, with its behaviour shown in figure (4.21). For the Froude number 0.25, 0.30 and 0.35 cases, the trends are all similar, with each showing the

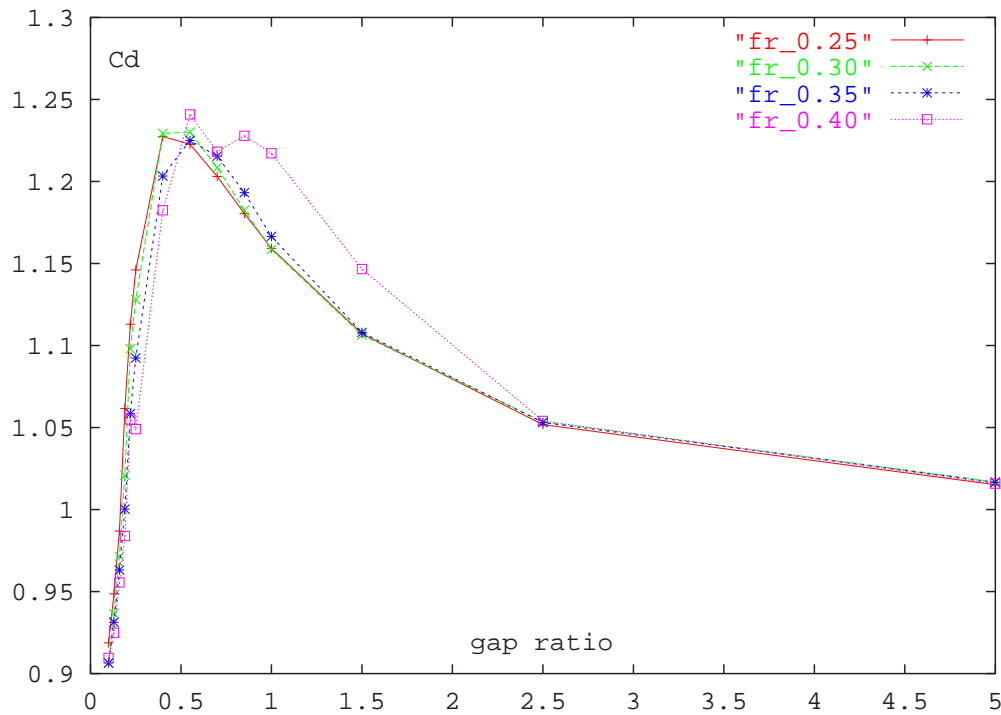


Figure 4.20: Variation of the normalized drag coefficient with gap ratio for Froude numbers of 0.25, 0.30, 0.35 and 0.40. The Reynolds number for each case is 180.

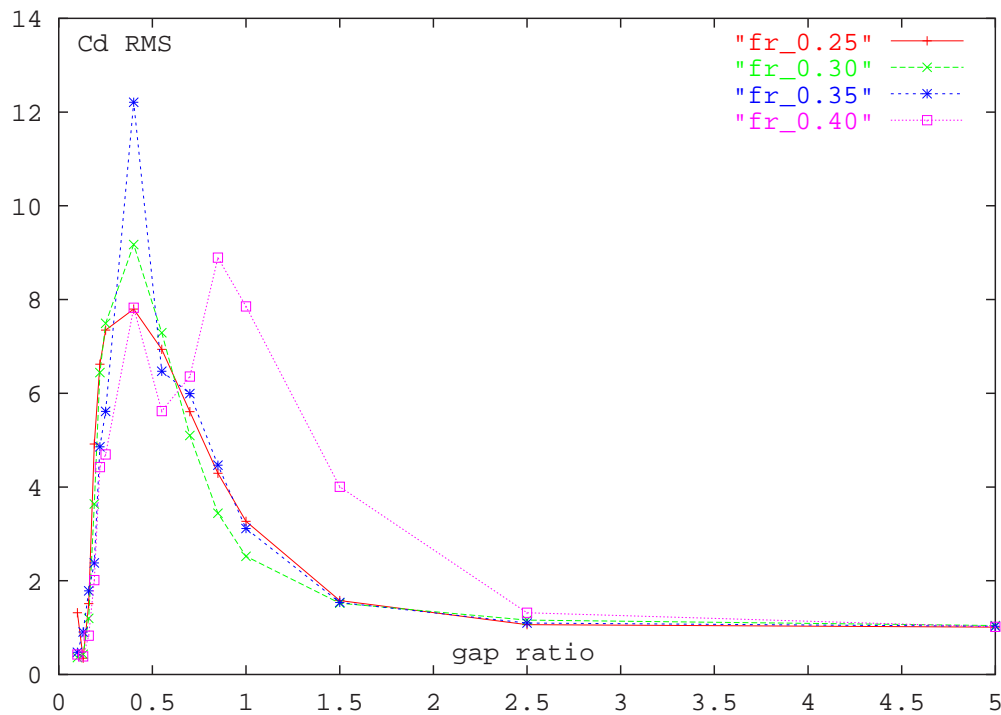


Figure 4.21: Variation of the normalized RMS drag coefficient with gap ratio for Froude numbers of 0.25, 0.30, 0.35 and 0.40. The Reynolds numbers for each case is 180.

maximum variation in the behaviour of the RMS drag at a gap of 0.40. It should be noted that the increase in the size of the normalized drag fluctuations were considerable, with the RMS component at all Froude numbers being approximately an order of magnitude greater at gaps between 0.25 and 0.85. As the Froude number is increased to 0.40, the trend in the behaviour of the RMS drag coefficient alters dramatically, with the dominant peak now occurring at a gap ratio of 0.85.

The shift in the trend at the Froude number of 0.40 is clearly related to the onset of wave breaking (that was observed for gaps between 0.25 and 0.70 and which is discussed later in section (4.9)), and it is suggested that it is redirection of the fluid passing over the cylinder in conjunction the altered levels of reverse flow in the wake that account for the considerable deviation in the behaviour.

4.4.5 Moment

While the moment is a function of the shear stress acting on the cylinder and hence upon the Reynolds number, the general trends do give some indication as to tendency for the cylinder to rotate. Figure (4.22) shows the behaviour of the mean moment coefficient acting upon the cylinder. This result clearly indicates that there is a reduction in the mean moment with increasing Froude number. Such a change is believed to be related to the shift in the position of both the stagnation and separation points, whose behaviour will now be considered.

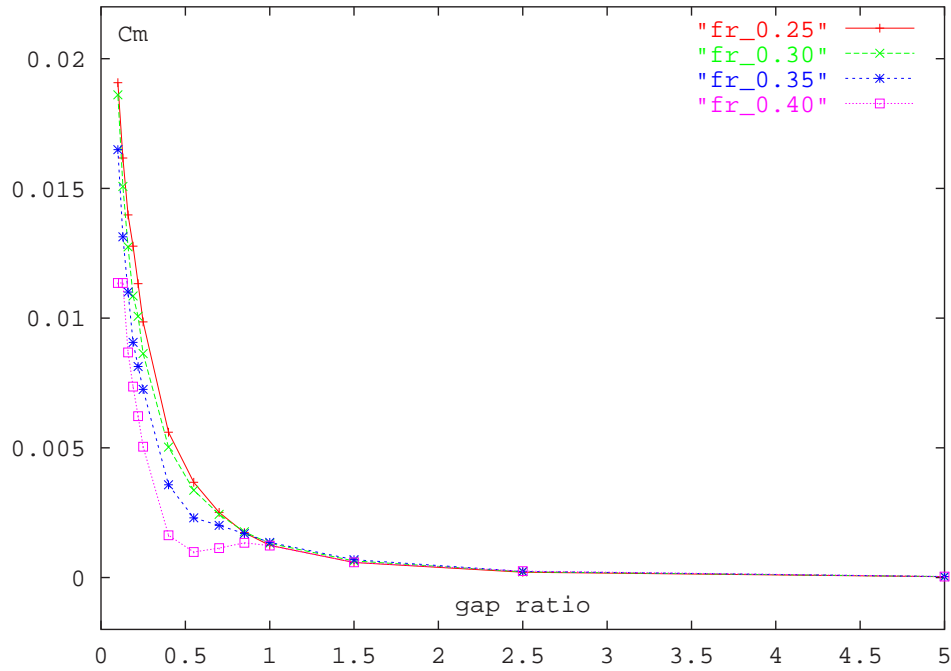


Figure 4.22: Variation of the mean moment coefficient with gap ratio for Froude numbers of 0.25, 0.30, 0.35 and 0.40. The Reynolds number is again 180.

4.5 Pressure Distribution, and the Stagnation and Separation Points

To get a better understanding as to why the forces and moments acting on the cylinder vary in the manner that they do, it is necessary to examine the behaviour of both the pressure distribution around the cylinder and the angular position of both the stagnation and separation points. Figures (4.23) to (4.26) show the variation in the pressure distribution with Froude number for four different gap ratios, while figures (4.27) to (4.32) show the behaviour of the stagnation and separation points at the two extremes in the lift cycle.

It is clear from the pressure distribution plots that the increase in the magnitude of the lift with decreasing gap ratio is due in part, to the clockwise rotation of the front stagnation point, with this angular shift also partly explaining the corresponding drop in the drag. The pressure distribution plots also illustrate the influence of the Froude number, with the results for the gap ratio 0.25 case (figure (4.25)) highlighting the significant change. For this gap ratio the results at a Froude number of 0.25 resemble those observed at the larger gaps ratios (i.e. cases in which largely unhindered vortex shedding occurs), while the distribution at a Froude number of 0.40

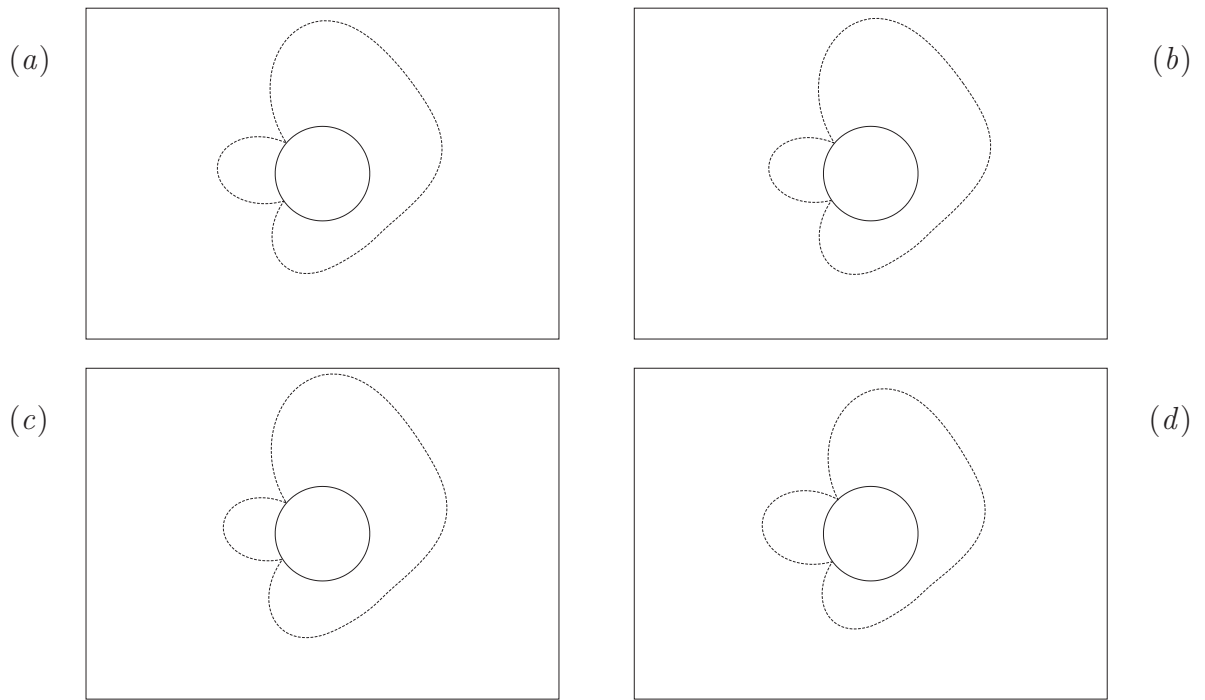


Figure 4.23: Pressure distributions plots at the point of maximum lift for a gap ratio of 0.70 and for Froude numbers of 0.25 (a), 0.30 (b), 0.35 (c) and 0.40 (d). The Reynolds number is again 180.

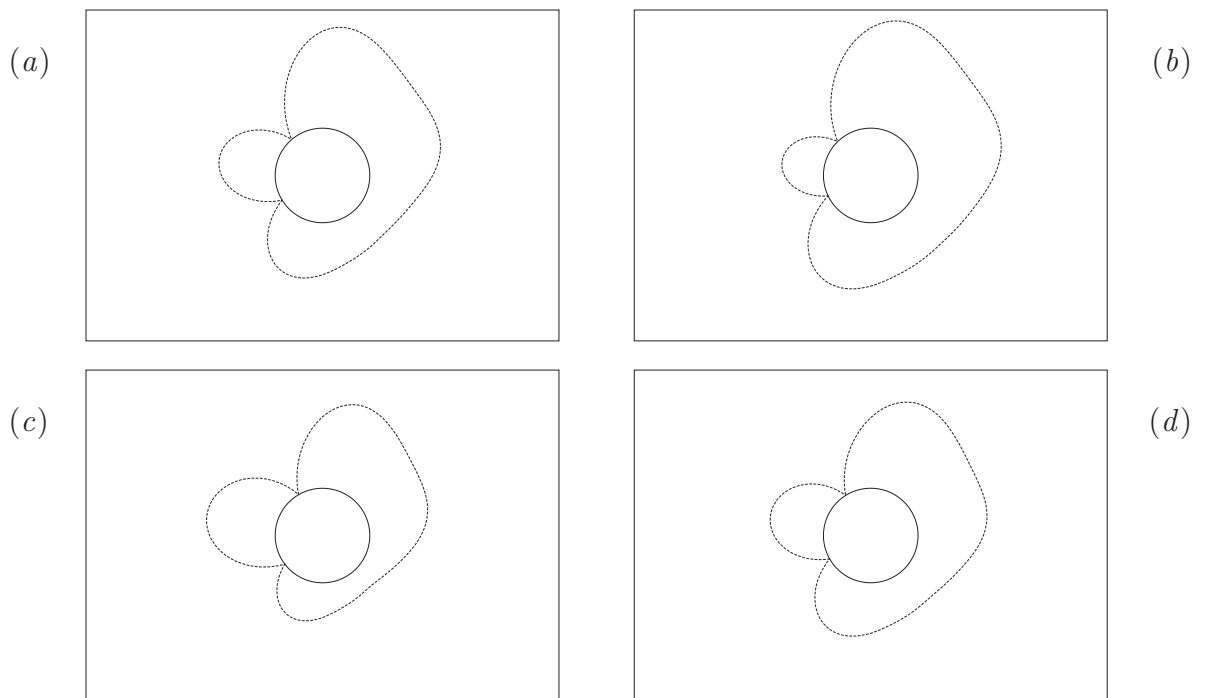


Figure 4.24: Pressure distributions plots at the point of maximum lift for a gap ratio of 0.40 and for Froude numbers of 0.25 (a), 0.30 (b), 0.35 (c) and 0.40 (d). The Reynolds number is again 180.

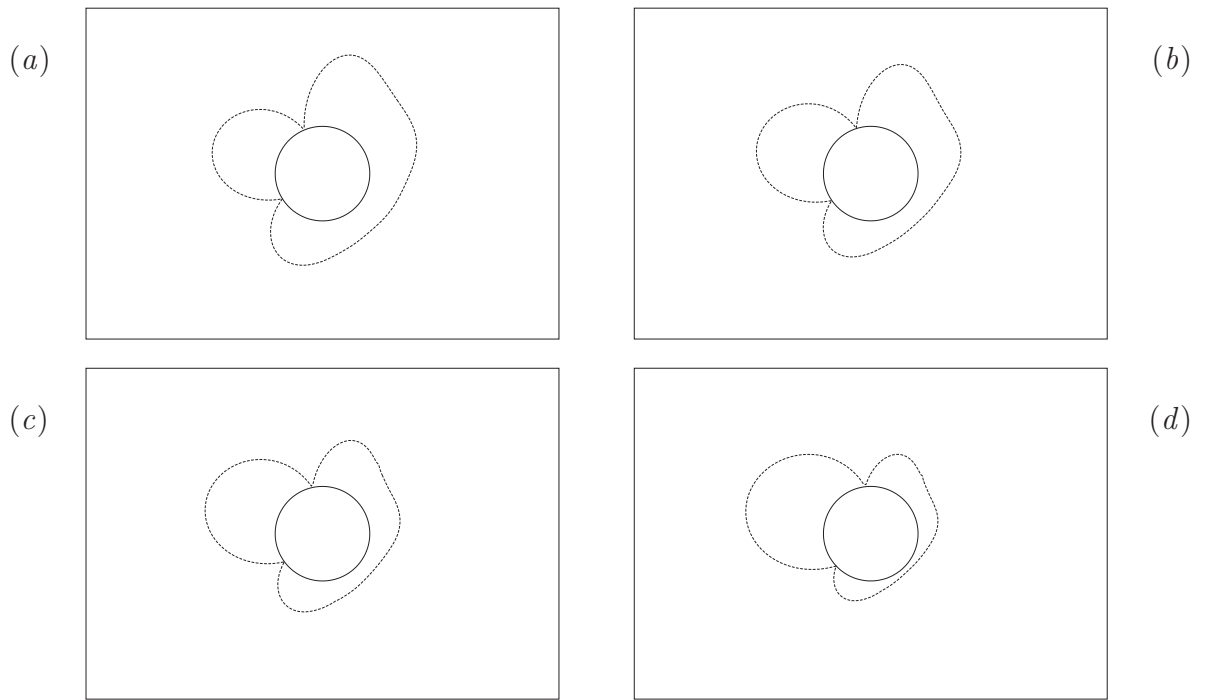


Figure 4.25: Pressure distributions plots at the point of maximum lift for a gap ratio of 0.25 and for Froude numbers of 0.25 (a), 0.30 (b), 0.35 (c) and 0.40 (d). The Reynolds number is again 180.

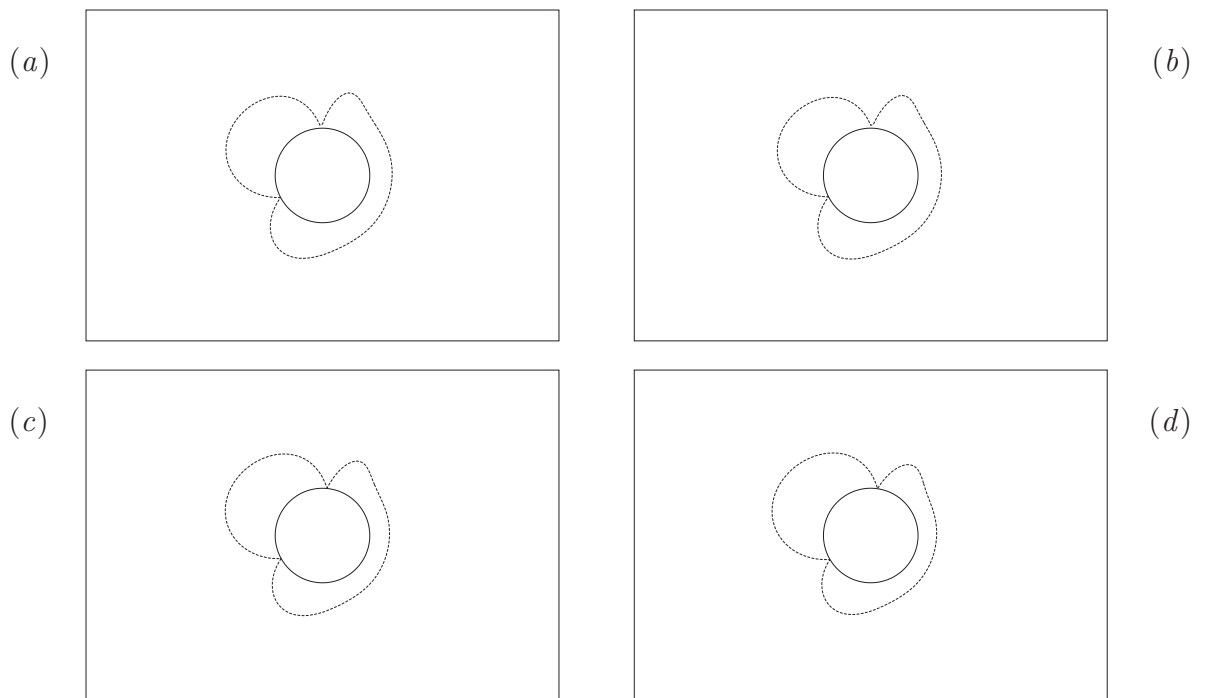


Figure 4.26: Pressure distributions plots at a random point in the lift cycle for a gap ratio of 0.10 and for Froude numbers of 0.25 (a), 0.30 (b), 0.35 (c) and 0.40 (d). The Reynolds number is 180.

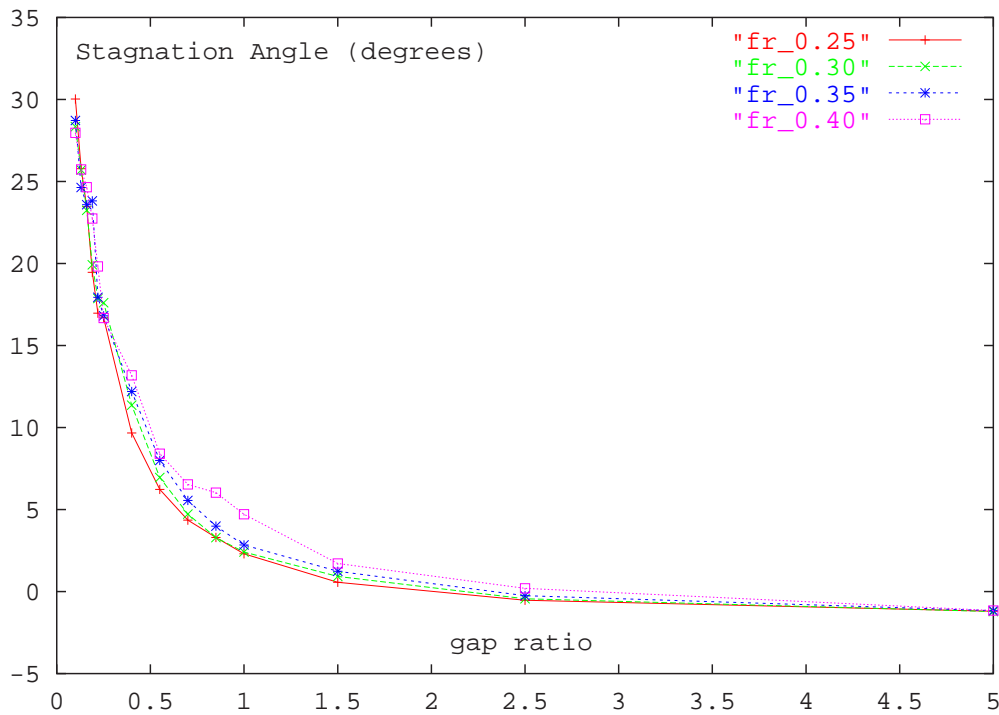


Figure 4.27: Variation of the stagnation angle with gap ratio at the point of maximum lift for Froude numbers of 0.25, 0.30, 0.35 and 0.40. The Reynolds number in each case is 180.

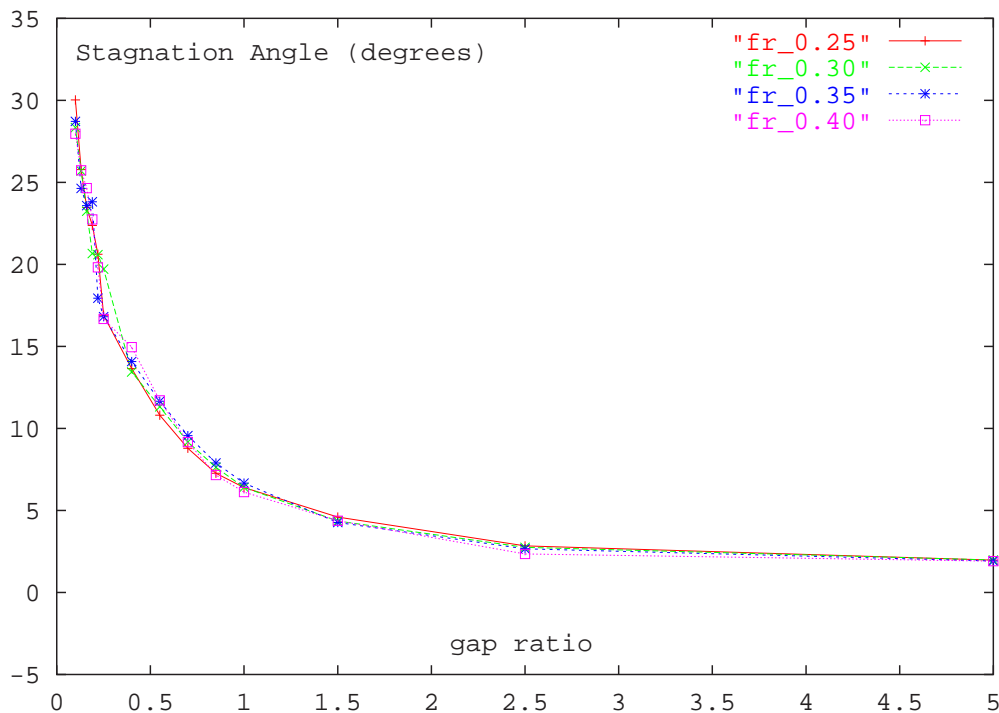


Figure 4.28: Variation of the stagnation angle with gap ratio at the point of minimum lift for Froude numbers of 0.25, 0.30, 0.35 and 0.40. The Reynolds number in each case is 180.

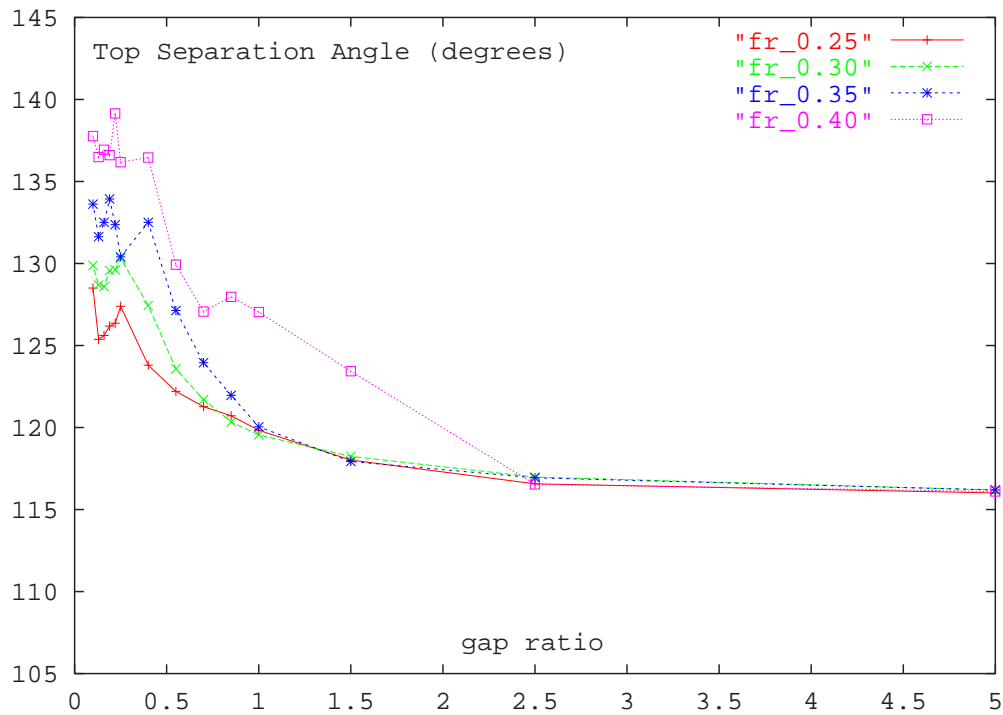


Figure 4.29: Variation of the top separation angle with gap ratio at the point of maximum lift for Froude numbers of 0.25, 0.30, 0.35 and 0.40. The Reynolds number in each case is 180.

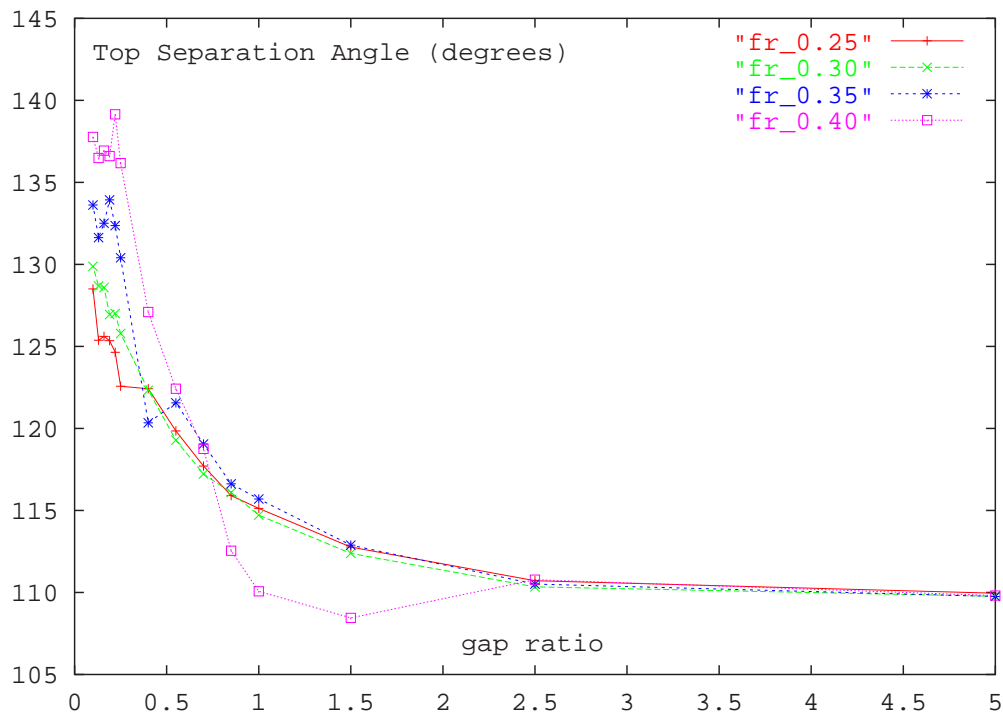


Figure 4.30: Variation of the top separation angle with gap ratio at the point of minimum lift for Froude numbers of 0.25, 0.30, 0.35 and 0.40. The Reynolds number in each case is 180.

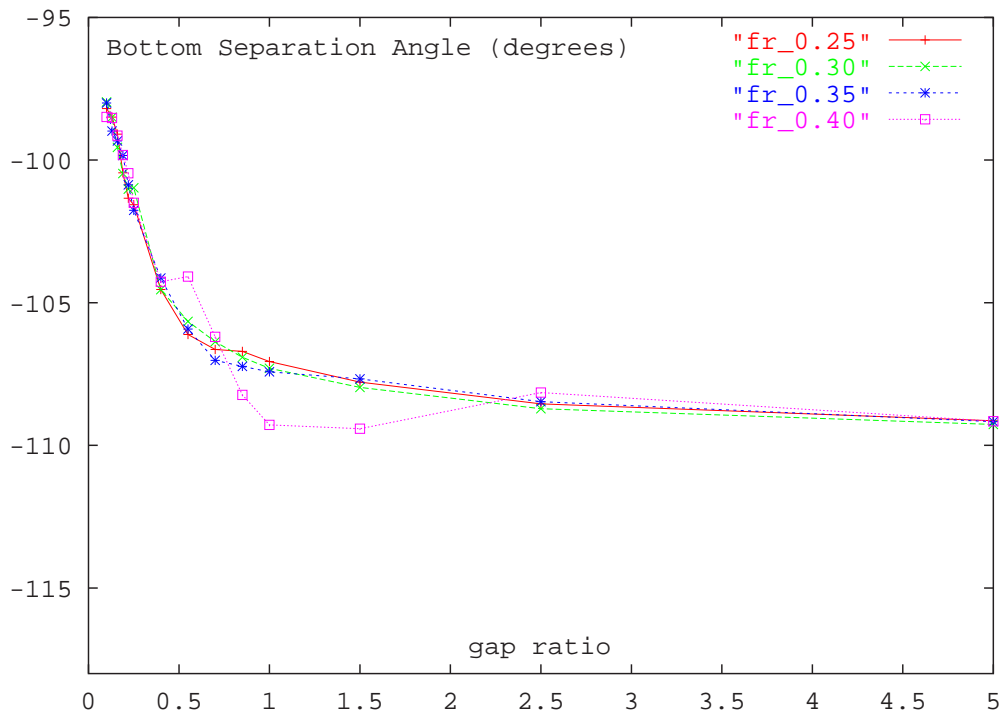


Figure 4.31: Variation of the lower separation angle with gap ratio at the point of maximum lift for Froude numbers of 0.25, 0.30, 0.35 and 0.40. The Reynolds number in each case is 180.

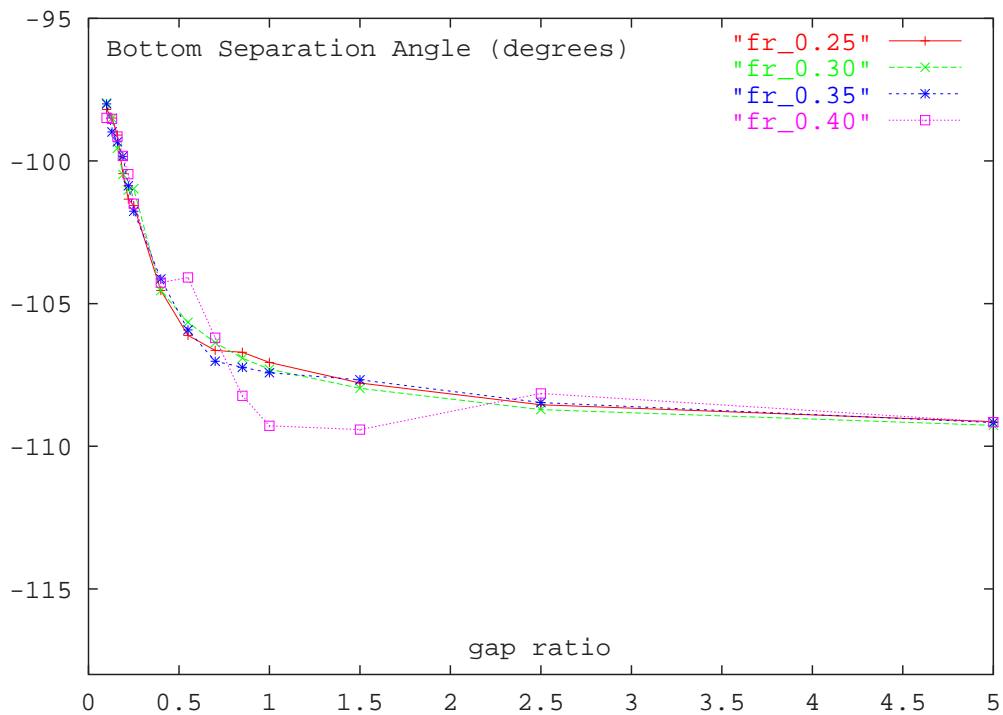


Figure 4.32: Variation of the lower separation angle with gap ratio at the point of minimum lift for Froude numbers of 0.25, 0.30, 0.35 and 0.40. The Reynolds number in each case is 180.

resembles those for smaller gap ratios where shedding is no longer observed.

The trends in the position of the front stagnation point (as shown in figures (4.27) and (4.28)) do not indicate that there is any significant shift in their position with Froude number. However, the position of the top separation point does vary, with the results at the two extremes in the lift cycle indicating that the size of the wake changes with time. This time varying behaviour must almost certainly be related to the time varying free-surface curvature, and it suggests that the entire system will be to some extent governed by the level of feedback between the free surface and the shedding of vortices from the cylinder. This is a point which will be considered in greater detail in the discussion at the end of this chapter.

It is also interesting to note that the size of the wake appears to decrease with increasing Froude number, with the delayed separation at the top of the cylinder having the greatest impact on the wake size. It is possible that it is this angular delay at larger Froude numbers that is responsible for the decrease in the mean moment coefficient acting upon the cylinder (as shown in figure (4.22)).

It should be noted that for the gap ratios at which shedding was not observed, the stagnation and separation points were calculated at random instants in time (as it was difficult to discern the points of maximum and minimum lift in a signal that displayed no underlying periodicity). This would to some extent explain the erratic behaviour observed in the position of separation points at small gap ratios.

The general behaviour of the stagnation and separation points suggests that they are for the most part governed at these low and intermediate Froude numbers by the geometry. However, when the Froude number is sufficiently large to permit significant surface distortion, and hence induce a notable geometry change, these points react accordingly. Thus it comes as no surprise that it is the top separation point that is closest to the time varying deforming surface, that displays the greatest level of fluctuation with Froude number

4.6 Formation Length

Some of the changes observed in the wake behaviour may be in part related to the position at which the vortices are forming in the region behind the cylinder. This location will have an impact on the magnitude of the time-dependent forces and hence will influence the lift, drag and moment acting upon the cylinder. While the definition of the formation length is somewhat

arbitrary, with Griffin (1995) listing a number of ways in which it has been calculated, it is the trend mapped out by its behaviour that is of concern here. As discussed in the previous chapter, the formation length was determined via two different methods. The first involved measuring the point at which the greatest standard deviation in the vertical component of velocity was observed, while the second was obtained by locating the point at which there was the greatest standard deviation in the vorticity at positions away from the cylinder. The location of these points are shown in figure (4.33). From figure (4.33) it is clear that as the gap ratio is reduced, the formation length diminishes up to a point, before increasing again as the gap ratio is reduced further. This behaviour ties in well with the variation of the RMS component of the lift force acting upon the cylinder, with the gap at which the peak in the RMS lift was observed (see figure (4.19)), corresponding to the closest approach of the formation length. The trend in the normalized distance of the formation length from the cylinder center also displays some distinct similarities with the behaviour of the Strouhal number (although the trends are inverted about the vertical line (which corresponds to either the Strouhal number or the formation length) equals 1). These trends are shown in figure (4.34), and they suggest that the Strouhal number also depends upon the formation distance, a result that may or may not be Reynolds number dependent. While the formation length provides some information with regard to the position at which the vortices form, it is the path and convective velocity associated with these vortices that determine the wake behaviour. Such behaviour is now considered in the next section.

4.7 Vortex Paths and Convective Velocities

While the path traced out by the vortex cores of a Kármán vortex street for a fully submerged cylinder is interesting in itself, it is of even more interest here, as the flow field exhibits considerable asymmetry due to the presence of the adjacent free surface. The influence of the deformable free surface on the path traced out by the vortices is of particular relevance, as it is expected that it is this interaction that largely determines the wake behaviour. Figure (4.35), shows the region in which the paths of the vortices were recorded, and it was noted that, for some cases in which the forces acting upon the cylinder were not purely periodic (for example at a gap ratio 0.40 and a Froude number 0.35, where the lift trace was slightly modulated), the path traced out by the vortex cores as they were convected downstream varied with time. This variation typically produced a small band of results on the vortex path plots.

Figure (4.36) shows the paths traced out by the vortex cores and the flux of vorticity into the

flow from the free surface (that typically occurs when small scale wake breaking is witnessed), for both a gap ratio of 0.40 and 0.70 over the entire range of Froude numbers considered within this section.

Measurements of the vortex convection speed were also made by simply recording the position of the vortex core over an interval in time. The variation of the convective velocity with Froude number is shown in figure (4.37). These results indicate that the convective velocity of the positive vortices decreases slightly with increasing Froude number, while for the negative vortices it behaves differently depending upon gap ratio. This is not all that surprising as the negative vortex tends to diffuse rapidly with distance at the smaller gap ratios.

An interesting feature to note for the gap ratios considered is the cross-over in the behaviour of the convective velocities. At low Froude numbers the negative vortices tend to move faster than the positive vortices, while the opposite is the case at larger Froude numbers. This tends to follow directly from what would be expected from potential theory; as the presence of the so called mirror cylinder on the other side of the interface acts to speed up the fluid close to the free surface. However, as the Froude number is increased and the level of surface curvature grows, the convective velocity of the negative vortices decreases and a cross over is observed. (i.e. positive vortices move faster than the negative vortices). The surface deformation at the larger Froude number then tends to invalidate the potential approximation, which is in agreement with the statement of Rood (1994*b*) that ‘vortex interactions with a deformable free surface are not generally represented by image vortex interactions’.

It should be noted that most of the vortex path results show the trace taken by the vortices over a few periods in the shedding cycle. For those in which the path was found to shift, the trail traced out over longer time samples are displayed. The presence of both the free surface and the vorticity located very close to the surface are not shown.

4.8 Comparison with Experiments

At this point it is worthwhile to compare the results of the current investigation with the experimental findings of Sheridan et al. (1997). Comparison was made difficult by the fact that there are no quantities measured in much of the parameter space they examined. Thus it was necessary to pictorially compare the flow states observed, which was in itself difficult, as such a comparison will only have meaning if it occurs at exactly the same instant in time.

To facilitate this, videos showing the evolution of the vorticity field, particle transport, and the surface position were made (see attached compact disk), and were found to be invaluable tools in helping to explain what was actually happening

To draw a meaningful conclusion from the results, it is necessary to compare the flow behaviour at the same points in parameter space. With regards to the dimensionless submergence depth or gap ratio, Sheridan et al. (1997) measure this quantity at a distance of 5.9 diameters upstream of the cylinder center, while the gap ratios here are based on the depth at 10.0 diameters upstream. To account for this, the gap ratio at both locations will be stated.

Careful investigation of figure (6) from Sheridan et al. (1997), and in particular the result at a Froude number 0.35 and a gap ratio 0.40, indicates that the flow may display some three-dimensional aspects. Their results indicate that the flow appears to be either going into, or coming out of, the page at regions roughly one and a half diameters downstream. However, their assertion that the predominant features are quasi-two-dimensional is largely supported by current investigation (with the results, and in particular those at higher Froude numbers which are considered in the next chapter), showing a remarkable level of agreement.

Figures (4.38) and (4.39) show the comparison between the current findings and those of Sheridan et al. (1997). These results illustrate moderate agreement, with only parts of the flow field displaying similar behaviour. A more favourable comparison was obtained with regard to the shear layer from above the cylinder, which remains close to the free surface in both instances. However, the presence of the positive vortex from beneath the cylinder, which is not observed in the experimental findings, clearly illustrates a distinct difference between the two sets of results. A possible explanation for the discrepancy is the difference in formation length, which for a fully submerged cylinder varies with Reynolds number (see Norberg (1998)). The results here also indicate that the formation length varies with gap ratio, and it is plausible to suggest that these two factors combined may alter the flow state slightly.

It is postulated that one of the major effects of the Reynolds number, apart from its influence on the scale of the vortical structures formed, is its impact on the formation length. It is expected that a longer or shorter value will influence the ability of the wake to accumulate a sufficient amount of both fluid and vorticity to enable the formation of discrete vortices.

4.9 Wave Breaking

The alteration in the behaviour of the lift, drag and moment suggests that the level of feedback between the deforming free surface and the flow both upstream and downstream of the cylinder has been altered. Some of the observed changes may be attributed to the behaviour of the local Froude number (i.e. a Froude number in which the length scale is based upon the local depth). The local Froude number ($\frac{u}{\sqrt{gh}}$) gives a measure of the ratio of the local flow velocity to the speed of small amplitude surface waves in shallow water (which is a result obtained from linear theory). As such, it is a parameter that dictates the level of feedback between the surface deformation and the local flow field, as small amplitude waves may only travel upstream at Froude numbers less than 1 (this statement is only strictly true for linear solutions, however it should give some insight into the non-linear problem being investigated here).

Acheson (1990) when considering a hydraulic jump, shows that such a jump represents a change from a supercritical flow (flow field in which the local Froude number is greater than 1) to a subcritical one (where the local Froude number is less than 1); with such a transformation inducing a significant change in the surface height (i.e. a hydraulic jump). Hence an examination of the local Froude number in the region directly above the cylinder is warranted, as it may provide some insight into the local flow conditions and help explain the significant sharpening and wave breaking observed at the larger Froude numbers.

The variation of the local Froude number, based on both the flux averaged velocity (mass flux divided by surface height, which gives a spatially averaged velocity in the gap) and the maximum velocity in the gap directly above the cylinder, at the point of maximum lift were used.

It should be noted that the peak velocity was usually observed slightly downstream from the cylinder, as shown in figure (4.40) (which also illustrates the line from which the current results are taken). As a consequence, the maximum local Froude number will generally occur downstream of the cylinder, with the maximum velocity typically being approximately 20% higher than it is in the region above the cylinder. However, it is expected that the velocity within this region should give some indication with regard to the trend in local Froude number. The variation of the local Froude number with gap ratio is shown in figures (4.41) and (4.42).

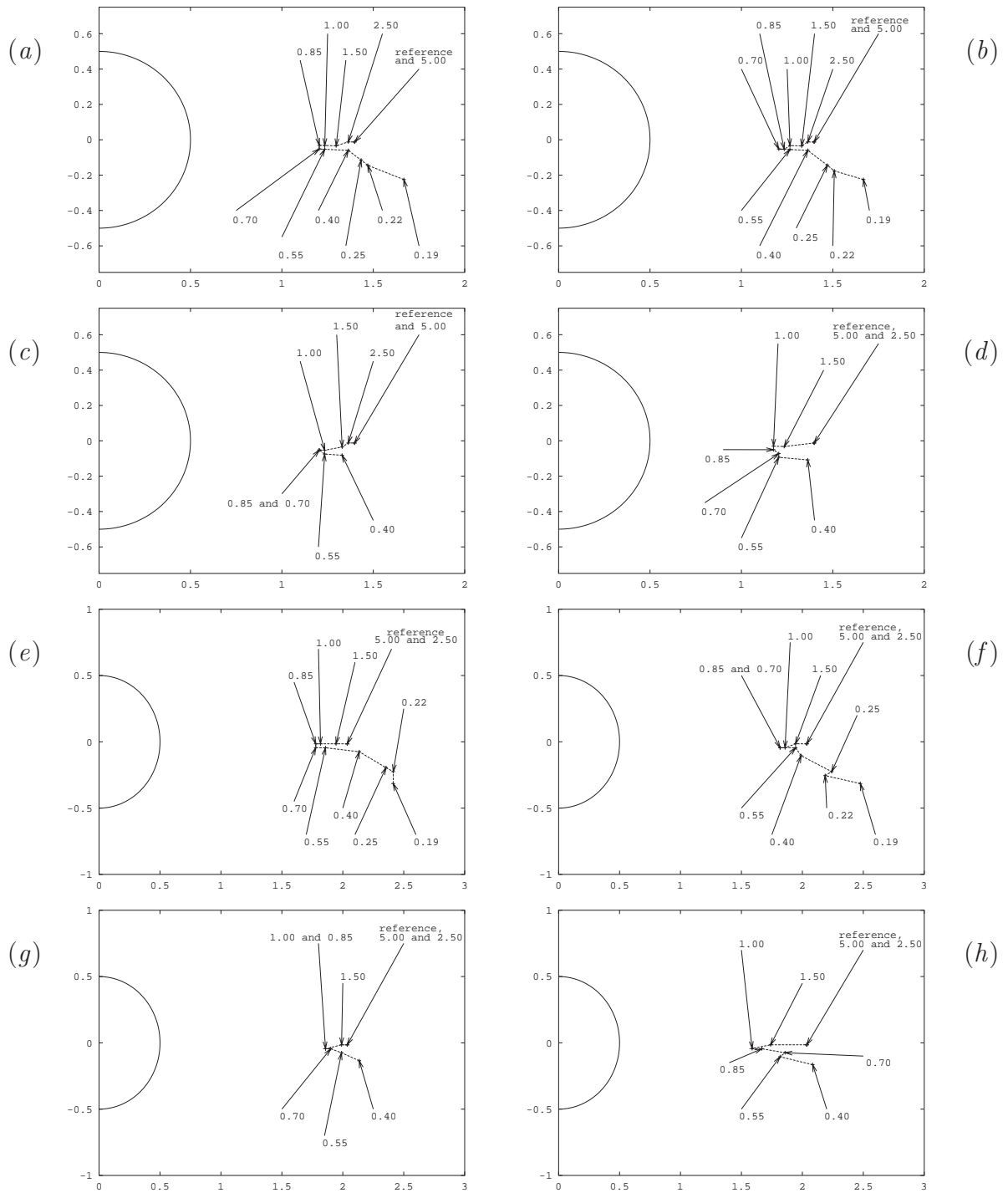


Figure 4.33: Figure showing the variation of the formation length with gap ratio and Froude number. Figures (a) to (d) show the formation length calculated using the standard deviation in the vorticity, while figures (e) to (h) show the formation length calculated using the standard deviation of the vertical component of the velocity. ((a) and (e) are for a Froude number of 0.25, (b) and (f) are for a Froude number of 0.30, (c) and (g) are for a Froude number of 0.35 and, (d) and (h) are for a Froude number of 0.40). The Reynolds number in each case is 180.

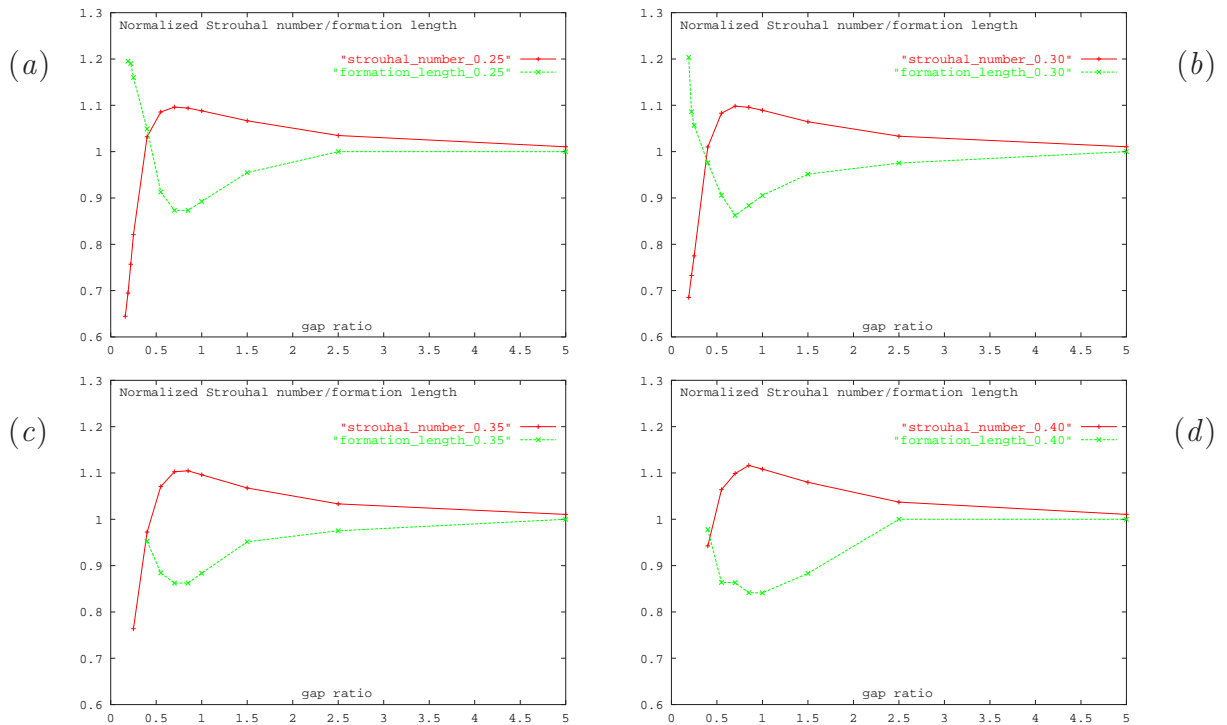


Figure 4.34: Variation of the normalized formation length (based on the standard deviation in the vorticity) and the normalized Strouhal number with gap ratio for Froude numbers 0.25 (a), 0.30 (b), 0.35 (c), and 0.40 (d). The Reynolds number in each case is 180.

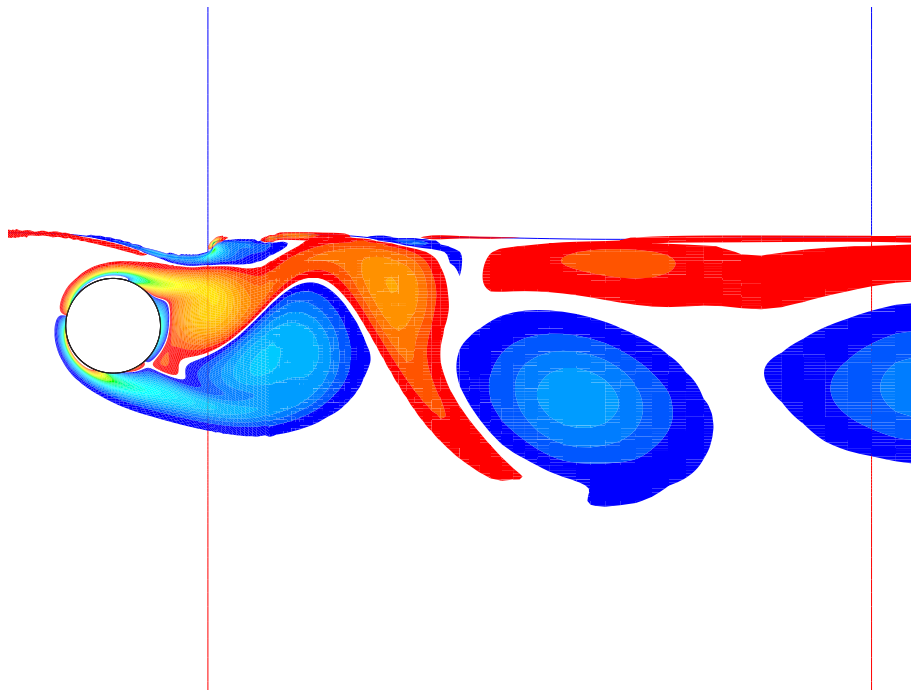


Figure 4.35: Plot showing the vorticity field for a gap ratio of 0.40 and a Froude number of 0.40. The Reynolds number for case is 180. The two vertical lines denote the domain size used for calculating the vortex convection speeds and tracking the vortex paths.

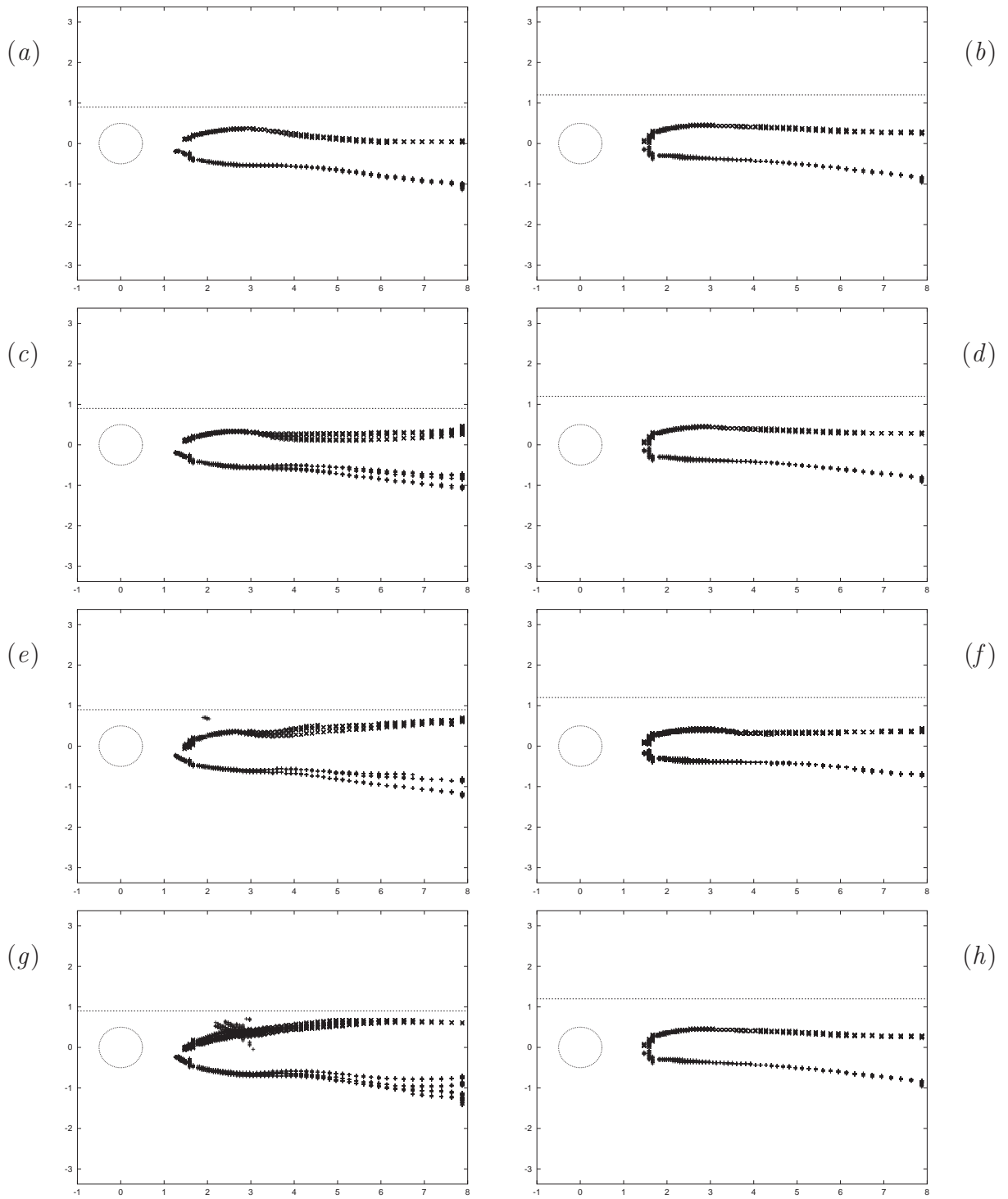


Figure 4.36: Plots showing the vortex paths for a gap ratio of 0.40 (a, c, e and g) and 0.70 (b, d, f and h) for Froude numbers of 0.25 (a and b), 0.30 (c and d), 0.35 (e and f) and 0.40 (g and h). The Reynolds number in each case is 180.

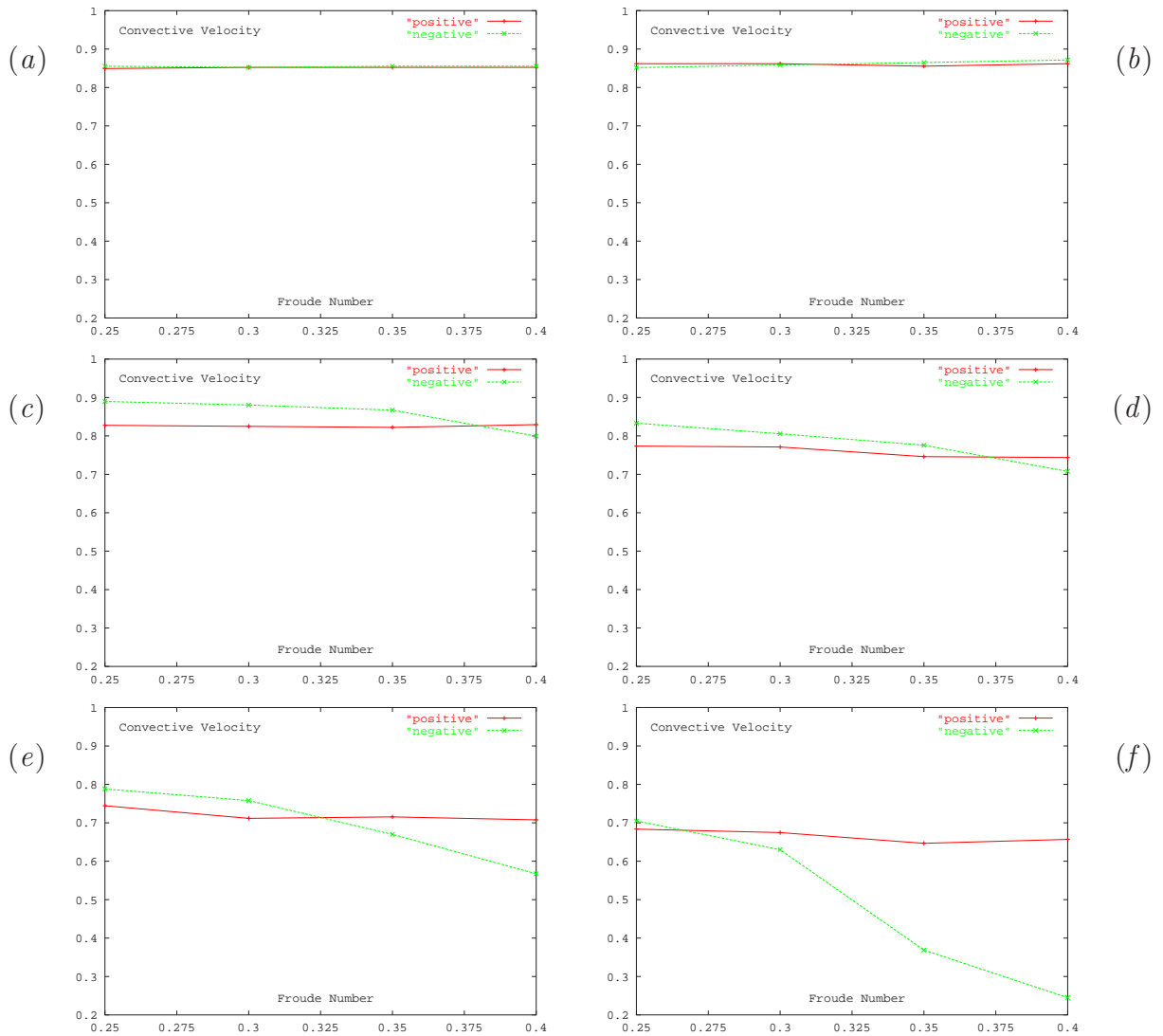


Figure 4.37: Plots showing the variation in vortex convection speed with Froude number for both the positive and negative vortices. ((a) gap ratio of 5.00, (b) gap ratio of 2.50, (c) gap ratio 1.00, (d) gap ratio 0.70, (e) gap ratio of 0.55 and (f) gap ratio 0.40). The Reynolds number in each case is 180.

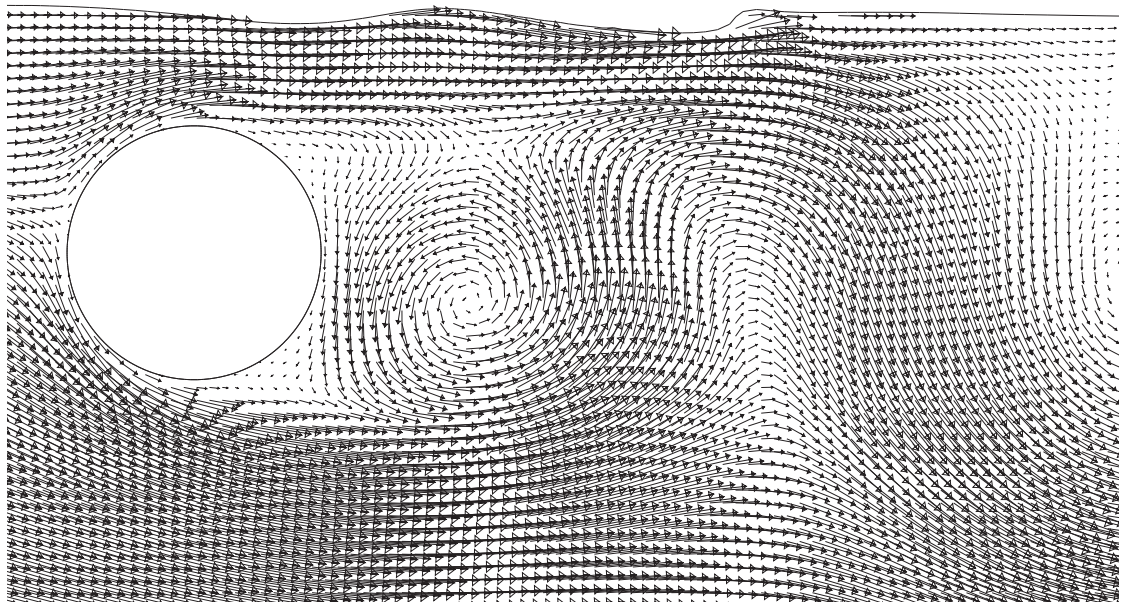
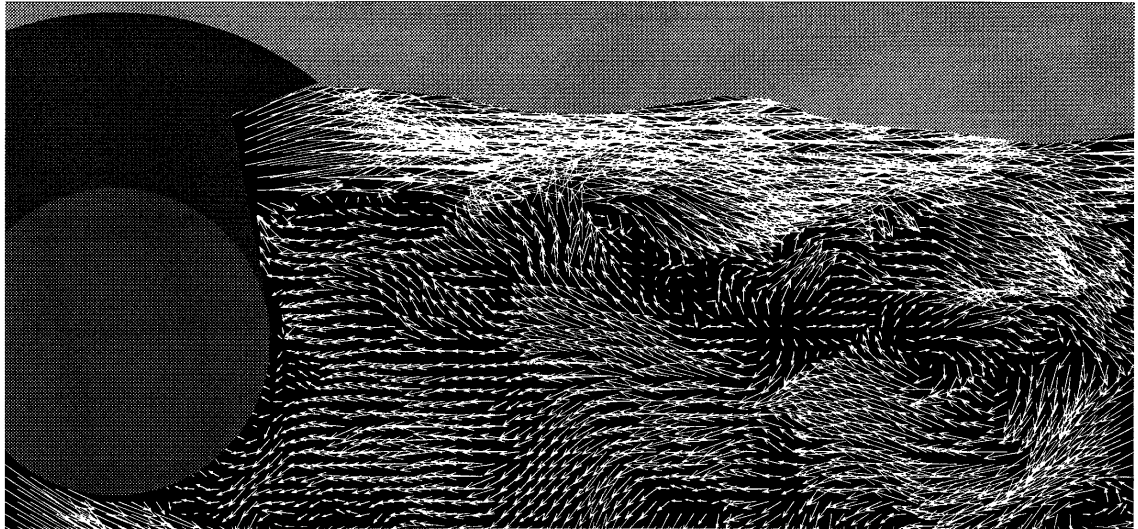


Figure 4.38: Comparison of the velocity fields between experimental findings of Sheridan *et al.* (1997) (top) and the current numerical study (bottom), for a gap ratio of 0.40 and a Froude number of 0.35 (gap at 5.9 diameters upstream is 0.42). The results of Sheridan *et al.* (1997) (top) are for a Reynolds number between 5990 and 9120, while in the numerical results the Reynolds number is 180.

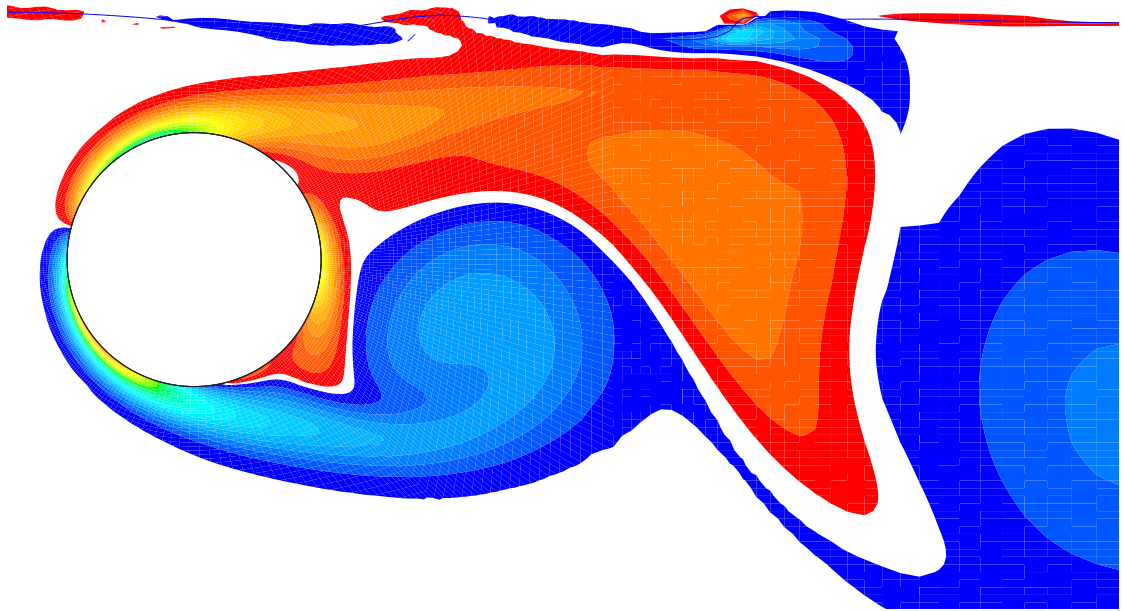


Figure 4.39: Comparison of the vorticity fields between experimental findings of Sheridan *et al.* (1997) (top) and the current numerical study (bottom), for a gap ratio of 0.40 and a Froude number of 0.35 (gap at 5.9 diameters upstream is 0.42). The results of Sheridan *et al.* (1997) (top) are for a Reynolds number between 5990 and 9120, while in the numerical result s the Reynolds number is 180.

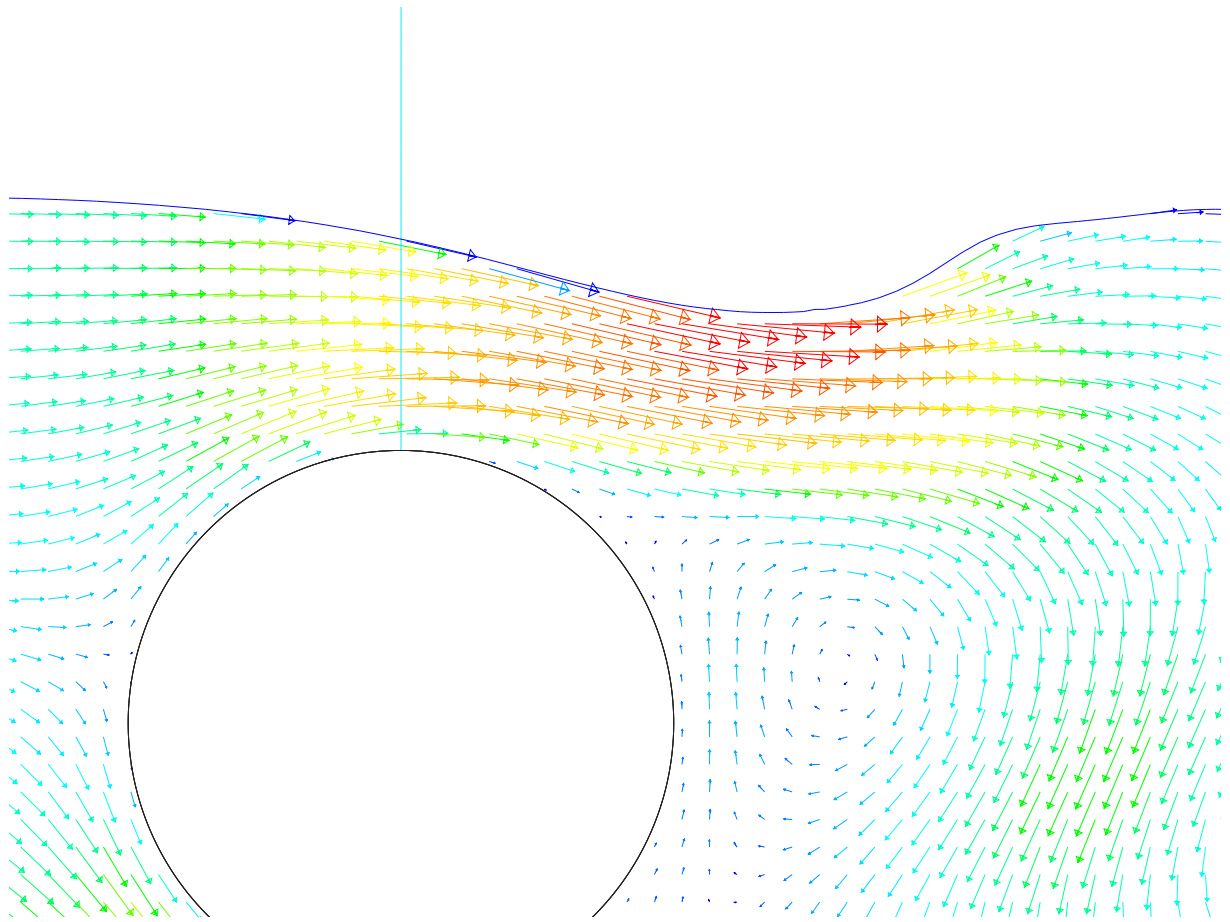


Figure 4.40: Plot showing velocity vectors at the point of maximum lift. The line through which the flux in calculated is also shown. The gap ratio for the case shown is 0.40 and the Froude number is 0.35. The Reynolds number is again 180.

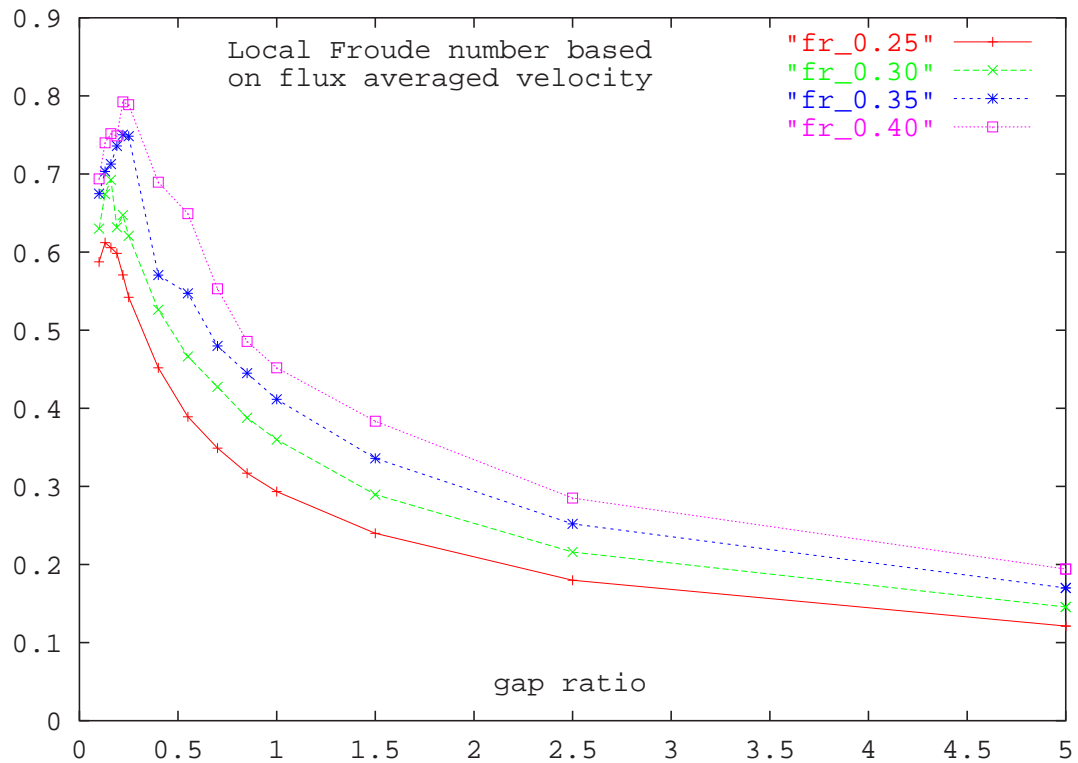
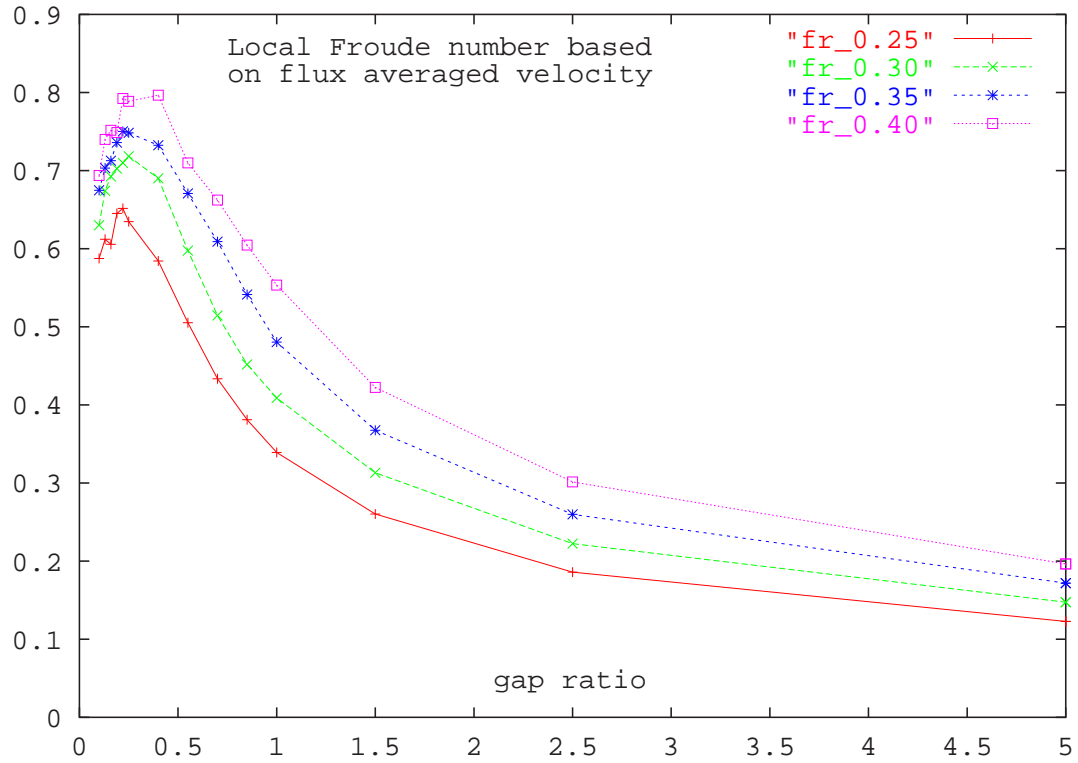


Figure 4.41: Variation of the local Froude number with gap ratio (the Froude number based on flux averaged velocity in the region above the cylinder), at both the points of maximum (top) and minimum (bottom) lift. The Reynolds number in each case is 180.

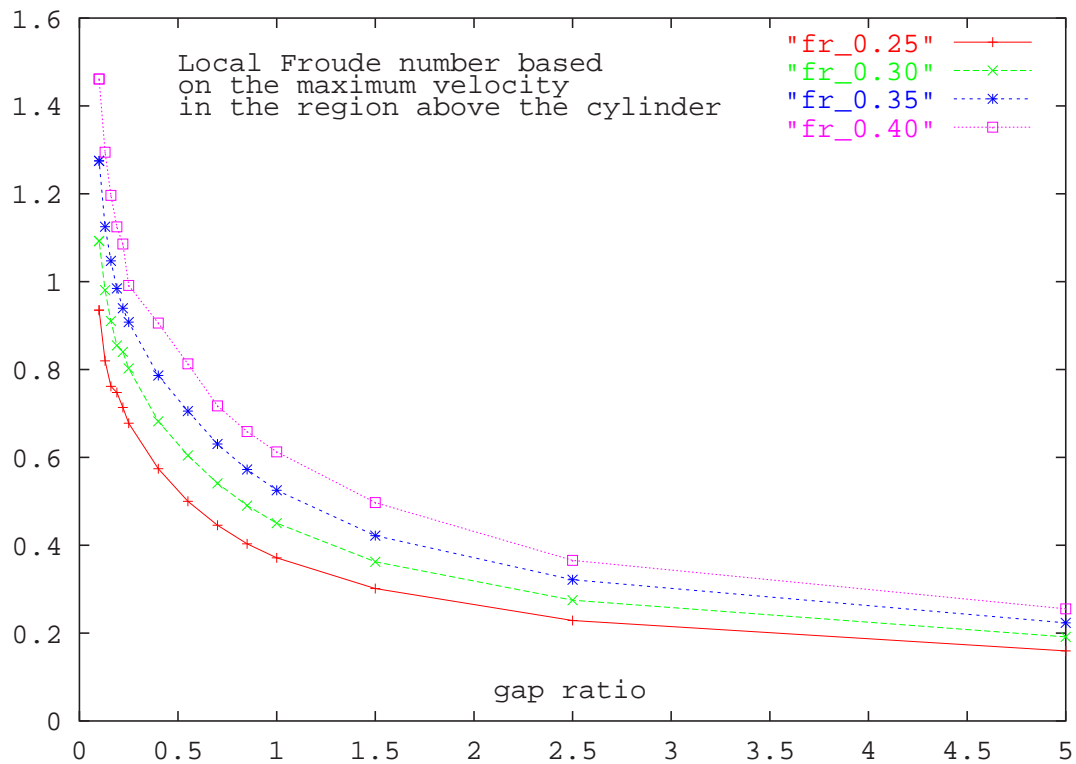
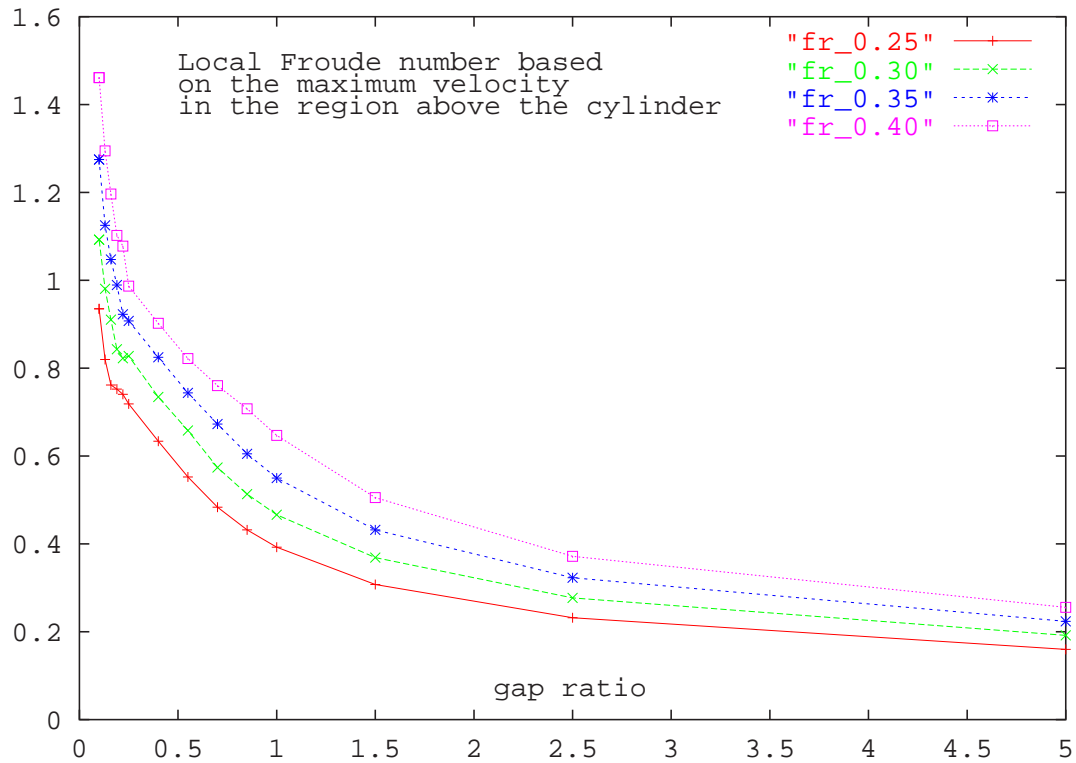


Figure 4.42: Variation of the local Froude number with gap ratio (the Froude number based on maximum velocity in the region directly above the cylinder), at both the points of maximum (top) and minimum (bottom) lift. The Reynolds number in each case is 180.

The closeness of the local Froude number to the value of unity for the gap ratio 0.25, Froude number 0.35 and 0.40 cases, suggests that the local Froude number exceeds unity for some interval of time during the course of a shedding cycle. The results of Acheson (1990) for a hydraulic jump would then suggest that the transformation of the flow back to a state in which it is subcritical (below 1), may then be accompanied by as small hydraulic jump or a significant sharpening in the local surface curvature.

The change in the local Froude number (from supercritical to subcritical) would thus explain the sharpened scar region which was observed during part of the shedding cycle at the larger Froude numbers. This behaviour is most clearly demonstrated via consideration of the videos which show the time dependent evolution of the vorticity field. Indeed, the movie for the gap 0.25 Froude number 0.35 case indicates that a sharp surface scar appears (with a scar being a region in which the surface curvature rapidly changes sign), and that positive vorticity then diffuses out from the scar (with this positive vorticity cross annihilating with the negative vorticity formed on the upper half of the cylinder).

It is expected that it is this sharpening in the surface curvature, combined with the significant local slowing/reversal of the flow velocity at positions close to the free surface, that will eventually result in wave breaking.

4.10 Mechanism

As was discussed in the previous chapter (that dealt with the flow at lower Froude numbers), the cessation of shedding was largely brought about by the reduction in the amount of fluid available to form vortices and by the reduction in the velocity close to the free surface (with such a reduction causing the wake velocity profile to become asymmetric, which according to Koch (1985) is a condition which does not support an absolute instability).

The weakening and eventual cessation of shedding at the intermediate Froude numbers considered here is believed to be due to the same process. Although the more malleable free surface alters the behaviour somewhat, with the interaction of the flow structures with the free surface influencing the supply of fluid available to form vortices, and in doing so skewing the wake at larger gap ratios. Hence it is expected that the wake behaviour will be governed by the time dependent surface deformation, and its influence upon the degree of skew in the wake.

When described in this way, the system essentially represents a form of feedback loop. Such

that the vortices shed from the cylinder influence the degree of surface deformation, which in turn controls the level of skew in the wake, hence altering the formation of discrete vortices.

Such a feedback loop supports the modulation of shedding, which was observed at some gap ratios (e.g. gap 0.25, Froude number 0.40); as vortex shedding is able to grow in strength until it reaches a point at which the surface deformation associated with its growing strength, results in a significant skew in the wake and hence leads to its weakening, and in some cases its suppression. This weakening then removes the vortical structures that gave rise to the surface distortion in the first place, and with this, the cycle is able repeat itself.

Thus as the surface becomes more malleable, it is the time-dependent nature of the flow that governs the entire wake behaviour, as the near wake need only become skewed for a short period of time for shedding to be weakened or even suppressed. It is hypothesized that it is this mechanism which governs the metastable behaviour observed by Sheridan et al. (1995), and which will be discussed in greater detail in the next chapter (which deals with the flow at higher Froude numbers).

At the Froude numbers being investigated here, the surface deformation appears to be insufficient to transiently suppress shedding, but it is large enough to considerably weaken its strength. The modulated lift trace observed at a gap ratio of 0.25 and for Froude numbers of both 0.35 and 0.40 illustrates this point.

The small-scale wave breaking that was also noted appears to occur when the local Froude number exceeds unity in isolated regions of the flow. When this occurs, information in the form of surface waves cannot travel upstream and the interaction of this fast moving fluid with the slow/reverse flow from above the positive vortices ensures that either surface sharpening or wave breaking takes place (with Lin & Rockwell (1995) indicating that the shift from a surface scar to breaking wave depends upon the Froude number).

When wave breaking is observed, it appears to share some similarities with the breaking of Branch I instability waves (wave breaking associated with the first branch of the dispersion relation) as discussed by Dimas & Triantafyllou (1994). In this case there exists a sharp horizontal velocity shear at the surface, with the wave height still remaining relatively small.

It is useful at this point to consider what is actually happening in the wake of the cylinder. An examination of the pressure and velocity fields together for a gap ratio of 0.40 and a Froude number of 0.35, reveal that the fluid from above the cylinder follows the surface before being wrapped around the negative shear layer from the upper side of the cylinder, and then diverted

downwards. At the same time, the fluid from downstream is also intromitted (or entrained) upstream by the large positive vortex that was shed from beneath the cylinder. This positive vortex tends to lift the surface at positions away from the cylinder, while drawing it downward at positions closer. This behaviour is most clearly illustrated with reference to the pressure and velocity fields at an instant as shown in figure (4.43).

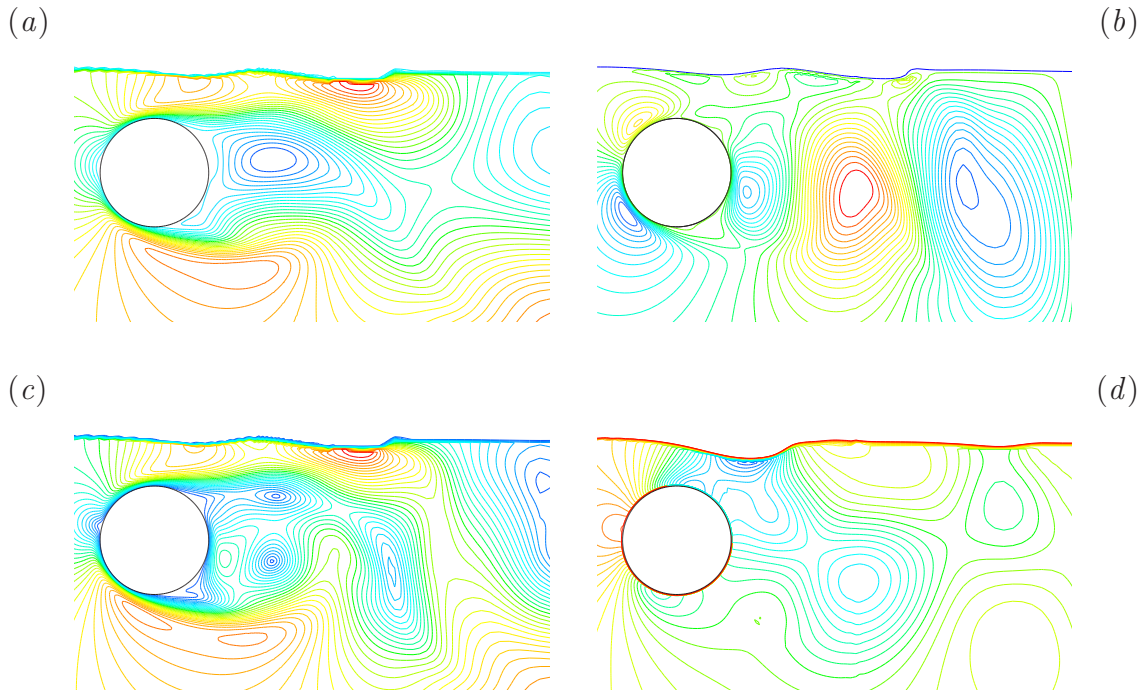


Figure 4.43: Contours of x velocity (a), y velocity (b), total velocity (c) and pressure (d), for a gap ratio of 0.40 and a Froude number of 0.35. The Reynolds number in each case is 180.

At the juncture point between the two oppositely signed vortices, fluid is drawn downward (hence the negative y velocity), and this assists in the sharpening of the free surface in the region directly above two vortices. The downward movement of the fluid from above the cylinder also tends to result in the positive vortex from beneath the cylinder being lifted upward slightly, with this process illustrated schematically in figure (4.44). The slight upward movement of the positive vortex has a twofold effect. Firstly, it moves the region of slow/reverse flow (region just above the positive vortex, which is rotating in a counter clockwise manner) closer to the free surface and hence increases the likelihood of wave breaking. Secondly, it moves the last shed positive vortex into a region in which its convective velocity diminishes.

The second point is important, as the reduction in the convective speed of the positive vortex enables larger-scale positive vortical structures to form in the wake. Such structures depending

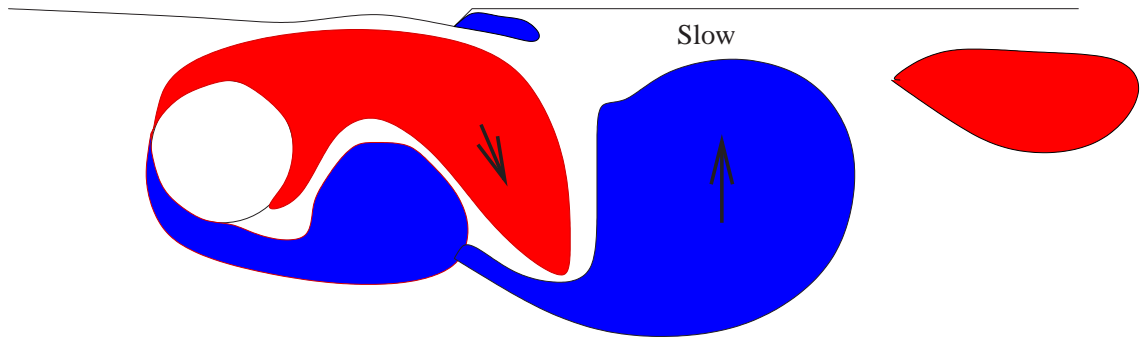


Figure 4.44: Schematic showing the movement of the vortices.

upon their proximity to the cylinder, then help to further deflect the fluid from above the cylinder downwards, and in doing so skew the wake. These larger-scale positive vortical structures typically form when the convective speeds of the shed positive vortices differ, such that one vortex catches the other, and the two are then observed to coalesce.

The extent of the upward movement of the last shed positive vortex depends upon both the surface curvature (and hence upon the Froude number) and upon the vortical structures already present in the wake. It is tentatively suggested here that the position at which this upward movement of the last shed positive vortex occurs, is dependent upon the formation length. As such a suggestion would explain the difference in the position at which wave breaking was observed.

With regard to the first point, the downward movement of the negative shear layer and the upward movement of the last shed positive vortex from beneath the cylinder result in either a significant slowing (at lower Froude numbers), or even a flow reversal (at higher Froude numbers), in the region close to the free surface. This behaviour then has a significant influence upon the surface curvature, with slowing typically resulting in a sharpened scar, while reversal results in wave breaking.

It is necessary to stress that this behaviour is all highly time-dependent, with the free surface curvature and wake skew varying throughout the course of the shedding cycle. As a consequence, the wake will tend to give rise to structures that differ significantly from those of a fully submerged cylinder, with these structures subsequently influencing the wake development.

The basic flow mechanism describing the surface / wake interaction is postulated to be as follows:

- The upward movement of the positive vortex induces surface curvature, which due to the nature of the positive vortex results in the surface rising at positions away from the

cylinder and falling at positions closer.

- The roll-up of the negative shear layer from above the cylinder further exacerbates this by drawing more fluid downward.
- The altered surface curvature then results in the fluid from above the cylinder being directed downwards, and depending upon the gap ratio, the slow/reverse flow from above the positive vortex and the flow from above the cylinder interact.
- This interaction causes some of the horizontal momentum associated with the flow above the cylinder to be converted into vertical momentum.
- Now depending upon the angle at which the two streams of fluid meet (which is largely determined by the surface curvature and hence to some extent by the Froude number), the interaction will result in either a local sharpening of the free surface for slight angles or in wave breaking at larger angles.

Any downward deflection of the fluid from above the cylinder will obviously reduce the horizontal momentum associated with this flow, and hence allow the positive vortex from beneath the cylinder to exert a greater influence on the flow near the free surface (at least at small gap ratios). As the fluid from above the cylinder is deflected downwards, satisfaction of continuity (conservation of mass) will then require that fluid from further downstream must be drawn upstream (otherwise the fluid height would drop dramatically). For the small gap ratio cases in which the vortices from beneath the cylinder are already at close proximity to both the cylinder and the free surface, it is these structures that are drawn upward and closer.

As mentioned earlier, the upward movement of the last shed positive vortex has a two fold effect, as it tends to reverse flow at locations close to the free surface while also moving into a region in which it has a diminished level of horizontal momentum (and hence a reduced convective speed). Thus, it is the path taken by the last shed positive vortex that dominates the near wake behaviour, with its influence on the both the surface curvature and the intromission of fluid upstream from further downstream, controlling both the level of skew and the supply of fluid into wake cavity (the region in between the two shear layers).

It should be emphasized that the upward movement of the last shed positive vortex is a gradual process, with the upward movement being strongly influenced by the structures present in the wake just downstream of the cylinder. Indeed, it is the positive vortical structures that form downstream that are partially responsible for the establishment of the gradient in the convective

velocity with height. And as such, they have a significant influence upon the vortices shed after their formation.

It should also be stressed that it is the slowed/reverse flow that deflects the fluid from above the cylinder away from the free surface. This deflection then skews the wake and hence alters the wake state, with the interesting features arising as a consequence of the inherent time-dependence of the entire process.

To emphasize the influence of the slow/reverse flow associated with the behaviour of the last shed positive vortex, it is perhaps best to consider two specific examples. The first will focus on the behaviour at a gap ratio of 0.25 and a Froude number of 0.30 (where the lift trace shows only slight levels of modulation), while the second will look at the flow at the same gap ratio but at a Froude number of 0.40 (where the lift trace is highly modulated). Before proceeding it is highly recommended that the reader view the videos for these cases.

For the smaller Froude number case (i.e. gap 0.25, Froude number 0.30) at the point of maximum lift, the faster moving flow from above the cylinder interacts with the slow moving fluid just above the positive vortex. Such an interaction causes the pressure to rise, and a pressure gradient is established which directs the flow from upstream in a diagonally downward direction (see figure (4.45)). The pressure gradient is such that if the fluid from above the cylinder were to continue moving forward, it would move into a region in which the pressure gradient rises. Hence this fluid will tend to move downwards and in between the forming vortices. At the minimum extreme in the lift cycle, the flow that issues from above the cylinder extends over a greater horizontal range, with the strong positive vortex, which is at this point further from the cylinder, directing the flow vertically downwards. Again, it is the positive vortex which was formed beneath the cylinder, but shed during the last cycle, that dominates the flow further downstream. Figure (4.45) shows the pressure fields at both the maximum and minimum positions in the lift cycle respectively, and it is clearly visible that the vortices from beneath the cylinder tend to represent the regions of lowest pressure, and hence have the greatest impact on the near wake behaviour.

For the larger Froude number case (i.e. gap 0.25, Froude number 0.40), the increased surface curvature ensures that more fluid is intromitted upstream (as the increased redirection of the fluid from above the cylinder ensures that there is a diminished level of horizontal momentum associated with the 'jet') and in doing so it deflects the fluid from above the cylinder further away from the free surface. This results in small scale wave breaking and in the upward movement

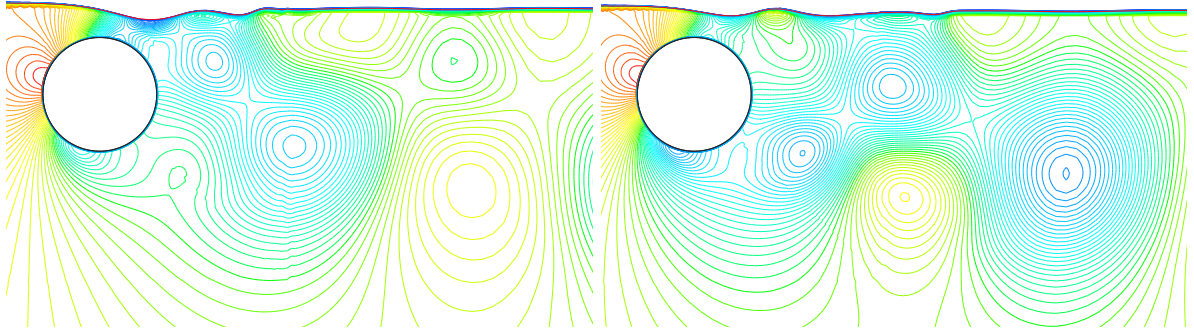


Figure 4.45: Plots showing the pressure field at the point of maximum (left) and minimum (right) lift for gap ratio of 0.25 and a Froude number of 0.30. The Reynolds number in each case is 180.

of the last shed positive vortex (this typically only occurs when the positive vorticity from both the free surface and from beneath the cylinder, envelope the negative shear layer from above the cylinder). The reader is strongly recommended at this point to consult the videos which illustrate this point, or at the very least consider figure (4.48) which will be discussed shortly.

The upward movement of the last shed positive vortex (which is also the most dominant, as it has the lowest pressure associated with it) into a region in which its convective velocity is reduced, results in a slowing of the flow near to the surface and in a stretching of the shear layer from beneath the cylinder. This behaviour typically results in an elongated wake in which vortex roll-up is delayed or stalled. Weak shedding then only re-establishing itself when the larger-scale positive vortical structure that forms during this process, moves further downstream, hence diminishing its influence on the near wake. This behaviour is best illustrated in both the particle transport and vorticity videos. However, a few key frames together with their relevant location on the lift trace are shown in figures (4.46) to (4.49). Figure (4.46) highlights the variation in lift coefficient with time, while the close up view of the region in between the two dashed vertical lines (where the lift undergoes a substantial reduction in magnitude), is shown in figure (4.47). The labels in figure (4.47) correspond to the frames taken from the videos of the evolution of the vorticity field and the particle transport plots, which are shown in figure (4.48) and figure (4.49).

The particle tracer plots, which color the particles based on their release height, were obtained by releasing inert particles from a series of vertical positions 8 diameters upstream of the cylinder center. In many instances, particles were released at exactly the point where the undisturbed surface would lie. Occasionally in these cases, slight variations in the surface position resulted

in these particles being injected into lighter phase just above the free surface. Hence some of the videos show a limited number of particles moving away from the surface, particularly for the cases in which wave breaking was observed. For the images presented here, these particles are not shown, but they are present in the videos.

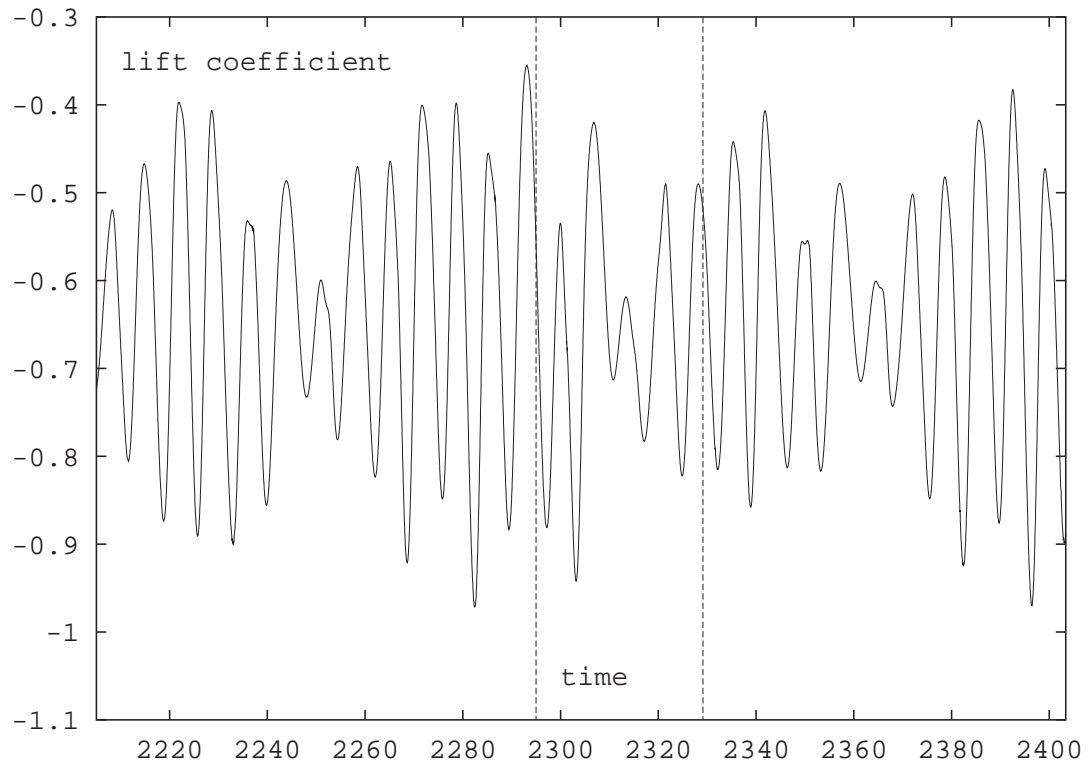


Figure 4.46: Variation of the lift coefficient with time for a gap ratio of 0.25 and a Froude number of 0.40. The region in between the two dashed vertical lines is shown in figure (4.47). The Reynolds number in each case is 180.

The movies showing both the particle transport and vorticity fields indicate that the movement of one of the positive vortices towards the free surface (and hence into a region where its convective velocity is slightly slower) tends to result in a loose pairing between the positive vortices shed from beneath the cylinder. The distance from the cylinder at which the two positive vortices coalesce is related to the difference in their convective velocities, which is in turn influenced by the vortical structures already present in the wake. The videos suggest that it is the positive vortical structures in the wake in combination with the level of surface deformation, that exert the controlling influence on the wake behaviour. Hence it is postulated that it is surface deformation that regulates the upward movement of the positive vortices, while the structures already in the wake dictate the variation in the convective speed with distance from the free surface.

It is believed that it is the surface curvature in conjunction with the positive vortical structures

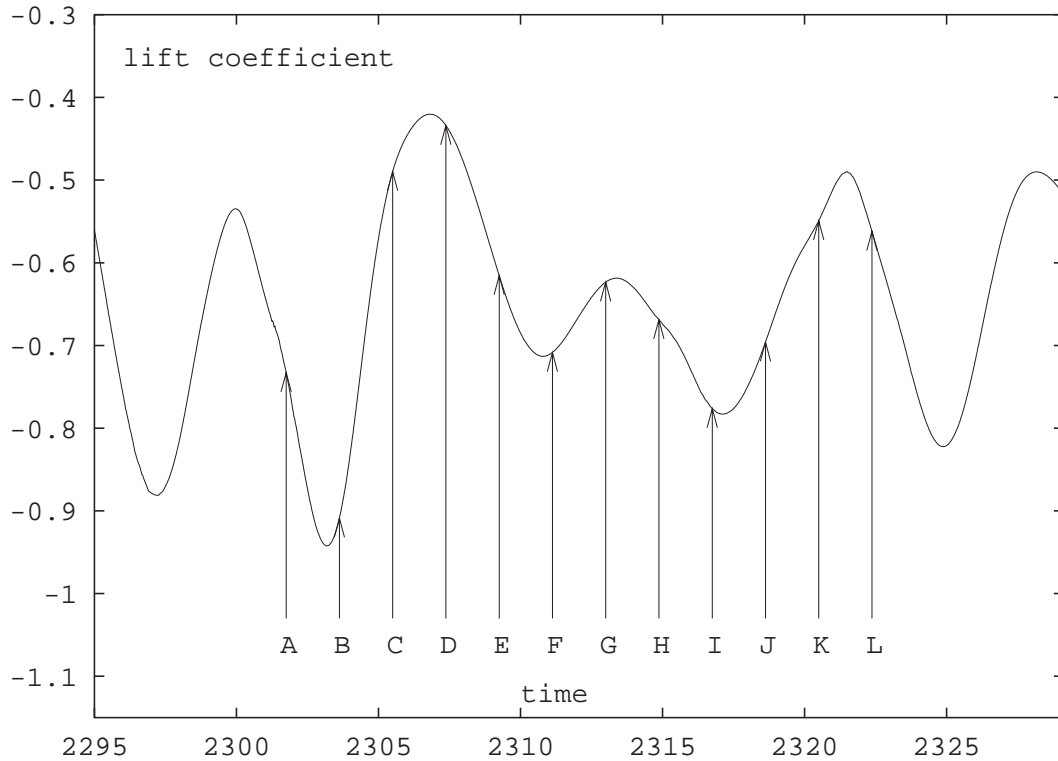


Figure 4.47: Close up view of the variation of the lift coefficient with time for a gap ratio of 0.25 and a Froude number of 0.40. The markers denote the frames shown in figures (4.48) and (4.49). The Reynolds number in each case is again 180.

in the wake, that are responsible for the modulated lift signal observed for a gap ratio of 0.25 and a Froude number of 0.40. For this case, it is speculated that it is the mutated vortices that form from the cylinder, that combine to skew the wake, and hence weaken the absolute instability. The period of significant weakening then allows for the offending structures which have accumulated in the wake and which are themselves a byproduct of the stronger vortex shedding, to be flushed further downstream. This process then effectively regulates the shedding, such that it grows and diminishes in a modulated manner.

The reader is recommended at this point to examine the particle transport videos, as they illustrate that it is the strength of the slowing/‘flow reversal’ that governs the wake behaviour (with this flow being largely determined by the position of the last shed positive vortex or series of vortices).

The two regions to the right of the first dashed line on the lift trace in figure (4.46), where the magnitude of the lift diminishes markedly, both occur when there is a significant reduction (and in some regions a reversal) in the convective speed of the fluid located close to the surface. The

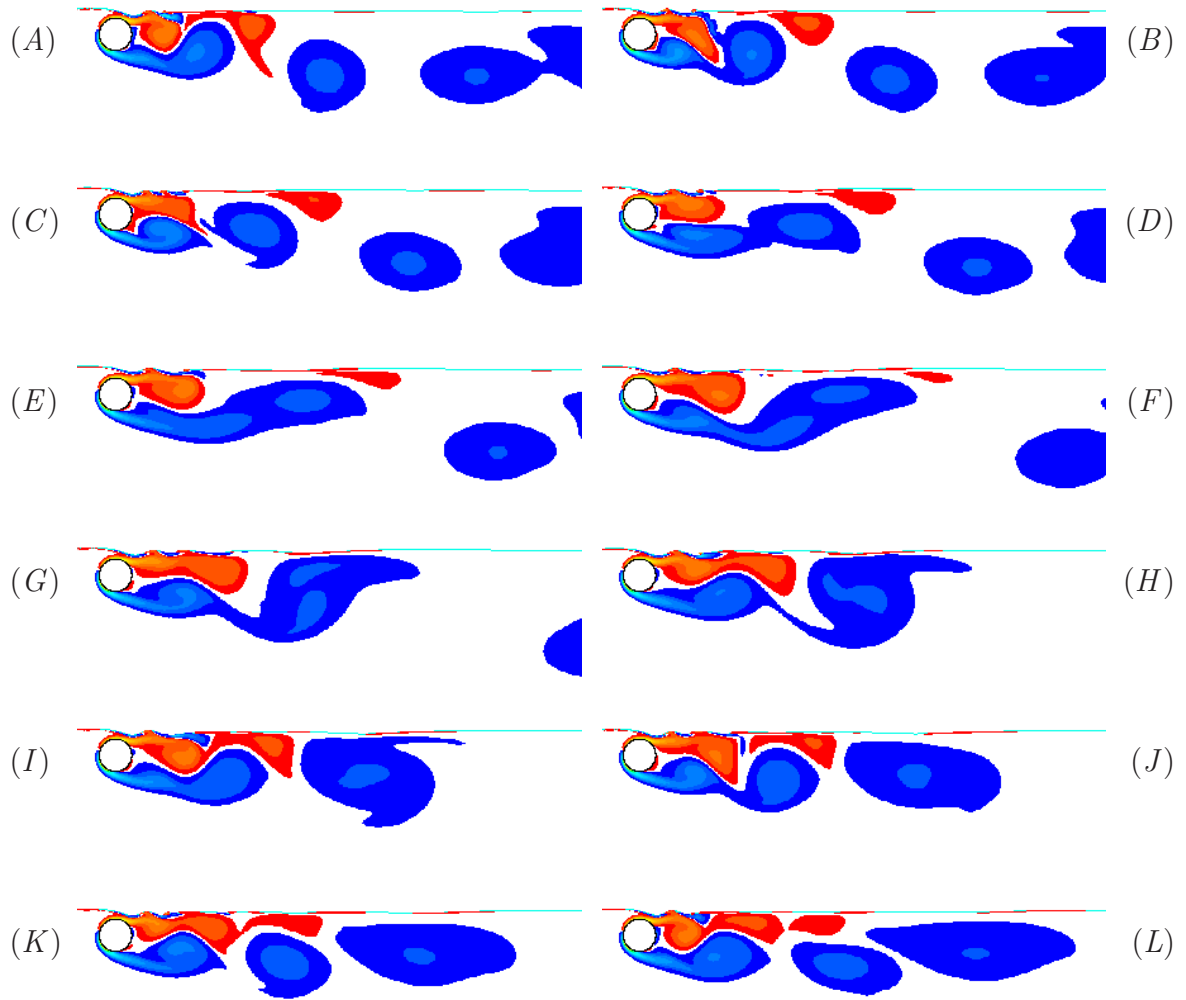


Figure 4.48: Vorticity fields at the corresponding instants shown figure (4.47) (gap ratio 0.25, Froude number 0.40, Reynolds number 180).

first zone (where the magnitude of the lift diminishes) occurs when the upward movement of the positive vortex is such that it comes into close contact with the free surface (see figures (4.48) and (4.49)). For this case it is the flow associated with the last shed positive vortex which induces the skew in the wake and hence stalls the shedding. The second zone occurs when the last shed positive vortex moves up slightly, but not into close contact with the surface. In this zone, it is the upstream flow associated with the dominant last shed positive vortex and the positive vortices shed previously, which combine to significantly impair the flow close to the surface. Figure (4.50) shows the vorticity field and particle tracer behaviour near the second zone (it should be noted that the videos for this case show both zones).

The common element in both cases, is the asymmetry or skew introduced into the wake velocity

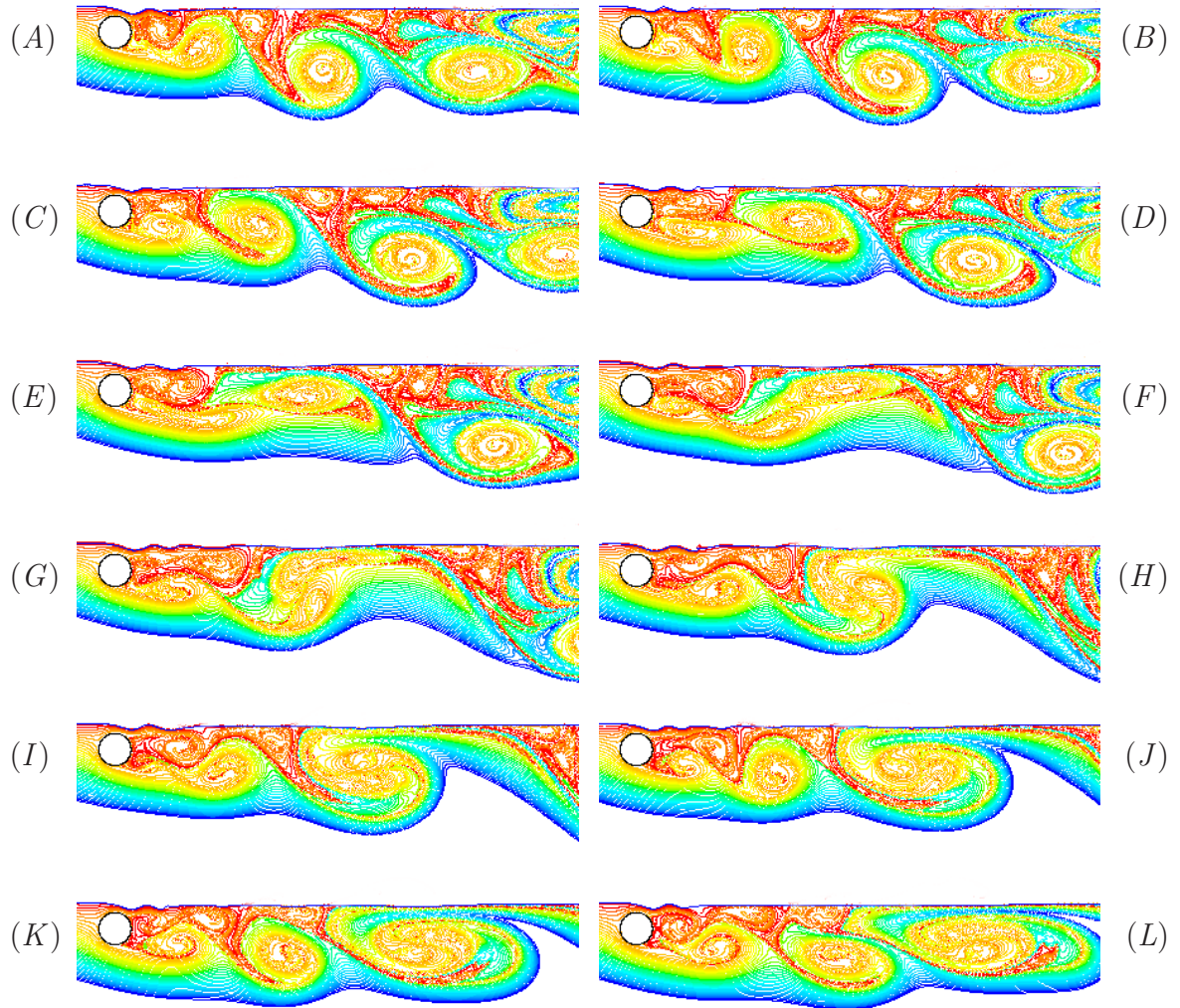


Figure 4.49: Particle transport plots at the corresponding instants shown figure (4.47) (gap ratio 0.25, Froude number 0.40, Reynolds number 180).

profile by the slowing/reversal of flow near the free surface. Koch (1985) indicates that the wake of a bluff body will tend to switch from being absolutely unstable to convectively unstable in the presence of an asymmetric velocity profile. Hence it is speculated that the vortex stalling, or the momentary delay in the vortex shedding observed here, is due to a shift in the nature of the instability governing the wake. This is a point that will be discussed in greater detail in the next chapter.

The particle tracer plots also illustrate that much of the downstream transport of the fluid that passes over the cylinder is via entrainment into the larger positive vortices, with a large portion of the fluid located close to the surface oscillating backwards and forwards with a small mean velocity downstream. This point is reinforced by reference to figure (4.51) which shows the

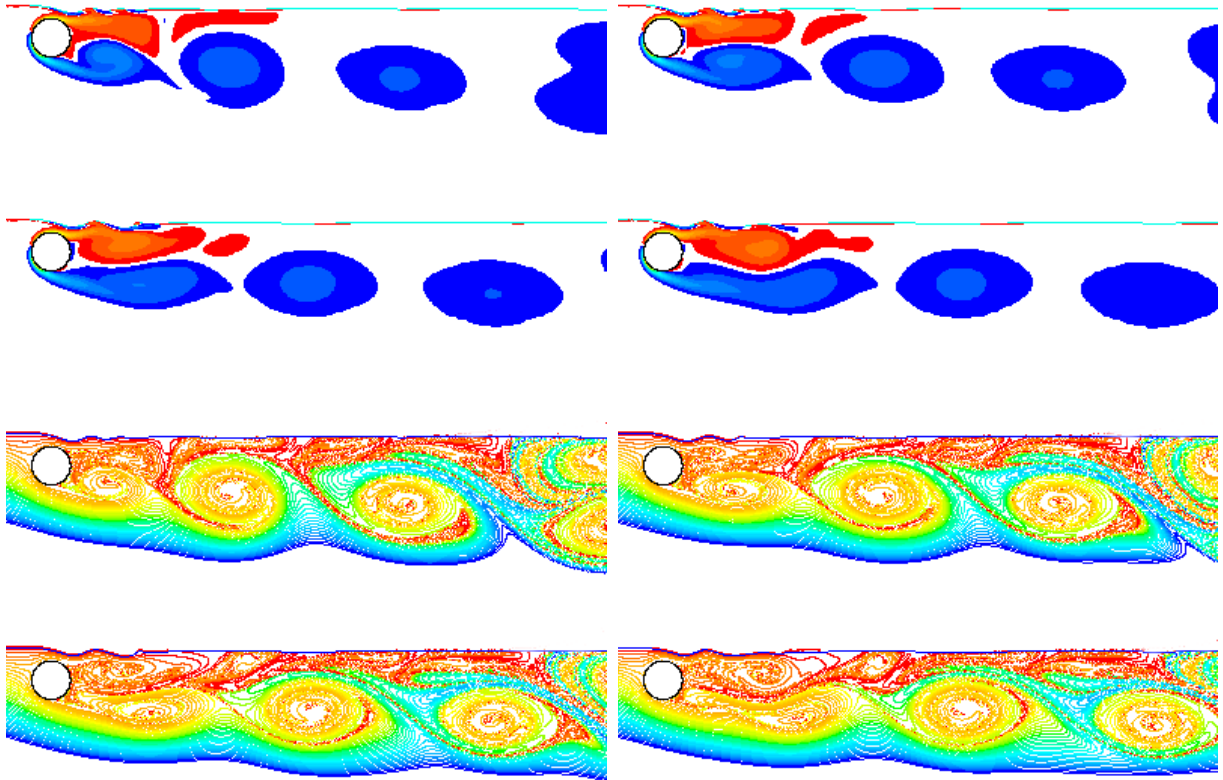


Figure 4.50: Vorticity and particle transport plots at four equispaced instants in the shedding cycle for the region to the right of the second dashed vertical line in figure (4.47). The plots show the flow behaviour in second zone in which the lift diminishes (left to right then top to bottom) (gap ratio 0.25, Froude number 0.40, Reynolds number 180).

particles colored by their residence time in the flow. It is clear from this plot that the particles closer to the surface tend to stay in the domain longer than those further from the free surface.

The residence time plot only helps to reinforce the notion that it is the behaviour of the positive vortical structures, that directly influences the near wake behaviour.

4.11 Summary

Before moving on to the next chapter (that considers the results at higher Froude numbers), it is worthwhile to reiterate some of the key findings for flow past a cylinder close to a free surface at Froude numbers between 0.25 and 0.40.

The key point that differentiates the behaviour observed here from that observed at the lower Froude numbers considered in the last chapter, is the level of surface deformation and its impact

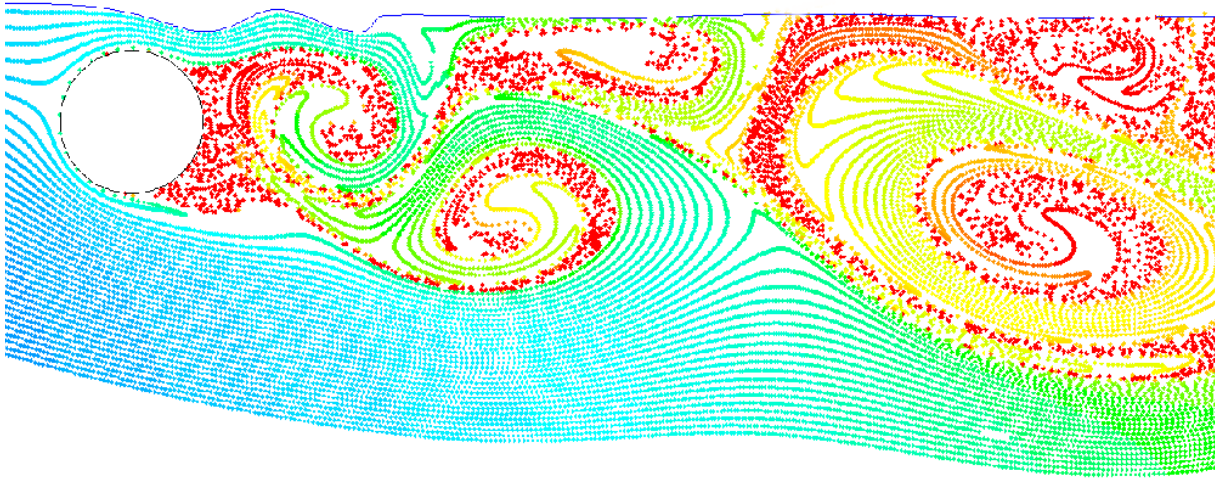


Figure 4.51: Particle tracer plot that shows the particles colored according to their residence time in the flow domain. The gap ratio for this case is 0.25 and the Froude number is 0.40. The Reynolds number is again 180.

upon the skew in the wake.

With regard to the surface deformation, it is clear that the increased Froude number has a significant effect, with small scale wave breaking being observed at some of the gap ratios for Froude numbers greater than or equal to 0.35. This wave breaking appears to be related to the angle at which the flow from above the cylinder and that from above the last shed positive vortex interact.

It is proposed that the general behaviour of the wake is governed by the level of feedback between the surface curvature and the absolute instability. At the smaller Froude numbers the surface is more rigid and skew is introduced by a reduction in the velocity of the fluid passing over the cylinder. However, at larger Froude numbers this skew is partially brought about by the angular redirection of the fluid passing over the cylinder. Hence while it is believed to be the skew that alters the instability in both cases, it is the nature of the skew that differs. Indeed, it is the time dependence of the skew at the larger Froude numbers that contributes to the more interesting flow behaviour.

It is anticipated that at larger Froude numbers the more significant surface curvature will permit the last shed positive vortex to move even further upward, and hence result in a significant separation of the flow from the free surface. It is also expected that the greater levels of time dependent curvature will give rise to wake states which vary significantly with time (such as

the metastable wake states observed by Sheridan et al. (1995)). The behaviour at these larger Froude numbers is now considered in the next chapter.

Chapter 5

Froude Numbers 0.50, 0.60 and above

As indicated in the discussion of the previous two chapters that dealt with the behaviour at lower Froude numbers, the level of surface deformation and hence the level of skew in the wake can have a large impact on its evolution. This chapter will now explore what happens when the Froude number is further increased, such that larger scale surface deformation and in some instances significant separation of the flow from the free surface is observed. In contrast to the preceding two chapters there has been considerably more experimental work done in this region of parameter space, with all of the results of Sheridan et al. (1995) and most of the results of Sheridan et al. (1997), Sheridan et al. (1998) and Hoyt & Sellin (2000) lying within the parameter range considered within this chapter.

All of the above mentioned authors observed significant changes in the wake behaviour for the Froude numbers considered here. Sheridan et al. (1995) note that the system was capable of supporting two differing wake states at a given point in parameter space. However, these two wake states were found to have limiting stability, in the sense that transformations between the two occurred in a pseudo periodic manner, and as such they were deemed by Sheridan et al. (1995) to be metastable.

The broadest range in parameter space (i.e. gap ratio and Froude number) was considered by Sheridan et al. (1997), who indicate that the flow can be loosely categorized into three basic wake states, which are characterized by the position of the fluid passing over the top of the cylinder (with this flow often being referred to by Sheridan et al. (1997) as a ‘jet’). The three

basic wake states, which are shown schematically in figure (5.1), are:

1. The ‘jet’ follows and remains attached to the free surface.
2. The ‘jet’ separates from the free surface, and occupies a region of space somewhere in between the cylinder and the surface.
3. The ‘jet’ stays attached to the rear of the cylinder, and only separates near the underside of the cylinder.

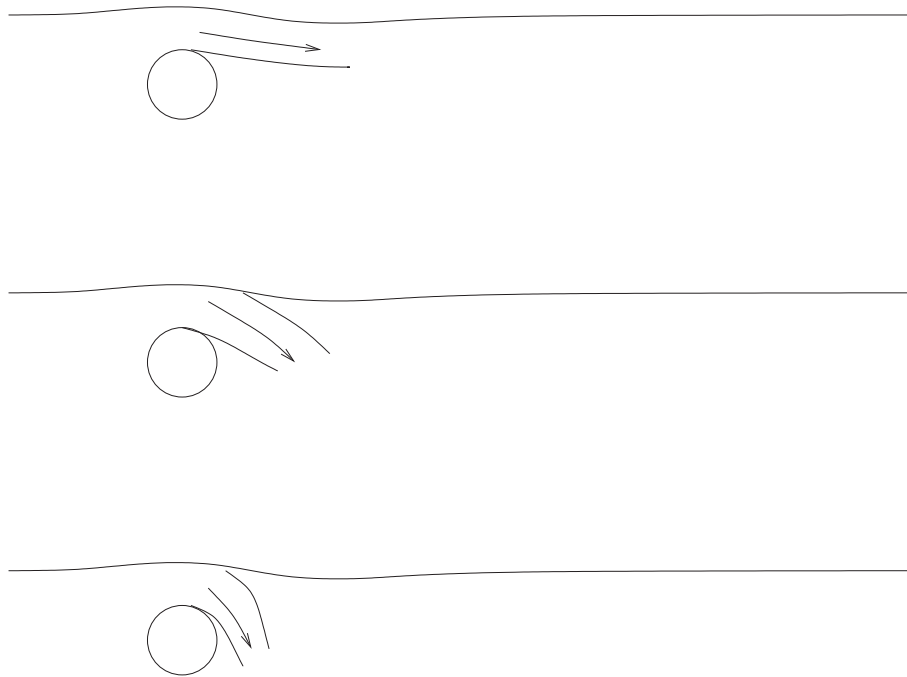


Figure 5.1: Schematic diagram illustrating the three basic wake states observed by Sheridan *et al.* (1997).

Each of these three states are observed to a limiting degree by Sheridan *et al.* (1997) at a Froude number of 0.60. Hoyt & Sellin (2000) also observe similar behaviour at a Froude number of 0.53, although they indicate that the flow often varies in a time-dependent manner, hence suggesting that some of these states may only be seen at a particular instant. It is thus expected that these three states should be observed in the current predictions.

It is perhaps best to begin this chapter with a description and a comparison of the flow fields over a range of gap ratios, for Froude numbers of both 0.50 and 0.60. It should be noted that significant changes in both the behaviour of the wake and the free surface are often observed as the Froude number is increased between these two values. Again comparison with experiment is

restricted to being purely pictorial, as to the author's knowledge no experimental measurements are available. However measurements of Strouhal number, lift, drag and moment will all be presented here, along with a description of the mechanism and a comment on the nature of the instabilities associated with each of the various flow states.

Before proceeding it is necessary to qualify some of the particle transport results (in particular the videos), which are presented on the Compact Disk accompanying this thesis. In many of these videos, a limited number of particles are observed on the other side of the free surface (which is modelled here as a fluid / fluid interface). These particles are observed for two reasons:

1. Firstly in some instances, and in particular cases in which the submergence depth is an integer multiple of 0.05, particles were released directly onto the free surface. Hence even the slightest drop in the surface position at the point of release, will result in some of these particles being injected just on the other side of the fluid-fluid interface. Such particles will then have their path determined by the flow field associated with the lighter fluid, and as such they are most notable in regions of high surface curvature (where the flow fields in the two phases are no longer parallel). While these particles could have been removed (i.e. never injected), they serve to highlight any drop in the fluid height near the inlet, while also providing more information with regard to the movement of the fluid close to the free surface.
2. Secondly, inaccuracies associated with the wave breaking process will permit neighboring particles (from within the fluid) to be carried up with the rising bubbles of the lighter phase which are entrained when wave breaking occurs. These particles should be ignored, and while their presence does provide some details with regard to the flow behaviour of the lighter phase (fluid), their appearance should not detract one's attention from the underlying flow behaviour.

It should be noted that these particles were removed from the particle transport (non-video) plots shown within this chapter.

5.1 Flow Behaviour

A brief description of the flow behaviour at each of the gap ratios for both a Froude number of 0.50 and 0.60 will now be given. It is necessary to stress that almost all of the flow behaviour was highly time dependent with the response of the system often being non-periodic. For these

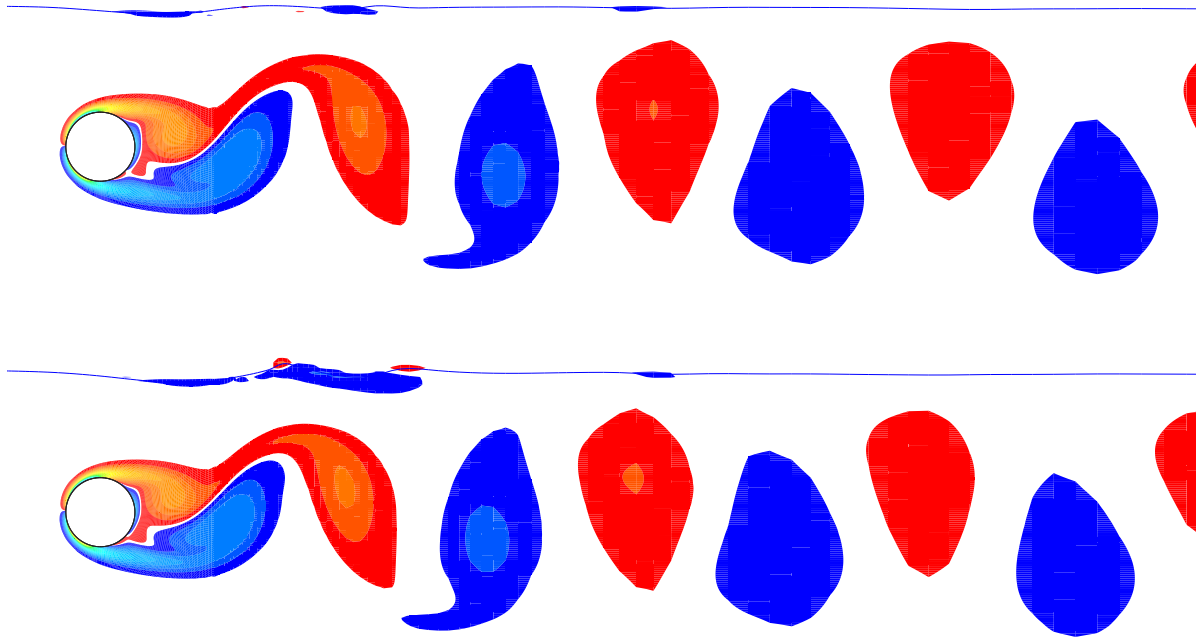


Figure 5.2: Vorticity fields at the point of maximum lift for a gap ratio of 1.50 and for Froude numbers of 0.50 (top) and 0.60 (bottom). The Reynolds number in each case is 180.

cases the videos showing the evolution of the flow field were invaluable and it is recommended that the reader view the videos on the attached compact disk while reading this chapter.

5.1.1 Large Gap Ratios, 5.00, 2.50, 1.50, 1.00 and 0.85

At the larger gap ratios (i.e. 5.00, 2.50), the flow about the cylinder is largely undisturbed by the adjacent free surface. However, as the gap ratio is reduced to 1.50 non negligible surface distortion is noted at both a Froude number of 0.50 and 0.60, with the surface curvature notably sharper at the higher Froude number. This behaviour is highlighted in figure (5.2), which shows the vorticity field for both Froude numbers at the point of maximum lift.

At the larger Froude number (i.e. 0.60), positive vorticity is clearly seen in the region close to the curved surface. However, its presence is insufficient to alter the vortex street formed from the cylinder. As the gap ratio is reduced to 1.00, small scale intermittent wave breaking is observed at both Froude numbers, however, it is much more substantial at a Froude number of 0.60. At the lower Froude number, the wave breaking and the associated surface vorticity is insufficient to alter the vortex street in a dramatic way, with the negative vortices, while

deformed, still maintaining an orientation similar to those for a fully submerged cylinder. At the larger Froude number however, the flux of vorticity from the surface is now sufficient to significantly alter the vortex street, such that the negative vortices are twisted as they interact and cross annihilate with the amalgamated positive vorticity from both the free surface and the cylinder. This behaviour is illustrated in figure (5.3), which shows the vorticity field for both Froude numbers at the point of minimum lift.

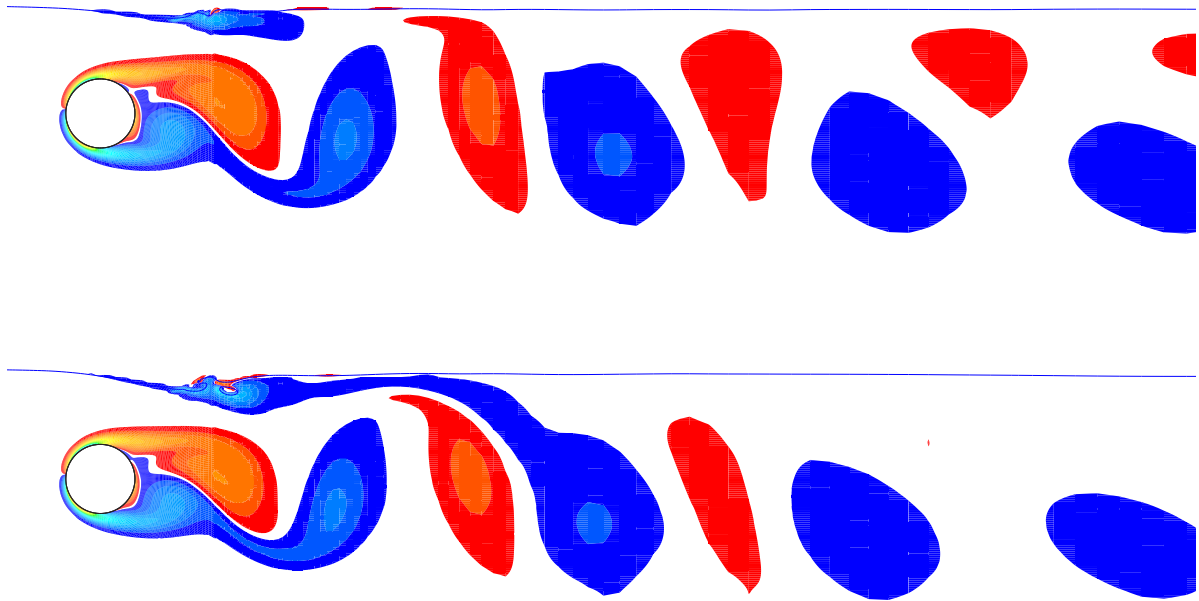


Figure 5.3: Vorticity fields at the point of minimum lift for a gap ratio of 1.00 and for Froude number of 0.50 (top) and 0.60 (bottom). The Reynolds number in each case is 180.

This process is further exacerbated when the gap ratio is reduced to 0.85, with the flow at a Froude number of 0.50 also displaying intermittent wave breaking. The negative vortices now become severely stretched, such that they are observed to have decayed after traveling roughly 10 to 12 diameters downstream. This stretching and decay is shown in figure (5.4), which illustrates the vorticity field at two instants. At a Froude number of 0.60, permanent small scale wave breaking is noted, with the breaking/(separation of the ‘jet’ from the surface) providing a source of positive vorticity which combines with that from beneath the cylinder, to envelop the forming negative vortex. This envelopment process increases the level of cross annihilation, which subsequently leads to the premature decay of the negative vorticity. The entire procedure is best illustrated with reference to the videos, however two frames from both

the particle transport and vorticity videos are shown in figure (5.5).

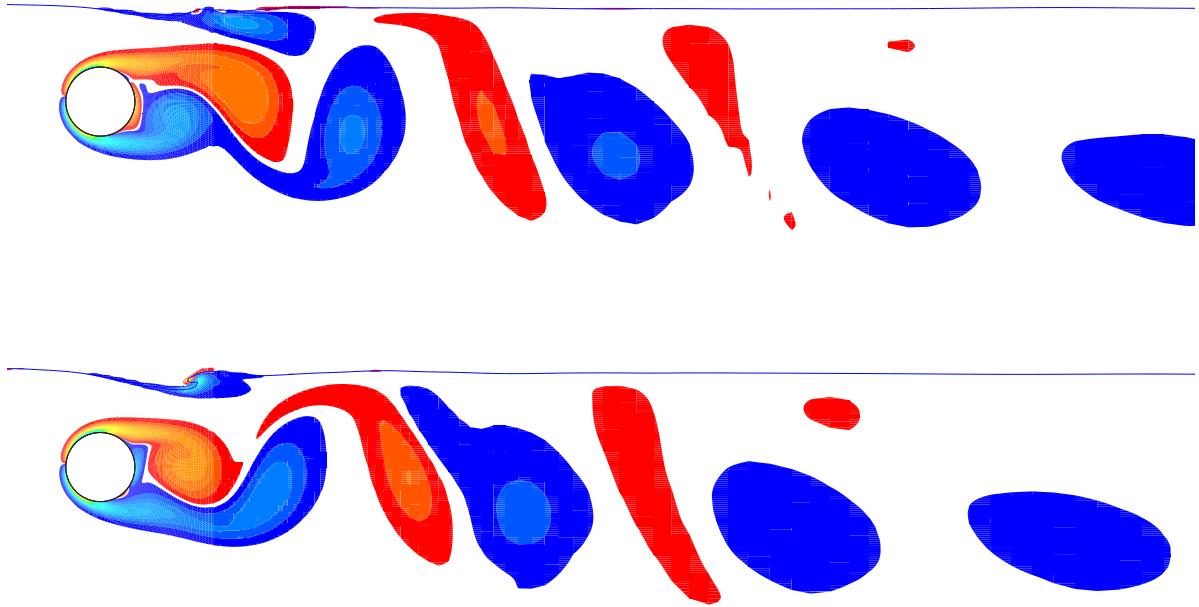


Figure 5.4: Vorticity field at two instants in time for a gap ratio of 0.85 and for a Froude number of 0.50. The Reynolds number in each case is 180.

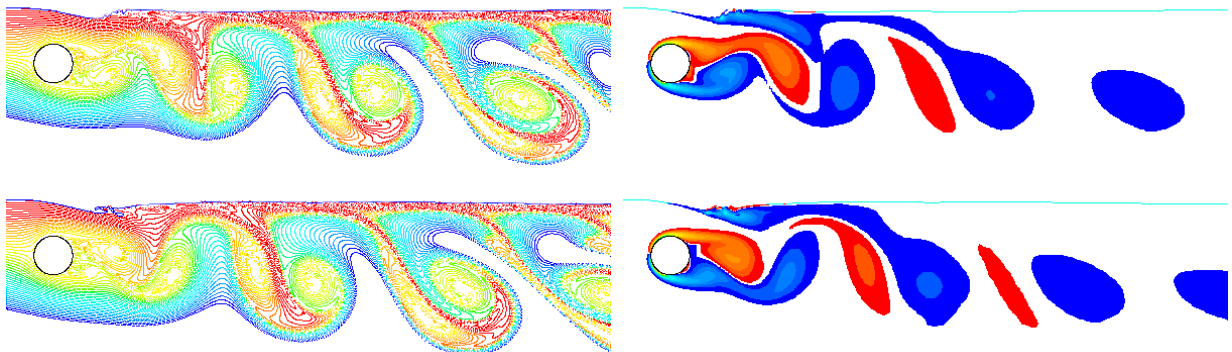


Figure 5.5: Key frames from the video showing the vorticity field and the particle transport plots for a gap ratio of 0.85 and for a Froude number of 0.60. The Reynolds number in each case is 180.

One can clearly see that the free surface becomes more malleable as the Froude number is increased, with the significant time varying curvature facilitating a greater transfer of vorticity into, and out of, the free surface. Rood (1994b) indicates that vorticity can appear spontaneously on free surface boundaries, with its appearance related to both the surface parallel velocity of the surface fluid, and the surface curvature. The time dependent variation of the surface will

thus alter the transport of vorticity through it, with the flux of vorticity through a free surface being dependent upon the viscous acceleration of the free surface fluid in the direction tangential to the free surface. This suggests that as the gap ratio is reduced further, one would expect a more significant transfer of vorticity across the free surface, with the time varying surface curvature acting to further weaken the forming negative vortex, while also introducing more positive vorticity.

5.1.2 Intermediate Gap Ratios 0.70, 0.55, 0.40, 0.25 and Metastable Wake States

This section will now discuss the flow behaviour observed at intermediate gap ratios, namely 0.70, 0.55, 0.40 and 0.25. As much of the work of Sheridan et al. (1995), Sheridan et al. (1997) and Hoyt & Sellin (2000) lies within this range of gap ratios, it should be possible to make a number of predictions with regard to the wake behaviour.

Before entering into a discussion on the metastable wake states which were observed by Sheridan et al. (1995) and Sheridan et al. (1997), it is perhaps profitable to draw attention to what types of flow behaviour have been seen in the intermediate gap ratio range that will be considered here. Sheridan et al. (1997) note that at a Froude number of 0.60 and for gap ratios between 0.75 and 0.24, that the flow passing over the cylinder, which in the foregoing will be referred to as a ‘jet’, tended to progressively move from being attached to the free surface through to being almost attached to the rear of the cylinder. These states were illustrated earlier in the schematic in figure (5.1).

As the particle image velocimetry (PIV) approach adopted by Sheridan et al. (1995) and Sheridan et al. (1997) yields instantaneous flow fields, they were not in a position to give much detail with regard to the transient nature of the flow states. However, it is reasonable to assume that the flow field is time dependent. Hoyt & Sellin (2000) also examine this flow but at a Froude number of 0.53, with their dye tracer technique indicating that the flow field was indeed time dependent, with Kármán vortex shedding clearly noted at a gap ratio of 0.75.

For a couple of key cases, both Sheridan et al. (1995) and Sheridan et al. (1997) found that more than one wake state could be observed at a fixed gap ratio and Froude number. For these cases the wake spontaneously underwent transformations between the two states in a pseudo periodic manner. However, Sheridan et al. (1995) were unable to attribute a dimensionless frequency to this behaviour, only indicating that the frequency was roughly two orders of magnitude lower

than that of Kármán vortex shedding for a fully submerged cylinder. Such behaviour was deemed by Sheridan et al. (1995) to be metastable, as each wake state was only observed to exhibit a slight margin of stability.

The metastable behaviour observed by Sheridan et al. (1995) at a gap ratio of 0.45 and a Froude number of 0.60, involved the ‘jet’ transiently switching between a state of attachment to the free surface, and a state of separation from it such that it occupied a region of space in between the free surface and the cylinder (i.e. the flow switched between the first and second states in figure (5.1)). For this case they note that the transition between the two states could be artificially induced by transiently piercing the free surface at a position downstream (presumably at distances greater than 4 diameters) to a depth of approximately 0.4 of a cylinder diameter. They also mention that it was possible to induce hysteretic effects by altering the flow velocity, with this variation typically resulting in a change of wake state.

Sheridan et al. (1997) also noted that metastable type behaviour occurred at a Froude number of 0.60, and for gap ratios of both 0.31 and 0.59. Their observations at the smaller gap ratio indicated that the ‘jet’ switched between a state of attachment to the rear of the cylinder, and detachment from it such that it occupied a region of space in between the free surface and the cylinder (the second and third states in figure (5.1)). For reasons which shall be given later (in the discussion at the end of this chapter), this behaviour will not be referred to as being metastable, but rather as being a time-dependent flow adjustment. At the larger gap ratio, they note that the ‘jet’ flips between the latter state observed above (i.e. occupying a region in between the free surface and the cylinder) and attachment to the free surface.

Hence one may assume that similar behaviour should be observed here for the numerical predictions. It already has been shown in the previous chapter which dealt with the flow at intermediate Froude numbers, that vortex shedding could be suppressed and in some cases stalled. Such behaviour is not that surprising when one considers that the depth at which shedding ceases tends to grow with increasing Froude number. Hence it is expected that as one approaches the limiting depth at which shedding is suppressed, that the wake will display increasingly altered behaviour.

Lugt & Ohring (1992) have shown for the interaction of a vortex pair with a free surface, that the larger the Froude number the greater the level of surface deformation. This increased curvature combined with the inherently time-dependent shedding of vortices from the cylinder (at least at some gap ratios), is thus likely to establish conditions or more appropriately introduce skew into

the wake, such that the capacity of the flow around the cylinder to shed, or rather the nature of the absolute instability, will be altered in a time dependent manner.

Of relevance are the findings of Koch (1985) and the speculation by Huerre & Monkewitz (1990), that only a limited degree of asymmetry is required before no time harmonic resonance (or absolute instability) is possible. Thus suggesting that the changes in the wakes behaviour may be linked to a change in the nature of the instability associated with the cylinder wake. However a further discussion with regard to this suggestion is deferred to later in this chapter.

The momentary stalling of vortex shedding, which was observed for a gap ratio of 0.25 at a Froude number of 0.40 in the previous chapter, highlights one possible path via which shedding may cease. For that case the flux of vorticity through the free surface severely weakened the negative shear layer. This weakening then resulted in the wake being dominated by positive vortical structures, which by nature are recirculatory (i.e. they have a counter clockwise rotation which results in the flow of fluid upstream at positions closer to the free surface). This recirculatory flow then hinders the downstream movement of the fluid passing over the cylinder and in doing so, it introduces an asymmetry (or skew) into the time-mean velocity profile. It is believed that if this asymmetry is sufficient, then the absolute instability associated with the wake will be significantly weakened to the point at which shedding is observed to stall. This stall was only momentary as it was dependent upon the proximity of the positive vortical structures that form at positions downstream of the cylinder. By removing or delaying the driving mechanism responsible for the generation of these structures (i.e. the formation and shedding of discrete vortices), it was thus possible to alter the wake such that the structures that stalled the shedding in the first place, were no longer being formed.

For the cases in which the free surface is more malleable, which is generally true at larger Froude numbers, the reverse (or slowing) of the fluid near to the surface at positions downstream of the cylinder (just above the positive vortices), and its subsequent interaction with the flow from above the cylinder, will generally, depending upon the gap ratio, result in the fluid from above the cylinder being deflected downwards. This deflection results in a significant curving of the free surface and in some cases small scale wave breaking, with the Froude number largely determining what happens.

As the fluid from above the cylinder (i.e. the 'jet') is deflected downwards, satisfaction of continuity (conservation of mass) will then require that fluid from further downstream must now move upstream (diagonally upwards). For a gap ratio of 0.25 and a Froude number of 0.40,

this resulted in the last shed positive vortex moving closer to the free surface, with its presence further restricting the downstream movement of fluid in the region close to the surface. This effectively alters the path via which fluid from above the cylinder may exit from the wake cavity, and it is believed that it is the increasing asymmetry in the wake which causes shedding to stall. It should be noted that the form of the asymmetry is different to that observed at small Froude numbers, where the asymmetry was introduced by a reduction in the flow velocity in the region above the cylinder. At these larger Froude numbers the asymmetry arises as a result of the 'jet' being deflected away from the horizontal. The observed stalling of the vortex shedding then delays the formation of new vortices and it persists until the offending positive vortical structure which is near to the surface, moves downstream, at which point shedding begins anew.

At the larger Froude numbers considered here, the increased surface curvature will naturally deflect more of the fluid from above the cylinder downwards. This will in turn require more of the fluid from further downstream to move upstream in order to satisfy continuity. The removal of increasing amounts of negative vorticity through the free surface (with the rate of removal (flux) being dependent upon the viscous acceleration), will tend to result in the fluid at locations downstream possessing a stronger positive sense of vorticity, and hence being more recirculatory. Thus the subsequent entrainment or intromission upstream of this fluid, will then slow or even reverse the convective velocity of the fluid near to the interface, with such behaviour then resulting in wave breaking. Hence one should entertain the possibility that similar stalling, or even a complete cessation of vortex shedding will coincide with wave breaking at the free surface.

The flow behaviour at each of the gap ratios within the intermediate range is now considered.

At a gap ratio of 0.70, the wave breaking is clearly synchronized with the shedding of vortices from the cylinder, and the envelopment of the forming negative vortex is noted for both a Froude number of 0.50 and 0.60. The negative vortices experience considerable stretching, and are observed to persist for only a short distance downstream for both Froude numbers, with this behaviour best illustrated via consideration of the vorticity videos. The particle transport movies indicate that some of the fluid that passes over the cylinder is transported downstream at locations near to the free surface; for all the investigations conducted here, this phenomenon appears to be strongly related to the formation and shedding of discrete vortices. However, for both Froude numbers most of the downstream transport of the fluid from above the cylinder occurs via its pairing with the stronger positive vortex from beneath the cylinder. This pairing then results in the formation of structures that resembles a skewed form of the mushroom-shaped

pattern, that is observed for flow past a fully submerged cylinder.

One interesting point to note for this case is that the particle transport videos at the lower Froude number (i.e. 0.50) reveal that cylinder-sized structures are noted near the surface, which are linked via tendrils of ‘jet’ fluid to the fluid making up a pair of previously shed negative vortices. These structures are shown in figure (5.6) and in the particle transport videos. At the larger Froude number (i.e. 0.60), these structures appear to link the fluid from many previously shed vortices (as opposed to two at a Froude number of 0.50), with this linking behaviour shown in figure (5.7) and in the video. The difference between the results at the two Froude numbers appears to be related to what is happening near the free surface, with more significant wave breaking and flow reversal noted at the larger Froude number.

The flow at a gap ratio of 0.75 and a Froude number of 0.53 is considered by Hoyt & Sellin (2000), with Sheridan et al. (1997) considering the same case but at a Froude number of 0.60. Figures (5.8) and (5.9) show the favorable comparison between the results, with the numerical prediction at a gap ratio of 0.70 and a Froude number of 0.50 showing the best match with the results of Sheridan et al. (1997).

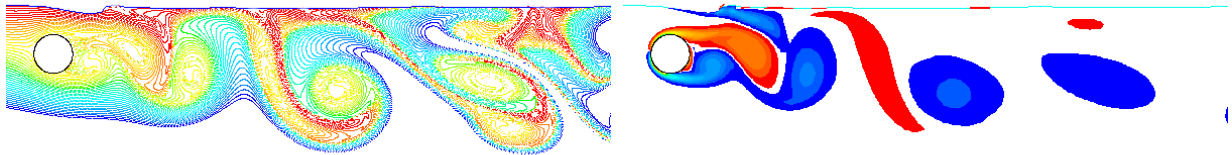


Figure 5.6: Key frames from the video showing the vorticity field and the particle transport plots for a gap of 0.70 and for a Froude number of 0.50. In particular, the structure in the particle transport plot which has tendrils connecting the fluid previously shed from above the cylinder should be noted. The Reynolds number in each case is 180.

The time-dependent response of the free surface to the shedding of vortices from the cylinder, results in a continuous alteration of the surface curvature. Hence as the gap ratio is reduced, the increased time dependent surface curvature will result in more negative vorticity fluxing through the interface and in a progressively weaker negative shear layer. Thus as the gap ratio is further reduced, one would expect that the wake will become increasingly dominated by positive vortical structures, which are largely recirculatory.

Hence, it is expected that the level of slowing/reverse flow will increase as the gap ratio is reduced further, with such behaviour likely to result in more significant wave breaking, and in the deflection of the ‘jet’ away from the free surface. The angle of the deflection will then be

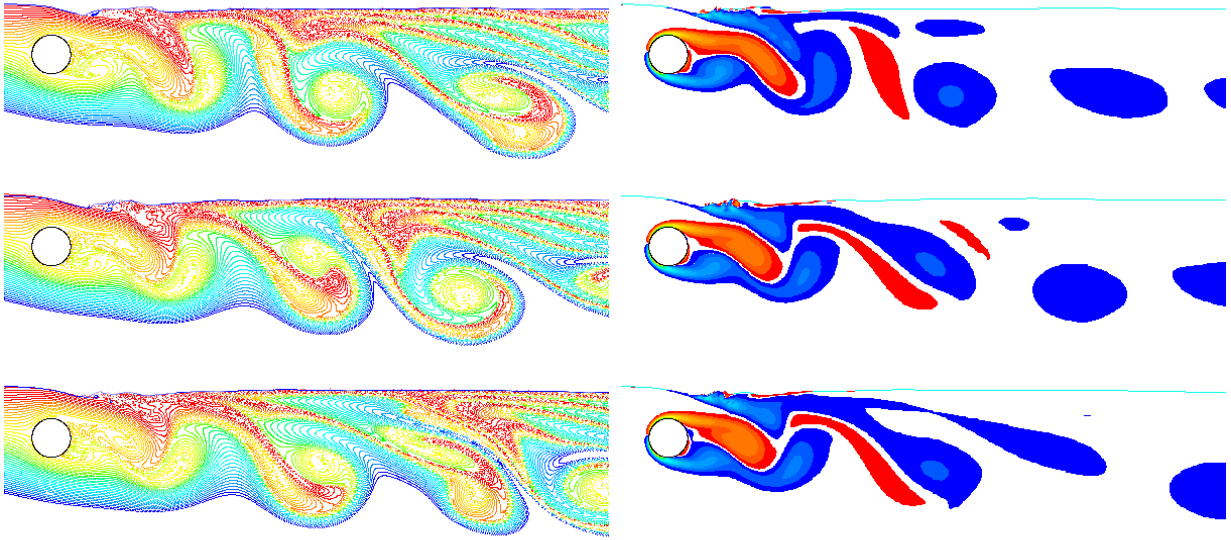


Figure 5.7: Three key frames from the video showing the vorticity field and the particle transport plots for a gap ratio of 0.70 and for a Froude number of 0.60. The Reynolds number in each case is 180.

determined by the relative difference in the strength of the vortices from both the top and the bottom of the cylinder.

Thus for a gap ratio of 0.55, it is anticipated that a more significant level of slowing/ reversal of the flow will be observed close to the surface, with the ‘jet’ deflecting through a slightly larger angle when it separates. It should be stressed that the change in the flow behaviour for a given gap ratio with Froude number, is due almost entirely to the more malleable free surface; with the time-dependent curvature altering both the path taken by the fluid as it passes over the cylinder, and the asymmetry in the wake flow.

A significant change in the wake behaviour is observed at a gap ratio of 0.55, when the Froude number is increased from 0.50 to 0.60. At the lower Froude number, the wake largely resembles that at a gap ratio of 0.70, with small-scale wave breaking synchronized to the shedding of vortices (with this behaviour clearly visible in the video). At the larger Froude number, metastable type behaviour is noted, with the ‘jet’ spending the majority of its time separated from the free surface, with only very short periods of attachment observed. For the period in which the ‘jet’ is attached, significant surface curvature is witnessed and is observed to grow until it is sufficient to cause wave breaking, and with this, the ‘jet’ detaches from the free surface. A form of weakened shedding is still noted throughout this process, however, the negative vorticity from the top of the cylinder is almost always enveloped by the vorticity emanating from the breaking

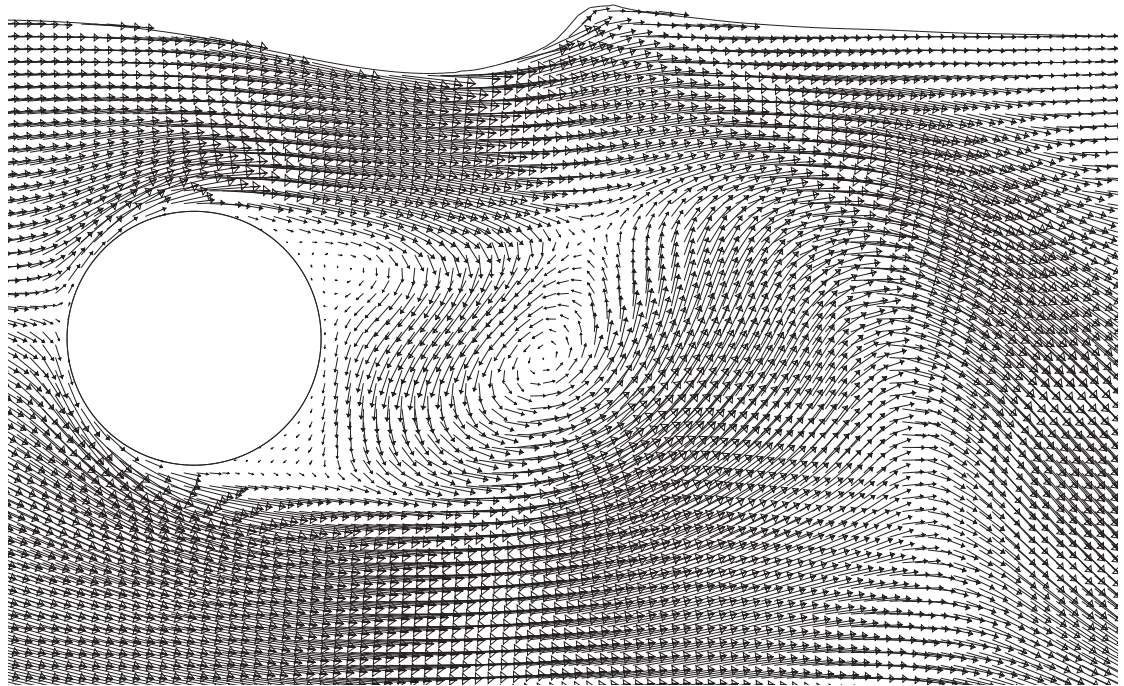
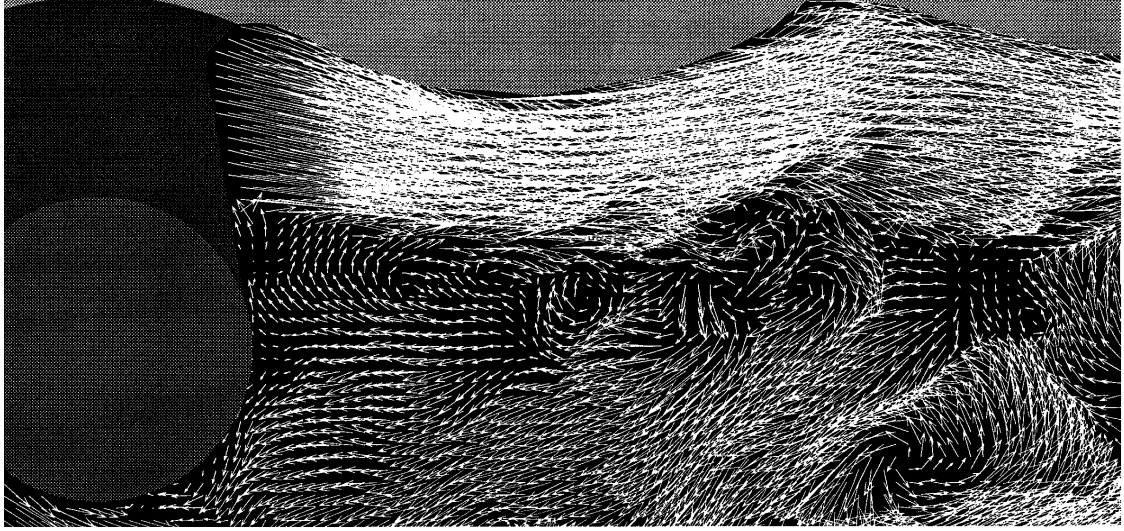


Figure 5.8: Pictorial comparison of the velocity fields. The result of Sheridan *et al.* (1997) (top) is at a gap ratio of 0.75, a Froude number of 0.60 and for a Reynolds number inbetween 5990 and 9120, while the result from the current investigation (bottom) is at a gap ratio of 0.70, a Froude number of 0.50 and a Reynolds number of 180.

wave and from beneath the cylinder. This transport of vorticity from the breaking wave largely matches that observed by Lin & Rockwell (1995), who indicate that the level of vorticity transport varies with Froude number. It is noted that the only time that wave breaking does not

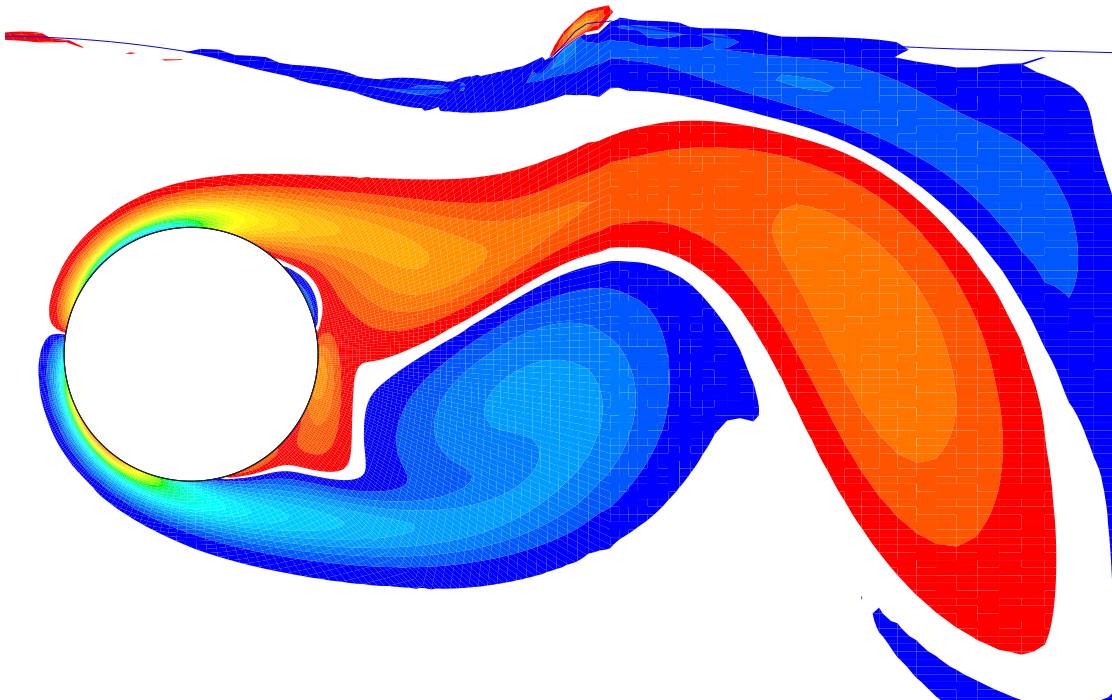


Figure 5.9: Pictorial comparison of the vorticity fields. The result of Sheridan *et al.* (1997) (top) is for a gap ratio of 0.75, a Froude number of 0.60 and for a Reynolds number inbetween 5990 and 9120, while the result for the current investigation (bottom) is for a gap ratio of 0.70, a Froude number of 0.50 and a Reynolds number of 180.

occur, is when the ‘jet’ is attached to the free surface. This time-dependent behaviour is best illustrated via consideration of the videos, with the particle transport movie indicating that the flow just downstream of the cylinder is largely recirculatory (i.e. the flow close to the surface

has a low or negative convective velocity, while the flow further from the free surface possesses a higher positive velocity). A few key frames from the video are shown in figure (5.10), which highlights the metastable behaviour. This result agrees very favourably with those of Sheridan et al. (1997), who also observe the ‘jet’ separating and then re-attaching to the free surface in a metastable fashion at a gap ratio of 0.59 and a Froude number of 0.60. Figures (5.11) to (5.14) show the pictorial comparison, which is remarkable when one considers the nearly 40 fold difference in the Reynolds number between the two cases. This result strongly supports the assertion by Sheridan et al. (1997) that the predominant features are quasi-two-dimensional.

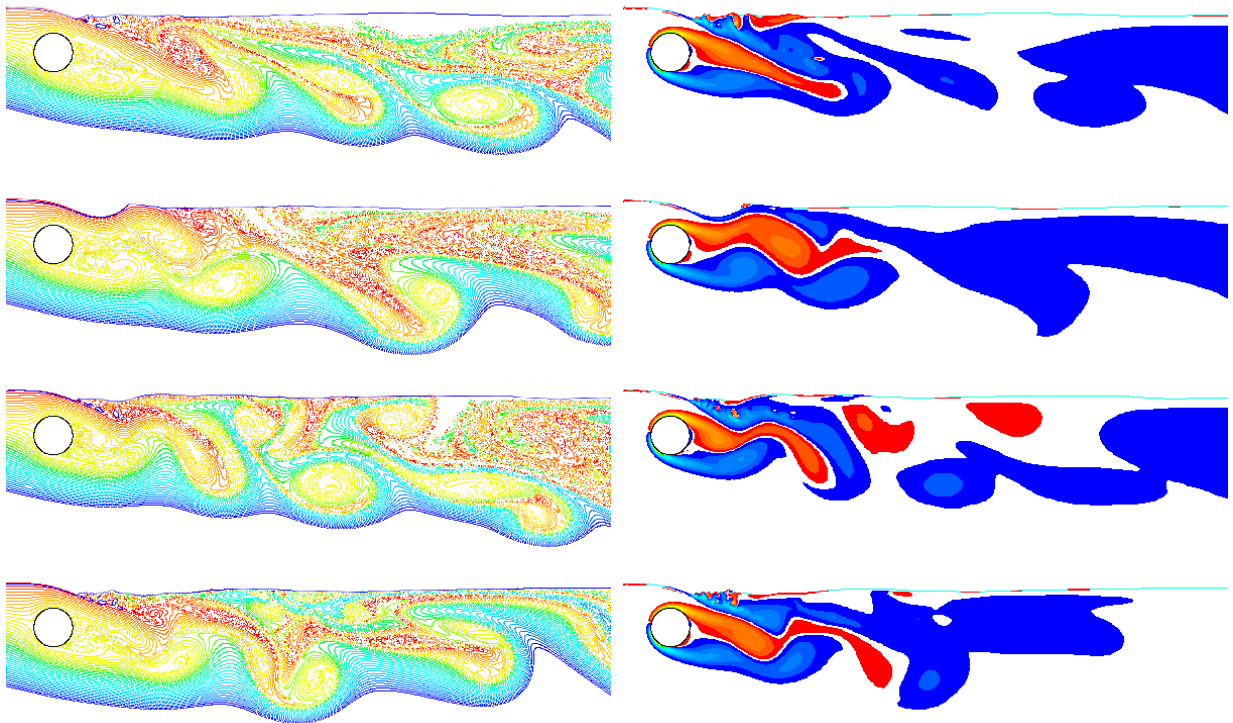


Figure 5.10: Key frames from the particle transport and the vorticity videos for a gap ratio of 0.55 and for a Froude number of 0.60. The Reynolds number in each case is 180.

It should be noted at this point that the separation of the ‘jet’ from the free surface highlights one of the potential limitations of the numerical model, with small amounts of the upper fluid (i.e. the less dense fluid which is akin to air) being entrained with the ‘jet’ as it separates and moves away from the free surface. In general, the amount of the lighter fluid entrained is small, with the slight quantities which are entrained tending to form small bubble-like structures which rise towards the surface. These bubbles have only relatively small amounts of momentum associated with them and hence are unlikely to influence the general flow dynamics. However they can, and do, generate small scale vortical structures which stand out in the vorticity field plots. While

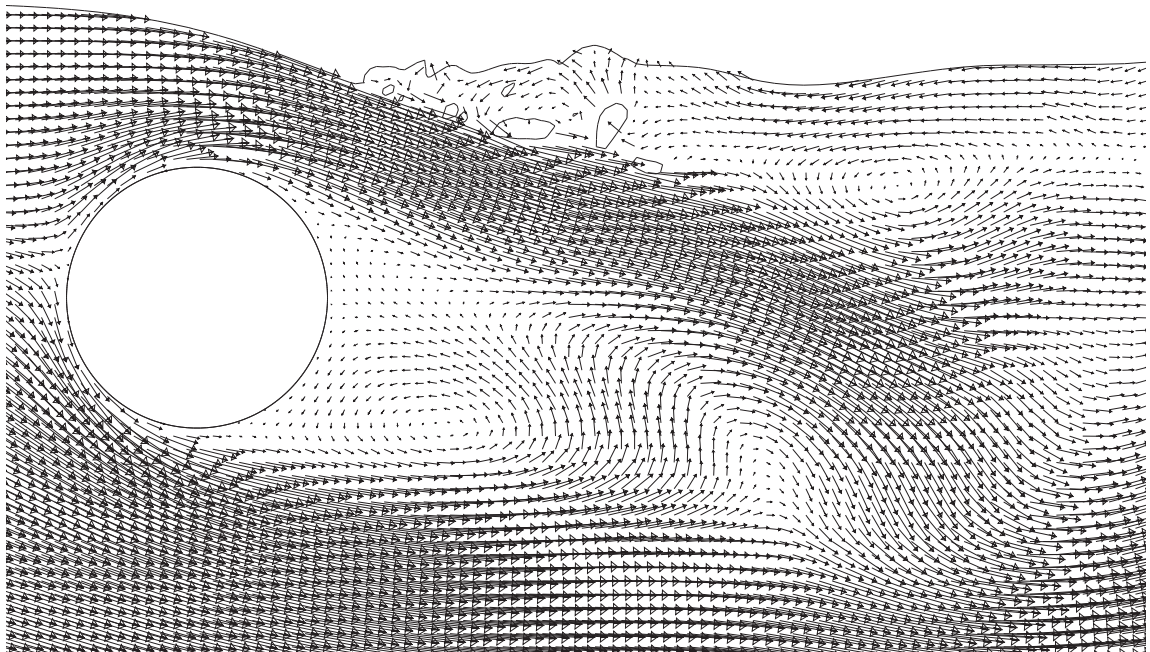
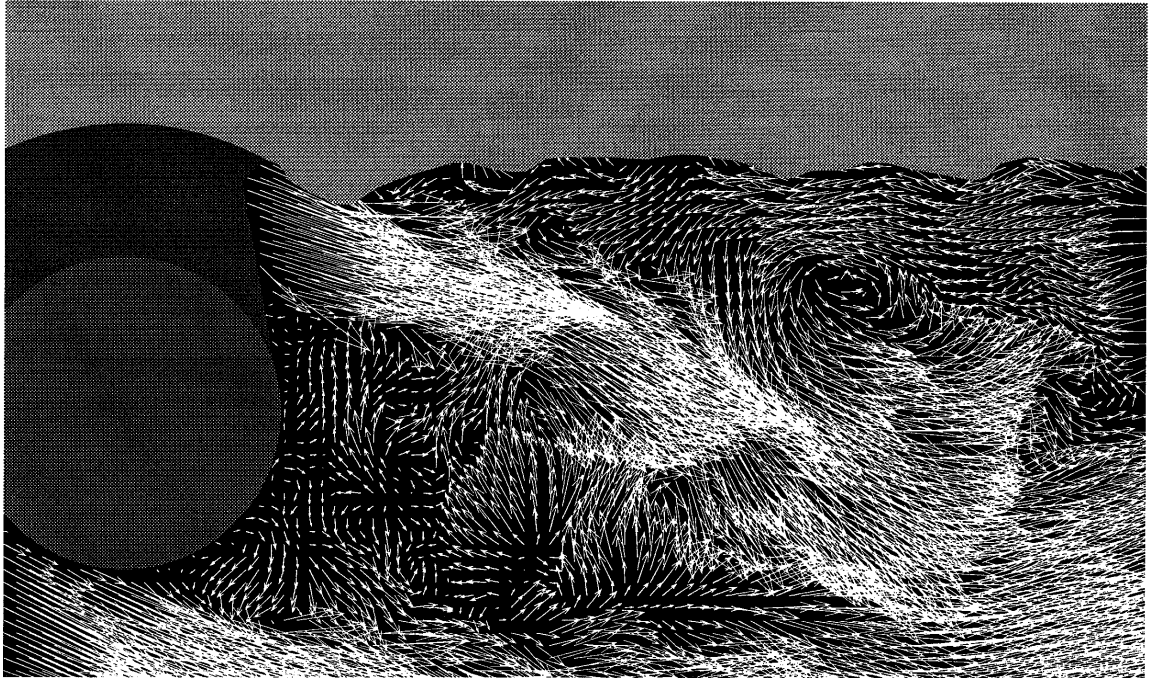


Figure 5.11: Comparison of the velocity fields between the experimental results of Sheridan *et al.* (1997) (top) for a gap ratio of 0.59, a Froude number of 0.60 and for a Reynolds number inbetween 5990 and 9120 at time t_1 , and the numerically predicted results (bottom) at a gap ratio of 0.55, a Froude number of 0.60 and for a Reynolds number of 180.

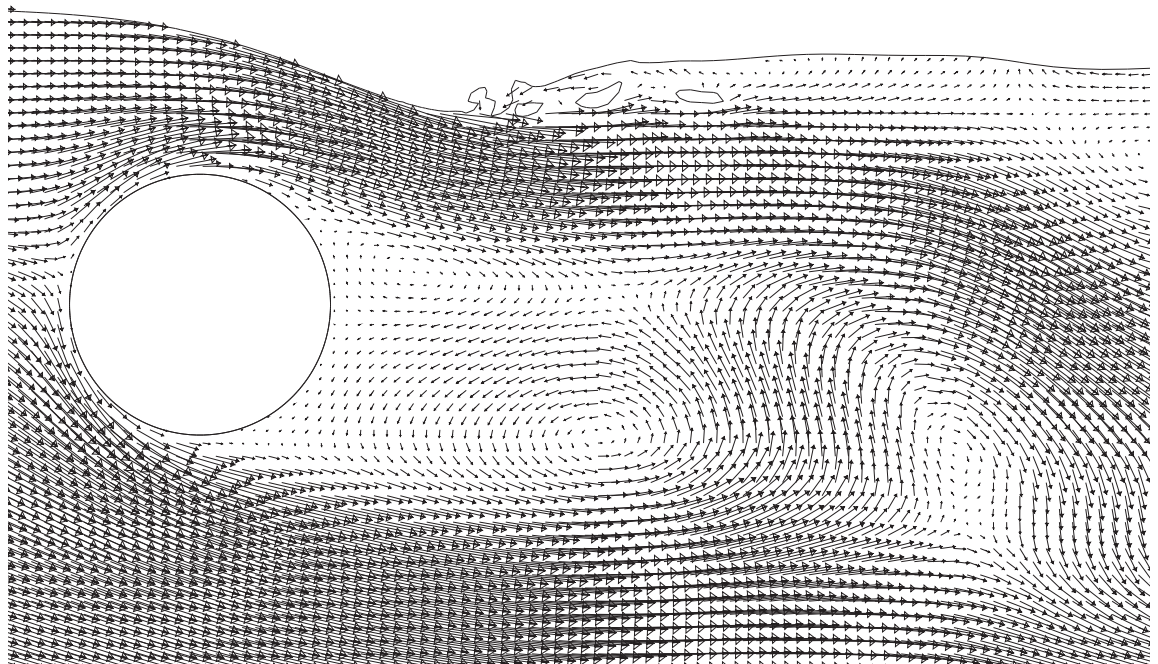
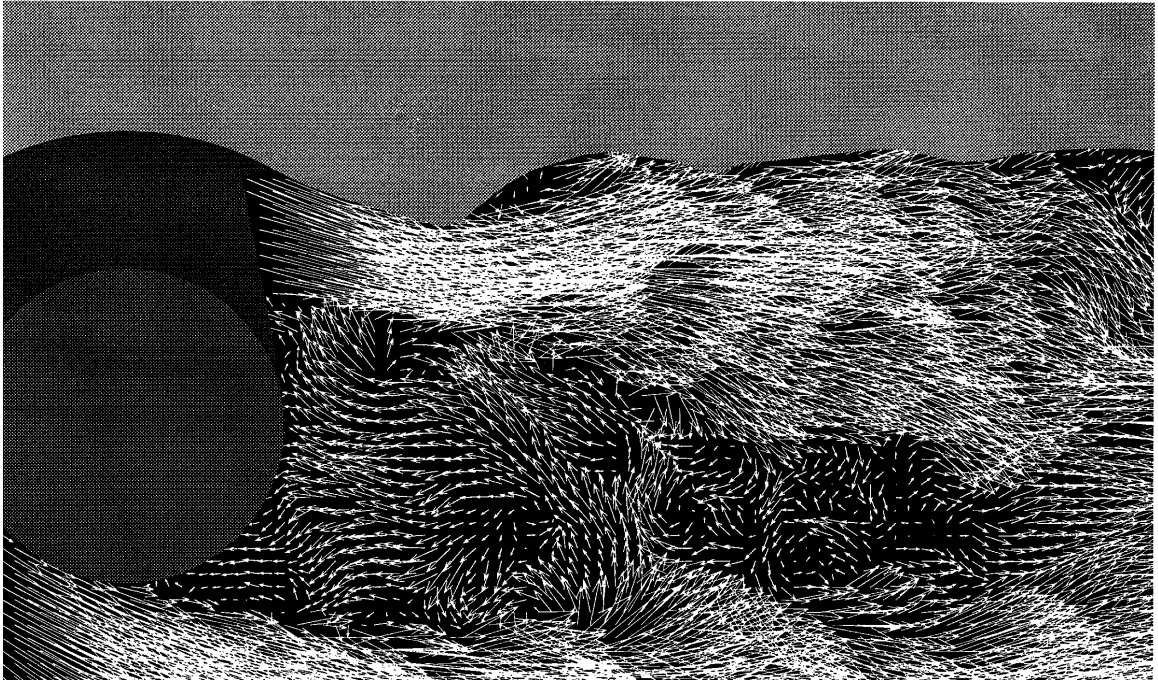


Figure 5.12: Comparison of the velocity fields between the experimental results of Sheridan *et al.* (1997) (top) for a gap ratio of 0.59, a Froude number of 0.60 and for a Reynolds number inbetween 5990 and 9120 at time t_2 , and the numerically predicted results (bottom) at a gap ratio of 0.55, a Froude number of 0.60 and for a Reynolds number of 180.

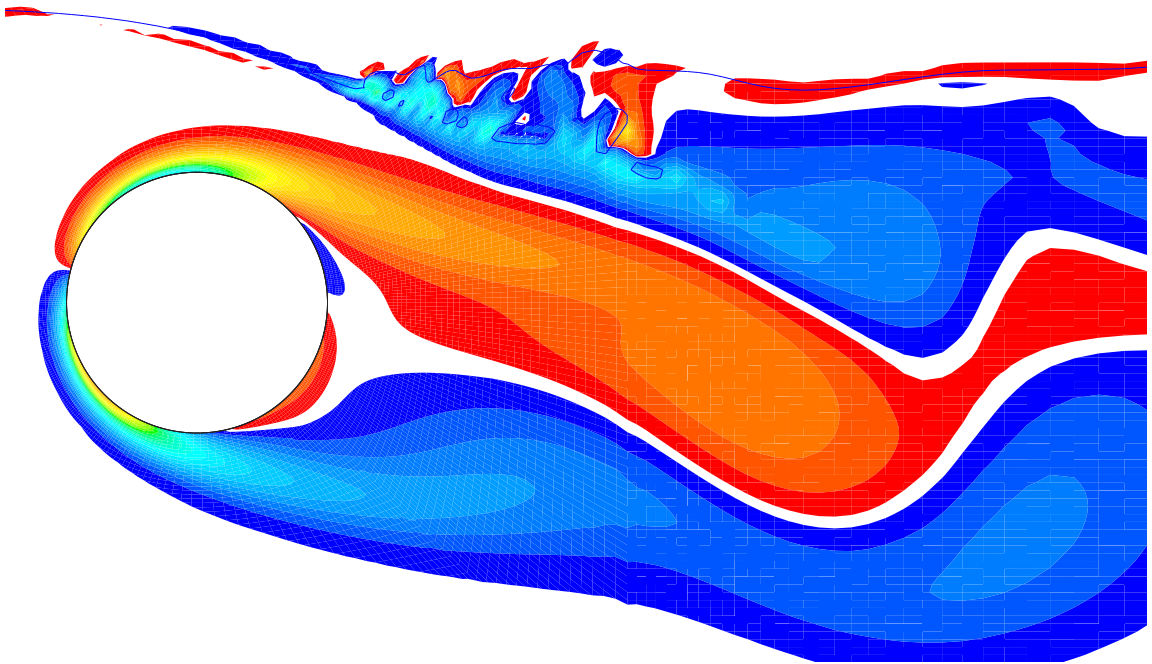


Figure 5.13: Comparison of the vorticity fields between the experimental results of Sheridan *et al.* (1997) (top) for a gap ratio of 0.59, a Froude number of 0.60 and for a Reynolds number inbetween 5990 and 9120 at time t_1 , and the numerically predicted results (bottom) at a gap ratio of 0.55, a Froude number of 0.60 and for a Reynolds number of 180.

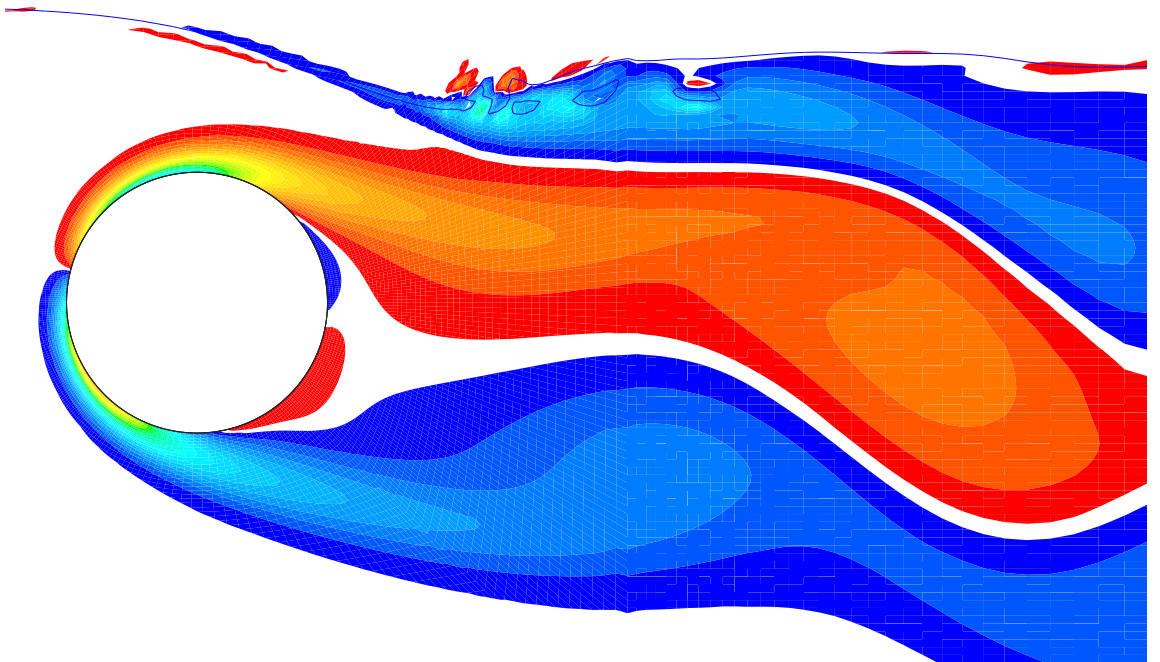
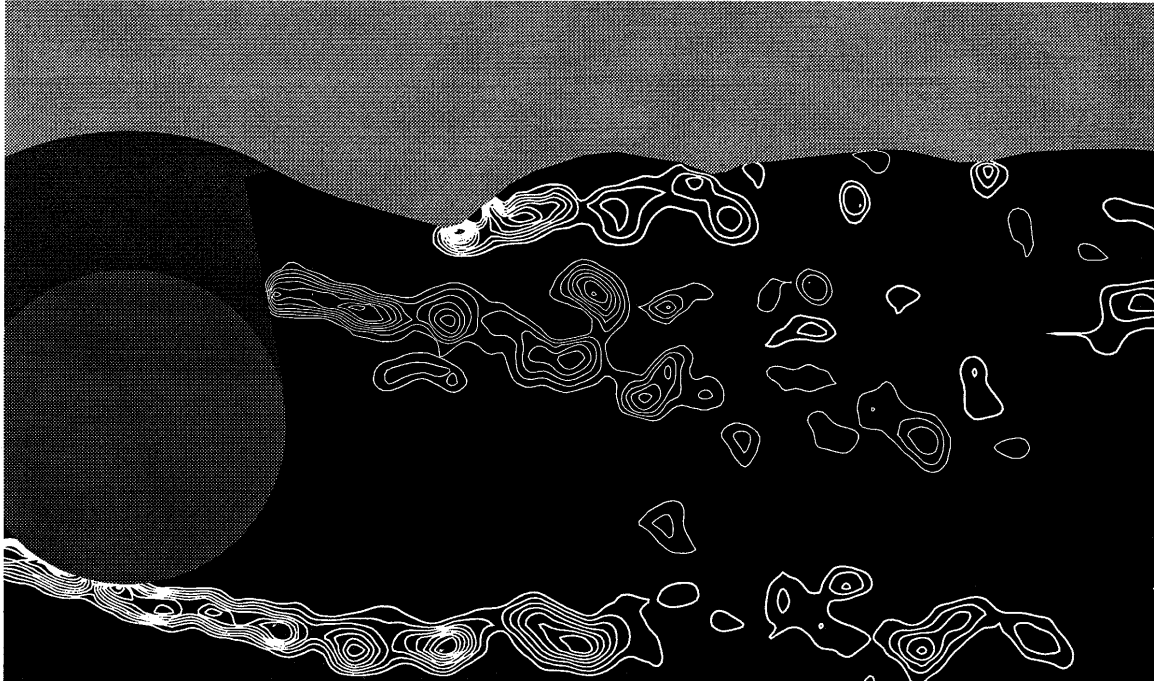


Figure 5.14: Comparison of the vorticity fields between the experimental results of Sheridan *et al.* (1997) (top) for a gap ratio of 0.59, a Froude number of 0.60 and for a Reynolds number inbetween 5990 and 9120 at time t_2 , and the numerically predicted results (bottom) at a gap ratio of 0.55, a Froude number of 0.60 and for a Reynolds number of 180.

this behaviour could be physically realistic, no mention of air entrainment is noted by Sheridan et al. (1997), although it is noted by Valluri (1996) when experimentally investigating flow past a flat circular disk near a free surface. Irrespective of whether this is a physical phenomenon, the breaking wave and the entrainment of the lighter fluid make the prediction of the surface location somewhat more uncertain, with the numerical model producing less accurate results in regions where only one or two of the neighboring cells contain the denser fluid.

As the gap ratio is reduced further, the associated increase in the surface curvature is likely to cause the ‘jet’ to separate at smaller Froude numbers. Hence it is expected that metastable type behaviour may be seen at a gap ratio of 0.40 over at least part of the Froude number range considered within this chapter (i.e. 0.50 to 0.60), with Sheridan et al. (1995) observing metastable behaviour at a gap ratio of 0.45 and a Froude number of 0.60. To examine this in greater detail an additional Froude number, namely 0.55, was also considered for the gap ratio 0.40 case.

The modulated lift trace observed at a Froude number of 0.50 indicates that some significant changes are occurring in the wake, with the video for this case showing the ‘jet’ switching between a state of attachment to, and later separation from, the free surface. The movies indicate that the ‘jet’ spends most of its time separated from the free surface, with only a short period of attachment noted. They also indicate that a form of shedding still persists, although the discrete negative vortices decay very rapidly with distance, such that they are no longer observed after a mere 5 diameters. Figure (5.15) shows both the particle transport plots and the vorticity fields at a few key instants.

Sheridan et al. (1997) give an instantaneous snap shot of the both the velocity and vorticity fields at a gap ratio of 0.40 and at a Froude number of 0.47; however they give no information with regard to the evolutionary characteristics of the wake with time (although the presence of the smaller-scale Kelvin-Helmholtz vortices which appear to dominate their vorticity plots obviously indicate some time-dependent behaviour). Figure (5.16) and (5.17) show the favorable comparison between the results of Sheridan et al. (1997) and those of the current investigation at one particular instant in time. Both results indicate the presence of a significant crest at a position just downstream of the cylinder, with positive vorticity noted at locations just upstream and downstream of this crest in both investigations.

The particle transport videos highlight the recirculatory behaviour of the wake at positions downstream of the cylinder, with an increasing proportion of the fluid passing over the cylinder

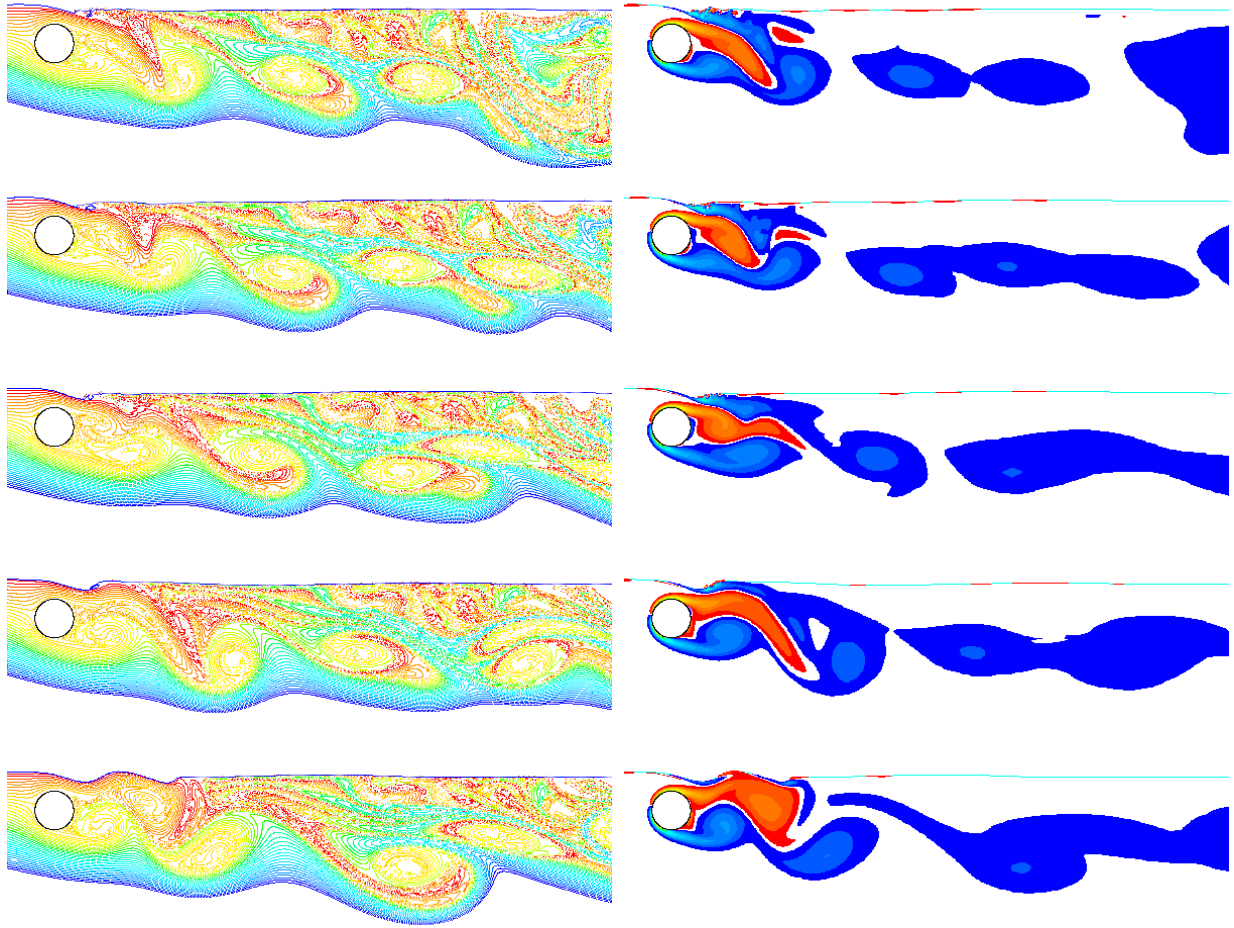


Figure 5.15: Key frames from the particle transport and vorticity videos for a gap ratio of 0.40 and for a Froude number of 0.50. The Reynolds number in each case is 180.

now being transported downstream via entrainment into the positive vortices. Indeed, the only significant transport of ‘jet’ fluid close to the surface occurs when the ‘jet’ is attached to the free surface. This recirculatory behaviour results in a significant slowing and at some points a reversal of the flow close to the free surface at positions downstream of the cylinder. The fluid within this zone has a particularly long residence time, with its dominant mode of removal being via entrainment into the larger scale vortical structures, which tend to form at locations further downstream.

Increasing the Froude number to 0.55 has little effect on the flow, with the video indicating that metastable behaviour is again observed, although it should be noted that the lift trace is more strongly modulated for this case (see figure (5.46) which is shown later in the section dealing with Strouhal number and Lift). The Fourier transform that is also shown later in figure (5.46) indicates that the modulation frequency is approximately 0.0163.

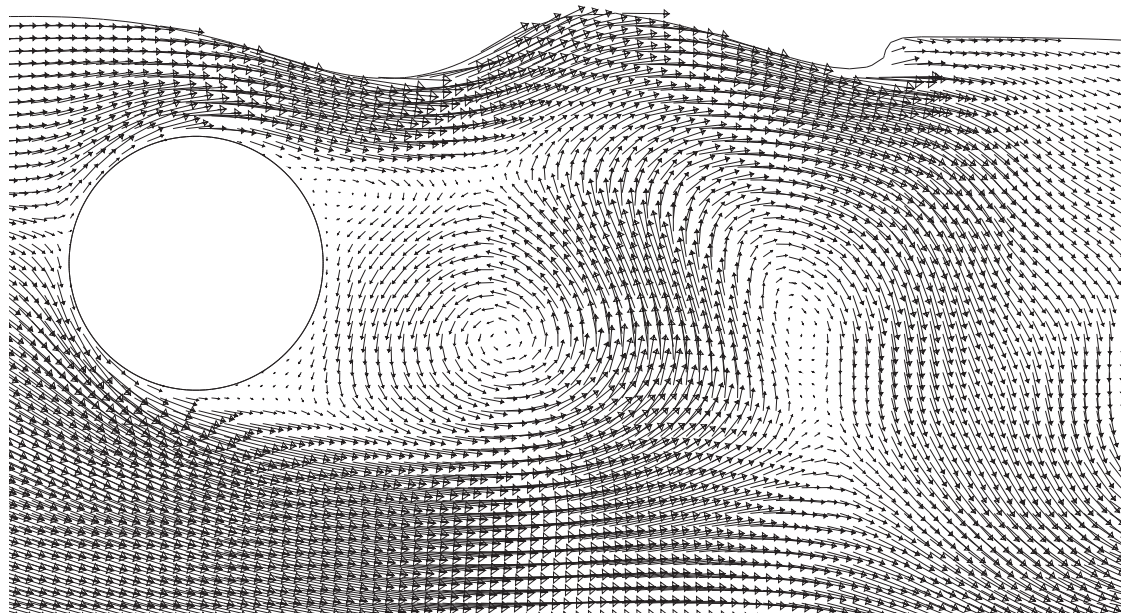
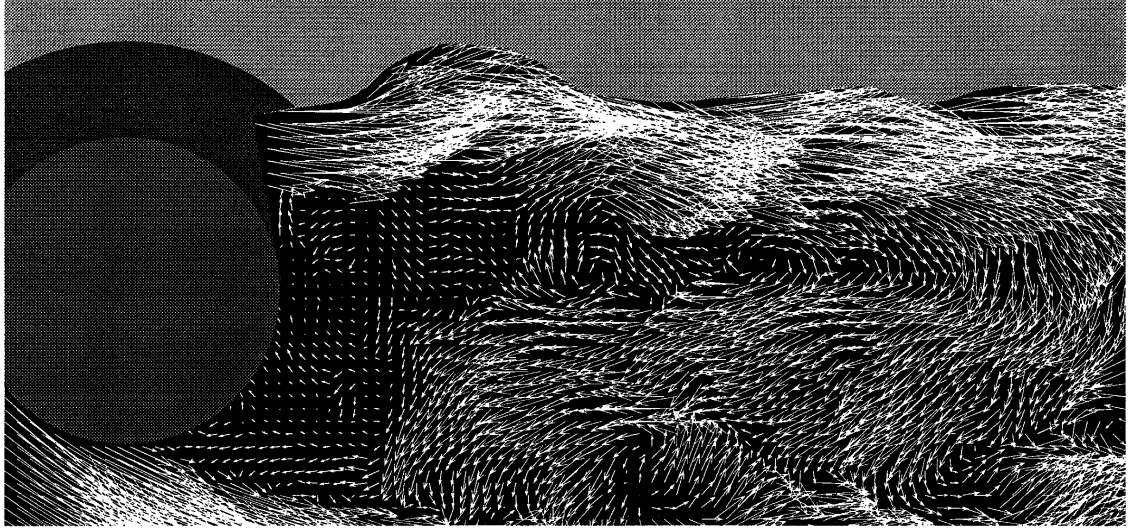


Figure 5.16: Comparison of the velocity fields between the experimental results of Sheridan *et al.* (1997) (top) for a gap ratio of 0.40, a Froude number of 0.47 and for a Reynolds number inbetween 5990 and 9120, and the numerically predicted results (bottom) at a gap ratio of 0.40, a Froude number of 0.50 and for a Reynolds number of 180.

An additional increase in the Froude number to 0.60 again yields metastable behaviour, although the oscillatory nature of the wake is reduced up until the point at which it is observed to stop momentarily. This behaviour suggests that the asymmetry introduced by the separated ‘jet’ is

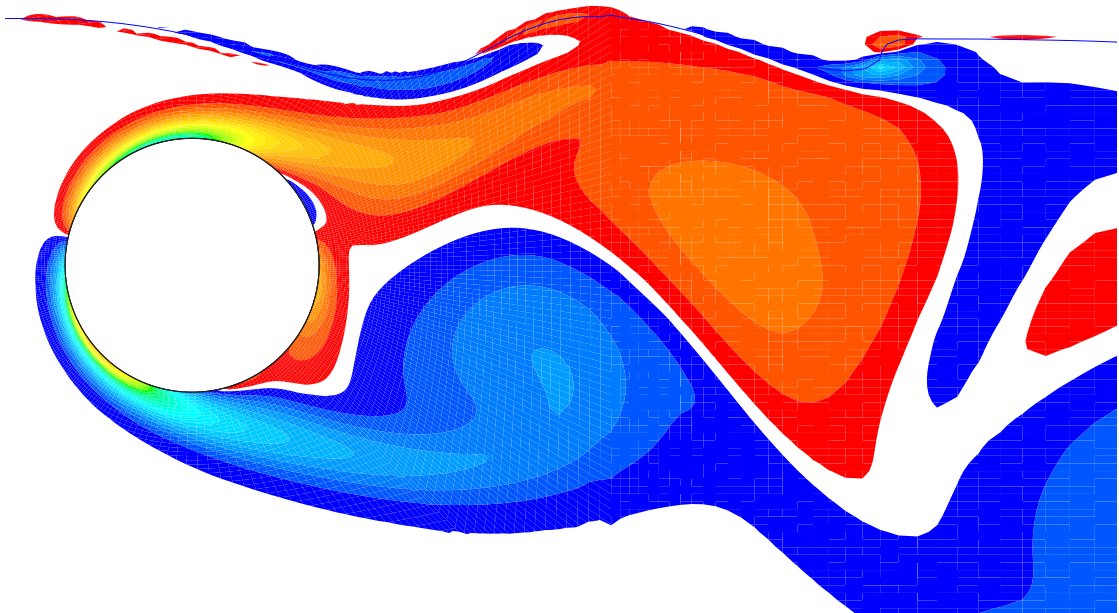


Figure 5.17: Comparison of the vorticity fields between the experimental results of Sheridan *et al.* (1997) (top) for a gap ratio of 0.40, a Froude number of 0.47 and for a Reynolds number inbetween 5990 and 9120, and the numerically predicted results (bottom) at a gap ratio of 0.40, a Froude number of 0.50 and for a Reynolds number of 180.

sufficient to suppress the absolute instability associated with the cylinder wake. The cessation of shedding appears to be in response to the flow structures generated just downstream of the cylinder, with such structures producing the sufficient skew required to cease shedding. However,

these structures are a by product of the mutated vortex shedding, and as such their influence is only temporary. The downstream convection of the larger positive vortical structures then removes the recirculatory flow conditions that lead to the cessation of vortex shedding in the first place.

Hence it would appear that the metastable wake states represent a form of feedback loop, in which the shedding of discrete vortices and their interaction with the free surface induce significant surface curvature, which in turn skews the wake. Such changes then alter the conditions which give rise to shedding in the first place, and the absolute instability is weakened or in some cases extinguished. With no discrete vortices the surface curvature diminishes, which in turn reduces the degree of asymmetry, and the absolute instability is again able to assert itself.

This appears to be what is happening at a gap ratio of 0.40 and a Froude number of 0.60, with the momentary cessation of vortex shedding, or more appropriately the weakening of the absolute instability, removing the driving oscillatory behaviour from the wake. Under such conditions, the 'jet' is able to re-attach to the free surface and long drawn-out shear layers that extend over a significant distance (roughly 8 diameters) are observed. Such behaviour heralds the re-establishment of conditions conducive to vortex shedding (reappearance of the absolute instability), as the wake under these conditions is largely parallel. However, for this case the formation of a staggered array of vortices quickly leads to significant surface deformation and eventual wave breaking which dramatically weakens of the shear layer above the cylinder. This in turn skews the wake and thus weakens the absolute instability, and hence completes the loop. Thus it is the structures that form as a result of vortex shedding that lead to its demise, and it is this demise that eventually leads to its re-establishment. Again, this process is best illustrated via consideration of the videos (see attached compact disk), however a number of key frames are shown here in figure (5.18). It should be noted that the 'jet' again spends most of its time separated from the free surface, with only a short period of attachment witnessed. When separated, it occupies a state similar to that observed by Sheridan et al. (1997) for a gap ratio of 0.43 and a Froude number of 0.60, with the favorable agreement between both the numerical prediction and the experimental findings shown in figures (5.19) and (5.20).

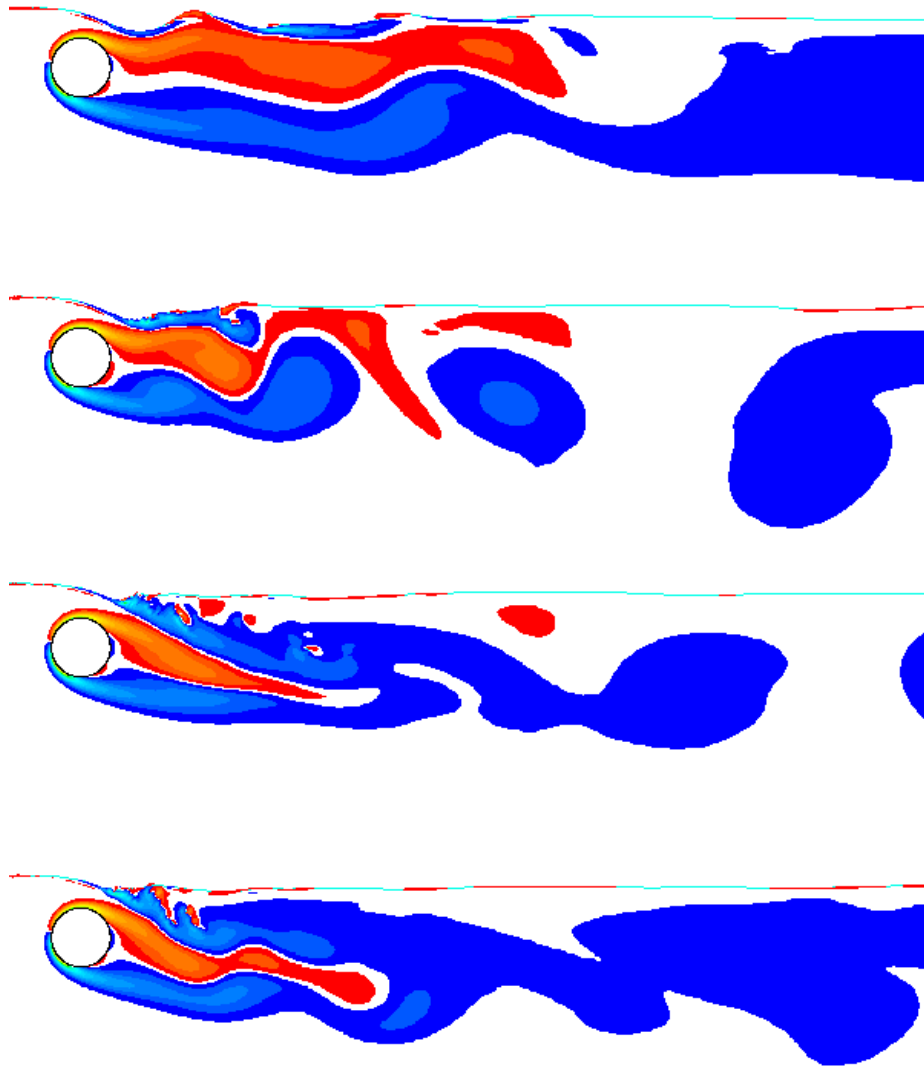


Figure 5.18: Key frames from the vorticity video for a gap ratio of 0.40 and a Froude number of 0.60. The Reynolds number in each case is 180.

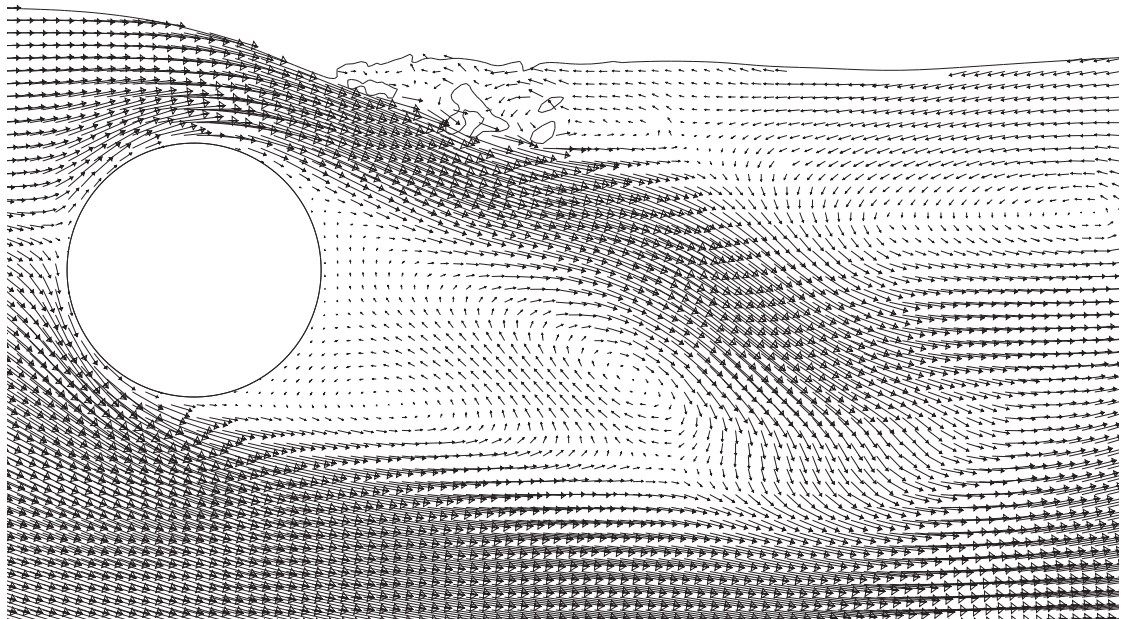
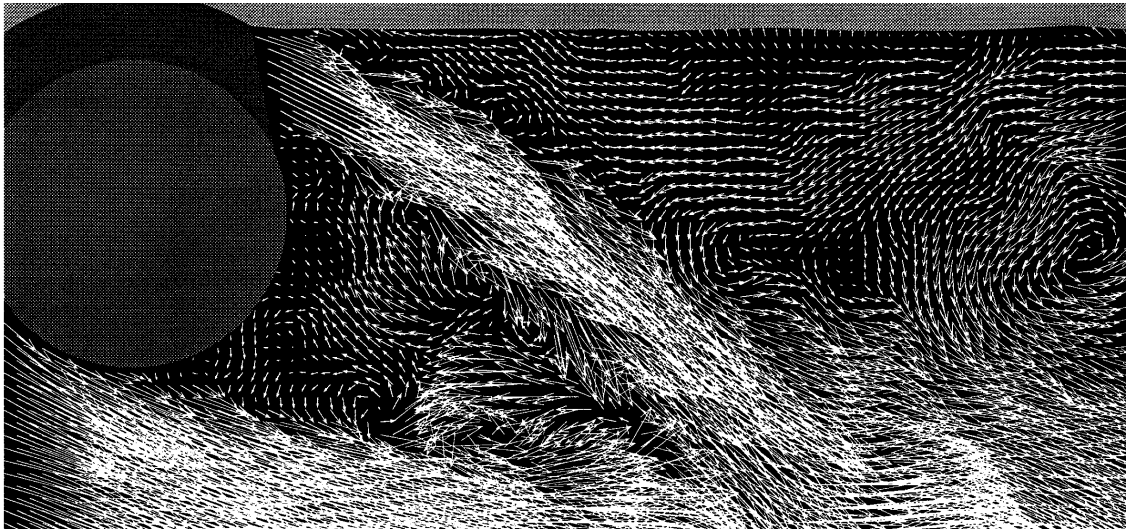


Figure 5.19: Comparison of the velocity fields between the experimental results of Sheridan *et al.* (1997) (top) for a gap ratio of 0.43, a Froude number 0.60 and for a Reynolds number inbetween 5990 and 9120, and the numerically predicted results (bottom) at a gap ratio of 0.40 (gap 5.9 diameters upstream is 0.45), a Froude number of 0.60 and for a Reynolds number of 180.

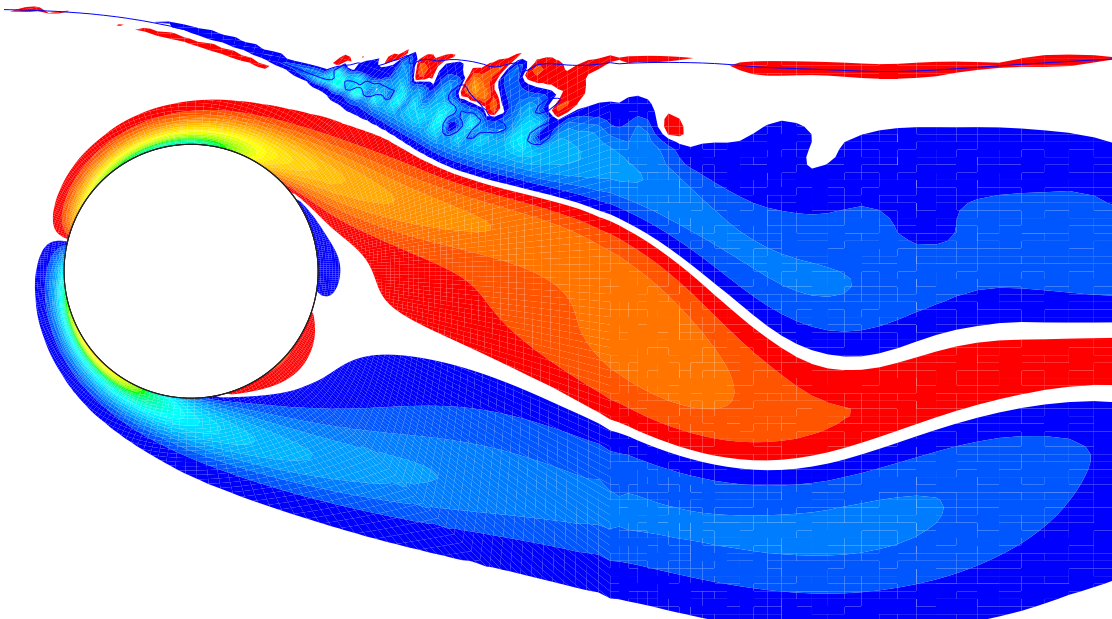
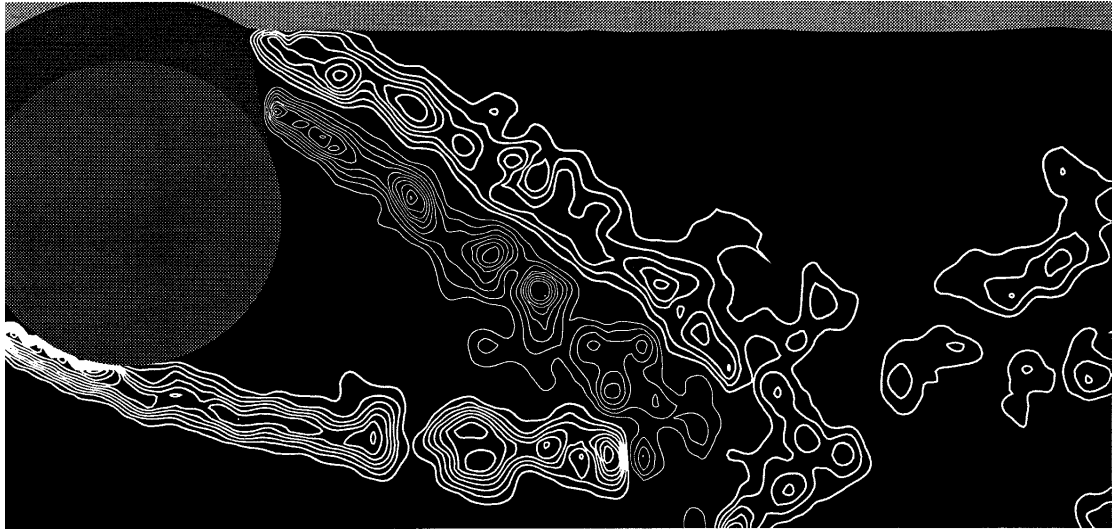


Figure 5.20: Comparison between the experimental vorticity field of Sheridan *et al.* (1997) (top) for a gap ratio of 0.43, a Froude number 0.60 and for a Reynolds number inbetween 5990 and 9120, and the numerically predicted vorticity field (bottom) at a gap ratio of 0.40 (gap 5.9 diameters upstream is 0.45), a Froude number of 0.60 and for a Reynolds number of 180.

The feedback loop idea suggests that some of the metastable wake states may represent a time-dependent switching between an absolute instability and a convective instability, with the level of skew in the wake determining which one governs at any particular instant. The metastable

behaviour at a gap ratio of 0.40 and at Froude numbers of 0.50 and 0.55 show signs that the wake is still absolutely unstable, with a clear time harmonic response observed. The behaviour at a Froude number of 0.60 suggests that the wake is switching between shedding and no shedding, or between an absolute and a convective instability.

Now as it is the structures that form downstream that influence the degree of skew, it is not surprising that Sheridan et al. (1995) found that external disturbances in the region downstream caused a switching between states. Indeed, their comment that the transformation between the two states could be artificially induced by transiently piercing the free surface at a region downstream (presumably at distances greater than approximately 4 diameters), strongly ties in with what was observed here. This piercing is likely to induce the roll-up of the negative shear layer and hence discrete vortex formation which eventually leads to separation, for the case in which the 'jet' is attached to the surface. Or on the other hand, when the 'jet' is in the separated state, the transient piercing is likely to restrict the reverse flow in the region behind the cylinder, thus allowing the 'jet' to re-attach to the surface. The hysteretic effect also noted by Sheridan et al. (1995) is similarly expected, as velocity changes will influence the Froude number and as such it will alter the curvature and the vorticity dynamics of the wake.

One would also expect similar metastable behaviour at smaller gap ratios, although it is likely that the more significant skew caused by the wake, even in the absence of vortex shedding, may be sufficient to ensure that the absolute instability never gets a chance to establish itself.

At a gap ratio of 0.25 and a Froude number of 0.50, the lift trace is again highly modulated which is consistent with metastable behaviour. The videos for this case show the cyclical nature of the metastable state, with the 'jet' again switching between a state of attachment to, and separation from, the free surface. It appears as if the formation of an extended pair of shear layers that precedes the shedding of discrete vortices, results in wave breaking first being noted at positions further downstream. For this case the wave breaking is first witnessed to occur at the second trough and it then migrates upstream until it moves to the first trough. This behaviour is again best illustrated in the video showing the evolution of the vorticity field. With reference to both the particle transport and vorticity movies (see attached compact disk), one observes that it is the evolutionary characteristics of the vortices as they travel downstream, that help determine the wake state. The videos indicate that it is the vortex shedding itself that gives rise to the structures that are responsible for its own demise. In this case, it is the upward movement of a discrete positive vortex and its subsequent coalescence with the next shed discrete positive vortex (to form a larger vortical structure), that reverses the flow near the

interface and hence deflects the ‘jet’ away from the free surface. This separation then skews the wake to such an extent that shedding is no longer sustainable. A number of key frames from the videos that highlight this behaviour are shown in figures (5.21), (5.22) and (5.23).

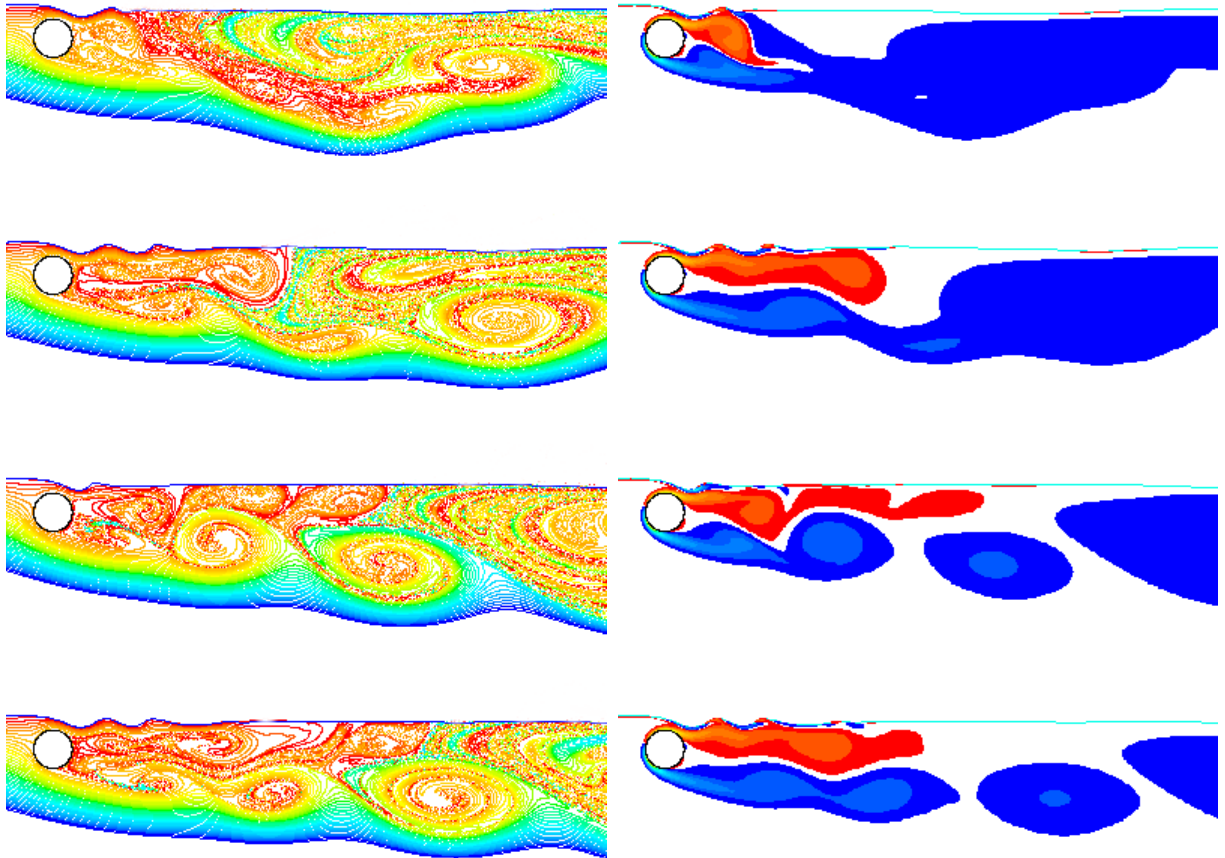


Figure 5.21: First set of frames from the particle transport and vorticity videos for a gap ratio of 0.25 and for a Froude number of 0.50. The Reynolds number in each case is 180.

The metastable wake behaviour observed here is essentially cyclical and should have a period associated with it. However, this period is expected to vary for each gap ratio and Froude number, as the complicated path giving rise to this behaviour will depend upon both the surface curvature and the proximity of the cylinder to the surface. The events making up the metastable cycle can be roughly described as follows;

1. The roll up of the negative shear layer at positions close to the free surface induces surface curvature and results in a slight redirection of the ‘jet’.
2. This roll-up and the time-dependent variation of the surface curvature in response to the shedding of discrete vortices, assists in the weakening of the negative shear layer as the

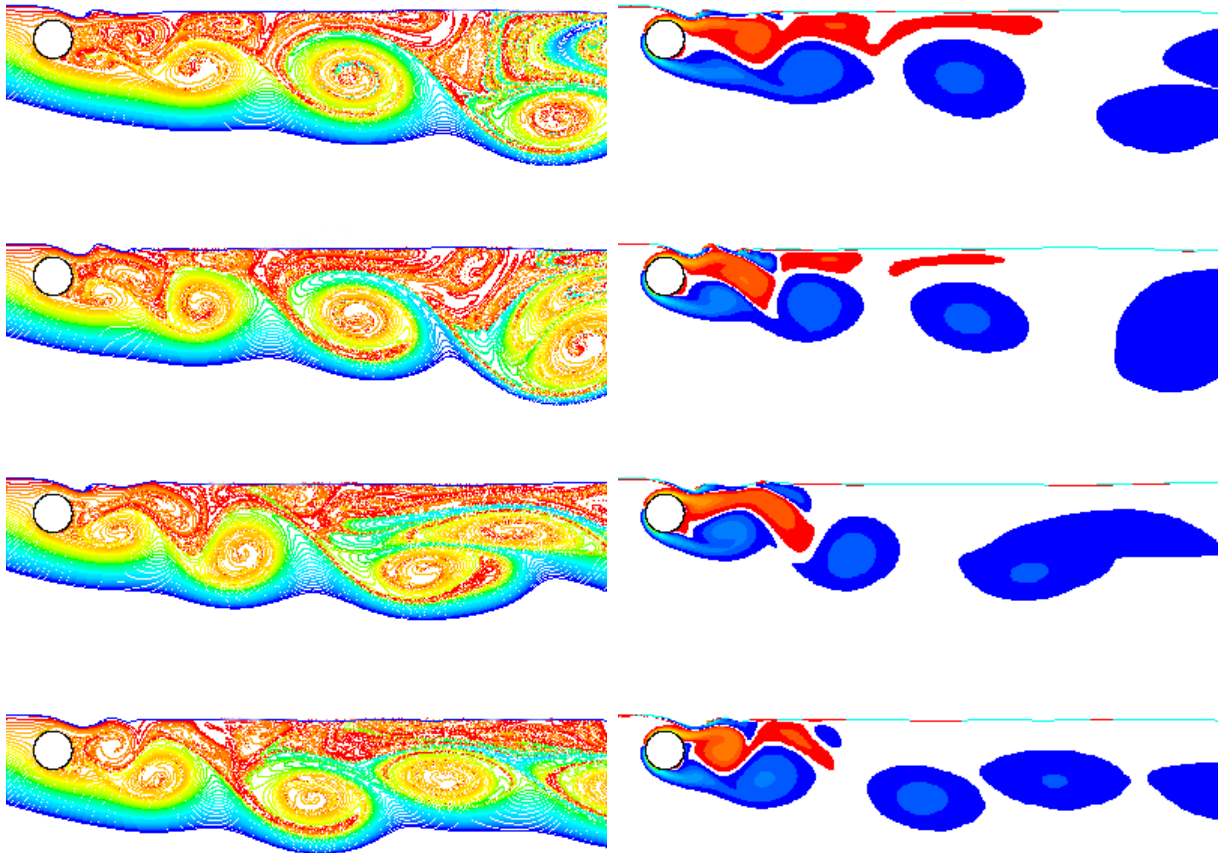


Figure 5.22: Second set of frames from the particle transport and vorticity videos for a gap ratio of 0.25 and for a Froude number of 0.50. The Reynolds number in each case is 180.

negative vorticity is able to flux across the interface.

3. The removal of this vorticity then establishes a bias in the vorticity distribution, such that the wake is now dominated by positive vortical structures.
4. These vortical structures, which typically form from the coalescence of two or more previously shed positive vortices, tend to be recirculatory, in that they slow and in some cases reverse the flow at positions close to the free surface.
5. This slower moving or reverse flow then interacts with the ‘jet’ from above the cylinder. The slight angle of the ‘jet’ as it passes over the cylinder ensures that it is diverted beneath the slower moving/reverse flow and small scale wave breaking is observed.
6. Such wave breaking then introduces more positive vorticity into the fluid, which further weakens the negative shear layer.

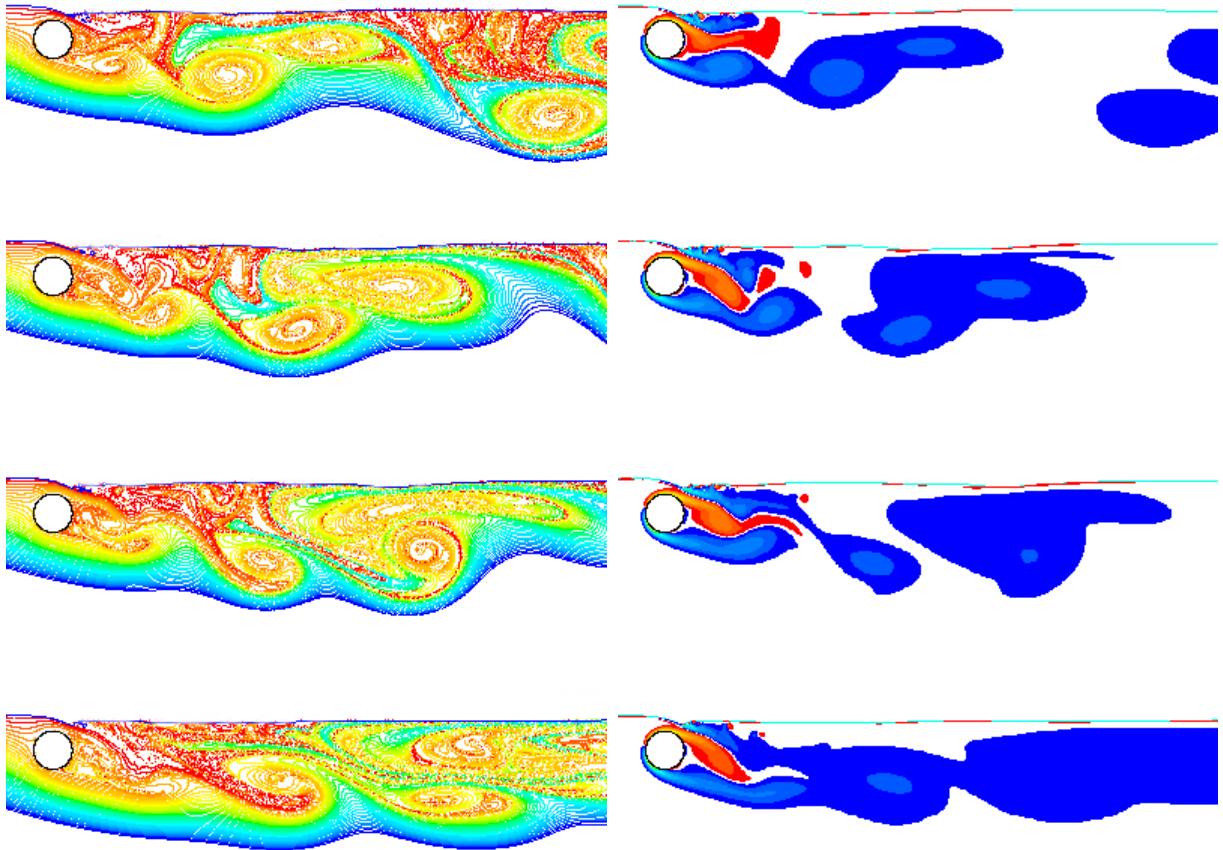


Figure 5.23: Third set of frames from the particle transport and vorticity videos for a gap ratio of 0.25 and for a Froude number of 0.50. The Reynolds number in each case is 180.

7. This growing bias in the wake vorticity distribution then increases the level of the reverse flow, which in turn deflects the ‘jet’ even further away from the surface.
8. This deflection of the ‘jet’ away from the free surface skews the wake and introduces an asymmetry into the velocity profile.
9. If the level of asymmetry or skew is sufficient, then the absolute instability is lost and the oscillatory nature of the wake ceases (i.e. cessation of vortex shedding).
10. If the level is insufficient, then the cylinder continues shedding mutated vortices.
11. The vortical structures which helped bring about these changes in the first place are not self sustaining and with time they are convected downstream.
12. The removal of the recirculatory structures allow the negative shear layer to re-attach to the free surface. And with this the entire process repeats itself.

It should be noted that the positive recirculatory vortical structures typically form when the path traced out by two consecutively shed positive vortices differs, such that each vortex has a different convective velocity. This difference then allows one vortex to catch up with the other, with the result being their coalescence.

It is anticipated that the nature of the wave breaking and its inadequate capture in the numerical simulation, along with minor disturbances introduced when the larger scale structures leave the computational domain, should alter the periodicity somewhat. The presence of small scale turbulent structures, an uneven surfactant distribution or even a biased or restrictive out-flow condition may also make the periodic behaviour of these structures difficult to measure in experiment. Put simply, it is expected that these larger scale structures will develop as they convect downstream, with their strength and proximity at any instant influencing the near wake state, and hence defining the metastable wake behaviour. It is for this reason that one would not expect the period for each of the metastable states to be similar.

When the Froude number is increased to 0.60 for the same gap ratio (i.e. 0.25), the wake permanently switches to the state in which the ‘jet’ occupies a region of space in between the cylinder and the free surface, with no metastable type behaviour any longer observed. Some flapping of the ‘jet’ is noted, however, it is insufficient to induce either attachment to the free surface or the rear of the cylinder. When in this state the wake looks remarkably like that observed by Sheridan et al. (1997) at a gap ratio of 0.31 and a Froude number of 0.60, and by Hoyt & Sellin (2000) for a gap ratio of 0.31 and a Froude number of 0.53. This comparison is shown in figures (5.24) and (5.25). It should be noted that the surface height at positions upstream fluctuated slightly for this case, with the gap ratio at 5.9 diameters upstream of the cylinder center (the point used by Sheridan et al. (1997) to determine the gap ratio) fluctuating between 0.28 and 0.35. The flows general behaviour is again best illustrated via consideration of the videos.

The slight fluctuations in the surface height with time were also observed when the distance from the inlet to the cylinder was increased and while such behaviour may be a transient feature (i.e. it may diminish with further evolution) it was observed to persist even after significant evolutionary time.

With regard to the fluid transport (with the reader recommended to consult the videos at this point), one can clearly see that the fluid from above the cylinder is drawn downwards and beneath the larger scale vortical structure that forms downstream of the cylinder.

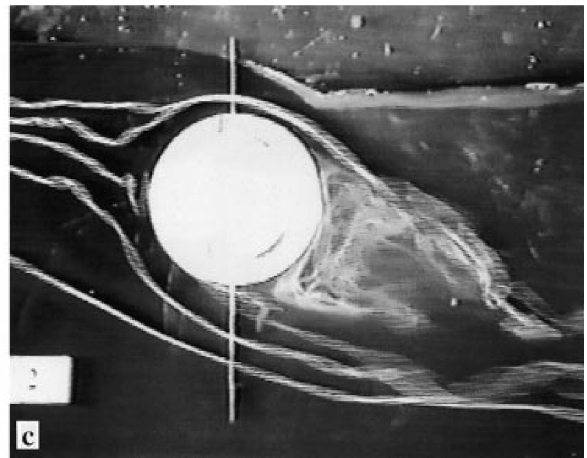
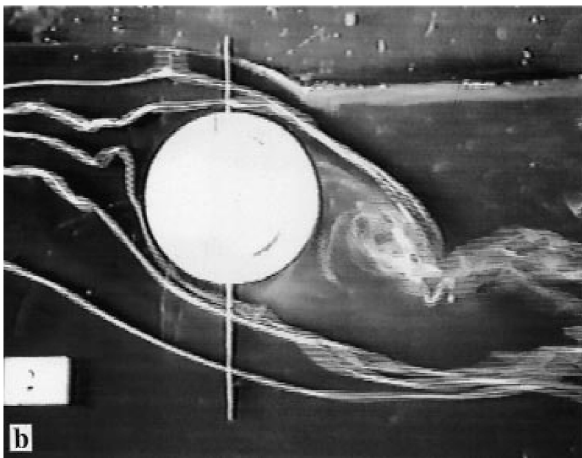
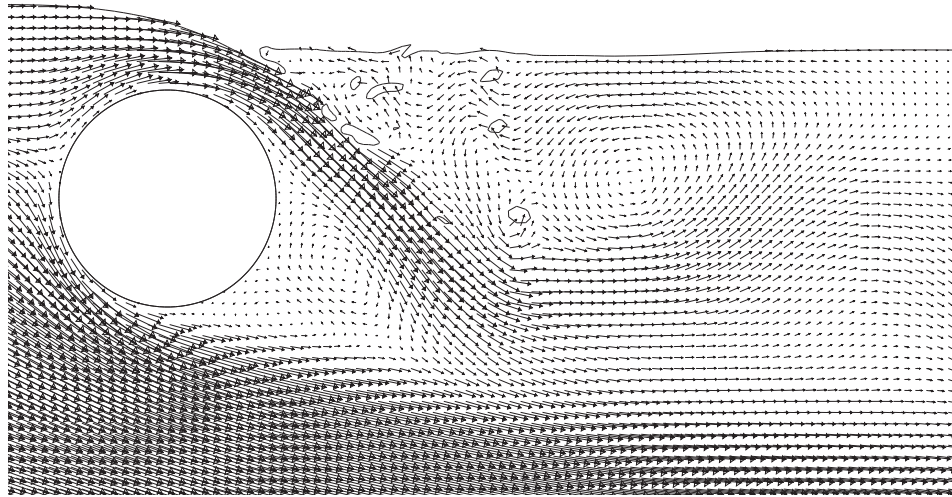
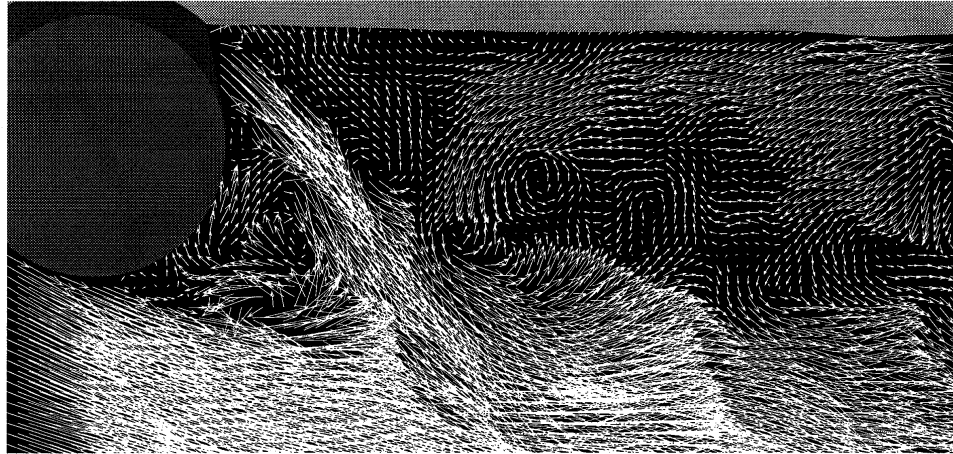


Figure 5.24: Comparison between the experimental results of Sheridan *et al.* (1997) (top) for a gap of 0.31, a Froude number 0.60 and a Reynolds number between 5990 and 9120, the current numerically predicted results (middle) at a gap ratio of 0.25 (gap 5.9 diameters upstream is 0.26), a Froude number 0.60 and a Reynolds number of 180, and experimental results of Hoyt and Sellin (2000) (bottom) at a gap ratio of 0.31, a Froude number of 0.53 and a Reynolds number of 27000.

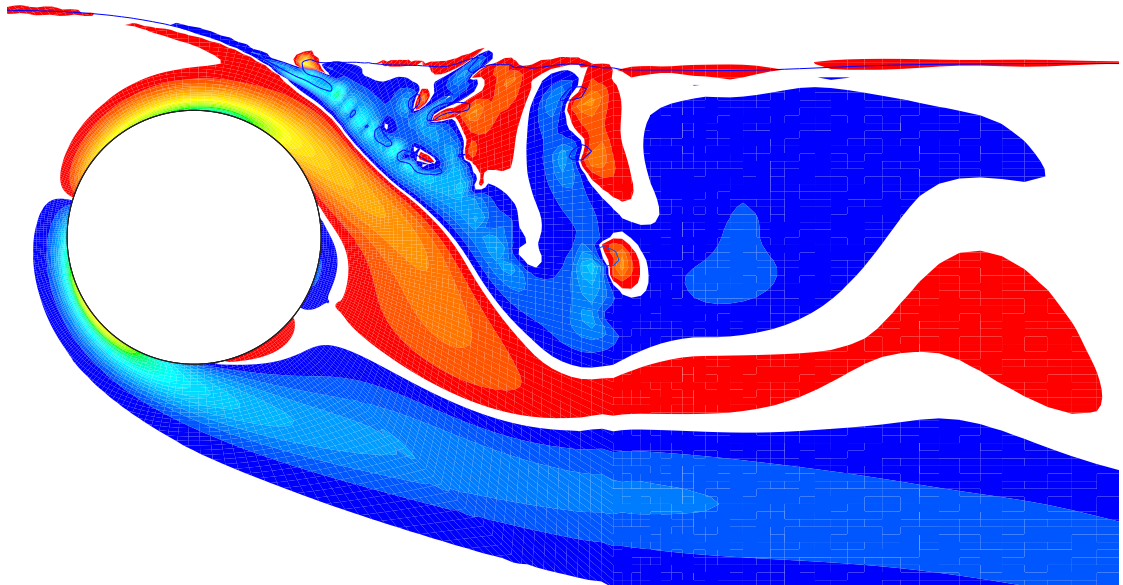
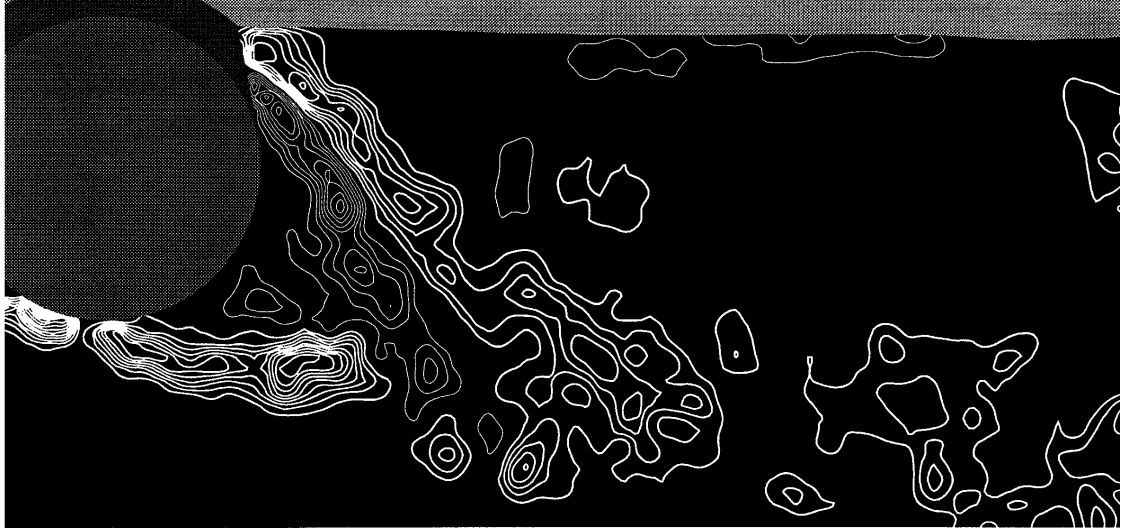


Figure 5.25: Comparison between the experimental vorticity field of Sheridan *et al.* (1997) (top) for a gap ratio of 0.31, a Froude number 0.60 and a Reynolds number between 5990 and 9120 and current numerically predicted results (bottom) at a gap ratio of 0.25, a Froude number of 0.60 and a Reynolds number of 180.

The particle tracer videos highlight the fluctuation in the surface height at locations upstream, with the variation in the horizontal momentum associated with the changing angle of the ‘jet’ and the breaking wave having some influence on this behaviour. The particles tracer movies

also illustrate one of the major aspects of this entire problem (i.e. flow past a cylinder close to a free surface), in that they highlight the importance of fluid transport. That is, they indicate the pathway via which the fluid can both enter and leave the wake cavity.

For this case in which no vortex shedding is noted the wake appears to be predominantly recirculatory and although it is clearly unsteady it does share some similarity with the wakes observed by Fornberg (1985) for symmetric flow past a cylinder (flow past a half cylinder with a symmetry condition imposed along the centerline).

From what has been observed so far it is anticipated that similar behaviour to that noted at a gap ratio of 0.25 should be seen as the gap ratio is further reduced, with the strength of time fluctuating behaviour diminishing.

5.1.3 Small Gap Ratios 0.22, 0.19, 0.16, 0.13 and 0.10

At the smaller gap ratios, the wake shows significant variation as the Froude number is increased, with the ‘jet’ in all cases moving from a state of attachment to the free surface at a Froude number of 0.50, to a state of separation at a Froude number of 0.60. At the lower Froude number (i.e. 0.50) the flow is unsteady, although only marginally so at the smaller gap ratios (i.e. 0.10, 0.13 and 0.16), with small scale wave breaking noted in the region just downstream of the cylinder. Unsurprisingly, the largest time dependent fluctuations are noted at the greater depths, namely 0.19 and 0.22, with a flux of positive vorticity into the fluid observed at two different positions downstream. Such behaviour is consistent with that found at a gap ratio of 0.25, with the two locations indicating that the shear layer from above the cylinder is rolling up (i.e. wave breaking is observed at the second trough). This behaviour indicates that the conditions at these gap ratios and at this Froude number, are at least marginally conducive to the establishment of a vortex shedding.

What is interesting about these results is that no metastable type behaviour is observed, which suggests that the strength of the negatively signed shear layer from above the cylinder plays an important part in the metastable wake development. Indeed, the results indicate that if the mutated negative vortices which form are of insufficient strength to induce significant surface curvature (which in turn results in a significant flux of vorticity into the fluid from the free surface), then the ‘jet’ will remain attached to the surface and no metastable type behaviour will be observed. Thus it appears to be a requirement that the vorticity from both the free surface and the cylinder join, for metastable type behaviour to be observed. Thus metastable

behaviour is only likely to occur when there is significant surface curvature or significant wave breaking at the free surface.

For the cases at a gap ratio of 0.22 and 0.19, the flow reversal at locations downstream of the cylinder now only acts to slow the fluid passing over the cylinder, as opposed to deflecting it away from the surface. Aspects of this behaviour are again best illustrated via consideration of the videos, however the flow fields at a couple of instants in time are shown in figures (5.26) and (5.27).

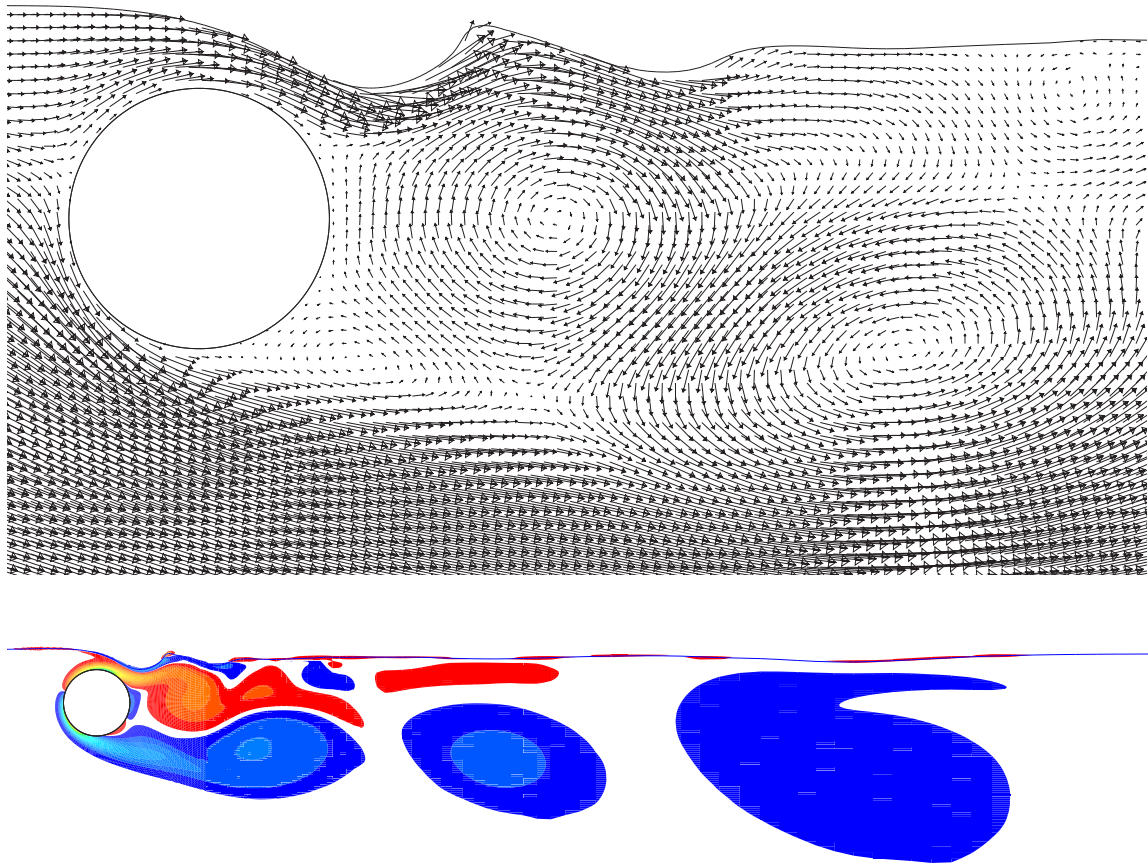


Figure 5.26: Velocity and vorticity fields for a gap ratio of 0.22, a Froude number of 0.50 and a Reynolds number of 180.

At the smaller gap ratios (i.e. 0.16, 0.13 and 0.10), the flow field is largely steady for a Froude number of 0.50, with two extended shear layers defining the wake, as shown in figure (5.28). While some small scale wave breaking is found in the region just behind the cylinder, it appears to have little effect on the wake, and it is noted that the length of the positive shear layer (the

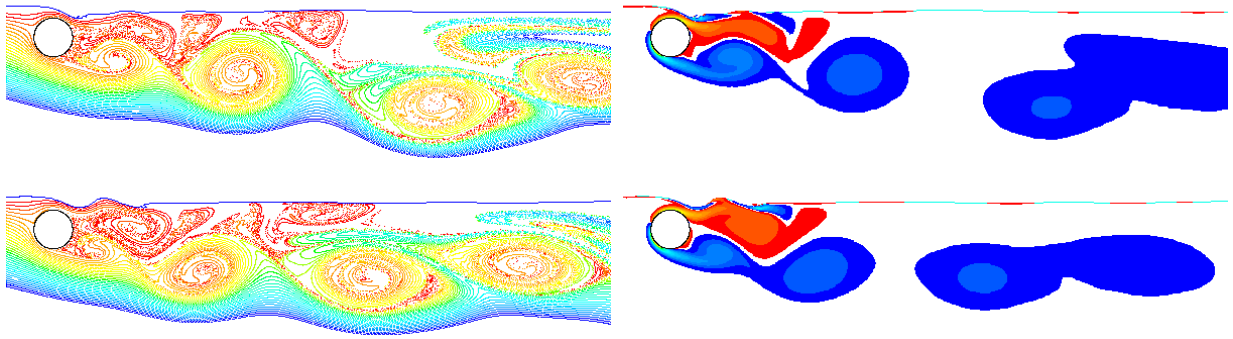


Figure 5.27: Two frames from the particle transport and vorticity videos for a gap of 0.19 and a Froude number of 0.50. The Reynolds number in each case is 180.

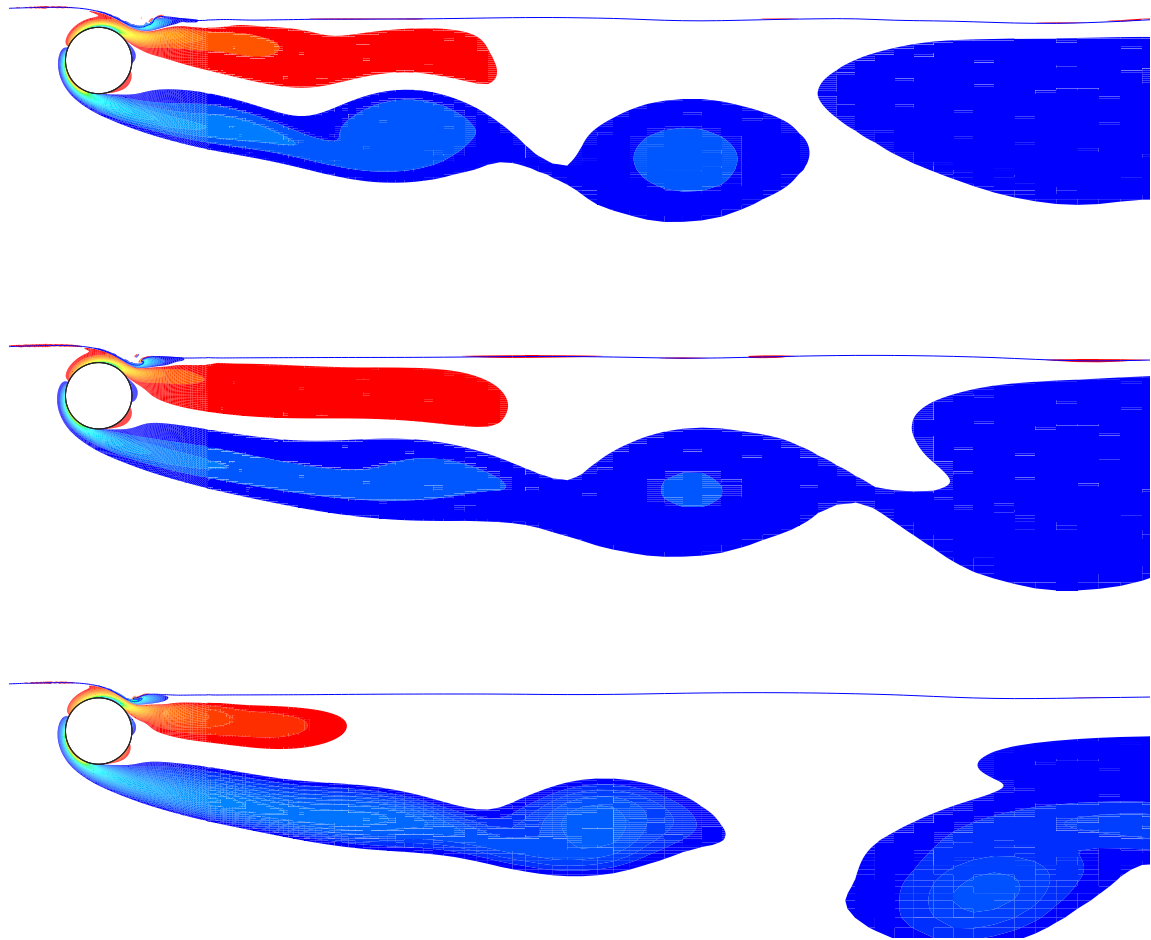


Figure 5.28: Vorticity fields at a Froude number of 0.50 for gap ratios of 0.16, 0.13 and 0.10 (top to bottom). The Reynolds number in each case is 180.

one from beneath the cylinder) grows with the reduction of the gap ratio, while the negative shear layer (the one from above the cylinder) contracts.

Increasing the Froude number causes the ‘jet’ to separate from the free surface for all of the gap ratios considered within this section (i.e. 0.22, 0.19, 0.16, 0.13 and 0.10), with this behaviour consistent with that observed by Sheridan et al. (1997). When the ‘jet’ separates from the free surface the flow becomes largely recirculatory, with a large circulating flow structure noted at positions downstream. This structure has low levels of vorticity associated with it (i.e. roughly 4 to 5 percent of the maximum vorticity), and strongly resembles the structures observed by Fornberg (1985) for symmetric flow past a cylinder. The videos for these cases highlight the extent of the recirculatory zone, while also indicating that the width of the recirculatory structure increases with decreasing gap ratio. Figure (5.29) shows a number of key frames from the video which illustrate this behaviour.

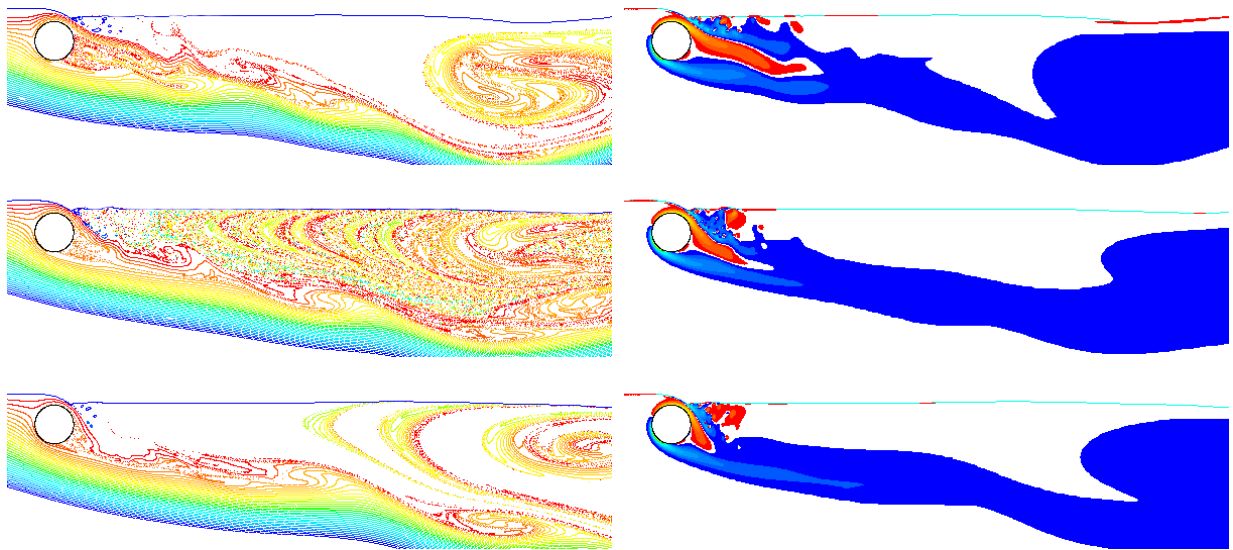


Figure 5.29: Particle transport and vorticity plots which highlight the extent of the recirculation bubble for gap ratios (from top to bottom) of 0.19, 0.16, and 0.13. The Froude number in each instance is 0.60 and the Reynolds number is 180.

It should be noted that the height at the inlet was found to vary significantly with time for the gap ratio 0.19, Froude number 0.60 case, with the influence of such height changes clearly discernible in the particle transport video. These fluctuations arise as the larger scale recirculatory structures that form downstream of the cylinder become more mobile, with their formation and downstream convection inducing significant surface curvature. This behaviour generates a surface depression, or more appropriately a wave, which appears to be reflected and to some extent amplified within the domain, with this amplification process reflected in the lift trace that is shown in the next section. This behaviour was found to persist even when the distance of the cylinder to the inlet and to the outlet was increased.

It is suggested here that at this larger Froude number (i.e. 0.60), the surface curvature introduces a greater level of skew to the wake that ensures that the weak shedding that was observed at the larger gaps within this range can no longer be sustained. It will be argued, with the reasoning being given later in this chapter, that this skew causes the wake to become convectively unstable, with the large recirculation zone simply representing a manifestation of this type of instability.

Before proceeding to consider the Strouhal number and the forces acting upon the cylinder, it is perhaps best to compare in greater detail the current results with those of Sheridan et al. (1997) for the flows at small gap ratios. The first thing that needs to be pointed out is that the state in which the ‘jet’ is attached to the rear of the cylinder was not obtained, although behaviour very close to this was noted at the smaller gap ratios, with such behaviour, particularly at a gap ratio of 0.13, shown previously in figure (5.29).

The results at a gap ratio of 0.10 and for a Froude number of 0.60 and 0.70, indicate that the ‘jet’ will tend to move towards the cylinder as the Froude number is increased, with the increased surface curvature limiting the amount of fluid passing over the cylinder (via the rotation of the front stagnation point), and hence increasing the amount passing under the cylinder and thus increasing such flows entrainment demands. It is also noted, although only briefly, that two recirculation bubbles are observed at a Froude number of 0.70 while only one is noted at 0.60, for a gap ratio of 0.10, with this change illustrated in figure (5.30).

At a gap ratio of 0.10 and a Froude number of 0.60, the current result strongly resembles those of Sheridan et al. (1997) for a gap ratio of 0.16 and a Froude number of 0.60, with both investigations showing the ‘jet’ separating from the free surface. In addition the angle between the shear layer from beneath the cylinder and the horizontal is roughly 20 degrees in the current investigation, which is close to that of Sheridan et al. (1997), with a measurement from their pictures yielding a result of approximately 22 degrees (see figure (5.31) for a comparison). The current results also confirm the presence of a small recirculating zone just next to the ‘jet’ which while mentioned by Sheridan et al. (1997), is difficult to determine from their velocity plot. This behaviour is clarified, with this recirculation zone for a gap ratio of 0.13 and a Froude number of 0.60 shown in figure (5.32).

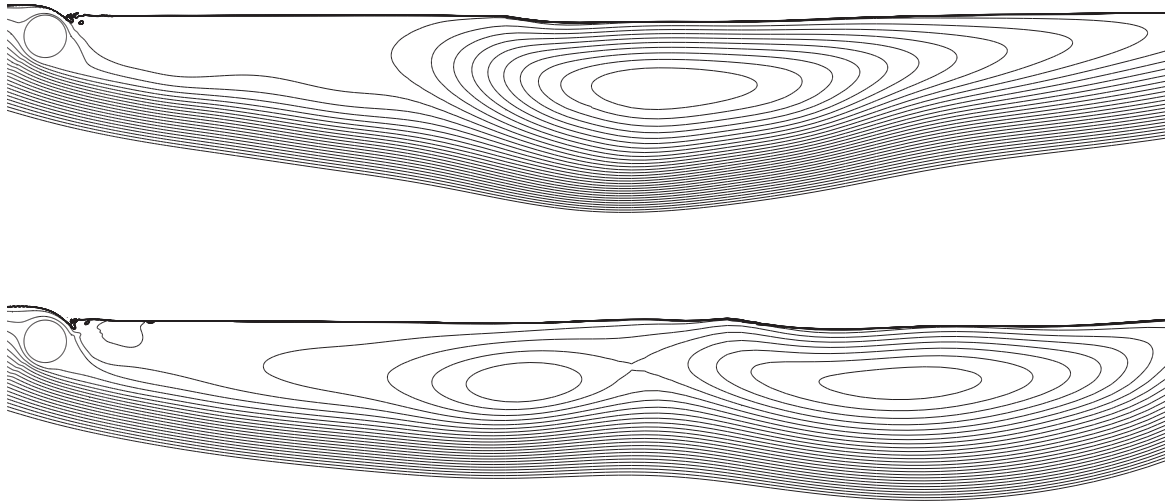


Figure 5.30: Stream function plots highlighting the size of the recirculation bubble for a gap ratio of 0.10 and a Froude number of 0.60 (top) and 0.70 (bottom). The Reynolds number in each case is 180.

5.2 Strouhal Number and Lift

The changes in the behaviour of the wake in response to the altered Froude number should make themselves apparent in the non-dimensionalized shedding frequency or Strouhal number. The Strouhal number should essentially detail the time-dependent manner in which the above mentioned changes in the wake occur. As the previous two chapters that dealt with the flow at lower Froude numbers have highlighted there is a tendency for shedding to cease at increasingly larger gap ratios as the Froude number is increased. Hence one would expect that shedding may cease, or at the very least vary more significantly, at greater and greater depths for larger and larger Froude numbers. Indeed, the metastable states observed here, by Sheridan et al. (1995) and by Sheridan et al. (1997), appear to represent a form of loose boundary in parameter space both in terms of the Froude number and the gap ratio, at which shedding is observed. Deviations away from these points then tend to result in either a complete cessation of shedding, or in the re-establishment of a mutated form of shedding.

While the nature of the changes observed in the wakes development alter with Froude number, the cessation of vortex shedding itself is not restricted to the problem being considered here. Bearman & Zdravkovich (1978), Angrilli et al. (1982), Grass et al. (1984), Lei et al. (1999) and Price et al. (2000) have all shown that shedding ceases for a cylinder placed adjacent to a no-slip

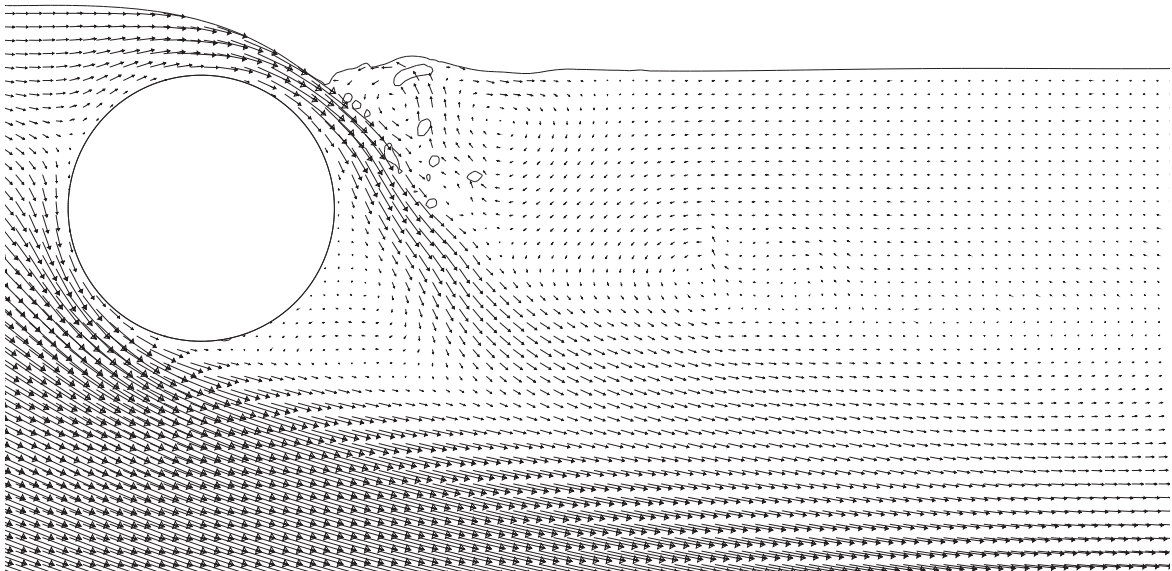
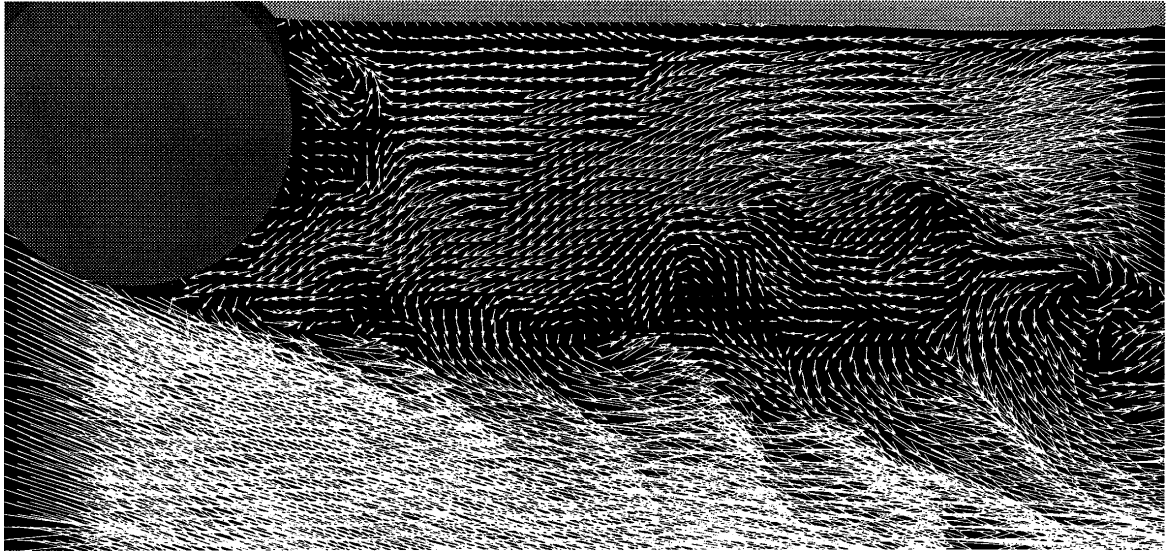


Figure 5.31: Comparison between the experimental velocity field of Sheridan *et al.* (1997) (top) at a gap ratio of 0.16, a Froude number of 0.60 and a Reynolds number between 5990 and 9120, and the numerically predicted velocity field (bottom) at a gap ratio of 0.10, a Froude number 0.60 and a Reynolds number of 180.

wall. Hence one must ask, what changes are induced by increasing the Froude number that result in such a dramatic change in the wake behaviour? The answer appears to be the level of skew in the wake orientation, which is determined by the free-surface boundary condition. This condition dictates both the local normal pressure gradient, and local tangential velocity gradient. Hence by increasing the Froude number, one allows for a greater level of surface curvature that

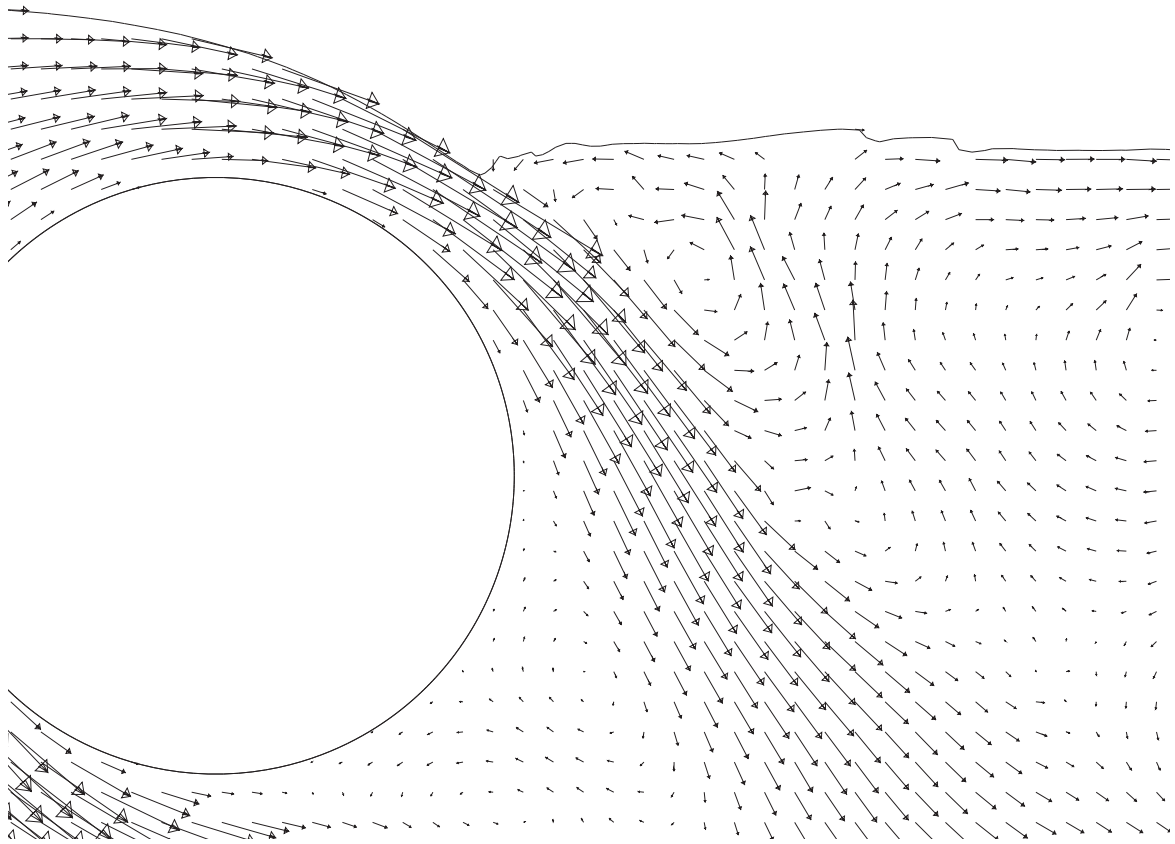


Figure 5.32: Numerically predicted recirculation zone next to the 'jet'. The result shown is for a gap ratio of 0.13 and for a Froude number of 0.60. The Reynolds number for this case is 180.

in turn alters the angle at which the 'jet' leaves the cylinder. This skew then alters the nature of the instability associated with the cylinder wake, with the findings of Koch (1985) and the speculation of Huerre & Monkewitz (1990), suggesting that the presence of an asymmetric base flow may lead to significant changes in the local stability properties.

The influence of the free surface boundary condition can not be under stated, with it governing the flow just beneath the surface, while also determining the surface shape. It also allows for the preferential removal of negative vorticity from the fluid, while also governing the ease via which fluid from downstream may be introritted upstream.

Hence, it is expected that the changes in the behaviour of the Strouhal number are likely to reflect, at least in part, the influence of the free surface boundary condition on the nature of the instability associated with the cylinder wake.

The behaviour of the Strouhal number as measured by the variation of the lift coefficient will now be considered. For many of the larger gap ratio cases (i.e. 5.00 to 1.50), almost regular vortex shedding was observed for Froude numbers of both 0.50 and 0.60, with the lift trace producing

one clearly discernible shedding frequency. However at intermediate gap ratios, metastable type behaviour was noted in which more than one frequency was often present, while at smaller gap ratios no shedding was detected at all, with the lift trace in these instances producing small erratic time-dependent fluctuations. The variation of the Strouhal number with gap ratio is shown in table (5.1), and in figure (5.33), with the lift trace and the associated spectra for gap ratios less than 1.50 shown in figures (5.34) to (5.44).

Gap ratio G/D	Normalized Strouhal number/s $Fr = 0.50$	Normalized Strouhal number/s $Fr = 0.55$	Normalized Strouhal number/s $Fr = 0.60$
0.10	NS	NA	NS 0.201268
0.13	NS 0.207549	NA	NS 0.211331
0.16	NS 0.121907, 0.081273	NA	NS 0.205462
0.19	NS 0.220951, 0.749308	NA	NS 0.208104, 0.192097,
		NA	0.016006
0.22	NS 0.763117, 0.215240	NA	NS 0.211331
0.25	MS 0.813502, 0.232430	NA	NS 0.196561, 0.184279
0.40	SFP 1.215055,	MS 1.131933,	MS 1.119805,
	1.135811,	0.086244,	1.077549,
	1.118199	0.862425	0.126772
0.55	1.096075	NA	MS 1.216112, 0.169456
0.70	1.120180	NA	1.198553
0.85	1.120861	NA	1.177750
1.00	1.115890	NA	1.156693
1.50	1.074802	NA	1.093576
2.50	1.036154	NA	1.037184
5.00	1.011057	NA	1.010264

Table 5.1: Variation of the Strouhal number with gap ratio for Froude numbers of 0.50, 0.55, and 0.60. NS = no shedding (frequencies), MS = metastable (frequencies), NA = no measurement, SFP = shedding but with a fluctuating period (frequencies).

The behaviour of the mean and RMS lift is shown in figure (5.45).

While the wake state often changes considerably as the Froude number is increased from 0.50 to 0.60, the mean lift on the other hand varies very little. The RMS lift however, does vary significantly and it is again a better indicator of the changes occurring in the wake. As figure (5.45) indicates, there is a hastened decrease in the RMS lift as the gap ratio is reduced at the larger Froude number, with this change illustrating the fact that the ‘jet’ has separated from the free surface.

Figure (5.46), shows the modulated lift trace and its spectra for a gap of 0.40 and a Froude number of 0.55. This modulation appears to be symptomatic of metastable type behaviour,

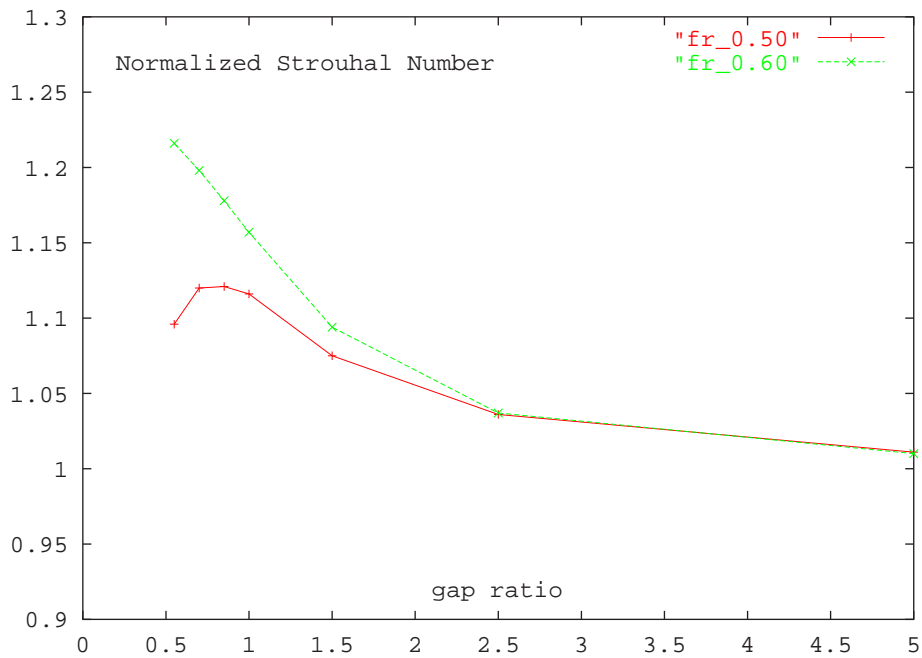


Figure 5.33: Variation of the normalized Strouhal number with gap ratio for Froude numbers of 0.50 and 0.60. The Reynolds number for all cases is 180.

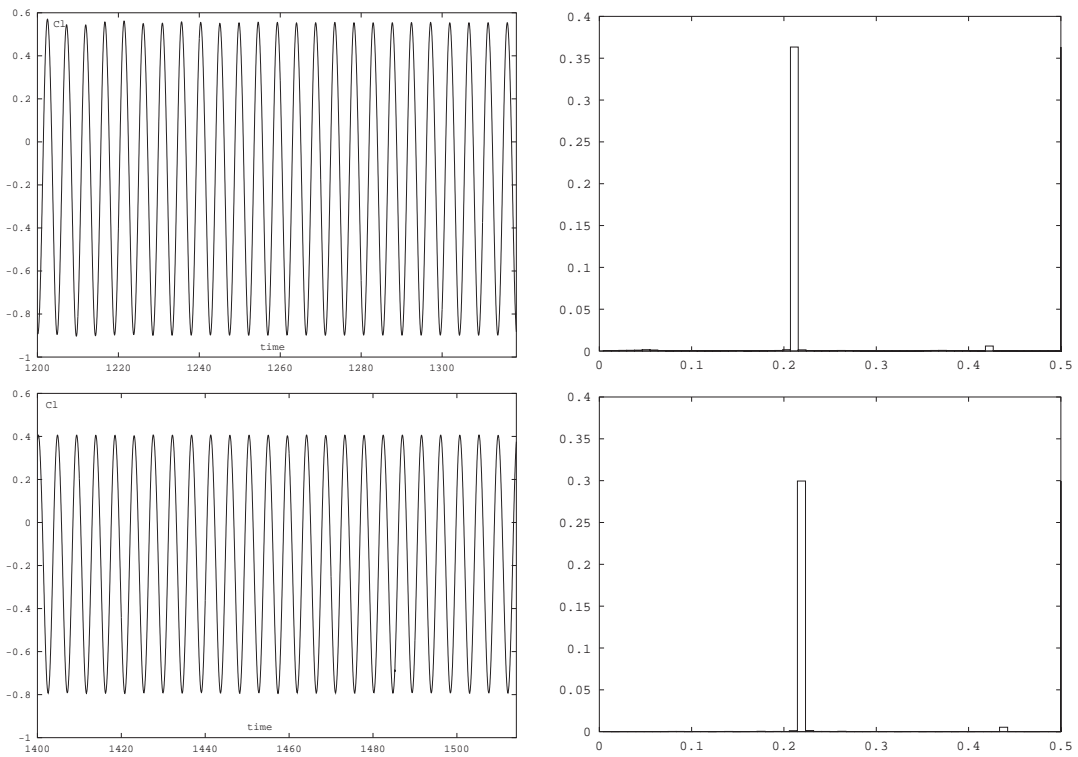


Figure 5.34: Plot showing the lift coefficient and its spectra for a gap ratio of 1.00 and for Froude numbers of 0.50 (top) and 0.60 (bottom). The Reynolds number for each case is 180.

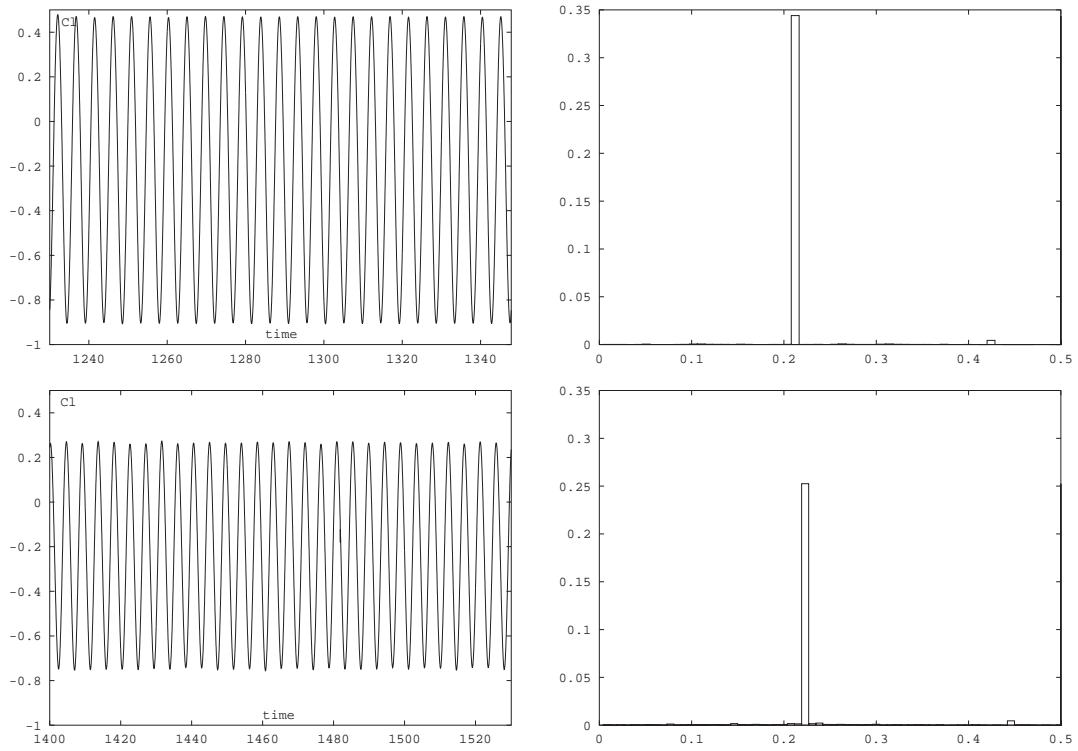


Figure 5.35: Plot showing the lift coefficient and its spectra for a gap ratio of 0.85 and for Froude numbers of 0.50 (top) and 0.60 (bottom). The Reynolds number for each case is 180.

with the video for this case clearly revealing the pseudo cyclical manner in which the ‘jet’ separates from the surface, only to re-attach again later. The closer inspection of the lift trace in figure (5.47) and the movie for this case show the evolution of the flow, for the interval to the right of the dashed vertical line. A few key frames from this video and their corresponding position on the lift trace are shown in figures (5.48), (5.49), (5.50) and (5.51).

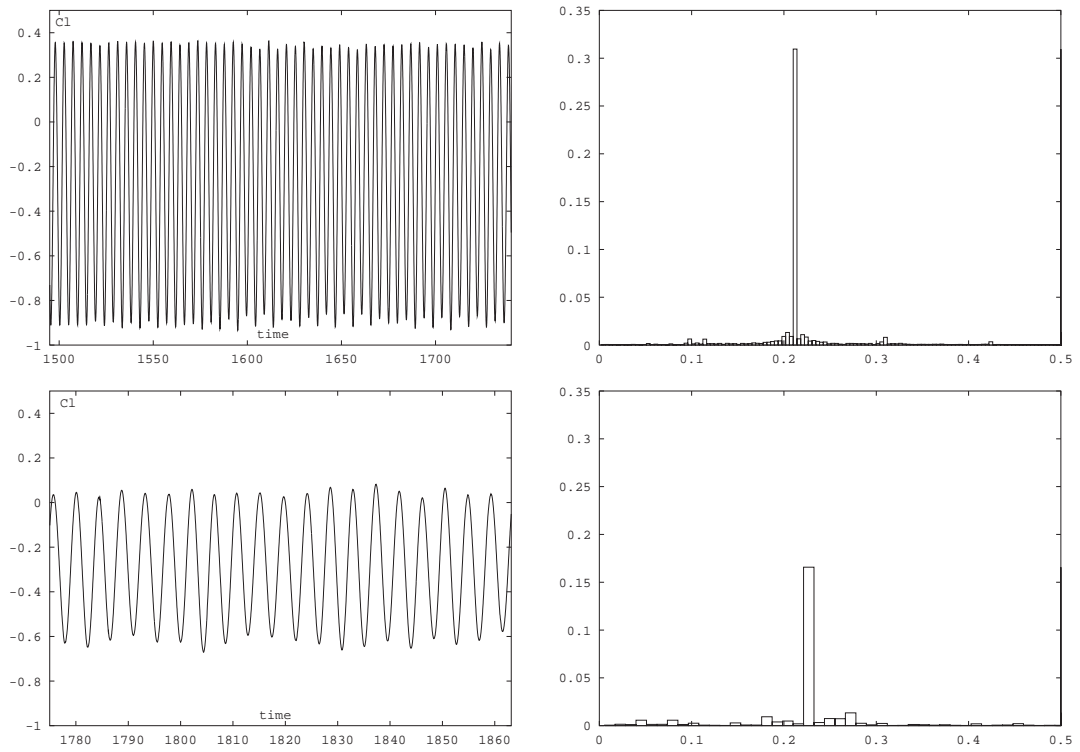


Figure 5.36: Plot showing the lift coefficient and its spectra for a gap ratio of 0.70 and for Froude numbers of 0.50 (top) and 0.60 (bottom). The Reynolds number for each case is 180.

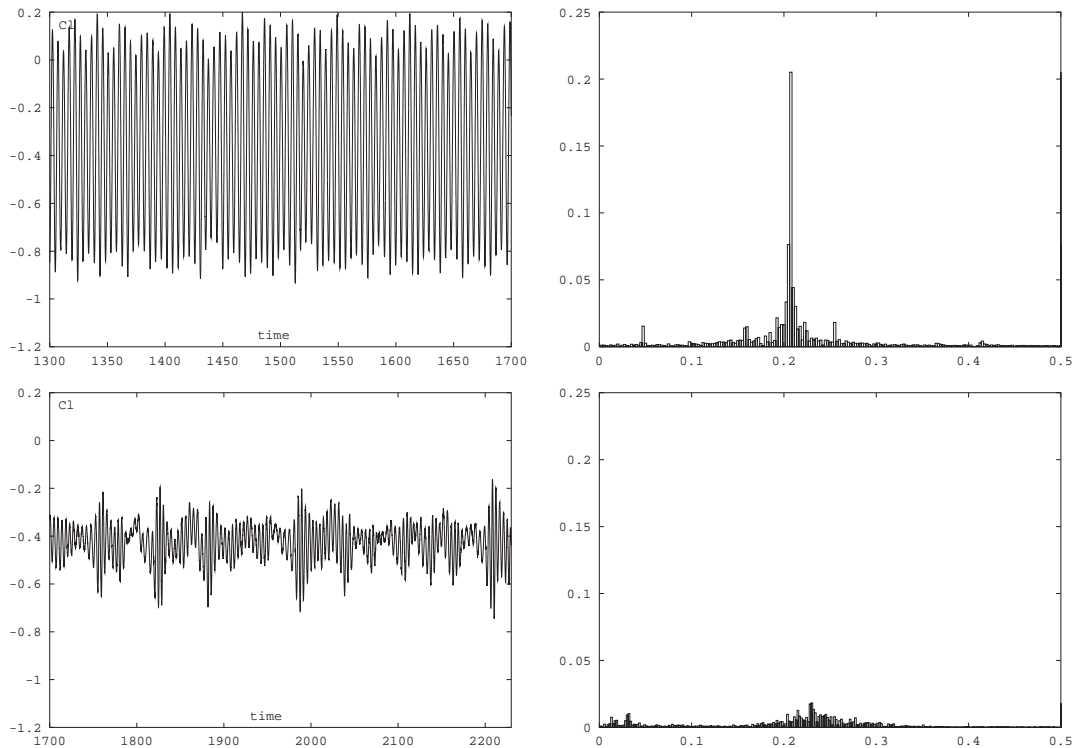


Figure 5.37: Plot showing the lift coefficient and its spectra for a gap ratio of 0.55 and for Froude numbers of 0.50 (top) and 0.60 (bottom). The Reynolds number for each case is 180.

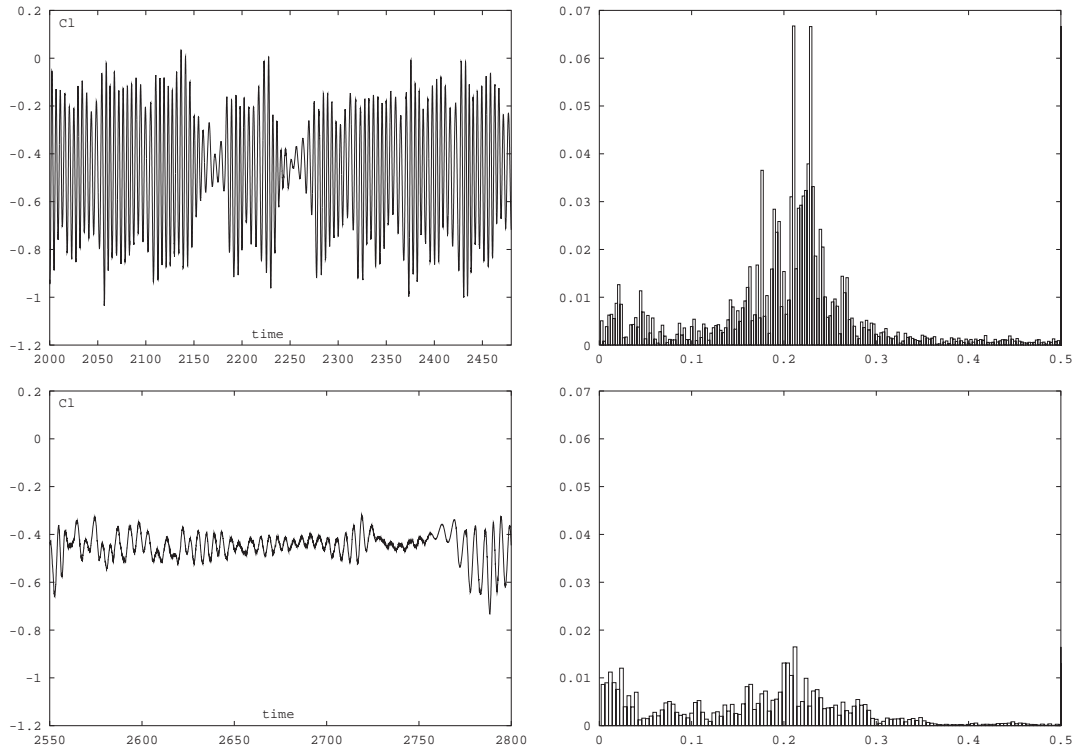


Figure 5.38: Plot showing the lift coefficient and its spectra for a gap ratio of 0.40 and for Froude numbers of 0.50 (top) and 0.60 (bottom). The Reynolds number for each case is 180.

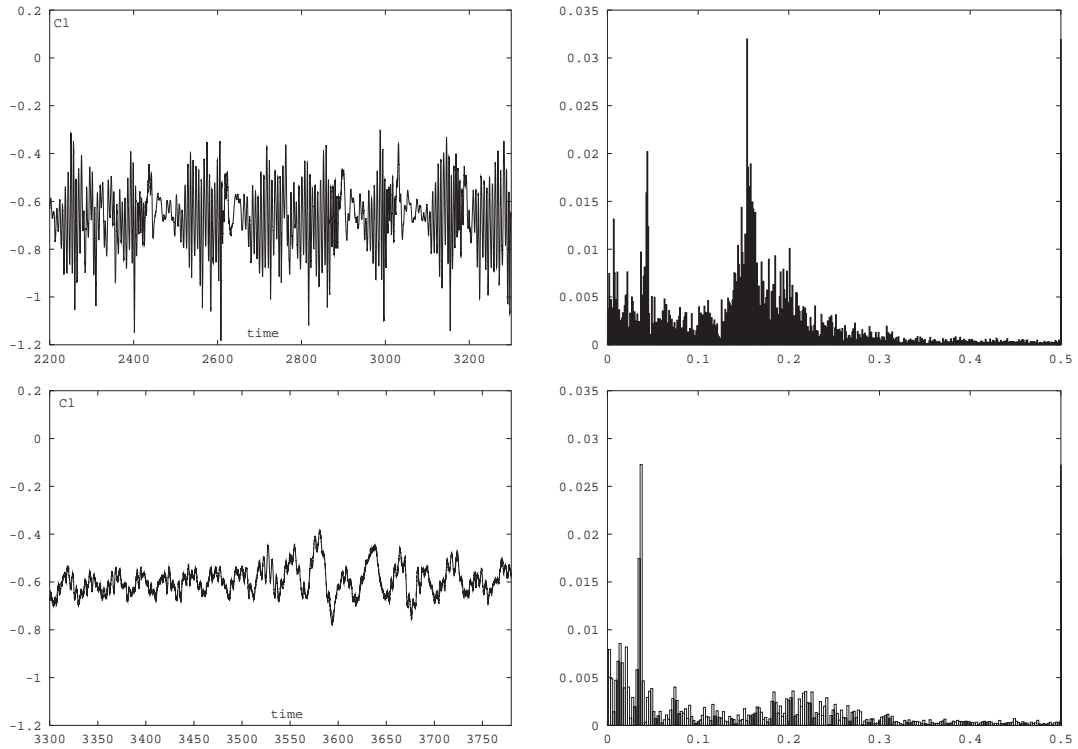


Figure 5.39: Plot showing the lift coefficient and its spectra for a gap ratio of 0.25 and for Froude numbers of 0.50 (top) and 0.60 (bottom). The Reynolds number for each case is 180.

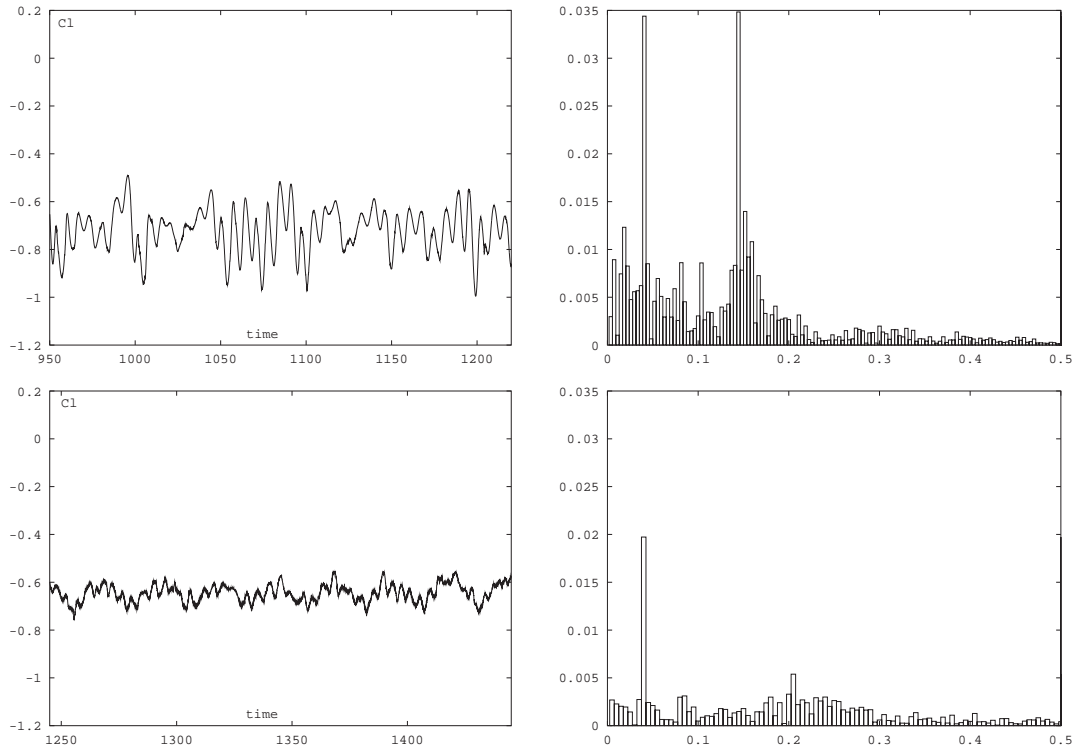


Figure 5.40: Plot showing the lift coefficient and its spectra for a gap ratio of 0.22 and for Froude numbers of 0.50 (top) and 0.60 (bottom). The Reynolds number for each case is 180.

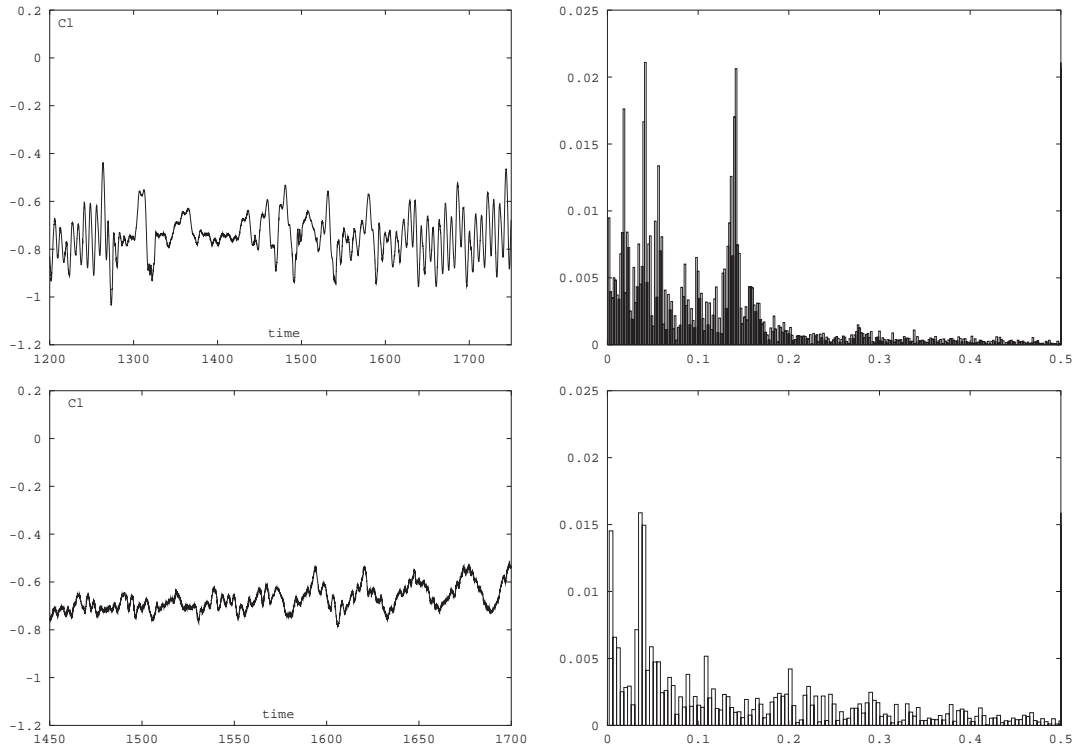


Figure 5.41: Plot showing the lift coefficient and its spectra for a gap ratio of 0.19 and for Froude numbers of 0.50 (top) and 0.60 (bottom). The Reynolds number for each case is 180.

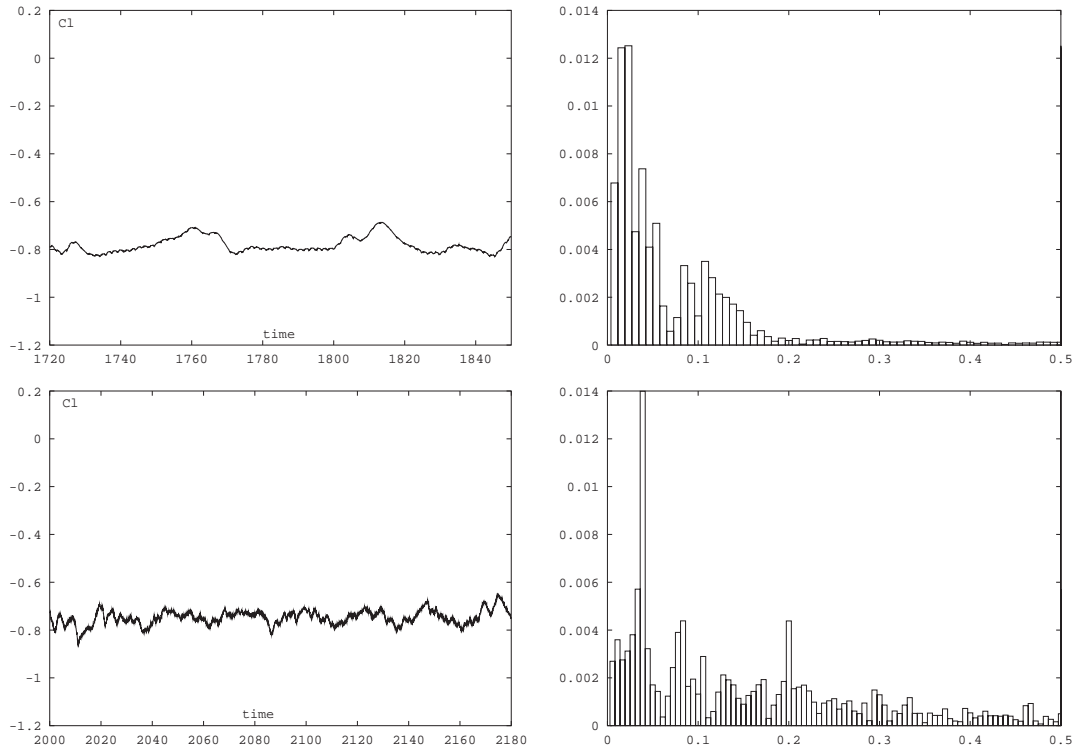


Figure 5.42: Plot showing the lift coefficient and its spectra for a gap ratio of 0.16 and for Froude numbers of 0.50 (top) and 0.60 (bottom). The Reynolds number for each case is 180.

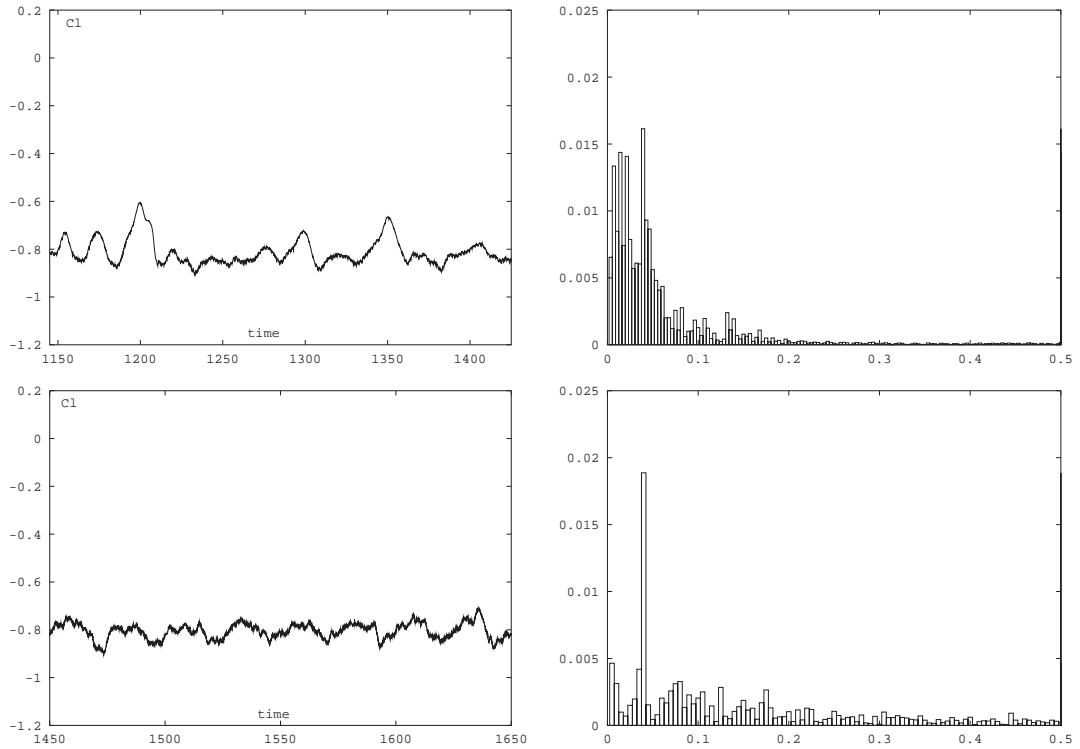


Figure 5.43: Plot showing the lift coefficient and its spectra for a gap ratio of 0.13 and for Froude numbers of 0.50 (top) and 0.60 (bottom). The Reynolds number for each case is 180.

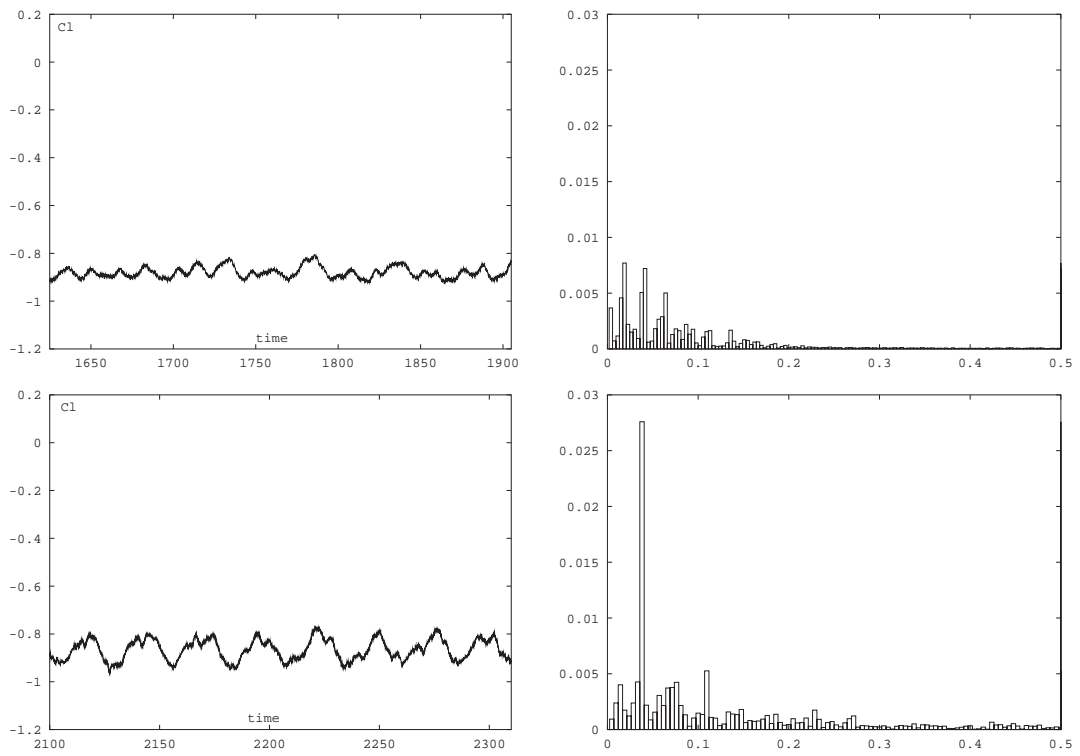


Figure 5.44: Plot showing the lift coefficient and its spectra for a gap ratio of 0.10 and for Froude numbers of 0.50 (top) and 0.60 (bottom). The Reynolds number for each case is 180.

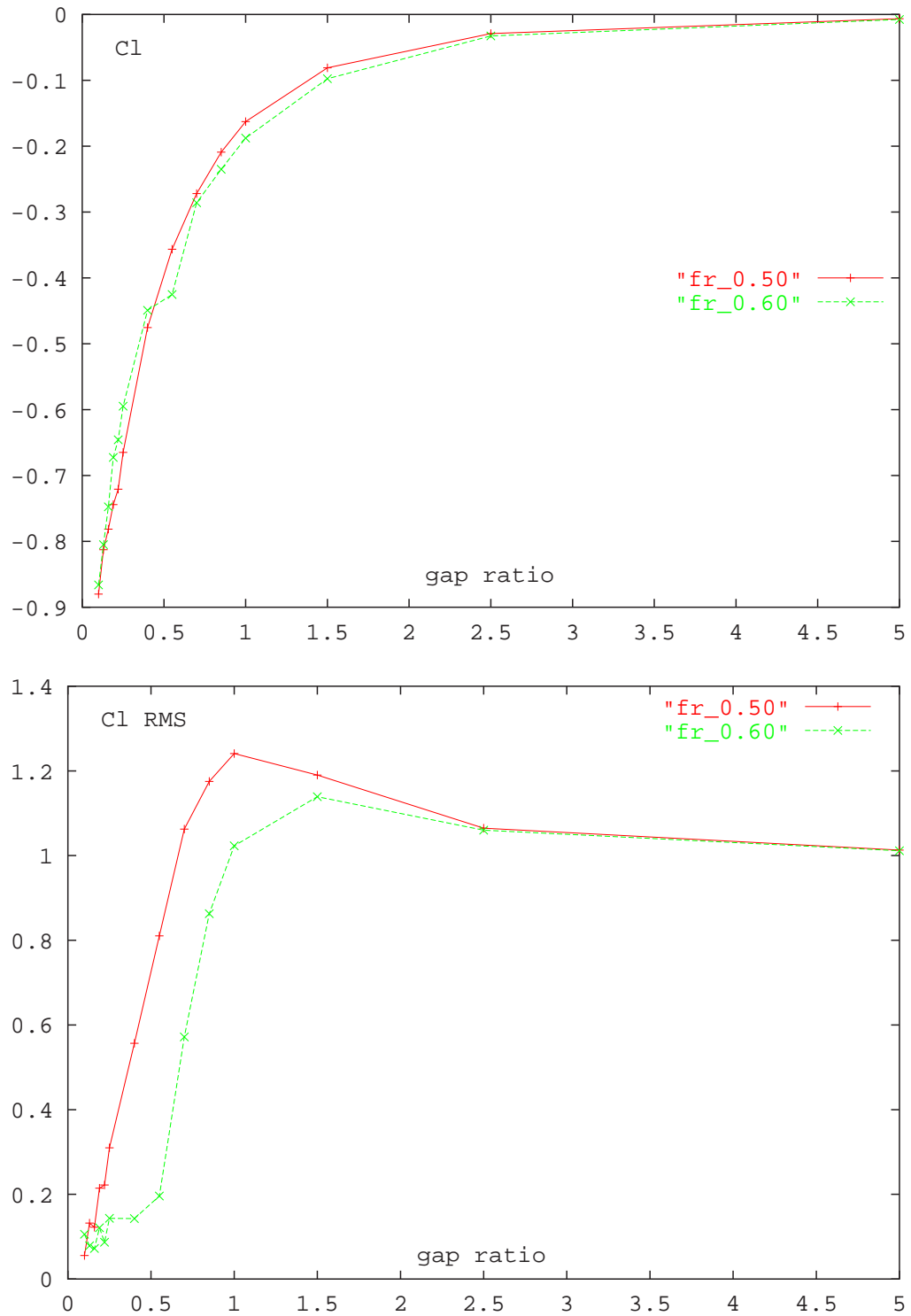


Figure 5.45: Variation of the mean lift and normalized RMS lift with gap ratio for Froude numbers of 0.50 and 0.60. The Reynolds number for each case is 180.

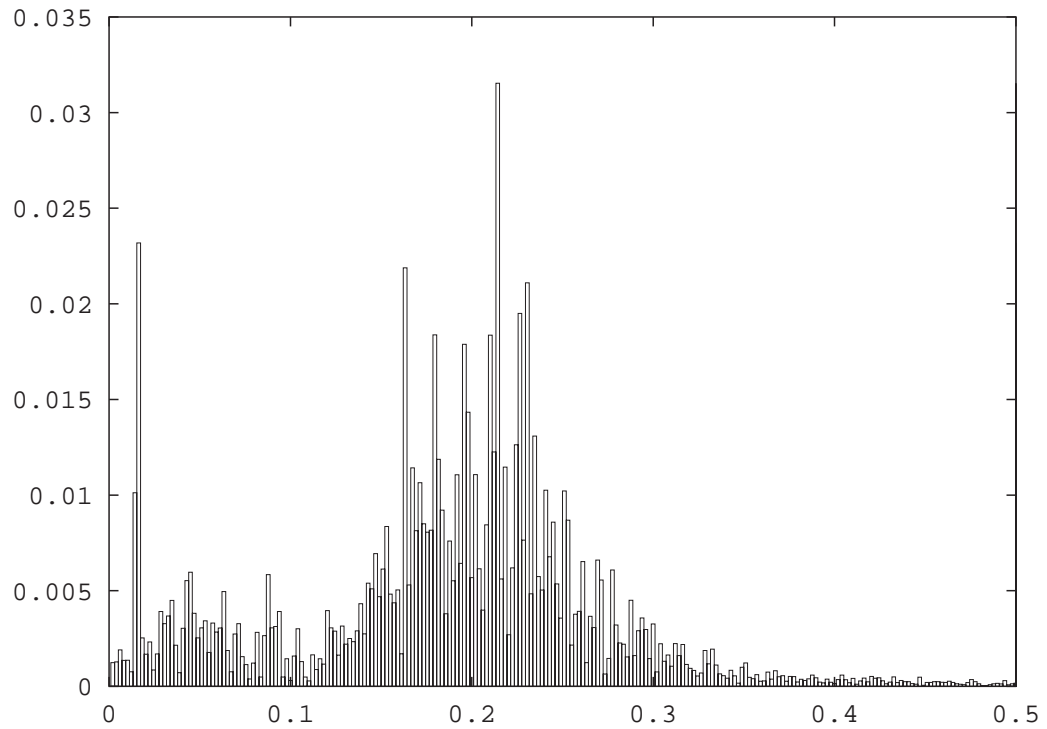
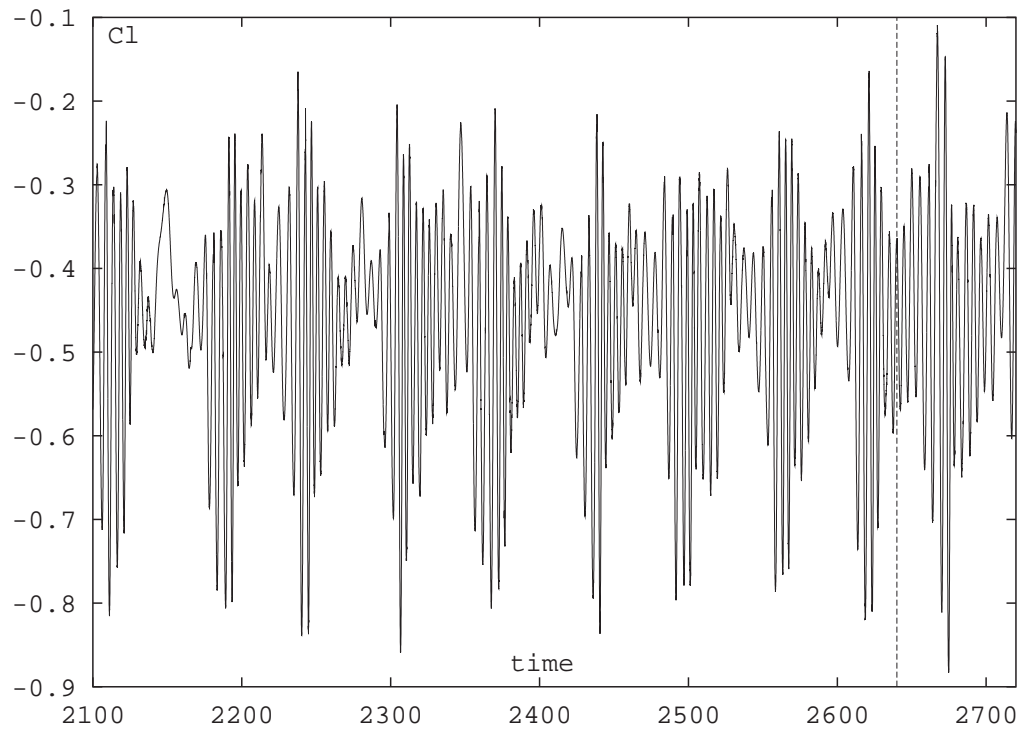


Figure 5.46: Plot showing the lift trace and its spectra for a gap ratio of 0.40 and a Froude number of 0.55. The Reynolds number for each of the cases shown is again 180. The region to the right of the dashed vertical line is shown in figure (5.47).

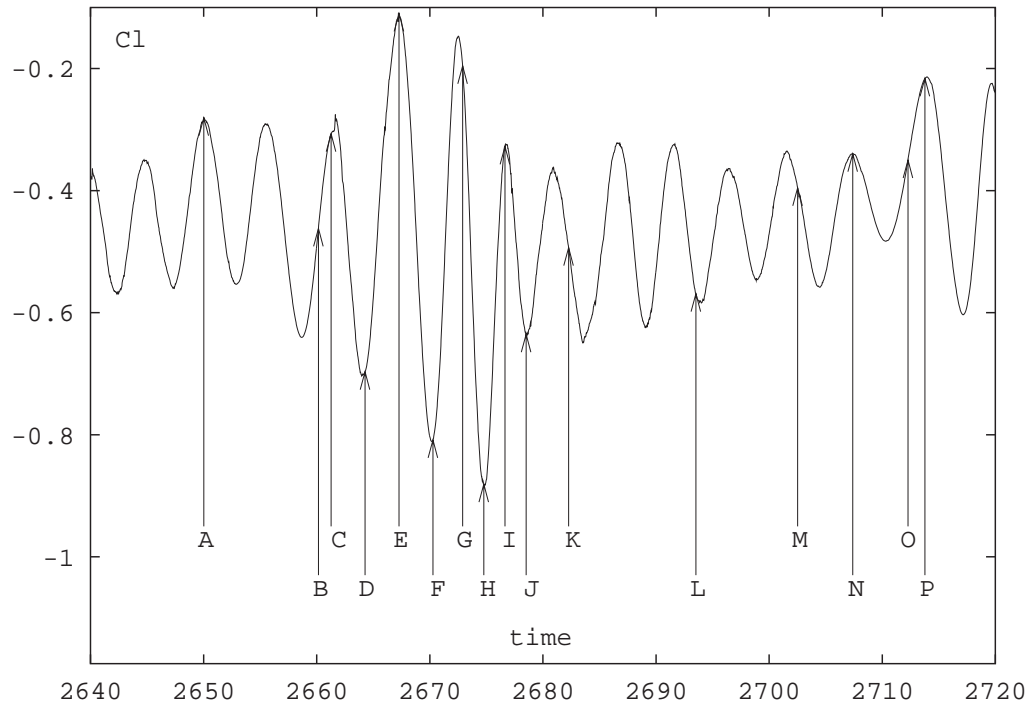


Figure 5.47: Close up view of the lift trace for a gap ratio of 0.40 and a Froude number of 0.55. The Reynolds number for each of the cases shown is again 180. The letters (A to P) denote the frames shown in figures (5.48) to (5.51).

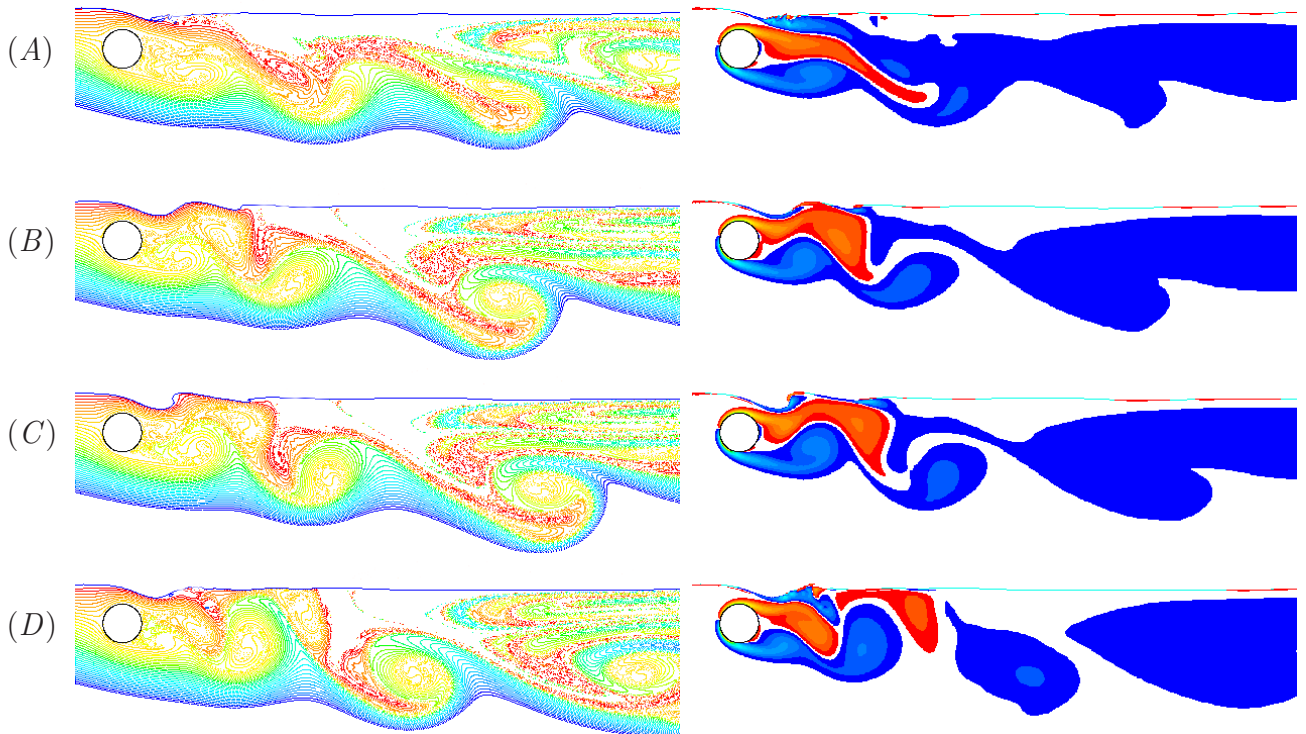


Figure 5.48: Particle transport and vorticity plots showing the first four points A to D denoted in figure (5.47) (gap ratio 0.40, Froude number 0.55). The Reynolds number is again 180.

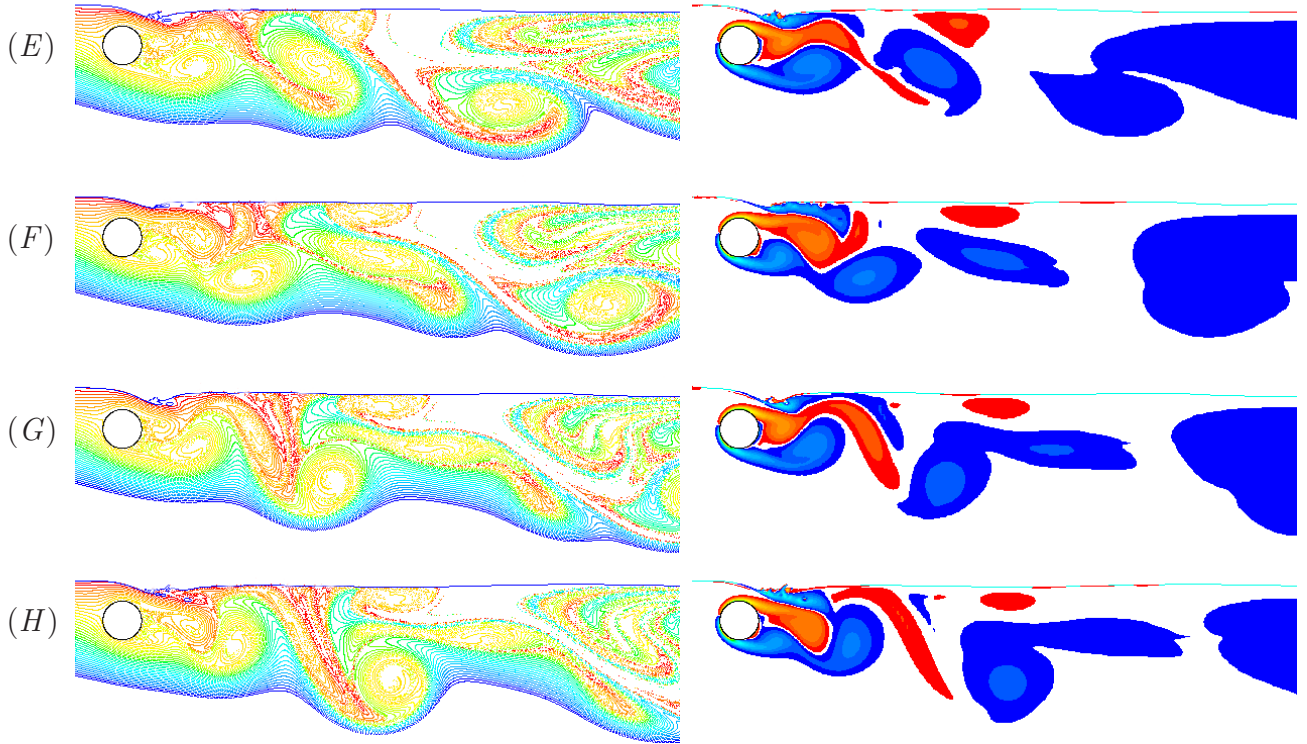


Figure 5.49: Particle transport and vorticity plots showing the four points E to H denoted in figure (5.47) (gap ratio 0.40, Froude number 0.55). The Reynolds number for each of the cases shown is again 180.

What is clear from these plots is that when the ‘jet’ is attached to the surface, the lift starts to increase (with the maximum not occurring while the ‘jet’ is attached, but shortly after it has separated), and that this attachment dramatically alters the surface curvature, with the sharpening surface eventually breaking. Soon afterwards the downward deflection of the ‘jet’ is observed. The attachment of the ‘jet’ to the surface also alters the way in which fluid from above the cylinder is convected downstream, with attachment coinciding with transport close to the surface, while separation (i.e. the ‘jet’ detached from the surface) results in the fluid making up the ‘jet’ being fed into the larger scale vortical structures from beneath.

This modulation is seen for all of the cases in which metastable type behaviour is observed, although the characteristics such as the magnitude, and the modulation frequency, appear to differ for each case. Similar behaviour is also observed at a gap ratio of 0.25 and a Froude number of 0.50, and at a gap ratio of 0.55 for a Froude number of 0.60.

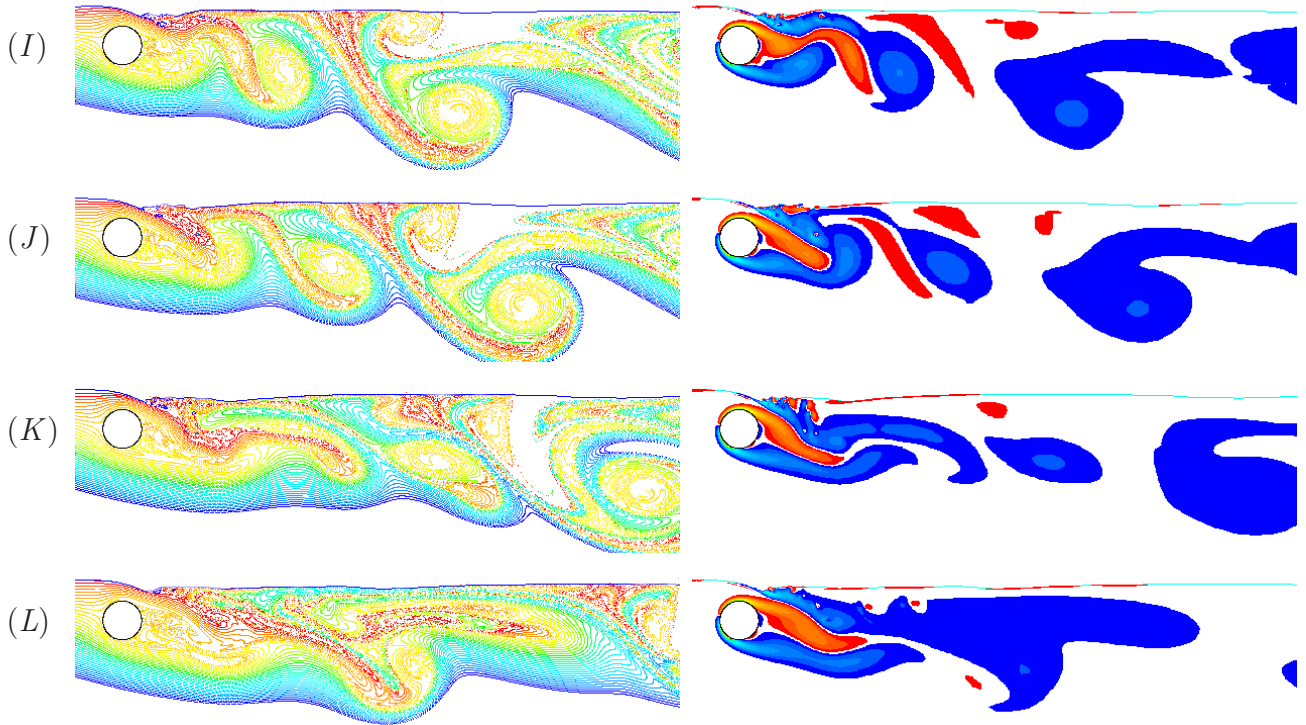


Figure 5.50: Particle transport and vorticity plots showing the four points I to L denoted in figure (5.47) (gap ratio 0.40, Froude number 0.55). The Reynolds number for each of the cases shown is again 180.

5.3 Drag

The behaviour of the drag is of interest as the formation of large-scale vortical structures in the wake, particularly at the smaller gap ratios, should alter the horizontal force acting upon the cylinder. The metastable behaviour is also likely to be highlighted in the time dependent variation of the drag, with the growth and attenuation of vortex shedding influencing the pressure distribution behind the cylinder. Figure (5.52) shows the behaviour of the mean and RMS drag. The trend in the mean drag indicates that the formation of the larger scale vortical structures and the separation of the ‘jet’ from the free surface, act to reduce the drag. These structures typically form at significantly large distances from the cylinder (i.e. 5 or more diameters), with their presence also suppressing vortex shedding. The notable drop in the RMS drag is thus not surprising as the larger scale structures prevent the formation of low pressure vortex cores in the near wake (hence the notable drop in RMS drag at the larger Froude number). Such structures also slow the fluid in the wake cavity and hence increase the dynamic pressure in this region. The reorientation of the wake explains the general drop off in the drag (and the increase in the magnitude of the lift) observed for both cases as the gap ratio is reduced. However, the

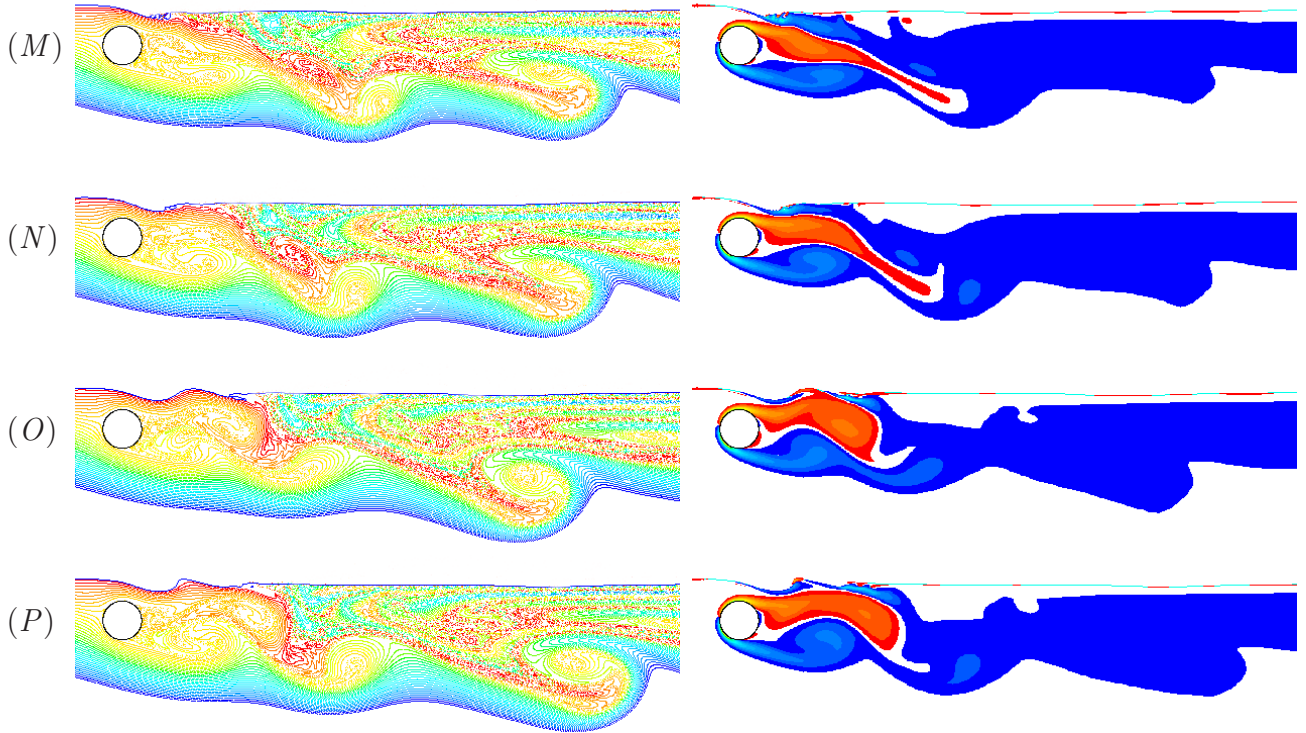


Figure 5.51: Particle transport and vorticity plots showing the last four points M to P denoted in figure (5.47) (gap ratio 0.40, Froude number 0.55). The Reynolds number for each of the cases shown is again 180.

separation of the ‘jet’ from the free surface reorients the wake even further, hence the more rapid decline in drag with gap ratio at the larger Froude number.

5.4 Moment

While the moment acting on the cylinder will be solely due to viscous effects, and hence dependent upon the Reynolds number, it is the trends that are of interest here. The behaviour of the moment with gap ratio, for both Froude numbers, is shown in figure (5.53). The interesting point to note is that the moment changes sign for some of the smaller gap ratio cases as the Froude number is increased (which appears to reflect the slowing or the reversal of flow in some regions of the wake).

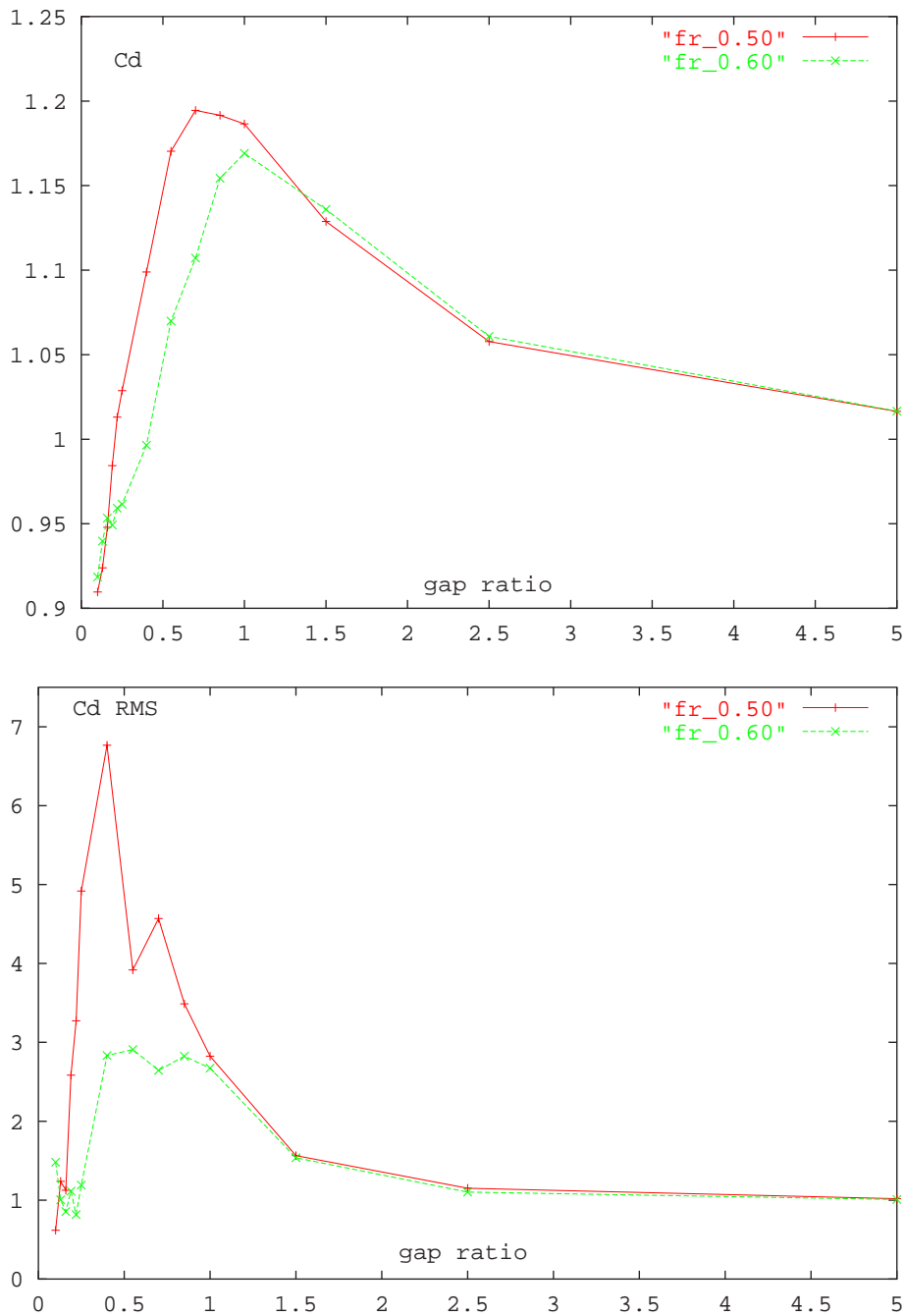


Figure 5.52: Variation of the normalized mean drag and normalized RMS drag with gap ratio for Froude numbers of 0.50 and 0.60. The Reynolds number for each of the cases shown is again 180.

5.5 Mechanism and the Stability of the Wake States

It is perhaps useful at this point to compare the current behaviour with that observed by Sumner et al. (1999) for flow past two side-by-side cylinders in cross-flow. In their investigation they note that at some gap ratios the flow in between the cylinders tends to be biased, in that it

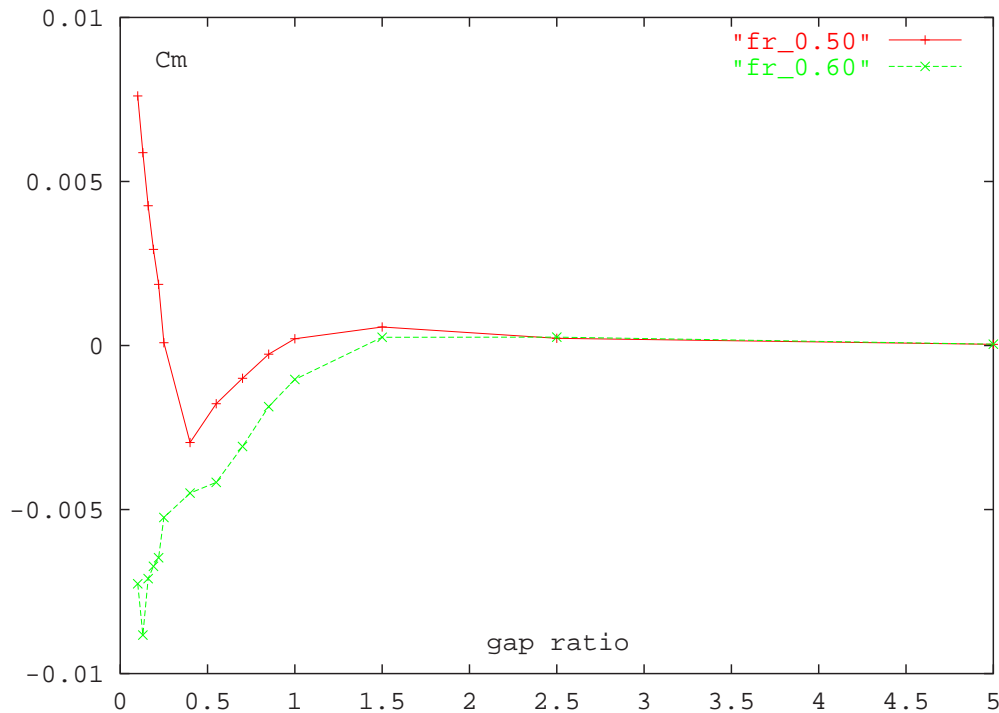


Figure 5.53: Variation of the mean moment with gap ratio for Froude numbers of 0.50 and 0.60. The Reynolds number for each of the cases shown is again 180.

preferentially favours one cylinder. At smaller gap ratios (i.e. 0.20 or below), the two cylinders behave in a fashion similar to that of a single bluff body. As the free-slip boundary is often assumed to be a symmetry plane in potential theory, one may roughly consider the problem here to be analogous to half of the problem considered by Sumner et al. (1999) (although it should be stressed that this is only a rough approximation as vortex interactions with a deformable free surface are not generally well represented by image vortex interactions (Rood (1994b))). Hence at the smaller gap ratios in which Sumner et al. (1999) observe the flow to be similar to that of a single bluff body, one would expect the flow here to represent flow past half a body (which is itself similar to symmetric flow past an obstacle). According to Gerrard (1966) and Green & Gerrard (1993), vortex shedding occurs when the shear layer from one side of the body is drawn across the centerline, such that it cuts off the upstream supply of vorticity to the growing vortex, and a discrete vortex is formed. For this half body analogy, the flow from beneath the cylinder can never cross the centerline, and hence this system can never produce single bluff body shedding.

If the flow is thus forced to be symmetric, then similar behaviour to that found by Fornberg (1985) is expected. For the case of symmetric flow past a cylinder, Fornberg (1985) observes

a large recirculation zone that spans significant distances both vertically and horizontally; and indeed, structures of similar extent are noted here. This observation applies equally at small gap ratios for all of the Froude numbers in the current investigation (i.e. Froude numbers from 0.00 to 0.60), although the value of the Froude number does appear to influence the gap ratio at which this recirculation zone is first observed.

It is speculated here, and it is necessary to stress the word *speculated*, that the flow is convectively unstable when in this state. This idea is asserted, as perturbations do not cause the system to exhibit a time harmonic response and hence the system does not appear to be governed by an absolute instability. It is well known that the wake of a fully submerged cylinder is absolutely unstable to pulse disturbances for Reynolds numbers exceeding roughly 40. It has also been shown by Triantafyllou & Dimas (1989) (with experimental confirmation by Lin et al. (1996)) that a half submerged cylinder is convectively unstable for Froude numbers below 1.77, which is always the case here. Hence it would seem plausible that as the cylinder is moved towards the surface, the instability should transform from being absolutely unstable (at large gaps) to being convectively unstable (at smaller gaps).

As convective instabilities are influenced by the nature of the disturbance, with some form of feedback such as forcing or reflections from boundaries, required for the disturbances to grow. It is thus expected that the flow at these smaller gap ratios may be more responsive to any reflected waves within the computational domain. This may in part explain the observed fluctuations in the surface height at the inlet at a gap ratio of 0.19 and a Froude number of 0.60, although the inadequate capture of the wave breaking could just as likely be responsible for this behaviour.

If one follows the assertion that the wake does indeed move from being absolutely unstable at larger depths to being convectively unstable at smaller ones (with the degree of skew and hence the Froude number determining the gap at which such changes occur), then the metastable wake states follow on as a natural extension, as they represent the loose border in parameter space between the two types of instability.

Hence the metastable wake states will be largely governed by the level of surface deformation, which is itself determined by the Froude number. Thus as the Froude number is increased the level of surface curvature should also increase and the range of gap ratios over which metastable behaviour is observed should grow. However, it is anticipated that only a finite range of gap ratios will support metastable behaviour, as the direct interaction of the vorticity from both the free surface and the cylinder appears to be required for the switching between the instabilities

to occur.

The current results demonstrate that significant changes in the wake behaviour are observed when the Froude number is increased, with these findings largely in agreement with those of Sheridan et al. (1995), Sheridan et al. (1997) and Hoyt & Sellin (2000). Indeed, the close comparison between the current numerical results and those obtained experimentally is remarkable when one considers the range of Reynolds numbers covered. Such agreement suggests that the problem is insensitive to Reynolds number, and is largely dominated the geometrical constraints. The agreement between the current results at low Froude number and those for a no-slip wall lend support to this argument.

It was speculated from the outset that this problem was governed by two primary mechanisms: the first being the supply of fluid to the near wake, and the second involving the degree by which the wake is skewed from being parallel. With regard to the first point, one needs only examine the particle transport video for a fully submerged cylinder to realize that the problem of flow past a cylinder close to a free surface will be strongly influenced by the entrainment demands of the cylinder wake. The supply of fluid is largely determined by the gap ratio.

The degree of skew on the other hand, is predominantly governed by the Froude number which represents the ratio between the inertial and gravitational forces. Its influence on the wake is simply via its determination of the surface curvature, with Ohring & Lugt (1991), and Lugt & Ohring (1992) having shown that vortices generally induce greater surface distortion at larger Froude numbers. It is both of these factors in combination that then determine the nature of the wake flow. The results in the chapter dealing with the flow at low Froude numbers highlight the influence of fluid supply, while the results in the current chapter emphasize the importance of skew. It is the influence of the skew in the wake that perhaps produces the most dramatic changes in the behaviour, as such changes are invariably time-dependent. The metastable wakes states are a clear example, with the time-dependent skew in response to the vortex structures formed on the cylinder resulting in an arresting change in the wake behaviour.

It is perhaps best at this point to clarify what was referred to earlier as being a flow adjustment. With regard to the movement of the ‘jet’ from a position closer to the rear of the cylinder to a point somewhere in between the cylinder and the surface. Such behaviour is not deemed to be metastable here, as it does not constitute a change in the nature of the instability of the wake, whereas the ‘attachment’/‘significant detachment’ of the ‘jet’ from the surface may be justifiably called a metastable state. While this classification is purely based on a definition, it is suggested

here that there are only two basic wake states: attachment or near attachment of the ‘jet’ to the free surface, and significant separation of the ‘jet’ from the free surface. Attachment or near attachment of the ‘jet’ to the surface then corresponds to an absolute instability, while the significant separation corresponds to a convective instability (as no time harmonic response is noted).

It is postulated that the time-dependent flow adjustment observed by Sheridan et al. (1997) is related to the temporal evolution of the large recirculation bubble, with the influence of the Reynolds number on the stability of these large structures being largely unknown (with Fornberg (1985) only having considered symmetric flow past a cylinder up to Reynolds numbers of 600). However, the favorable comparison between the current results and those of Sheridan et al. (1997) indicate that such structures are also likely to be observed at much higher Reynolds numbers. It is possible that these recirculation zones are less stable at larger Reynolds numbers, and hence may produce some time dependent behaviour, which would explain the flow adjustment observed by Sheridan et al. (1997). While the flow adjustment in which the ‘jet’ attaches and then detaches from the rear of the cylinder is not observed here, it should be noted that some flapping of the separated ‘jet’ was observed. One can not rule out that these larger recirculatory structures become three-dimensional, with the three-dimensional evolution then being responsible for the flow adjustment.

The evidence at present for the current investigation will only permit one to suggest that certain behaviour is characteristic of a convective or an absolute instability, without being able to directly classify such behaviour. However, it is strongly speculated here that recirculatory behaviour is synonymous with a convective instability, while near wake vortex shedding is synonymous with an absolute instability.

5.6 Summary

The results of this chapter demonstrate the influence that skew has on the wake, with the gap ratio at which shedding ceases growing with Froude number. The flow mechanics are discussed and it is speculated that the level of skew determines that nature of the instability associated with the cylinder wake (i.e. absolute or convective instability). Furthermore, it is speculated that the metastable wake states, which are covered in this chapter, represent a loose border in parameter space between the two types of instability.

Chapter 6

Conclusion

From the outset the major goal of the current study was to provide a mechanism that explains the observed changes in the wake behaviour for flow past a cylinder close to a free surface. It was envisaged that such a mechanism may then provide some information with regard to the nature of the instabilities associated with the wake over a range in parameter space.

The initial suggestion that this problem was largely governed by two primary mechanisms, with the first being the supply of fluid into the near wake, and the second being the degree by which the wake is skewed from being parallel, appears to have largely been vindicated.

With regard to the first point, one needs only examine the particle transport video for a fully submerged cylinder, to realize that the problem of flow past a cylinder close to a free surface will be strongly influenced by the entrainment demands of the forming vortices behind the cylinder. Such videos highlight the fact that considerable amounts of the fluid that would have gone into forming a fully submerged vortex street, are clearly unavailable for the case of the cylinder close to an adjacent surface.

The resultant wake behaviour for the cylinder close to a free surface reflects these changes, with the influence of the supply of fluid into the wake cavity being demonstrated by the significant changes in the response of the system observed at small gap ratios. It is believed that it is this supply which largely governs the behaviour of the wake at small Froude numbers where the flow is largely parallel, and it is suggested that it is this behaviour that also dominates the flow for the case of a cylinder close to a no-slip surface.

The suggestion by Koch (1985) and the speculation of Huerre & Monkewitz (1990) that only a limited range of asymmetry is required before an absolute instability can no longer be sustained,

intimates that the cessation of shedding (or the extinguishment of the absolute instability) at the small gap ratios is likely to involve the skewing of the wake velocity profile.

The low Froude number results for variation of the maximum time averaged velocity in the region directly above the uppermost part of the cylinder with gap ratio, that shows a significant reduction in the average flow velocity with decreasing gap, suggest that the wake does indeed become skewed, even for cases in which the flow is still largely parallel.

Indeed it appears to be skew in the velocity profile that leads to the cessation of shedding for all of the Froude numbers considered, although having said that, the nature of the skew appears to be different for each Froude number. At low Froude numbers the wake is largely parallel and the skew introduced is due to a reduction in the horizontal velocity near the top of the cylinder. At the intermediate and larger Froude numbers the skew arises as there is an increasing vertical and decreasing horizontal component of the flow passing over the cylinder. Such skew is then introduced by the increased level of surface curvature which alters the horizontal component of the flow passing over the cylinder.

It is the level of skew, or perhaps more appropriately the reduction in the horizontal component of the flow passing over the cylinder, that is the common thread linking all of the results concerning the cessation of shedding for the entire Froude number range considered. At the larger Froude numbers the surface curvature and hence the level of skew varies with time, and it is this time dependence that gives rise to the more interesting wake states.

Indeed, it is tentatively proposed here that the metastable wake states represent a time dependent switching between an absolute and a convective instability. For the metastable cases, it is believed that the absolute instability gives rise to structures which lead to its own demise, and as such the system when in this state represents a feedback loop.

The argument that the the flow becomes convectively unstable at small gap ratios is supported by the findings of Triantafyllou & Dimas (1989), who indicate that the wake of a half submerged cylinder (at an infinite Reynolds number) is convectively unstable for Froude numbers below approximately 1.77 (which is always the case here). As the wake of a fully submerged cylinder is absolutely unstable for Reynolds numbers above roughly 40 (Triantafyllou & Dimas (1989)), it would seem plausible that the nature of the instability must change as the cylinder is moved closer and closer towards the surface.

The altered levels of skew with increasing Froude number reflect the response of the free surface to the vorticity field generated by the cylinder. At the lower Froude numbers where the surface

is relatively flat, the upward movement of the positive vortex from beneath the cylinder (at small gap ratios) induces little or no surface deformation and the slowed/reverse flow above the positive vortex interacts with the flow passing over the cylinder in a direct manner (i.e. the collision is ‘head-on’). At the larger Froude numbers, the upward movement of the last shed positive vortex from beneath the cylinder results in more significant surface deformation, and hence alters the angle at which the slow/reverse flow from above the positive vortex and that from above the cylinder interact. Finally when the Froude number is sufficiently large, the angle between the two counter flowing streams increases to the point at which the flow from above the cylinder is deflected away from the surface. This simplified procedure is shown schematically in figure (6.1).

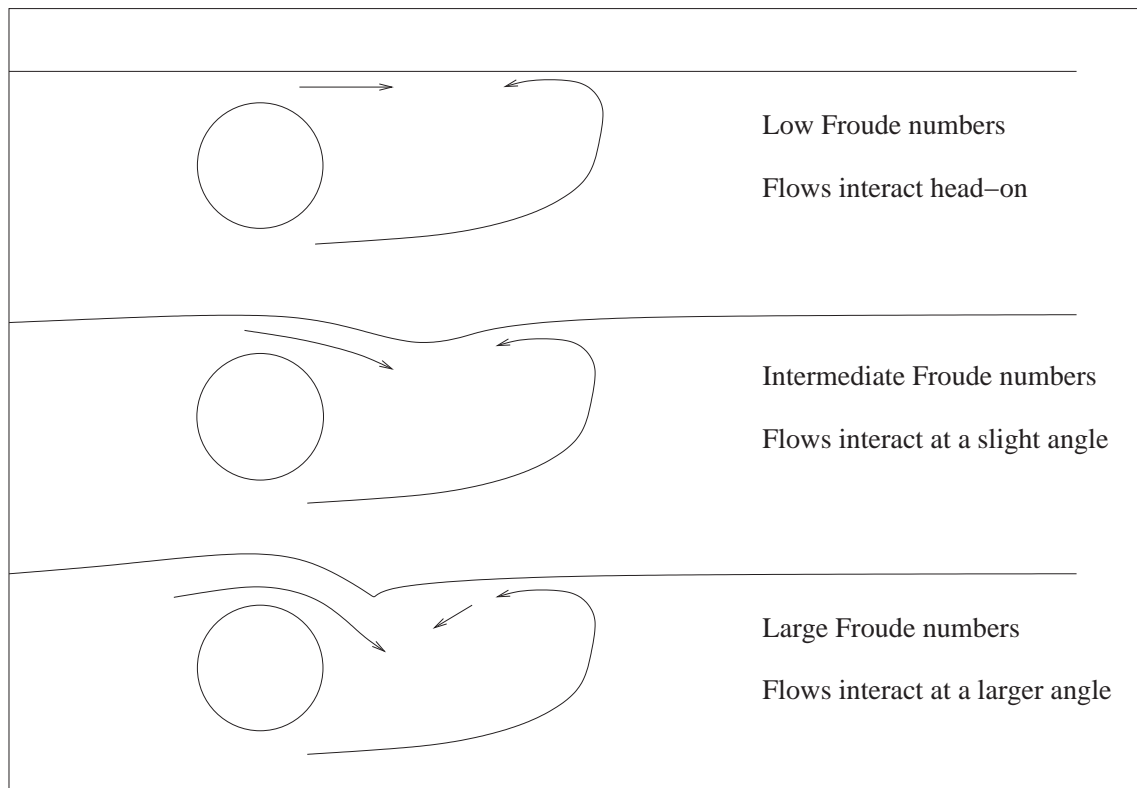


Figure 6.1: Schematic illustrating the influence of the Froude number on the wakes behaviour.

It should be noted that the slow/reverse flow near the free surface is due to all of the positive vortical structures in the wake, and not just the last shed positive vortex, although it is the closest structures that have the most influence.

In the introduction at the start of this document, a number of other aims/goals were set, and it is perhaps useful at this point to consider how well they have been satisfied. The first goal was to confirm that the flow field is largely two dimensional, as suggested by Sheridan et al. (1997).

The comparison between the current results and those of Miyata et al. (1990), Sheridan et al. (1995), Sheridan et al. (1997) and Hoyt & Sellin (2000), suggest that the two-dimensionality of the results is somewhat dependent upon both Froude number and gap ratio.

At the smaller Froude numbers the pictorial comparison is not particularly good with the results of Sheridan et al. (1997), although it is favourable with those of Miyata et al. (1990). The major difference is the lack of anything resembling discrete vortices in the wake for the results of Sheridan et al. (1997) at low Froude numbers. Both the current results and those of Miyata et al. (1990) indicate that shedding takes place for a range of gap ratios at low Froude numbers, and it is possible, although unlikely, that the contouring chosen by Sheridan et al. (1997) hides such vortices.

At the intermediate and larger Froude numbers the comparison between the results of the current two dimensional study and that of Sheridan et al. (1997) improves. Remarkable agreement is observed at the larger Froude numbers, both in terms of the point in parameter space at which the metastable effects occur, and with respect to the flow behaviour at these points in parameter space.

The flow also appears to become more two dimensional at smaller gap ratios, and it suggests that the closer one comes to the wake being convectively unstable, the more two dimensional the flow field becomes.

The second goal was to map out a larger region of the parameter space, which to the author's knowledge was largely uncharted. It is believed that the current results go some way in satisfying this goal, with the behaviour of the Strouhal number, the mean and RMS components of the lift and drag, the mean moment, the position of the stagnation and separation points, the variation of the formation length, the paths and convective velocities of the vortices, the time averaged flow, the behaviour of the local Froude number and both the vorticity fields and particles transport plots all having been considered.

6.1 Future Work

It is hoped that the current investigation has shed some light on the problem of flow past a cylinder close to a free surface. However, it has also raised a number of issues that warrant further investigation. Some of these include:

- Confirmation of the variation of the formation length with gap ratio, and the effect of the

Reynolds number on both the formation length and the Strouhal number.

- A more substantial investigation of the three dimensionality of the flow.
- The influence of a body with fixed separation points (i.e. a square or a rectangular plate).
- A stability analysis of the wake profiles for the cases close to the point at which shedding ceases.

Bibliography

- Acheson, D. J. (1990), *Elementary Fluid Dynamics*, Oxford University Press.
- Angrilli, F., Bergamschi, S. & Cossalter, V. (1982), ‘Investigation of wall induced modifications to vortex shedding from a circular cylinder’, *Transactions of the ASME Journal of Fluids Engineering* **104**, 518–522.
- Anthony, D. G., Hirska, A. & Willmarth, W. W. (1991), ‘On the interaction of a submerged turbulent jet with a clean or contaminated free surface’, *Physics of Fluids A* **3**(2), 245–247.
- Apelt, C. J. & West, C. J. (1975), ‘The effects of wake splitter plates on bluff-body flow in the range $10^4 < r < 5 \times 10^4$. part 2’, *Journal of Fluid Mechanics* **71**(part 1), 145–160.
- Barkley, D. & Henderson, R. D. (1996), ‘Three-dimensional floquet stability analysis of the wake of a circular cylinder’, *Journal of Fluid Mechanics* **322**, 215–241.
- Bearman, P. W. & Wadcock, A. J. (1973), ‘The interaction between a pair of circular cylinders normal to a stream’, *Journal of Fluid Mechanics* **61**, 499–511.
- Bearman, P. W. & Zdravkovich, M. M. (1978), ‘Flow around a circular cylinder near a plane boundary’, *Journal of Fluid Mechanics* **89**(part 1), 33–47.
- Berger, E. & Wille, R. (1972), ‘Periodic flow phenomena’, *Annual Review of Fluid Mechanics* **4**, 313.
- Blackburn, H. M. & Henderson, R. D. (1995), Near-wake vorticity dynamics in bluff body flows, *in* ‘Proceeding of the 12th Australasian Fluid Mechanics Conference, Sydney, Australia’, pp. 17–20.
- Briggs, R. J. (1964), *Electron-stream Interaction with Plasmas*, M.I.T. Press, Cambridge, Massachusetts.

- Chapra, S. C. & Canale, R. P. (1991), *Numerical Methods for Engineers*, 2nd edn, McGraw-Hill.
- Chomaz, J. M., Huerre, P. & Redekopp, L. T. (1988), ‘Bifurcation to local and global modes in spatially developing flows’, *Physics Review Letters* **60**, 25–28.
- Dimas, A. A. & Triantafyllou, G. S. (1994), ‘Nonlinear interaction of shear flow with a free surface’, *Journal of Fluid Mechanics* **260**, 221–246.
- Dimopoulos, H. G. & Hanratty, T. J. (1968), ‘Velocity gradients at the wall for flow around a cylinder for reynolds numbers between 60 and 360’, *Journal of Fluid Mechanics* **33**(part2), 303–319.
- Fletcher, C. A. J. (1991), *Computational Techniques for Fluid Dynamics*, Vol. 1-2, 2nd edn, Springer-Verlag.
- Fornberg, B. (1985), ‘Steady viscous flow past a circular cylinder up to reynolds number 600’, *Journal of Computational Physics* **61**, 297–320.
- Freymuth, P., Finaish, F. & Bank, W. (1986), ‘Visualization of the vortex street behind a circular cylinder at low reynolds number’, *Physics of Fluids* **29**(4), 1321–1323.
- Gerrard, J. H. (1966), ‘The mechanics of the formation region of vortices behind bluff bodies’, *Journal of Fluid Mechanics* **25**(part 2), 401–413.
- Göktun, S. (1975), The drag and lift characteristics of a cylinder placed near a plane surface, Master’s thesis, Naval Postgraduate School, Monterey, California, USA.
- Grass, A. J., Raven, P. W. J., Stuart, R. J. & Bray, J. A. (1984), ‘The influence of boundary layer velocity gradients and bed proximity on vortex shedding from free spanning pipelines’, *Transactions of the ASME Journal of Fluids Engineering* **106**, 70–78.
- Green, R. B. & Gerrard, J. H. (1993), ‘Vorticity measurements in the near wake of a circular cylinder at low reynolds number’, *Journal of Fluid Mechanics* **246**, 675–691.
- Green, S. I., ed. (1995), *Fluid Vortices*, Kluwer Academic Publishers.
- Griffin, O. M. (1995), ‘A note on bluff body vortex formation’, *Journal of Fluid Mechanics* **284**, 217–224.
- Griffin, O. M. & Hall, M. S. (1991), ‘Review-vortex shedding lock-on and flow control in bluff body wakes’, *Transactions of the ASME Journal of Fluid Engineering* **113**, 526–537.

- Griffin, O. M. & Ramberg, S. E. (1974), ‘The vortex street wakes of vibrating cylinders’, *Journal of Fluid Mechanics* **66**, 553–576.
- Griffin, O. M. & Ramberg, S. E. (1976), ‘Vortex shedding from a cylinder vibrating in line with an incident uniform flow’, *Journal of Fluid Mechanics* **75**, 257–271.
- Hirt, C. W. & Nichols, B. D. (1981), ‘Volume of fluid (vof) method for the dynamics of free boundaries’, *Journal of Computational Physics* **39**, 201–225.
- Hoyt, J. W. & Sellin, R. H. J. (2000), ‘A comparison of the tracer and piv results in visualizing water flow around a cylinder close to the free surface’, *Experiments in Fluids* **28**, 261–265.
- Huerre, P. & Monkewitz, P. A. (1990), ‘Local and global instabilities in spatially developing flows’, *Annual Review of Fluid Mechanics* **22**, 473–537.
- Hughes, W. F. & Brighton, J. A. (1991), *Fluid Dynamics*, 2nd edn, Schaum’s Outline Series.
- Issa, R. I. (1986), ‘Solution of the implicitly discretized fluid flow equations by operator splitting’, *Journal of Computational Physics* **62**, 40–65.
- Koch, W. (1985), ‘Local instability characteristics and frequency determination of self-excited wake flows’, *Journal of Sound and Vibration* **99**(1), 53–83.
- Lamb, H. (1924), *Hydrodynamics*, 5th edn, Cambridge University Press.
- Lei, C., Cheng, L., Armfield, W. & Kavanagh, K. (1998), A numerical study of vortex shedding from a circular cylinder near a wall, in ‘International Conference on Computational Hydrodynamics, Seoul, Korea, 1988’, pp. 699–704.
- Lei, C., Cheng, L. & Kavanagh, K. (1999), ‘Re-examination of the effect of a plane boundary on force and vortex shedding of a circular cylinder’, *Journal of Wind Engineering and Industrial Aerodynamics* **80**, 263–286.
- Leonard, B. P. (1979), ‘A stable and accurate convective modelling procedure based on quadratic upstream interpolation’, *Computational Methods in Applied Mechanical Engineering* **19**, 59–98.
- Lighthill, M. J. (1963), *Laminar Boundary Layers* (ed. Rosenhead, L., Oxford University Press.
- Lin, J.-C. & Rockwell, D. (1995), ‘Evolution of a quasi-steady breaking wave’, *Journal of Fluid Mechanics* **302**, 29–44.

- Lin, J.-C. & Rockwell, D. (1996), ‘Force identification by vorticity fields: Techniques based on flow imaging’, *Journal of Fluids and Structures* **10**, 663–668.
- Lin, J.-C., Sheridan, J. & Rockwell, D. (1996), ‘Near wake of a perturbed, horizontal cylinder at a free surface’, *Physics of Fluids* **8**, 2107–2116.
- Lin, J.-C., Towfighi, J. & Rockwell, D. (1995), ‘Instantaneous structure of the near wake of a circular cylinder: On the effect of reynolds number’, *Journal of Fluids and Structures* **9**, 409–418.
- Lugt, H. J. (1987), ‘Local flow properties at a viscous free surface’, *Physics of Fluids* **30**, 3647–3652.
- Lugt, H. J. & Ohring, S. (1992), ‘The oblique ascent of a viscous vortex pair toward a free surface’, *Journal of Fluid Mechanics* **236**, 461–476.
- Lundgren, T. & Koumoutsakos, P. (1999), ‘On the generation of vorticity at a free surface’, *Journal of Fluid Mechanics* **382**, 351–366.
- Martin, J. C. & Moyce, W. J. (1952), ‘Part iv. an experimental study of the collapse of liquid columns on a rigid horizontal plane’, *Transactions of the Philosophical Society of London* **244**, 312–334.
- Miyata, H., Shikazono, N. & Kani, M. (1990), ‘Forces on a circular cylinder advancing steadily beneath the free-surface’, *Ocean Engineering* **17**(1/2), 81–104.
- Monaghan, J. J. (1992), ‘Smoothed particle hydrodynamics’, *Annual Review of Astronomy and Astrophysics* **30**, 543–574.
- Monaghan, J. J. (1994), ‘Simulating free surface flows with sph’, *Journal of Computational Physics* **110**, 399–406.
- Monkewitz, P. A. (1988), ‘The absolute and convective nature of instability in two-dimensional wakes at low reynolds numbers’, *Physics of Fluids* **31**(5), 999–1006.
- Morkovin, M. K. (1964), Flow around circular cylinder- a kaleidoscope of challenging fluid phenomena, in ‘ASME Symposium on Fully Separated Flows’, Philadelphia, Pennsylvania, USA, pp. 102–118.
- Morsi, S. A. & Alexander, A. J. (1972), ‘An investigation of particle trajectories in two-phase flow systems’, *Journal of Fluid Mechanics* **55**, 193–208.

- Morton, B. R. (1984), ‘The generation and decay of vorticity’, *Geophysical and Astrophysical Fluid Dynamics* **28**, 277–308.
- Noca, F., Shiels, D. & Jeon, D. (1997), ‘Measuring instantaneous fluid dynamic forces on bodies, using only velocity fields and their derivatives’, *Journal of Fluids and Structures* **11**, 345–350.
- Norberg, C. (1998), Ldv-measurements in the near wake of a circular cylinder, *in* ‘Proceedings of the ASME Fluids Engineering Division Summer Meeting, FEDSM98-5202, Washington DC., U.S.A.’.
- Oertel, H. J. (1990), ‘Wakes behind blunt bodies’, *Annual Review of Fluid Mechanics* **22**, 539–564.
- Ohring, S. & Lugt, H. J. (1991), ‘Interaction of a viscous vortex pair with a free surface’, *Journal of Fluid Mechanics* **227**, 47–70.
- Ongoren, A. & Rockwell, D. (1988*a*), ‘Flow structure from an oscillating cylinder. part 1: Mechanisms of phase shift and recovery in the near wake.’, *Journal of Fluid Mechanics* **191**, 197–223.
- Ongoren, A. & Rockwell, D. (1988*b*), ‘Flow structure from an oscillating cylinder. part 2: Model competition in the near wake’, *Journal of Fluid Mechanics* **191**, 225–245.
- Pantankar, S. V. & Spalding, D. B. (1972), ‘A calculation procedure for heat, mass and momentum transfer in three-dimensional flows’, *International Journal of Heat and Mass Transfer* **15**, 1787–1806.
- Price, S. J., Smith, J. G., Leong, K., Paidoussis, M. P. & Sumner, D. (2000), Flow-visualization around a circular cylinder near to a plane wall, *in* Z. . Staubli, ed., ‘Flow Induced Vibration, Balkema, Rotterdam 2000’, pp. 105–112.
- Reichl, P. J., Morris, P., Hourigan, K., Thompson, M. C. & Stoneman, S. A. T. (1997*a*), Coating flow simulations using smooth particle hydrodynamics, *in* ‘Computational Fluid Dynamics in Mineral & Metal Processing and Power Generation, Melbourne Australia’, pp. 345–352.
- Reichl, P. J., Morris, P., Hourigan, K., Thompson, M. C. & Stoneman, S. A. T. (1997*b*), Free surface flows using smooth particle hydrodynamics, *in* ‘Proceedings of the ASME Fluids Engineering Division Summer Meeting, FEDSM97-3403, Vancouver, British Columbia, Canada’.

- Reichl, P. J., Morris, P., Hourigan, K., Thompson, M. C. & Stoneman, S. A. T. (1998), ‘Smooth particle hydrodynamics simulation of surface coating’, *Applied Mathematical Modelling* **22**, 1037–1046.
- Reichl, P. J., Morris, P., Stoneman, S. A. T., Thompson, M. C. & Hourigan, K. (1998), Smooth particle hydrodynamics modelling of vertical jet impingement, *in* ‘Proceedings of the 13th Australasian Fluid Mechanics Conference, Melbourne, Australia’, pp. 103–106.
- Rood, E. P. (1991), Vortex interactions with a free-surface, *in* ‘Proceedings of the FAA International Wake Vortex Symposium, Washington D.C., 1991’, Vol. 2, pp. 43–1 – 34–5.
- Rood, E. P. (1994a), ‘Interpreting vortex interactions with a free surface’, *Transactions of the ASME Journal of Fluids Engineering* **116**, 91–94.
- Rood, E. P. (1994b), Myths, math, and physics of free-surface vorticity, *in* A. S. Kobayashi, ed., ‘Proceedings of the Twelfth US National Congress of Applied Mechanics, June 1994, Seattle, Washington (Applied Mechanics Reviews)’, Vol. 47, pp. 152–156.
- Rood, E. P. (1995), Vorticity interactions with a free surface, *in* S. I. Green, ed., ‘Fluid Vortices’, Kluwer Academic Publishers, chapter XVI, pp. 687–730.
- Rosenhead, L., ed. (1963), *Laminar Boundary Layers*, Unabridged Dover republication of the edition published by Oxford University Press.
- Roshko, A., Steinolfson, A. & Chattoorgoon, V. (1975), Flow forces on a cylinder near a wall or near another cylinder, *in* ‘Proceedings of the 2nd US Conference of Wind Engineering Res., Fort Collins. Paper IV-15’, pp. 1–3.
- Sarpkaya, T. (1996), ‘Vorticity, free surface, and surfactants’, *Annual Review of Fluid Mechanics* **28**, 83–128.
- Shariff, K., Pulliam, T. H. & Ottino, J. M. (1991), A dynamical systems analysis of kinematics in the time-periodic wake of a circular cylinder, *in* C. R. Anderson & C. Greengard, eds, ‘Lectures in Applied Mathematics, Vortex Dynamics and Vortex Methods’, Vol. 28, American Mathematical Society, pp. 613–646.
- Sheridan, J., Lin, J.-C. & Rockwell, D. (1995), ‘Metastable states of a cylinder wake adjacent to a free surface’, *Physics of Fluids* **7**(9), 2099–2101.

- Sheridan, J., Lin, J.-C. & Rockwell, D. (1997), ‘Flow past a cylinder close to a free surface’, *Journal of Fluid Mechanics* **330**, 1–30.
- Sheridan, J., Lin, J.-C. & Rockwell, D. (1998), The interaction of a cylinder wake with a free surface, in ‘Proceedings of the ASME Fluids Engineering Division Summer Meeting, FEDSM98-5689, Washington DC., U.S.A.’.
- Smith, G. D. (1985), *Numerical solution of partial differential equations : finite difference methods*, 3rd edn, Oxford University Press.
- Strouhal, V. (1878), ‘Über eine besondere art der tonerregung.’, *Ann. Physik Chemie* **5**, 216–251.
- Strykowski, P. J. & Sreenivasan, K. R. (1990), ‘On the formation and suppression of vortex ‘shedding’ at low reynolds numbers’, *Journal of Fluid Mechanics* **218**, 71–107.
- Sumner, D., Wong, S. T., Price, S. J. & Paidoussis, M. P. (1999), ‘Fluid behaviour of side-by-side circular cylinders in steady cross-flow’, *Journal of Fluids and Structures* **13**, 309–338.
- Takeda, H., Miyama, s. M. & Sekiya, M. (1994), ‘Numerical simulation of viscous flow by smoothed particle hydrodynamics’, *Progress of Theoretical Physics* **92**, 939–960.
- Taneda, S. (1965), ‘Experimental investigation of vortex streets’, *Journal of the Physics Society of Japan* **20**, 1714–1721.
- Taniguchi, S. & Miyakoshi, K. (1990), ‘Fluctuating fluid forces acting on a circular cylinder and interference with a plane wall’, *Experiments in Fluids* **9**, 197–204.
- Thompson, M. C., Hourigan, K. & Monaghan, J. J. (1994), Simulation of free surface flows with sph, in ‘ASME Symposium on Computational Methods in Fluid Dynamics, Lake Tahoe, U.S.A.’.
- Thompson, M. C., Hourigan, K. & Sheridan, J. (1996), ‘Three-dimensional instabilities in the wake of a circular cylinder’, *Experimental and Thermal Fluid Science* **12**, 190–196.
- Triantafyllou, G. S. & Dimas, A. A. (1989), ‘Interaction of two-dimensional separated flows with a free surface at low froude numbers’, *Physics of Fluids A* **1**(11), 1813–1821.
- Triantafyllou, G. S., Triantafyllou, M. S. & Chryssostomidis, C. (1986), ‘On the formation of vortex streets behind stationary cylinders’, *Journal of Fluid Mechanics* **170**, 461–477.
- Tritton, D. (1988), *Physical Fluid Dynamics*, second edn, Oxford Science Publications.

- Truesdell, C. (1953), *The Kinematics of Vorticity*, Indiana University Press.
- Tryggvason, G. (1988), ‘Deformation of a free surface as a result of vortical flows’, *Physics of Fluids* **31**(5), 955–957.
- Tryggvason, G., Unverdi, S. O., Song, M. & Abdolahi-Alibeik, J. (1991), Interaction of vortices with a free surface and density interfaces, *in* C. R. Anderson & C. Greengard, eds, ‘Lectures in Applied Mathematics, Vortex Dynamics and Vortex Methods’, Vol. 28, American Mathematical Society, pp. 679–699.
- Tsai, W.-t. & Yue, D. K. P. (1996), ‘Computation of nonlinear free-surface flows’, *Annual Review of Fluid Mechanics* **28**, 249–278.
- Unal, M. F. & Rockwell, D. (1988*a*), ‘On vortex formation from a cylinder. part 1. the initial instability’, *Journal of Fluid Mechanics* **190**, 491–512.
- Unal, M. F. & Rockwell, D. (1988*b*), ‘On vortex formation from a cylinder. part 2. control by splitter-plate interference’, *Journal of Fluid Mechanics* **190**, 513–529.
- Valluri, S. (1996), Bluff Body Flows in the Presence of a Free Surface, PhD thesis, Graduate Aeronautical Laboratories California Institute of Technology.
- Versteeg, H. K. & Malalasekera, W. (1995), *An Introduction to Computational Fluid Dynamics: The Finite Volume Method*, Longman Scientific & Technical.
- Wang, H. T. & Leighton, R. (1991), Direct calculation of the interaction between subsurface vortices and surface contaminants, *in* ‘Proceedings of the 9th OMAE Conference, Houston, Texas, U.S.A.’, pp. 271–277.
- Warburton, T. C. & Karniadakis, G. E. (1997), Spectral simulations of flow past a cylinder close to a free-surface, *in* ‘Proceedings of the ASME Fluids Engineering Division Summer Meeting, FEDSM97-3389, Vancouver, British Columbia, Canada’.
- White, F. M. (1994), *Fluid mechanics*, 3rd edn, McGraw-Hill.
- Williamson, C. H. K. (1985), ‘Evolution of a single wake behind a pair of bluff bodies’, *Journal of Fluid Mechanics* **159**, 1–18.
- Williamson, C. H. K. (1989), ‘Oblique and parallel modes of vortex shedding in the wake of a circular cylinder at low reynolds numbers’, *Journal of Fluid Mechanics* **206**, 579–627.

- Williamson, C. H. K. (1991), 2-d and 3-d aspects of the wake of a cylinder, and their relation to wake computations, *in* C. R. Anderson & C. Greengard, eds, ‘Lectures in Applied Mathematics, Vortex Dynamics and Vortex Methods’, Vol. 28, American Mathematical Society, pp. 719–751.
- Williamson, C. H. K. (1996), ‘Vortex dynamics in the cylinder wake’, *Annual Review of Fluid Mechanics* **28**, 477–539.
- Yeung, R. W. (1982), ‘Numerical methods in free-surface flows’, *Annual Review of Fluid Mechanics* **14**, 395–442.
- Yu, D. & Tryggvason, G. (1990), ‘The free surface signature of unsteady two dimensional vortex flows’, *Journal of Fluid Mechanics* **218**, 547–572.